A MODIFIED AIRLIFT FIBER-BED BIOREACTOR

FOR ANIMAL CELL CULTURE

by

TZYY-WEN CHIOU

B.S. Agricultural Chemistry
National Taiwan University, Taipei, R.O.C
(1982)

M.S. Agricultural Chemistry
National Taiwan University, Taipei, R.O.C.
(1984)

Submitted to the Department of Applied Biological Sciences in
Partial Fulfillment of the Requirements for the Degree of

DOCTOR OF PHILOSOPHY

in

BIOCHEMICAL ENGINEERING

at the

MASSACHUSETTS INSTITUTE OF TECHNOLOGY

April, 1992

Signature of Author _____
Department of Applied Biological Sciences
January 29, 1992

Certified by _____
Professor Daniel I.C. Wang
Thesis Supervisor, Professor of Chemical and Biochemical Engineering

Accepted by _____
Professor Steven Tannenbaum
Chairman, Committee on Graduate Student

This doctoral thesis has been examined by a Committee of the Department of Applied Biological Sciences as follows:

Professor Charles L. Cooney — Chairman

Professor Anthony J. Sinskey

Professor Gregory N. Stephanopoulos

A modified airlift fiber-bed bioreactor for animal cell culture

by

Tzyy-Wen Chiou

Submitted to the Department of Applied Biological Sciences in partial fulfillment of the requirements for the degree of Doctor of Philosophy in Biochemical Engineering

ABSTRACT

The problems in animal cell bioreactors have been low surface-to-volume ratio of anchorage-dependent animal cell systems, oxygen transfer limitations, and shear sensitivity of the animal cells. The objectives of this thesis are to enhance bioreactor productivity through a better engineering design and to overcome some of the problems which are presently faced.

A new bioreactor for animal cell cultivation has been developed for both anchorage-dependent and anchorage-independent cells. This design is based on a modified configuration of the airlift bioreactor. The cells are retained in the annulus section of the airlift bioreactor which is packed with sub-micron glass fibers. Air is introduced from the base of the draft tube and oxygenates the medium in the draft tube, and bubbles disengage at the upper fluid surface. The hydrostatic pressure difference between the aerated fluid in the draft tube and the bubble-free fluid in the annular fiber-bed results in the global circulation of the medium in the bioreactor. The design provides an efficient oxygen supply *in situ* and minimizes the detrimental effects of gas-liquid interfacial forces and hydrodynamic forces. Additional advantages of the bioreactor include its simple construction, high surface-to-volume ratio, convective nutrient supply, avoidance of mechanical agitation, ability for continuous/perfusion operation, and high scaleup potential.

A hydrodynamic model was developed to characterize the bioreactor. By applying the model, liquid flow rates and volumetric mass transfer coefficients can be predicted and are shown to be in agreement with experimental data. Oxygen transfer in this reactor, calculated based on liquid flow rate and mass transfer coefficient, can be improved by optimizing the ratio of draft tube diameter (Di) to bioreactor diameter (Do). Effects of permeability of the fiber bed on oxygen transfer and optimal Di/Do ratio of the reactor have been studied. Desired permeability can be obtained by selecting appropriate void fraction, fiber diameter and fiber arrangement in the fiber bed. It was found that permeability is also affected by the accumulation of cells in the fiber bed. A model of multilayer cell growth in the fiber bed was developed to describe the effect of cell growth on permeability. The information is useful for choosing the correct Di/Do ratio to achieve high oxygen transfer rate at high cell densities.

The operation and technical feasibility of the bioreactor were successfully demonstrated by the cell cultivation experiments conducted in a 4-liter prototype reactor. In these continuous/perfusion cultivations, recombinant Chinese Hamster Ovary cells were used as model system for anchorage-dependent cell line and hybridoma ATCC-CRL-1606 for anchorage-independent cell line. Experimental results showed that high cell density,

high oxygen transfer rate, sustained production of desired product, and high productivity corresponding to high product concentration were achieved for both types of cells. This bioreactor is able to maintain the necessary conditions for stable operation at high cell density with continuous product synthesis for a long period of time. Channeling in the high-density fiber bed was studied by observations of the cell distribution in the fiber bed, change in channel radius due to cell growth and residence time distribution of the fiber bed before and after cell cultivation.

Theoretical scaleup potential of the airlift fiber-bed bioreactor has been considered for volumes ranging from 2.5 to 1000 liters. The optimal geometry and achievable oxygen transfer rate at various cell densities are presented.

Thesis Supervisor: Dr. Daniel I.C. Wang
Title: Professor of Chemical Engineering

ACKNOWLEDGEMENTS

I would like to express my sincere appreciation to all who have contributed to this thesis and made my stay at M.I.T. a very enjoyable and memorable experience.

My deepest appreciation goes to my thesis advisor, Professor Daniel I.C. Wang for his constant wise guidance, inspiration and great support in my thesis research. His brilliance, toughness, demand for excellence, dedication and discipline will always be a role model for my career development. I am also very grateful to my thesis committee, Professors Charlie Cooney, Tony Sinskey, and Greg Stephanopoulos for their encouragement and insightful and constructive comments. I have benefitted much from their invaluable advice.

I cannot thank Professor Wen-Tung Wu enough for his essential contribution at the early stage of this thesis. Professor Wu taught me a lot of engineering concepts as well as the philosophy of life. His words of wisdom will continue to guide me for many years to come. I am also indebted to Sei Murakami and Professor Yoon-Ching Chang for their inputs when they were visiting scientists at BPEC. The productive and hard-working team we had formed will always be remembered. Many thanks to the undergraduates, Marie Traverse, Beth Huizenga, Amy Meyers, Cynthia Chuang, Hui-Lin Lai, Karen Lee, Christine Jang and Ivana Markovic whose companionship and assistance in certain experiments have made the labwork very enjoyable and fruitful.

My past and present colleagues in BPEC have provided their care and support in many ways. In particular, I would like to thank Ruth Ayers, Audrey Childs, Sonia Foster, Diana Kenney, Lynn Lenker, Anushri Singhvi and Marguerite Walsh for their cheerful

spirit and constant administrative assistance. I would also like to thank Enno Adema, Mark Applegate, John Aunins, Jeff Cleland, Matt Croughan, Linda Desmarais, Gino Grampp, Anna Hagen, Beth Junker, Brian Kell, Brian Kelley, Dan Lasko, Per Lindell, Christine Moore, Gautam Nayar, Greg O'Connor, "Easter Bunny" Dawn Orton, Ed Osawa, Steve Perry, Jamie Piret, Dave Robbins, Eric Scharin, Marc Shelikoff, Rahul Singhvi, Dave Stevenson, Thanassis Sambanis, Karen Troxel, Nick Valkanas, Bruce Woodson, Craig Zupke and many others for the good times and the lasting friendship we shared. The informative talks, valuable discussions and all the technical assistance are heartily appreciated, not forgetting the humor that you have injected into my life. We Chinese have a saying, "People coming from four seas all belong to a big family"; you have indeed made me realize the truth in the idiom. Special thanks to Dan Lasko, Brian Kell, and Bruce Woodson for their time and effort in installing and the maintenance of the computers, without which a lot of this thesis work will be impossible to accomplish. Brian and Per, aren't you glad that it's time to end our early-bird computer fight !

Gratitude is also extended to some of the Chinese students at MIT whose timely support had kept me going. To David Chang, Chi-Fang Chen, Rong-Juin Shyu, Chris Hwang, Chen-Chin Lee, Steve Lee, Frank Lin, Jin-Yuan Liu, Kai-Chee Loh, Shiping Wang, David Wu, Chu-Fu Wuu, Liangzhi Xie, Jinyou Zhang, and many others, thanks and all the best in your future endeavors.

I owe a debt of gratitude to my husband, Dean, for his unwavering love, endurance and support through these years. He has been a great partner and a source of encouragement and strength. Thank you also to my lovely daughter, Jeanne, for all the amazement and happiness she brings to us. It is hard (sweat and tears) but indeed wonderful to be a mother and graduate student at the same time.

Last but not the least, I would like to acknowledge the Ministry of Education, Taiwan, Republic of China for the fellowship support during my coursework. I also wish to acknowledge the National Science Foundation of the United States of America for financially supporting this research through the Engineering Research Center Initiative to the Biotechnology Process Engineering Center, M.I.T. under the cooperative agreement ECD-88-03014. The generous supply of glass fibers from PPG, Inc (Pittsburgh) is also greatly appreciated.

To my family

TABLE OF CONTENTS

Page

Title Page 1

Committee Page 2

Abstract 3

Acknowledgements 5

Table of Contents 9

List of Figures 14

List of Tables 19

I. Introduction, Background and Proposed Bioreactor Design 20

1. Systems for Cultivating Anchorage-Dependent Cells 22

2. Systems for Cultivating Anchorage-Independent Cells 24

3. Comparison between Oxygenation Methods 26

4. Thesis Objective and Specific Aims 28

5. Proposed Bioreactor 30

II. Literature Review 32

1. Cell Damage from Sparging and Agitation 32

    1.1 Effects of Sparging 32

    1.2 Effects of Agitation 33

2. High Cell Density Configurations 36

    2.1 Cell Retention Devices 36

    2.2 Hollow Fibers 38

    2.3 Ceramic Matrices 39

    2.4 Fluidized Macroporous Microcarriers 40

2.5 Fixed Beds 41

2.6 Gel Entrapment and Microencapsulation 42

3. Liquid Circulation Velocity in Concentric Airlift Reactors 43

4. Permeability of Fibrous Porous Media 47

5. Channeling in a Packed Bed 50

III. Theoretical Analysis 53

1. Liquid Flow Rate 53

2. Mass Transfer Coefficient 56

3. Oxygen Transfer Rate 57

4. Permeability of Fibrous Bed 59

4.1 Fibrous Bed without Cells 59

4.2 Fibrous Bed with Cells

- Model of Multilayer Cell Growth for Permeability 60

IV. Materials and Methods 65

1. Cell Line Used and Its Maintenance

1.1 γ-CHO 65

1.2 CRL-1606 67

2. Materials 69

2.1 Glass Fibers 69

2.2 Antifoam 69

2.3 Bioreactor 69

3. Experimental Methods 71

3.1 Treatment of the Glass Vessels Surfaces 71

3.2 Determination of Liquid Flow Rate 72

3.3 Determination of Mass Transfer Coefficient 72
3.4 Determination of Pressure Drop 73
3.5 Determination of Hydrodynamic Permeability of Fiber Bed 73
3.5.1 Comparison of Permeability between Different Fiber Packing 76
3.6 Cell Growth on 24 μm and 30 μm Glass Fibers 77
3.7 Effect of Antifoam on the Cell Growth and Productivity 78
3.7.1 For γ-CHO 78
3.7.2 For Hybridoma ATCC-CRL-1606 78
3.8 Operations and Technical Feasibility Studies 79
3.8.1 Cell Entrapment Kinetics 79
3.8.1.1 Single-Pass Process 79
3.8.1.2 Inoculation Studies 80
3.8.2 Model Systems 80
3.8.2.1 Anchorage-Dependent Cell Culture 80
3.8.2.2 Suspension Cell Culture 81
3.8.3 Operations 81
3.9 Effect of Cell Growth on Permeability and Residence Time Distribution 84
4. Analytical Methods 87
4.1 Cell Enumeration 87
4.2 Glucose and Lactate 88
4.3 γ-Interferon 88
4.4 Anti-Fibronectin Immunoglobulin G 89

V. Results and Discussion 90

Chapter 1. Biological Considerations 91

1.1 Small Diameters Glass Fibers As an Alternative Support for Anchorage-Dependent Cells 91

1.2 Study of Antifoam Effect 96

1.2.1 Antifoam Requirement 96

1.2.2 Antifoam Toxicity 98

1.2.2.1 Anchorage-dependent Cells 98

1.2.2.2 Suspension Cells 98

Chapter 2. A Hydrodynamic Model 107

2.1 Liquid Flow Rate 107

2.2 Mass Transfer Coefficient 109

2.3 Oxygen Transfer Rate 109

2.4 Effect of Permeability on Oxygen Transfer Rate 112

2.4.1 Permeability as a Function of Void Fraction, Fiber Diameter and Fiber Arrangement 116

2.4.2 Effect of Cell Growth on Permeability 123

Chapter 3. Operations and Technical Feasibility 136

3.1 Entrapment Kinetics 136

3.2 Cultivating Anchorage-Dependent Cells 140

3.3 Cultivating Suspension Cells 158

3.4 Effects of Channeling 176

3.4.1 Cell Distribution 178

3.4.2 Change in Channel Radius 184

3.4.3 Residence Time Distribution (RTD) 185

Chapter 4. Scaleup Potential 194

4.1 Reactor without Cells 195

4.2 Reactor with Cells 200

VI. Summary and Conclusions 209

VII. Recommendations for Future Research 214

1. Uniformity in Axial Cell Distribution for Suspension Cells 214

2. Devising Control Strategies Based on On-Line Measurements 215

3. Medium Formulation for High Cell Density 216

4. Cell Distribution on a Fiber Mat 218

5. Local Liquid Velocity within Fiber Bed 219

6. Determination of the Optimum Fiber Diameter and the Effect of Curvature on Cell Metabolism 219

7. Fiber Bed with Alternative Fiber Arrangement 220

8. Mechanisms for Protein Product Instability during Sparging 220

Nomenclature 222

Refererices 224

Appendix 242

LIST OF FIGURES

Page

I. Introduction

Figure I.1 Outline of the research 29

Figure I.2 Configuration of the proposed bioreactor (cross-sectional view) 31

II. Literature Review

Figure II.1 Non-dimensional permeability as a function of fiber volume fraction for various porous media 49

III. Theoretical Analysis

Figure III.1 Close-packing of spheres in two dimensions 63

IV. Materials and Methods

Figure IV.1 Configuration of the reactor 74

Figure IV.2 Experimental schematic for permeability and residence time distribution studies 75

Figure IV.3 Schematic diagram and associated equipment of the airlift fiber-bed bioreactor 82

V. Results and Discussions

Chapter 1

Figure 1.1 Cell growth on 24μm and 30μm glass fibers 93

Figure 1.2 Photographs of γ-CHO cells grown on 24 μm and 30 μm glass fibers 94

Figure 1.3 Cumulative glucose consumption and lactate production for CHO

cells growing on 24 μm and 30 μm glass fibers 95

Figure 1.4 Antifoam requirement at various gas flow rates 97

Figure 1.5 Antifoam effect on glucose uptake (CHO) 99

Figure 1.6 Antifoam effect on lactate production (CHO) 100

Figure 1.7 Antifoam effect on γ-interferon production (CHO) 101

Figure 1.8 Effect of antifoam on cell growth (CRL-1606) 102

Figure 1.9 Effect of antifoam on glucose uptake (CRL-1606) 104

Figure 1.10 Effect of antifoam on lactate production (CRL-1606) 105

Figure 1.11 Effect of antifoam on IgG production (CRL-1606) 106

Chapter 2

Figure 2.1 Liquid flow rate at various Di/Do ratios and air flow rates 108

Figure 2.2 Volumetric mass transfer coefficient at various Di/Do ratios and air flow rates 110

Figure 2.3 Effect of Di/Do on oxygen transfer rate at various air flow rates 111

Figure 2.4 Optimal Di/Do at various air flow rates 113

Figure 2.5 Effect of permeability on oxygen transfer rate 114

Figure 2.6 Effect of permeability on maximum oxygen transfer rate and optimal Di/Do ratio 115

Figure 2.7 Dimensionless permeability versus void fraction for various arrangements 118

Figure 2.8 Effect of void fraction on permeability at various fiber diameters -Case 1 (perp) 119

Figure 2.9 Effect of void fraction on permeability at various fiber diameters -Case 2 (para) 120

Figure 2.10 Effect of void fraction on permeability at various fiber diameters -Case 3 (alig) 121
Figure 2.11 Effect of void fraction on permeability at various fiber diameters -Case 4 (randorn) 122
Figure 2.12 The progression of cell growth on the glass fibers 125
(a) 1.2x10^7 cells/cm^3 of γ-CHO 126
(b) 5.6x10^7 cells/cm^3 of γ-CHO 127
(c) 6.1x10^7 cells/cm^3 of CRL-1606 129
Figure 2.13 Layer number versus cell density 130
Figure 2.14 Effect of cell density on channel radius 131
Figure 2.15 Effect of cell growth on permeability 132

Chapter 3

Figure 3.1 Single-pass entrapment of cells by the packed fiber bed 137
Figure 3.2 Kinetics of inoculum entrapment of suspension cells (CRL-1606) 139
Figure 3.3. Initial cell distribution 141
Figure 3.4 Gas flow rate and antifoam concentration during the cultivation process (CHO)..... 142
Figure 3.5 Cumulative glucose consumption, lactate production and γ-interferon production during the cultivation process (CHO) 144
Figure 3.6 Liquid flow rate in the fiber bed during cultivation (CHO) 146
Figure 3.7 Oxygen uptake rate during the cultivation process (CHO) 147
Figure 3.8 Normalized permeability and corresponding cell density in the fiber bed during cell cultivation (CHO) 149
Figure 3.9 Cell distribution within the fiber bed at the end of

cultivation process (CHO) 151
Figure 3.10 Normalized cell density versus cultivation time (CHO) 153
Figure 3.11 Dissolved oxygen concentration at the top and bottom of the reactor and glucose concentration in the spent medium during the cell cultivation (CHO) 154
Figure 3.12 Effect of specific perfusion rate on growth rate (CHO) 155
Figure 3.13 Gas flow rate and antifoam concentration during the cultivation process (CRL-1606) 159
Figure 3.14 Inlet gaseous oxygen composition during cultivation (CRL-1606) ... 160
Figure 3.15 Dilution rate during cell cultivation (CRL-1606) 161
Figure 3.16 Cumulative glucose consumption and lactate production during the cultivation process (CRl-1606) 163
Figure 3.17 Liquid flow rate during the cultivation process (CRL-1606) 164
Figure 3.18 Oxygen uptake rate during the cultivation process (CRL-1606) 165
Figure 3.19 IgG concentration and cumulative IgG production during the cultivation process (CRL-1606) 166
Figure 3.20 Photograph of fiber bed at the end of cultivation (CRL-1606) 168
Figure 3.21 Photographs of glass fibers before and after CRL-1606 cultivation ... 169
Figure 3.22 Cell distribution at termination of cultivation (CRL-1606) 170
Figure 3.23 Free cell concentration and corresponding viability during cultivation (CRL-1606) 172
Figure 3.24 Normalized cell density versus cultivation time (CRL-1606) 174
Figure 3.25 Effect of specific perfusion rate on growth rate (CRL-1606) 175
Figure 3.26 Cell distribution within fiber bed (CHO) 179
Figure 3.27 Radial cell distribution at the end of cultivation (CRL-1606) 181
Figure 3.28 Photograph of blockage of small channels 183

Figure 3.29 Residence time distribution in the fiber bed for CHO cells at different cell concentrations 186

Figure 3.30 Residence time distribution for Hybridoma ATCC-CRL-1606 at different cell concentrations 187

Figure 3.31 Shift in channel radius due to cell growth 190

Chapter 4

Figure 4.1 Oxygen transfer rate at various aspect ratios and reactor volumes 196

Figure 4.2a Maximal oxygen transfer rate versus reactor volume 198

Figure 4.2b Optimal Di/Do ratio versus reactor volume 199

Figure 4.3 Effect of aspect ratio on oxygen transfer at $1x10^7$ cells/cm^3 203

Figure 4.4 Effect of aspect ratio on oxygen transfer at $5x10^7$ cells/cm^3 204

Figure 4.5 Effect of aspect ratio on oxygen transfer at $1x10^8$ cells/cm^3 205

Appendix

Figure A.1 Effect of dissolved oxygen concentration on penetration depth 244

Figure A.2 Effect of dissolved oxygen concentration on number of layers penetrated 246

LIST OF TABLES

Page

IV. Materials and Methods

Table IV.1 Bioreactor dimensions 70

V. Results and Discussions

Chapter 2

Table 2.1 Comparison between theoretical and experimental values 124

Table 2.2. Estimation of cells within reactor through permeability studies 134

Chapter 3

Table 3.1 Summary of cell cultivation results (γ-CHO) 157

Table 3.2 Summary of cell cultivation results (CRL-1606) 177

Table 3.3 Data on residence time distribution studies 188

Chapter 4

Table 4.1 Parameters used in the scaleup calculation for reactors at various cell densities 202

Table 4.2 Optimal geometry and the maximal achievable oxygen transfer rate for 2.5-, 250-, and 1000-liter reactor at various cell densities 206

I. INTRODUCTION, BACKGROUND, AND PROPOSED BIOREACTOR DESIGN

Animal cell culture has attracted great interest because procaryotic cells are currently incapable of correctly accomplishing post-translational modifications of proteins, such as glycosylation, protein cleavage, disulfide bond formation, amidation, carboxylation, and phosphorylation. However, the correct glycosylation, conformation, and proteolytic processing of protein products have been shown to be essential to have maximal specific activity, be nonimmunogenic, and have appropriate blood clearance rates (Cumming 1991). Therefore, animal cells are important for the production of various diagnostic and therapeutic proteins such as monoclonal antibodies, interferons, blood factors, vaccines, and growth hormones.

The demand for those therapeutic and diagnostic protein products has motivated recent efforts to develop large scale systems of animal cell culture. The major barriers for the economics and technical feasibilities of scaleup (Glacken *et al*, 1983; Nilsson, 1987) have been the requirement of surface for anchorage-dependent cells, the sensitivity of animal cells to shear forces, and the high demand for oxygen.

In some instances, cell lines either will not grow in suspension, or have a significantly low productivity, or express proteins with altered properties when they grow in suspension (Spier and Clarke, 1980). Due to the dependence of a surface for attachment and subsequent growth of these cells, anchorage-dependent culture systems have been widely used. High surface-to-volume ratios of these systems are desired to achieve high

cell number per unit reactor volume and high volumetric productivity.

Animal cells are shear-sensitive because they lack protective cell walls and their sizes are relatively large (10 to 20 μm). Thus, anchorage-dependent cells are very susceptible to shear forces caused by agitation and aeration because they cannot reduce fluid forces and torques by rotation when attached to a support. Therefore, an important consideration in the reactor design for animal cell culture is the ability to operate in a reduced shear environment. Based on the studies of the shear effect on cell attachment and cell metabolism, it is generally assumed that shear stress from the environment has to be less than some critical shear stress, which happens to be the highest shear stress cells can tolerate, in order to obtain normal cell growth (Mohandas, 1976; Dewey *et al*, 1981; Sprague *et al*, 1987; Croughan *et al*., 1987). This critical shear stress will govern the reactor design and place constraints on the reactor operation.

Due to its low solubility in the medium (7 mg/l at air saturation), oxygen is usually a limiting nutrient in high density cell cultures. Unlike most other nutrients which can be added in large amounts at a time, oxygen has to be supplied continuously. It has been reported that the dissolved oxygen level has critical effects on cell metabolism (Green *et al*, 1958; Brosemer and Rutter, 1961; Danes *et al*, 1963; Kilburn and Webb, 1968; Taylor *et al*, 1978). Although the respiration rate of animal cells is lower than that of procaryotic cells, at high cell density sufficient oxygen must be supplied and this represents a problem when vigorous agitation and aeration are employed due to the shear sensitivity of animal cells. These problems have led to the design of various cell culture systems and oxygenation methods, and these are briefly described below.

1. Systems for Cultivating Anchorage-Dependent Cells

In order to meet the surface requirement for cell attachment and cell growth, a number of cultivating systems have been developed. These systems can be classified according to whether the cells grow on a two dimensional surface (surface propagation) or in a three dimensional matrix (volume propagation).

Surface propagators include plate systems, suspension systems and fixed bed systems. T-flasks, roller bottles, multiplate propagators, spiral film, and gyrogen (a bioreactor with multiple tubes) are examples of plate systems. Anchorage-dependent cells have traditionally been produced in stationary T-flasks or roller bottles. Plates, trays, spiral films and gyrogen have also been used to introduce additional surface area to the reactor. These relatively small units have the advantages of being reliable, simple, and easy to operate. In case of contamination, only one unit out of a batch would be lost. However, their low surface-to-volume ratios result in low attainable cell density (Glacken *et al*, 1983). In addition, scaleup of the production process can only be achieved by increasing the number of cultivation units. These factors render the process labor intensive, less controllable and high demands of space.

Microcarrier is a classical example of cultivating anchorage-dependent cells suspended in an agitated reactor system. This was first introduced by van Wezel (1967). This system provides the following advantages: high surface-to-volume ratio, capability of operating in stirred vessels, non-diffusion limited transport, achievable continuous/perfusion operation, scaleable and controllable system, and reusable microcarriers. However, microcarrier systems have some disadvantages. The cells on the microcarriers are exposed to fluctuating shear fields resulting from agitation and rising gas bubbles in sparged

systems (Croughan,1988); this limits the agitation speed and hence the oxygen transfer capacity (Hirtenstein and Clark, 1980). Collisions among microcarriers can result from high microcarrier loading and this increases susceptibility to cell damage. Finally, microcarriers may clump during expended culture times, leading to poor suspension and adversed environment to the cells.

Fixed beds, such as packed bed of spheres, are frequently used as surface propagation systems. There are several beneficial features of the fixed bed systems. Physical damage to cells caused by stirring can be avoided. Continuous perfusion can be achieved. The medium-to-cell ratio can easily be changed. Products can easily be separated from the cells. The most common support material in the packed bed bioreactors has been a matrix of 3 mm glass beads (Wohler et al, 1972; Spier and Whiteside, 1976; Burbidge, 1979; Whiteside and Spier, 1981). The main criticisms to these systems include the inability to monitor the cells directly and the potential nutrient and pressure gradients within the reactor.

The structural features of three-dimensional lattices, such as hollow fibers, ceramics, and porous collagen microcarriers, provide a high surface area and facilitate the supply of nutrients and removal of wastes (Jensen, 1981; Tharakan *et al*, 1988). Cells entrapped in these systems can be protected from shear stresses. Hollow fibers and ceramics are usually used as matrices or beds and porous collagen microcarriers such as Verax^{R} beads are operated in a fluidized bed system.

For matrices and packed beds, possible drawbacks are the low transport of nutrients, the presence of undesirable nutrient gradients due to the axial pressure gradient, inhomogeneous inoculation, and different microenvironments for cells. In addition, as with

packed beds, the cell growth in these configurations is usually monitored indirectly. However, Tharakan and Chau (1986 a) showed that nutrient cross flow diminishes the problems with pressure and nutrient gradients, and the transport is not limited by diffusion in this configuration. Additionally, the selective permeability property of ultrafiltration hollow fibers allows reduction in serum usage and preliminary product separation.

Porous microcarriers when employed in suspended state are controllable and scaleable, and provide a homogeneous external environment. In addition, the porous collagen provides a natural growth surface for cell growth. However, the mechanical property of porous microcarriers, diffusion-limited transport in the inner volume of the beads, and aggregation of beads over a long period of time are among the disadvantages of these systems.

2. Systems for Cultivating Anchorage-Independent Cells

There is a wide variety of bioreactors available for cultivating anchorage-independent cells. They can be classified into those in which cells are growing freely suspended, and those in which cells are entrapped or immobilized.

Freely suspended cell culture has been achieved in traditional stirred-tank reactors, and airlift fermentors. They are commonly operated at commercial scale (Birch *et al*, 1985; Backer *et al*, 1988). The advantages for these reactors include a homogeneous environment, ease of scaleup, low space utilization, convenience in monitoring and control, and ability to directly sample cells. However, there are concerns about cell damage resulting from high agitation rates (Dodge and Hu, 1986; Kunas and Papoutsakis, 1990) and vigorous sparging

(Handa *et al*, 1987 ab) in suspension culture systems. In addition, the typical final cell concentrations obtained in stirrer-tank reactors are only 2-5x10^6 cells/ml. In order to achieve higher cell concentrations and productivities, various cell retention devices have been designed and used in suspension culture systems. Spin filter is a common example for internal cell retention (Himmelfarb *et al*, 1969; Griffiths, 1988). However, it was found that depending on the mesh size and screen material, the clogging of the filter has been encountered during operation (Esclade *et al*, 1991). The ratio of screen surface area to reactor volume also restricts its scaleability. Cell separation by external centrifugation (Shimazaki *et al*, 1986), internal dialysis membrane (Comer *et al*, 1990), or gravity sedimentation (Takazawa *et al*, 1988; Batt *et al*, 1990) provides another alternative means for cell retention and further increase in the cell density.

Suspension cells can be immobilized through microencapsulation and physical entrapment. Microencapsulation through alginate or agarose polymers have been successfully used to entrap and culture suspension cells (Nilsson *et al*, 1983; Duff, 1985 Wohlpart *et al*, 1991). High cell densities were achieved within the capsules (over 1x10^8 cells/ml), but the logistical and technical complexities limit its scaleability. Examples for physical entrapment in matrices or beds are the use of hollow fibers (Belfort, 1989), ceramic, polyurethane foams (Murdin *et al* 1987 a; Lazar *et al* 1988) and glass beads (Ramirez and Mutharasan, 1989). Similar to anchorage-dependent cells, these matrices can protect cells from shear stress, but concentration gradients within the matrix and difficulty involved in monitoring cell density are the major drawbacks.

A useful candidate for a packed bed system would be supports which anchorage-dependent cells can grow externally on the support, or can physically entrap anchorage-independent cells within its porous structure. In these instances, the cells can be exposed to

convective nutrient flow. Packed beds of spheres have been used for such cell culture systems (Wohlers *et al*, 1972; Spier and Whiteside,1976; Burbidge, 1979; Whiteside and Spier, 1981; Ramirez and Mutharasan, 1989). However, in order to provide high surface area for anchorage-dependent cells, the bead diameter must be small. As the radius of the support becomes smaller, the cell anchorage becomes more difficult. For example, the threshold diameter of glass beads for cell growth was reported to be 50 μm (Maroudas, 1972). This problem can be overcome by the use of fibrous supports. Perry and Wang (1989) have successfully grown γ–CHO cells on 80 μm glass fibers. It has been speculated that since cytoskeletal elements can align along the fiber axis (Dunn and Heath, 1976; Fisher and Tickle, 1981), it may be possible to obtain better cell growth on equal radius fibers than on spheres. Moreover, Osawa has shown that the pressure drop through beds with equal external surface area favors the use of fibers over spheres (Osawa, 1992).

3. Comparison between Oxygenation Methods

Several oxygenation methods have been used (Pollard and Khosrovi, 1978; Spier and Griffiths, 1982; Nelson, 1988 b) for animal cell culture and these include surface aeration, membrane oxygenation, saturation of medium by an external device, electrolysis of water, addition of oxygen-bearing chemicals, and direct sparging (including airlift).

Surface aeration, which is accompanied by low shear, is only adequate for the oxygen requirement at small scale. As volume increases, the available surface area per unit volume decreases rapidly, and reduces the effectiveness of surface aeration in large-scale bioreactors. In such cases, oxygen transfer can be enhanced by increasing the oxygen content in the headspace, or raising the back pressure of the culture reactor (Mizrahi *et al*,

1972), as long as the problem of oxygen toxicity does not occur.

Membranes with high oxygen permeability and autoclavability such as silicon tubing are widely used for oxygenation in various scales of animal cell cultures (Miltenburger and David, 1980; Fleischaker and Sinskey, 1981). They provide efficient oxygen transfer without gas interfaces. For scaleup at constant power per unit volume in membrane oxygenation system, the loss of interfacial area per unit volume greatly affects the mass transfer rate achievable in the reactor. Aunins *et al* (1986) thoroughly investigated the scale up of *in situ* membrane-oxygenated reactors, and concluded that the most likely solutions are improvements related to the interfacial area and driving force for transfer.

Saturating the medium externally has the advantage that the oxygenation system and other harsh environmental conditions such as sparging and agitation can be carried out in a cell free chamber and thus does not interfere with cell growth. However, on a large scale, a very high medium flow rate or a high pressure will be required to maintain oxygen concentration, and these may be detrimental to cells.

Among the different proposed methods, sparging has been proven to be a simple, efficient, and scaleable method for aerating microbial cultures. Successful airlift reactor operation has been reported recently for a variety of animal, insect and plant cell lines (Katinger *et al*, 1979). It has not been used successfully in attached cell culture due to two factors. These are physical damage to cells on surfaces exposed to gas bubbles (Tramper *et al*, 1986; Handa 1987 ab), and degradation of medium components (Donaldson *et al*, 1980; Aunins *et al*, 1986). It can be a simple, scaleable, *in situ* method of providing aeration for anchorage dependent cells once these effects are overcome. A reactor configuration which

separates the cells from the bubbles can avoid exposing the cells to damaging sparging. This has been done previously in the form of "caged aeration" of microcarriers (Whiteside *et al*, 1985), and has recently been incorporated into commercial stirred tank reactors by New Brunswick Scientific (Celligen), and by Chemap (Chemcell). Sparged aeration has not been conducted in a fixed bed system.

4. Thesis Objective and Specific Aims

The overall objective of this thesis is to enhance the productivity of animal cell culture in both anchorage-dependent and anchorage-independent cell systems through a novel bioreactor design. In the proposed bioreactor, glass fibers are packed into a bed to immobilize animal cells within its structure. Oxygen transfer is achieved without detrimental effects to the cells from turbulence and gas interfaces.

The specific aims of this research are the following (as outlined in Figure I.1):

1. To examine unique problems associated with fiber glass in airlift bioreactors: fiber glass diameter and antifoam addition on cell growth and product formation.

2. To develop a rational and systematic method for reactor design.

3. To construct and characterize the proposed bioreactor with respect to transport phenomena.

4. To apply the results toward an optimal bioreactor geometry.

5. To investigate the performance of the reactor for cultivating anchorage-dependent cells and suspension cells, and experimentally verify the rationale of the bioreactor design.

6. To analyze the scaleup potential of the designed bioreactor.

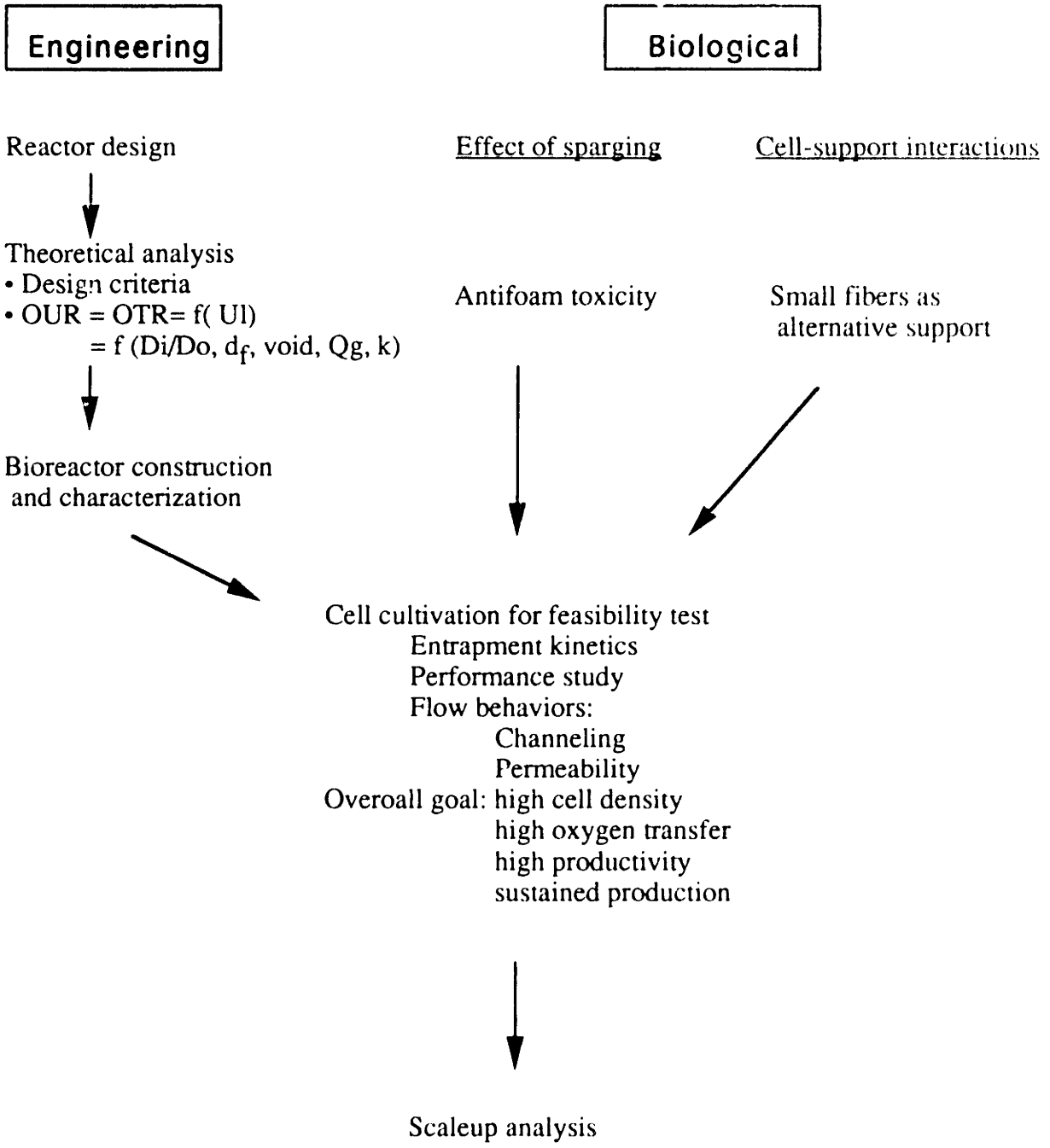

Figure I.1 Outline of the research

5. Proposed Bioreactor

A concentric cylinder airlift reactor, whose annulus is a packed bed of fibers, has been designed and investigated in this thesis. The configuration of the reactor is illustrated in Figure I.2. The sparging of air through the inner draft tube causes a liquid flow through the outer fiber bed which provides both oxygenation and convection for nutrient transport. The cells immobilized in the annular region do not come in contact with the bubbles, and thus avoids any detrimental effects from gas bubbles. The reactor design is simple and no mechanical agitation or external pump is required. This simple construction and the avoidance of moving parts prevent cell damage by local high-shear regions and also decreases the risk of contamination. Since the cells are immobilized, they can be easily separated from the product. Additionally, the reactor can be operated in a continuous/perfusion mode.

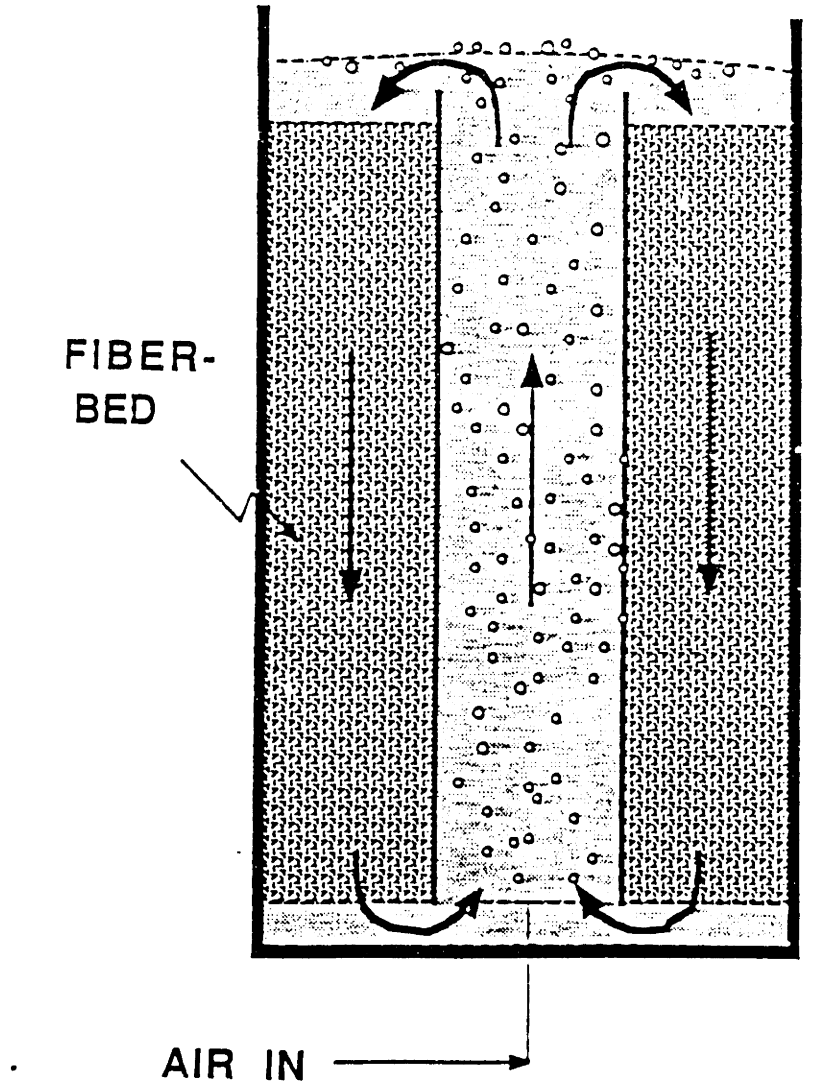

Figure I.2 Configuration of the proposed bioreactor (cross-sectional view). Arrows depict the flow of medium through the reactor.

1. Cell Damage from Sparging and Agitation

Traditionally, the cultivation of animal cells is primarily carried out with roller bottles, stirred tanks with suspension cells or microcarrier culture, and airlift reactors. These cultivating systems have been described in Section I. The scale-up of these systems for suspension cells has been relatively successful, and systems operating at 8000-10000 liters for stirred tank (Nelson, 1988 a) and 2000 liters for airlift reactors (Pullen *et al.*, 1985, Bliem *et al.*, 1991) are currently in commercial operation. For anchorage-dependent cells, microcarrier cultivation has also been scaled up and operated at scales of 1200-4000 liters (Montagnon *et al.*, 1984). However, it is perceived that cell damage by direct sparging and hydrodynamic effects resulting from agitation are potential problems using these technologies. These problems stem from the shear sensitivity of animal cells. Therefore, current trends in bioreactor design are concerned with elucidating the mechanisms of cell death by direct sparging and agitation to overcome these problems. The investigations on cell damage due to direct sparging and hydrodynamic effects resulting from agitation are reviewed below.

1.1. Effects of Sparging

Although being simple, efficient and scaleable for oxygenation, direct sparging results in interfacial contact between cells and gas bubbles and subsequent cell damage. Many researchers have studied the effects of physical forces on cell damage (van Wezel,

1982; Tramper *et al.*, 1987; Murhammer and Goochee, 1990). It appears that cell damage is associated with gas-liquid interfacial effects at the region of bubble disengagement and not with shear stresses occurring during bubble rise in the column or during bubble injection at the orifice (Katinger *et al.*, 1979; Handa *et al.*, 1987 a; Orton and Wang, 1990). Tramper *et al.* (1987) modeled cell death due to sparging based on a hypothetical killing volume, but this may be related to the liquid entrainment volume as a bubble bursts (Orton and Wang, 1990).

It is therefore suggested that a combination of altered medium formulations and altered sparger and bioreactor design should be considered to minimize bubble breakup at the free surface. Examples of preventing such damage include decreasing the culture surface to culture volume ratio, sparging with very small (micron-sized) bubbles, adding surface active agents such as Pluronic F-68 (Emery et al, 1987; Handa et al, 1987 b; Murhammer and Goochee, 1990) or high serum and protein concentrations which can result in more stable foams at the culture surface (Handa-Corrigan, 1990), or adding an oil layer on the top of the fluid to eliminate the bubble bursting zone (Wudtke, 1988). Alternative reactor configurations including Caged aeration, Celligen, Chemcell and an integrated module bioreactor (Reiter *et al.*, 1991) which separate the cells from sparging regions are also effectively employed.

1.2. Effects of Agitation

Suspension and microcarrier cultures are commonly agitated in order to increase oxygen transfer and provide a homogeneous environment for cell growth. However, due to the shear sensitivity of animal cells, cell death and detachment from microcarriers are

often observed in conjunction with vigorous agitation (Dodge and Hu, 1986; Backer *et al.*, 1988; Cherry and Papoutsakis, 1990). Therefore, understanding the bioreactor hydrodynamics and the mechanisms of cell injury in agitated bioreactors is essential for reactor engineering and design.

Significant progress towards elucidating the hydrodynamic effects on animal cells in microcarrier bioreactors has been made (Croughan and Wang, 1991; Papoutsakis, 1991). For dilute microcarrier cultures under high agitation, cell damage primarily results from forces generated by the interaction of the microcarrier with small turbulent eddies (Croughan and Wang, 1989). Only under rare circumstances does cell damage result from time-average flow fields. For concentrated cultures under high agitation, cell death might also occur through hydrodynamic interactions between microcarriers (Papoutsakis, 1991).

Cell death in microcarrier culture is dependent on eddy size, where eddies smaller than the microcarriers cause the greatest damage. The size of the smallest eddies is in the viscous dissipation regime and depends on the Kolmogorov length scale. This length scale increases with the kinematic viscosity and decreases with power input. Larger eddies do not generally cause damage as they entrain the entire microcarrier so that it is not subject to large velocity gradient. Additionally, if the time-averaged velocity components vary considerably over a small length scale, strong hydrodynamic forces could result and cells could be killed. Although it is mentioned earlier that cell damage is rarely a result of time-averaged flow fields, these may be important when there is a jet region off the impeller or when there is a close clearance between the impeller and the vessel wall. In microcarrier cultures, two neighboring microcarriers might collide with each other due to the action of turbulent eddies and this interaction causes cell damage.

Based on the understanding of the cell damage mechanisms, reactor design can be altered so as to reduce shear stress without compromising fluid mixing. Factors important in the design include liquid-height-to-vessel-diameter ratio, bottom shape, clearance between the impeller and vessel, and impeller shape and size. The other potential method to reduce hydrodynamic death from turbulence is the use of viscoelastic polymers (Quraishi *et al.*, 1977; Croughan and Wang, 1991). The polymers should have a characteristic relaxation time equivalent to the burst duration for the smallest eddies so that they do not strongly interfere with mass transfer.

For suspension cells, it is expected that cell damage in agitated bioreactors occurs at high agitation rates where the Kolmogorov eddy length begins to approach the size of a single cell. However, it has been reported that cell damage starts at agitation rates of 150-350 rpm (Kunas and Papoutsakis, 1989; Backer *et al.*, 1988; Murhammer and Goochee, 1988; Dodge and Hu, 1986). As discussed by Papoutsakis (1991), the Kolmogorov-eddy size under these conditions can be calculated to be at least 6-10 times higher than the typical sizes of animal cells. Therefore, for suspension cells, damage is unlikely to result from cell-to-cell, or cell-to-solid-surface interactions. Papoutsakis (1991) concluded that suspension cell damage in agitated bioreactors usually results from air entrainment with subsequent bubble breakup or fast-draining liquid films around rearranging gas-liquid interfaces. Qualitatively, the mechanisms for cell damage of suspension cells resulting from agitation are similar to those resulting from air sparging. Therefore, modified reactor design which can eliminate bubble entrainment should minimize cell damage even at high agitation rates for suspension cell culture.

2. High Cell Density Configurations

One major concern has been the relatively low cell concentrations attainable in traditional cell cultivating systems. As a result, the typical cell densities of less than $1x10^7$ cells/ml are usually obtained. In order to reduce the bioreactor size for large facilities, high cell concentration systems are favored. Moreover, high cell concentration reactors operating in a perfusion mode can lead to high unit productivity. Thus, much effort has been directed towards the development of high cell density processes (*e.g.* > $5x10^7$ cells/ml).

High cell density culture are commonly operated in a perfusion mode. In perfusion, cells are immobilized or physically retained by some mechanical means, so that continuous medium feed and spent medium removal are achieved without any decrease of the cell density. Perfusion systems require the separation of medium and cells to avoid cell wash-out. Anchorage-dependent cells, attached to a substrate, are naturally amenable to perfusion operation. Suspension cells are more difficult to immobilize, and many systems based on immurement (*e.g.* hollow fibers, gel encapsulation, and membranes) and entrapment (*e.g.* textured ceramic surfaces, porous beads, and sponges) have been devised (Griffiths, 1988).

The high cell density configurations include reactors employing cell retention devices, hollow fibers, ceramic matrices, macroporous microcarriers, fixed beds, and gel entrapment or microencapsulation. A detailed comparison is reviewed below.

2.1. Cell Retention Devices

One commonly used cell retention device is the spin-filter system. First introduced by Himmelfarb et al. (1969), various configurations of this system have been developed. For the interested reader, these are reviewed by Griffiths (1988). Usually, the spin filter consists of a cylindrical wire cage attached to the rotating impeller shaft. Under certain operating conditions, cell concentration outside the wire cage is lower than that inside the cage. Due to cell retention, cell densities of $1\text{-}5 \times 10^7$ cells/ml can be achieved. Oxygenation for the spin-filter systems is usually achieved by silicone tubing, direct sparging or using perfluorocarbon as an oxygen carrier (Tokashiki, 1991). In order to demonstrate its capacity in cultivating anchorage-dependent cells, the spin filter system has also been effectively used for aggregates or microcarrier culture (Avgerinos *et al.*, 1990). The mechanism for retention of aggregates or microcarrier culture is understood to be centrifugation, although the mechanism for suspension cell retention is not yet fully understood. Once the optimal operating conditions are defined, the spin-filter system could be a very effective means for large scale cell cultivation (Hu and Peshwa, 1991).

Filtration systems have also been commonly used to increase suspension cell concentrations (Shiloach *et al.*, 1986 ; Brennan *et al.*, 1987; Jager *et al.*, 1989; Maiorella *et al.*, 1991). The filtration process can take place externally or internally. In external filtration, cells and spent medium containing product are continuously pumped through an external loop to a fiber cartridge and the cells are returned to the reactor. In internal filtration, medium perfuses through the fibers located in the reactor. The external filtration method has the advantage of continuous harvest of the product and increasing cell density due to cell recycle. However, continuous pumping may impart mechanical stresses on the cells and decrease the cell viability, especially at high pumping rate. The loss of environmental control in the tubing when cells are circulating in the loop may be another potential problem. As for internal filtration systems, Comer *et al.*, (1990) used membrane

filters immersed in the culture fluid within the vessel for the cultivation of hybridoma cells. This not only obviates the need for external pumping but also simplifies the sterilization procedures during start-up operations. However, membrane fouling due to protein deposition and eventual membrane clogging still remain problematic (Hu and Peshwa, 1991).

Additional methods which have been used for cell retention include sedimentation by gravity in specially designed sedimenters (Tokashiki and Arai, 1989; Batt *et al.*, 1990), and external centrifugation (Shimazaki *et al.*, 1986; Tokashiki *et al.*, 1990).

2.2. Hollow Fibers

Knazek *et al.*, (1972) first recognized the potential of using hollow fiber devices for high-density animal cell culture. The objective of the system is to immobilize suspension cells or anchorage-dependent cells in a fixed-volume compartment. Medium is then perfused through the filter material, which also retains the cells at densities exceeding 10^8 cells/ml (Heifetz *et al.*, 1989; Gammon *et al.*, 1990). This cylindrical cartridge with bundles of thin ultrafiltration fibers provides a large surface area for perfusion of nutrients into the extracapillary space. Since diffusion is the main mode of nutrient transport, these systems suffer from problems with increased pressure drop and concentration gradients along the length of the cartridge (reviewed by Tharakan *et al.*, 1988; Tharakan and Chau, 1986 a). Hence, the scaleup of the system is limited. However, various modifications such as cross flow convection of nutrients (Ku *et al.*, 1981), flat bed systems to reduce the nutrient path length (Ku *et al.*, 1981), radial convective flow (Tharakan and Chau, 1986 a), and the Acusyst system (Tyo, *et al.*, 1988) have been developed to overcome this limitation. The

Acusyst uses cyclical pressure pulses to circulate the medium alternatively into and out of the capillary fibers and is currently a very successful technique for hollow fiber reactors. Ultrafiltration-type fibers are commonly used since the product can also be retained depending on the molecular weight cutoff of the fibers. In this way partial product concentration is affected. However, filtration-type fibers cause less problems with blockage and gradients since a higher flux rate is permitted (Brown *et al.*, 1985). Scholz and Hu (1990) used mixtures of fiber types to achieve separation of product molecules from spent feed or waste metabolites.

Although hollow fibers provide high surface-to-volume ratio, its application to anchorage-dependent cell culture has been limited mainly because the original hollow fibers, which are made of cellulose acetate, are not appropriate for cell attachment. Nevertheless, studies using polypropylene fibers (Ku *et al.*, 1981) or coating the fibers with poly-D-lysine (Tharakan and Chau, 1986 b; Tyo *et al.*, 1988) have shown that the attachment efficiency for these cells can be enhanced. Modifications of this type of technology such as the In Vitron static maintenance reactor (Tolbert *et al.*, 1985) and the membroferm (Scheirer, 1988) have been used for the commercial production of animal cell-derived products.

2.3. Ceramic Matrices

The ceramic system is a cylinder of porous ceramic monolith with square channels crossing through the cylinder. Cells inoculated into the channels either adhere to the surface or are entrapped in the pores of the monolith (Lydersen, 1987). Cell immobilization protects cells from hydrodynamic forces and facilitates separation of the

medium from the cells. Medium is passed through the channels to provide nutrients and to remove the metabolites. The ceramic matrices are low-cost, inert, and suitable for cultivating both anchorage-dependent and suspension cells. A small scale ceramic matrix bed bioreactor was reported by Marcipar *et al.*, (1983) for the entrapment of hybridomas. A commercial form of the ceramic matrix for cell cultivation, known as Opticell bioreactor, is currently available (Lydersen *et al.*, 1985 ab; Berg and Bodeker, 1988). Recently, the cell growth and oxygen transport processes in such ceramic matrices bioreactor have been characterized (Applegate, 1991).

2.4. Fluidized Macroporous Microcarriers

The macroporous microcarrier fluidized-bed culture operating at a continuous mode has been developed to produce pharmaceutical proteins from animal cells (Hayman *et al.*, 1987; Runstadler and Cernek, 1988; Nilsson *et al*, 1991; Vournakis and Runstadler, 1991). These cells have been cultivated in a fluidized bed configuration by immobilizing them inside weighted, porous macroporous microcarriers. The efficient oxygen supply and carbon dioxide removal are achieved by the efficient mass transfer characteristics of the fluidized bed and of the gas exchanger in a recycle loop. The fluid velocities in the bioreactor are sufficient to suspend the cell-containing macroporous microcarriers in the culture fluid, and yet do not render damage to the fragile animal cells. The macroporous microcarriers have the advantages of immobilizing cells in a tissue-like three dimensional structure. Other advantageous properties include achievable high cell density (greater than 10^8 cells/ml of bead volume), potential scaleability, operable for both attached and suspension cells, suitable for long-term continuous processes, and efficient nutrient transport into the microcarrier (Nilsson *et al.*, 1986). The materials used for porous

microcarriers have been collagen (Hayman *et al.*, 1987; Vournakis and Runstadler, 1991; Ray *et al.*,1991), gelatin (Reiter *et al.*, 1990; Nilsson *et al.*, 1991), porous glass (Looby and Griffiths,1988; Griffiths, 1990) or mixtures of appropriate polymers (Spier, 1991). These macroporous microcarriers can be specially tailored to various specifications. For example, the collagen beads can be made into sizes ranging from 100 to 1000 μm and pore openings ranging from 5 to 100 μm. The specific gravity can be varied from 1.05 to 3.0 by changing the number, size, and composition of the weighting particles.

2.5. Fixed Beds

Various packing materials such as glass spheres, cellophane, glass helices, glass rings, glass tubing, glass rods, polystyrene spirals, plastic films, and stainless steel springs can provide a supporting substratum for animal cell cultures (Griffith,1990). The reason that they have not been widely used for commercial production processes is mainly the intrinsic problems with nutrient and pressure gradients and low unit productivity, and the limited value for suspension cells (Griffiths and Looby,1991) Porous packing materials have drawn great attention due to the higher surface-to-volume ratio (consequently, higher cell concentration), three-dimensional structure, working equally well for suspension and anchorage-dependent cells, and efficient nutrient transport. However, due to their mechanical properties, not all the macroporous microcarriers are suitable for fixed bed operation. Successful examples for cell culture include the utilization of polyurethane foam (Murdin *et al.*, 1987 a b; Lazar, 1988), ceramic beads (Stephanopoulos *et al.*, 1989), and porous glass (Looby and Griffiths,1988; Griffiths, 1990).

2.6. Gel Entrapment and Microencapsulation

Gel entrapment is another potential technique to achieve high cell density culture. Because of their mild gelation reaction and biocompatibility, calcium alginate and agarose have been popularly used and well-described for immobilizing of animal cells (Nilsson *et al.*, 1983; Duff, 1985; Wohlpart *et al.*, 1991). However, gel particles can be easily damaged by mechanical stress, and, in some cases, the use of stirred tank and packed-bed reactors are not practical. An expanded bed configuration was adopted for continuous production of monoclonal antibody (Shirai *et al.*, 1987). Without destruction of gel particles, a fluidized bed reactor with stable long term cell cultivation was achieved by coating alginate gel with urethane polymer (Iijima *et al.*, 1988; Yoshida *et al.*, 1989).

Microcapsules can act as microculture vessels and allow high cell densities to be achieved inside the capsule (Lim, 1988). The enclosing membrane which encapsulates cells is semipermeable to allow the transfer of nutrients and metabolites. Using an appropriate pore size cutoff, contaminating immunoglobulins or viruses can be excluded, and desired products can accumulate inside the capsule. Thus, downstream processing can be simplified. Alginate-polyamino acid pair has been proved to be able to form the required permeable membrane (Lim, 1988). Controlled membrane molecular weight cutoff of the alginate-poly-L-lysine microcapsule system has been demonstrated by varying viscosity average molecular weight of the alginate-poly-L-lysine (King *et al.*, 1987).

Most of the high cell density configurations discussed above provide a heterogeneous environment, and the possible existence of nutrients and/or metabolite gradients may result in uneven distribution of cell viability, metabolic activity and growth rate in the reactors. To achieve better reactor performance, these have to be eliminated

using proper bioreactor design, process optimization, and better monitoring and control of the reactors.

3. Liquid Circulation Velocity in Concentric Airlift Reactors

Since bubble columns and airlift loop reactors do not require mechanical agitation, and their oxygen transfer and mixing can be achieved by air sparging with a minimal energy input, various modifications of these reactors are commonly used for aerobic fermentations. Due to the random motion of flow in the bubble columns, sieve tray, packings, or multishaft are commonly installed to redisperse the gas and to prevent unstable flow conditions (Weiland and Onken, 1981). In contrast, airlift loop reactors have a stable and directed well defined circulation flow. The flow behavior is distinct due to predictive circulation and, in some cases, geometric similarity of the flow cross-sections in the up-and down-flow portions of the reactor. Basically, airlift loop reactors can be classified into internal and external loops. The liquid circulations in both bubble columns (Schugerl *et al.*, 1977; Shah, *et al.*, 1982) and airlift reactors (Blenke, 1979; Blenke, 1985· Chisti and Moo-Young, 1987; Joshi, *et al.*, 1990) have been reviewed. Due to its geometric similarity to our reactor design, only the one in the concentric draft tube internal loop reactor is considered in this section.

Lamont (1958) is one of the earliest researchers who studied the concentric airlift reactors. He predicted the liquid circulation rates in puchuca tanks using airlift pump theory. In his semi-empirical model, the energy transferred as the air expands in rising through the vessel is corrected for energy dissipation due to bubble "slip" and the remainder gives rise to velocity heads associated with liquid flow in the vessel.

De Nevers (1968) showed that the mechanism for bubble driven fluid circulations is quite similar to the mechanism of natural convection but with much larger driving forces. Bubble driven fluid circulations are caused by the density difference between regions richer and poorer in bubbles. These circulations are stable in baffled bubble columns and concentric draft tube airlift reactors, but are chaotic in unbaffled bubble columns.

Based on minimum entropy generation and a momentum balance, Rietema and Ottengraf (1970) presented a theoretical model to predict the diameter of the "bubble street" and laminar liquid circulation velocities in a gas sparged column filled with glycerol. Freedman and Davidson (1969) also modeled the liquid circulation in a concentric airlift reactors based on an energy balance and measured gas holdup at low gas velocities.

Later on, many other researchers employed similar approaches based on momentum balances with empirical gas holdup and two-phase pressure drop correlations to predict the liquid circulation velocities in airlift reactors (Chakravarty,*et al.*, 1974; Kubota, *et al.*, 1978; Blenke, 1979; Hsu and Dudukovic, 1980; Bello, 1981; Merchuk and Stein, 1981; Weiland and Onken, 1981; Koide, *et al.*, 1984; Jones, 1985; Miyahara *et al.*, 1986; Verlaan *et al.*, 1986 b; Chisti and Moo-Young, 1988; Koide, *et al.*, 1988). The principle is that at steady state, the driving force for circulation resulting from the hydrostatic pressure difference (due to gas holdup differences between the riser and the downcomer) is balanced by the total pressure drop in the circulation path due to friction, valves, bends, flow area changes and internals. Most theories have been reviewed by Blenke (1979), Rietema (1982), and Chisti and Moo-Young (1987).

It has been found that liquid circulation in airlift systems is determined by the

superficial gas velocity (Onken and Weiland, 1983; Bello, *et al.*, 1984; Merchuk, 1986) and the relationship can be shown to be in the following form:

$$U_l = \alpha U_{sg}^{\beta} \tag{II.1}$$

where α is a function of reactor geometry and of the properties of the liquid, and β depends on the flow regime as well as reactor geometry (Onken and Weiland, 1983). Merchuk (1986) and Onken and Weiland (1980) found the exponent β in EquationII.1) to be approximately 0.4 for water or water-like solutions in different external loop reactors. Bello *et al.* (1984) investigated water and salt solution in several external and concentric internal loop reactors and showed that β was 1/3 and α depended on the reactor type and geometry as follows:

$$\alpha = \varphi \left(\frac{A_d}{A_r}\right)^m \tag{II.2}$$

where α was 1.55 and 0.66 for the external and internal loop reactors respectively, m had the respective values of 0.74 ± 0.04 and 0.78 ±0.08, and A_d/A_r is the cross-sectional area ratio of the downcomer to the riser.

Bello *et al.* (1984) also conducted further investigations in non-Newtonian CMC solutions and found decreasing liquid circulation with fluid viscosity according to the equation given below:

$$U_l = \alpha U_{sg}^{0.322} \left(\frac{A_d}{A_r}\right)^{0.794} \mu_{app}^{-0.395} \tag{II.3}$$

(ms^{-1}) (ms^{-1}) (Pas)

where α is 0.052 and 0.0204 for bubble- and slug-flow regimes respectively. Other researchers (Chakravarty,*et al.*, 1974; Weiland, 1984; Jones, 1985) have observed that increasing liquid viscosity leads to a decrease in liquid circulation rates.

Fields and co-workers (1984) found that liquid circulation in solutions containing small amounts of a drag reducing polymer such as xantham gum was greater than that in water. They also found that increased viscosity at higher polymer concentration decreased the liquid circulation even in these fluids. Verlaan and coworkers (1986 a) reported that the increase in the loading of relatively large solids (particle diameter = 2.7 mm) dispersed in water in an external loop device would reduce liquid circulation. Chisti and Moo-Young (1987) observed similar results for mycelia-like solids in external and internal loop reactors.

The liquid circulation velocity in the concentric airlift reactors was found to be strongly dependent on the area ratio of the downcomer to the riser (A_d/A_r). A variety of optimum ratio of draft tube diameter to reactor diameter for maximum liquid circulation rates has been reported in the literature. Largest liquid circulation rates were obtained when the ratio of draft tube diameter to reactor diameter was 0.59 (Weiland, 1984; Koide *et al.*, 1984), approximately 0.5 (Jones,1985), or 0.64 (Blenke, 1985) in various cases. Rousseau and Bu'lock (1980) found a minimal mixing time when the ratio of draft tube diameter to the reactor diameter is between 0.6 and 1.0, and they suggested equal riser and downcomer cross-sectional areas (*i.e.* the ratio of draft tube diameter to reactor diameter is $1 : \sqrt{2}$) to achieve highest liquid circulation rate.

In addition, since liquid circulation is very sensitive to the gas holdup difference between the riser and the downcomer of an airlift vessel, incorporation of high efficiency

gas-liquid separators (Siegel, *et al.*, 1986) or a gas deflector (Blenke, 1985) in the headspace would enhance circulation in airlift reactors.

4. Permeability of Fibrous Porous Media

Although most of the porous media are granular, some of them are composed of very long particles and can be described as fibrous. A significant characteristic of fibrous porous media is that the fraction of solid material is often much lower than that for a granular material. For a fibrous media, the solid volume fraction can be as low as 0.01 to form a structure; however, for granular media, the grains generally occupy about 60% to 70% of the total volume because they are inherently compact (Jackson and James, 1986).

Hydrodynamic permeability is the property of porous media which characterizes the ease of a fluid to flow through the media resulting from an applied pressure gradient. In other words, permeability is the fluid conductivity of the porous media (Collins,1961; Greenkorn, 1983). Darcy (1856) first demonstrated that a parameter characterizing the fluid conductivity of a porous material can be meaningfully defined. The equation which is called Darcy's law defines permeability in terms of measurable quantities:

$$k = \frac{\mu \frac{Q}{A}}{\left|\frac{\Delta P}{L}\right|} \qquad \text{(II.5)}$$

where Q is the volumetric flow rate through a cross-section of area A, μ is the fluid viscosity, and ΔP is the pressure drop over a length L. This widely used equation is valid for Newtonian fluids at low flow rates, that is, at low Reynolds numbers where fluid inertial effects are negligible.

From the definition of Equation II.5, it is observed that k, the permeability, has the dimension of length squared. k is roughly a measure of the mean square of the pore diameter in the material (Bejan, 1984). Since the square root of the hydrodynamic permeability is a characteristic length scale of channel diameter, if the channel diameter changes by a factor of x, the permeability will change by a factor of x^2 (Chen, 1991).

Fibrous media have been studied less extensively because they are not as common as granular materials. However, a few comparisons on the basis of hydrodynamic permeability have been made. Jackson and James (1986) performed a thorough review of experiments and theories related to low-Reynolds-number flow through fibrous porous media. Since the permeability of a fibrous medium depends on the size, concentration and arrangement of fibers, parameters such as the radius, r, and the volume fraction of solid material, ϕ, have to be selected to characterize fiber size and concentration respectively. The permeability is then a function of r, ϕ, and fiber arrangement. In non-dimensional terms, the relation is:

$$k/r^2 = f(\phi) \qquad \text{(II.6)}$$

for a particular fiber arrangement.

In Jackson and James' review (1986), experimental data of a wide variety of fibrous media from polymer chains to fiberglass were found. Most of the data are plotted in Figure II.1. The graph shows that permeability data for diverse fibrous materials correlate reasonably well when the coordinates k/r^2 and ϕ are used. The scatter is caused by

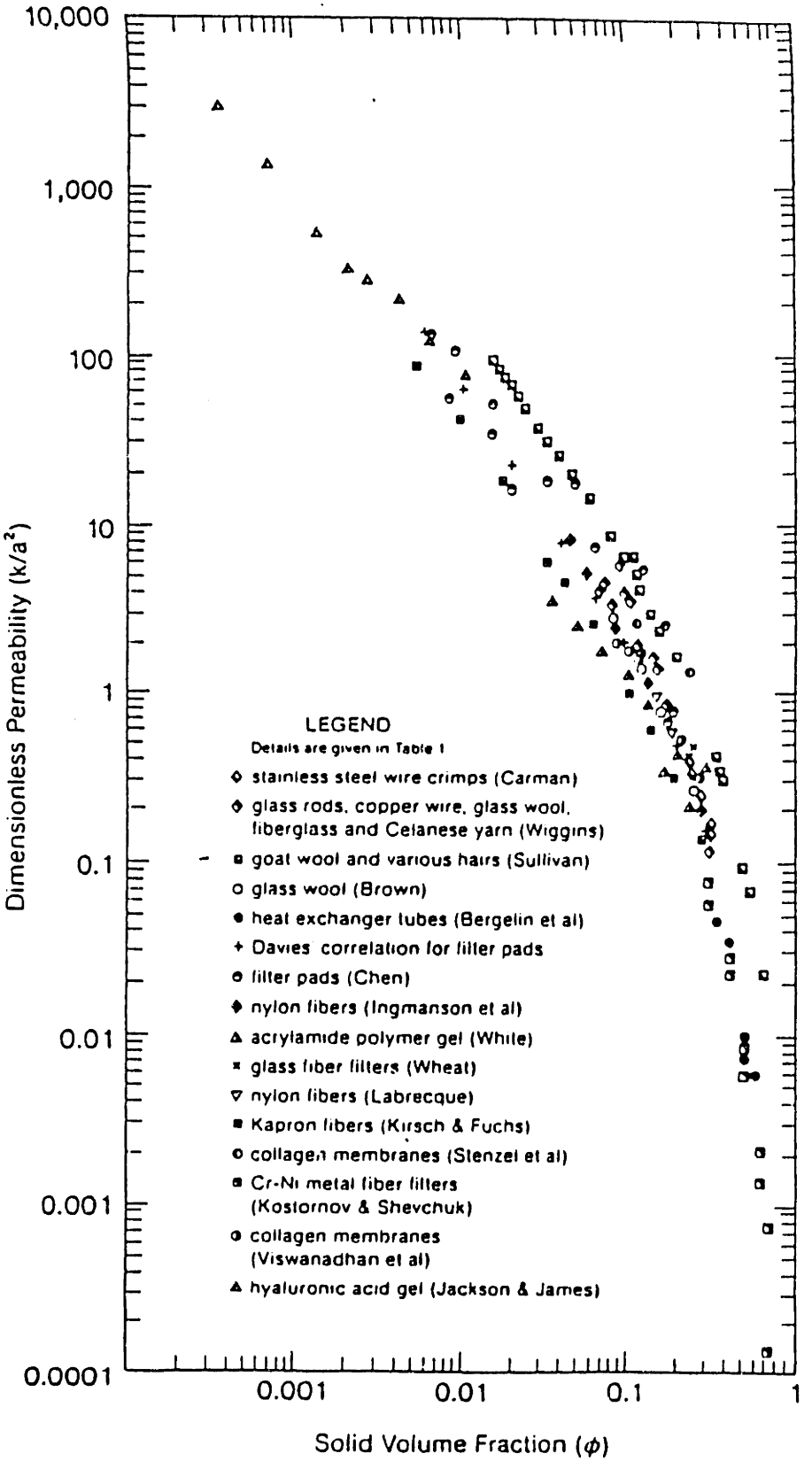

Figure II.1 Non-dimensional permeability as a function of fiber volume fraction for various porous media (from Jackson and James, 1986).

inhomogeneity and by variations in fiber shape and arrangement. Even with the scatter, the graph is useful for an order of magnitude estimate of flow resistance when fiber size and volume fraction of a porous material are known.

As for theoretical predictions, the general approach taken by theoreticians has been to idealize the porous medium as a matrix of rods and then to solve Stokes equation, or a similar equation, for a particular configuration. Based on the structure of the matrix and on the flow direction, the theories can be divided into three groups: (1) flow parallel to an array of parallel rods, (2) flow normal to an array of parallel rods, and (3) flow through three dimensional arrays. Accurate solutions of the Stokes equation for regular arrays of parallel rods, either aligned with the flow or normal to the flow, have been reported widely in the literature (Langmuir, 1942; Happel, 1959; Sparrow and Loeffler, 1959; Kuwabara, 1959; Hasimoto, 1959; Spielman and Goren,1968; Yu and Soong,1975; Sangani and Acrivos, 1982; Drummond and Tahir, 1984). For irregular arrays and three-dimensional media, some flow models are available to calculate approximate permeabilities (Spielman and Goren,1968; Jackson and James, 1982, and 1986). Jackson and James (1986) analyzed the experimental data and theories and found that the data agree reasonably well with the predictions by the models.

5. Channeling in a Packed Bed

Channeling causes inhomogeneity of the liquid velocity in porous material. The inhomogeneity is likely to affect processes occurring in packed bed columns. Very often, it should be considered in the design of such equipments.

Few studies were performed on the flow patterns in a fibrous packed bed. However, flow patterns in granular bed structure have been the subject of many investigations (Morales *et al.*, 1951; Schwartz and Smith, 1953; Bayer, 1960; Huyten *et al.*, 1960; Lipmaa and Luiga, 1966; Aerov *et al.*, 1979; Klawiter *et al.* 1982; Kaminsky *et al.* 1982; LaVan and Vermeulen, 1984; Volkov *et al.* 1986 a,b). When these packed beds are analyzed, plug flow through the bed and constant void fraction, ε, over the bed cross-section are usually assumed. The existence of a non-uniform, parabolic velocity profile in the bed cross-section was, however, discovered, with a maximal rate near the wall (Bayer, 1960; Huyten *et al.*, 1960) and near the axis (Lipmaa and Luiga, 1966; Hupe *et al.* 1969; Volkov *et al.* 1972) of the column.

The "wall effect " is a major source of the channeling (Arthur *et al.*,1950; Schwartz and Smith, 1953; Stanek and Szekely, 1972). Some researchers have found areas with accelerated gas flow rates at a distance of half to one particle diameter from the wall (Morales *et al.*, 1951; Schwartz and Smith, 1953; Aerov *et al.*, 1979), and others have reported that this area was much wider (Abaev *et al.*, 1981; Struminsky and Pavilikhina, 1981). LaVan and Vermeulen (1984) analyzed channeling combined with radial and axial dispersion in a fixed-bed adsorber both theoretically and experimentally, and they found that this low hydraulic resistance near the wall can be reduced by choosing a high ratio of bed diameter to particle diameter. Using Doppler laser anemometry, Volkov and co-workers (1986 a,b) studied the velocity field at the bed outlet for various parameters in order to find a relation between the non-uniformity of bed packing and the bed parameters. They also found that increasing the column diameter generally reduces the non-uniformity in large-scale velocity field, although this dependence is unclear.

The method of packing a bed can induce channeling by particle size segregation

(Volkov *et al.*, 1986 a,b). Precautions were taken by LaVan and Vermeulen (1984) to disperse the particles uniformly over the cross sections of the beds and to settle them gradually to prevent particle size segregation.

Particle size and shape can also be a major source of channeling. Significant deviations from the axial dispersion coefficient for small particles at low Reynolds number were measured by Edwards and Richardson (1968). Perkins and Johnston (1963) found that packings of small particles became increasingly non-uniform as the particle diameter decreased to below 1 mm. They also noted that substantially non-spherical particles lead to greater dispersion than packings of equal size spheres. LaVan and Vermeulen (1984) obtained results consistent with these observations. Furthermore, Volkov and co-workers (1986 a) found that wider particle size distribution leads to both larger aggregate sizes and larger velocity variations.

The velocity field measured at the packed bed outlet makes it possible to characterize the local velocity variations quantitatively. By measuring the velocity field at the bed outlet, the granular bed structure and the flow through the bed can be investigated indirectly. Based on this reasoning, Volkov and co-workers (1979) employed Doppler laser anemometry and found that the velocity varied widely from point to point in the cross-section of the apparatus. Similar results were later obtained by thermal anemometry (Struminsky and Pavilikhina, 1981). Liquid velocity profiles have also been investigated by Klawiter *et al.* (1982) and Kaminsky *et al.* (1982).

The above description pertains mainly to studies in granular packed bed, and minimal attention has been paid to beds packed with fibrous materials. It is hoped that this thesis work will shed some light on channeling effects in fibrous packed bed.

III. THEORETICAL ANALYSIS

In order to provide cells with an optimal environment and especially to avoid oxygen depletion, sufficient circulation of the oxygenated medium is necessary. Both medium circulation and oxygenation are dependent on the air sparging. Therefore, liquid flow rate and mass transfer coefficient are determined individually as a function of air flow rate. Oxygen transfer rate is then estimated incorporating these physical parameters. A hydrodynamic model is proposed to outline the pertinent variables necessary to quantify the transport processes.

1 Liquid Flow Rate

Liquid velocity can be estimated by equating the driving force resulting from the hydrostatic pressure difference against the hydraulic resistance of the draft tube and the annular packed bed through an overall momentum balance. Introducing air from the base of the draft tube into the bioreactor leads to gas holdup and an increase in liquid height. In addition, the hydrostatic pressure difference between the two-phase fluid in the draft tube and the liquid in the annular region provides the driving force for the circulation of liquid upwards in the draft tube (upriser) and down through the annular region (downcomer). A force balance of this system is shown below with all of the nomenclature for the equations presented at the end of this thesis.

$g\,\varepsilon_g L_i\,(\rho_l - \rho_g)$ = (Driving force from hydrostatic pressure difference)

$$\frac{4 f_{TP} L_i}{D_i}\left(\frac{\rho_{TP} U_{TP}^2}{2}\right) + \quad \text{(Frictional loss in the draft tube)}$$

$$\frac{\rho_g U_{gi}^2}{2} + \frac{\rho_l U_{li}^2}{2} + \quad \text{(Exit loss of the draft tube)}$$

$$K_c \frac{\rho_l U_{sli}^2}{2} + \quad \text{(Contraction loss at the draft tube inlet)}$$

$$\rho_l U_{sli} (U_{li} - U_{sli}) + \quad \text{(Acceleration loss across the air sparger)}$$

$$\mu_l U_{slo} L_o k \quad \text{(Frictional loss in the fiber bed)} \qquad \text{(III.1)}$$

Among the parameters in Equation III.1, gas holdup, ε_g, is the most important value in determining the driving force for liquid flow. Many equations for the prediction of gas holdup in traditional air-lift bioreactors have been reported (Zuber and Findlay, 1965; Turner, 1966; de Nevers, 1968; Hach, 1973; Hsu and Dudukovic, 1980; Jones, 1985; Bello *et al.*, 1985 ab; Verlaan *et al.*, 1986 b; Chisti and Moo-Young, 1987; Siegel *et al.*, 1988). In the packed-bed portion of the bioreactor, the glass fibers cause a much greater hydraulic resistance in the annulus and consequently reduce the liquid flow rate considerably. This added complexity does not readily allow one to directly apply the empirical equations developed for traditional air-lift reactors. One of the applicable and physically meaningful expressions for gas holdup is the draft flux model of Zuber and Findlay (1965) and is shown in Equation III.2.

$$\varepsilon_g = \frac{U_{sgi}}{C(U_{sgi} + U_{sli}) + U_{b,\infty}} \qquad \text{(III.2)}$$

Distribution parameter, C, in Equation III.2 varies from 1 to 1.5 in accordance with the flow profiles in the draft tube (Zuber and Findlay, 1965), but for a usual symmetrical flow, a value of C=1.07 can be used (Verlaan *et al.*, 1986 b).

Terminal rise velocity of a single bubble, $U_{b,\infty}$, can be expressed as :

$$U_{b,\infty} = \frac{d^2 (\rho_l - \rho_g) g}{18 \mu_l} \qquad \text{(III.3)}$$

The Lockhart-Martinelli correlation (Lockhart and Martinelli, 1949) is used to calculate the two phase frictional loss in the draft tube.

$$\frac{4 f_{TP}}{D_i g} \left(\frac{\rho_{TP} U_{TP}^2}{2} \right) = \left(\frac{\Delta P}{\Delta L} \right)_{TP} = \Phi_l^2 \left(\frac{\Delta P}{\Delta L} \right)_l \qquad \text{(III.4)}$$

$$\Phi_l = f(\chi) \qquad \text{(III.5)}$$

$$\chi^2 = \left(\frac{\Delta P}{\Delta L} \right)_l / \left(\frac{\Delta P}{\Delta L} \right)_g \qquad \text{(III.6)}$$

Contraction coefficient, K_c, is obtained from the following equation (Verlaan *et al.*, 1986 b) :

$$K_c = 0.45\left(1 - \frac{D_i^2}{D_o^2}\right) \qquad \text{(III.7)}$$

By combining the Equations III.2 to III.7 to the Equation III.1 and performing the necessary iterative calculations, the liquid superficial velocity, U_{sli}, can be obtained.

The liquid flow rate, Q_l, is then given by :

$$Q_l = \frac{\pi}{4} D_i^2 U_{sli} \qquad \text{(III.8)}$$

2 Mass Transfer Coefficient

Air sparging from the bottom of the draft tube not only leads to the liquid circulation but also provides oxygenation of the medium inside the draft tube. In order to evaluate the oxygen transfer with different reactor configurations, a mass transfer coefficient, k_l, and a specific gas-liquid interfacial area, a, are estimated individually.

According to the review by Shah *et al.* (1982), for a single bubble with Reynolds number greater than 1, the Sherwood number is given by:

$$Sh = \frac{k_l d}{\delta_{O2}} = 2.0 + 0.60\, Re^{1/2}\, Sc^{1/3} \qquad \text{(III.9)}$$

Assuming that surface oxygenation is negligible compared to sparging, the gas-

liquid interfacial area per reactor liquid volume, a, can be expressed as the following equation.

$$a = \frac{3 \pi D_i^2 L_i \varepsilon_g}{2 V_l d} \qquad \text{(III.10)}$$

From Equations III.9 and III.10, the mass transfer coefficient, k_l, and the specific gas-liquid interfacial area, a, can be obtained and thus the volumetric mass transfer coefficient, k_la, can be calculated.

3 Oxygen Transfer Rate

Assuming that the specific oxygen consumption rate of the single cell is constant, axial oxygen dispersion is negligible, and radial distribution of liquid velocity and dissolved oxygen concentration are negligible, the following one dimensional mass balance equations for stationary phase are obtained.

$$OTR = k_la \frac{(C^*_{in} - C_{lb}) - (C^*_{out} - C_{lt})}{\ln \frac{(C^*_{in} - C_{lb})}{(C^*_{out} - C_{lt})}} \qquad \text{(III.11)}$$

$$OTR = \frac{3600 Q_g}{V_l R T} (pO_{2in} - pO_{2out}) \qquad \text{(III.12)}$$

$$C^* = \frac{10^6 \rho_l pO_2}{H M_{H2O}} \qquad \text{(III.13)}$$

$$OUR = \frac{3600 Q_l}{V_l} (C_{lt} - C_{lb}) \qquad \text{(III.14)}$$

$$OUR = \frac{10^3 Y_{O2} X V_f}{V_l} \qquad \text{(III.15)}$$

At steady state, $OUR = OTR$ (III.16)

By solving the Equations III.11 to III.16, the expression of $Y_{O2}X$ was obtained as follows:

$$Y_{O2}X = \frac{\frac{10^6 \rho_l pO_{2in}}{H M_{H2O}} - C_{lb}}{10^3 V_f \Psi \left(1 + \frac{1}{e^{k_l a V_l \psi} - 1}\right)} \qquad \text{(III.17)}$$

where $$\psi = \frac{1}{3600} \left(\frac{10^6 \rho_l R T}{H M_{H2O} Q_g} + \frac{1}{Q_l} \right) \qquad \text{(III.18)}$$

Equations III.15 to III.18 show the dependence of the oxygen transfer rate on both liquid flow rate, Q_l, and volumetric mass transfer coefficient, $k_l a$.

4 Permeability of Fibrous Bed

The theoretical value of permeability for various mat geometries without cells can be calculated via Spielman and Goren's model (1968). For cells growing in the fiber bed, a model of multilayer cell growth is proposed to obtain the relationship between permeability and cell density. The analyses for the fiber bed with and without cells are presented below.

4.1 Fibrous Bed without Cells

Spielman and Goren (1968) considered the drag and the viscous hydrodynamic forces on flow through fibrous media to predict pressure drop for various fiber arrangements. The hydrodynamic permeability which is dependent on void fraction and fiber diameter can be obtained through the following analysis. The orientations of the fiber in the fiber mat which have been considered in the model include: (1) fiber oriented randomly within planes normal to the bulk flow, (2) fibers all parallel to the direction of the flow, (3) fibers all lying parallel to the direction of the flow, but having completely random angles in those planes (alignment), and (4) fibers axes completely randomly oriented in all directions (isotropic bed). The solution for each case is listed below:

For Case 1,

$$\frac{r^2}{k} = (1-\varepsilon_2)\left[2\frac{r^2}{k} + 4\frac{r}{k^{1/2}}\frac{K_1\left(\frac{r}{k^{1/2}}\right)}{K_0\left(\frac{r}{k^{1/2}}\right)}\right] \qquad \text{(III.19)}$$

For Case 2,
$$\frac{r^2}{k} = (1-\varepsilon_2)\left[2\ \frac{r}{k^{1/2}}\ \frac{K_1\left(\frac{r}{k^{1/2}}\right)}{K_0\left(\frac{r}{k^{1/2}}\right)}\right] \qquad \text{(III.20)}$$

For Case 3,
$$\frac{r^2}{k} = (1-\varepsilon_2)\left[2\frac{r^2}{k} + 3\ \frac{r}{k^{1/2}}\ \frac{K_1\left(\frac{r}{k^{1/2}}\right)}{K_0\left(\frac{r}{k^{1/2}}\right)}\right] \qquad \text{(III.21)}$$

For Case 4,
$$\frac{r^2}{k} = (1-\varepsilon_2)\left[\frac{4}{3}\frac{r^2}{k} + \frac{10}{3}\ \frac{r}{k^{1/2}}\ \frac{K_1\left(\frac{r}{k^{1/2}}\right)}{K_0\left(\frac{r}{k^{1/2}}\right)}\right] \qquad \text{(III.22)}$$

where ε_2 is the void fraction of fiber bed, and K_n is the modified Bessel function of the second kind of order n.

4.2 Fibrous Bed with Cells

- Model of Multilayer Cell Growth for Permeability

It was observed from the samples during the cell cultivations that both anchorage-dependent and suspension cells are attached onto the glass fibers as well as accumulation on the glass fiber forming multilayers as cell growth progressed. The layers of cells growing on the fibers obviously affect the channel diameter and consequently the permeability of the fiber bed.

Since the square root of the permeability is a characteristic length scale of channel diameter (Greenkorn, 1983; Chen,1990), a decrease in the channel diameter of a porous bed by a factor of x will lead to a decrease of permeability by a factor of x^2. Based on this

argument, model of multilayer cell growth for permeability is hence proposed .

In order to study the change in channel size, the layer thickness resulting from cell accumulation on the fibers has to be calculated. Firstly, the relationship between the number of cell layer and the cell density must be specified.

When cells are anchored on the glass fibers, cell number on the nth layer (N(n)) is given by :

$$N(n) = \frac{\left[2\pi \frac{d_f}{2} + 2\pi \, Th \, (n - 1)\right] L \; N_f}{A_c} \qquad \text{(III.23)}$$

where d_f is the fiber diameter, Th is the thickness of one layer of cell, L is the length of a fiber, N_f is the number of fibers, and A_c is the contact area for a cell on the fiber.

The total cell number in n layers ($N_t(n)$) is given by :

$$N_t(n) = \sum_{1}^{n} N(n) = \frac{\left[n \, 2\pi \frac{d_f}{2} + 2\pi \, Th \frac{n(n - 1)}{2}\right] L \; N_f}{A_c} \qquad \text{(III.24)}$$

Fiber number N_f can be determined by :

$$N_f = \frac{V \phi_f}{\pi \left(\frac{d_f}{2}\right)^2 L} \qquad \text{(III.25)}$$

where V is the reactor volume, ϕ_f is the fiber fraction of the reactor.

Equation III.24 can be solved for n :

$$n = \frac{-\left(\frac{d_f}{2} - \frac{Th}{2}\right) + \sqrt{\left(\frac{d_f}{2} - \frac{Th}{2}\right)^2 + \frac{Th\ d_f^2 A_c\ X_c}{\phi_f}}}{Th} \qquad \text{(III.26)}$$

where X_c is cell density in cells/cm^3.

Therefore, the thickness of n layers of cells (Th(n)) is

$$Th(n) = n\ Th \qquad \text{(III.27)}$$

For γ-CHO cells, a contact area of 7.9×10^{-6} cm^2 per cell, Rc of 7.5 μm, and Th of 10 μm were used for the layer calculation. Assuming that the effect of fiber curvature is negligible, the contact area was calculated based on confluency number, 1.2×10^5 cells/cm^2, which was previously experimentally determined.

Hybridoma cells do not spread onto the surface of glass fibers, thus, the cells are assumed to appear as individual spheres. The cells are assumed to arrange themselves in such a way as to occupy the minimum volume. Figure III.1 shows the close-packing of spheres in two dimensions. In close-packing Type A, the thickness of a layer is about twice the cell radius, and the Ac equals to $(2Rc)^2$. In close-packing Type B, thickness of one layer is approximately $\sqrt{3}$ Rc, and the contact area can be approximated by the occupied area:

$$Ac = \pi R_c^2 \frac{2\sqrt{3}}{\pi} = 2\sqrt{3} R_c^2 \qquad \text{(III.28)}$$

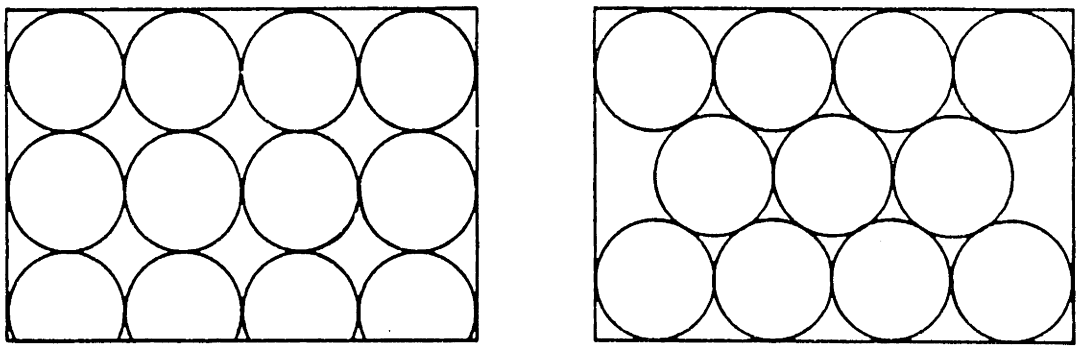

Figure III.1 Close-packing of spheres in two dimensions (from Addison, 1961)
(a) Type A; (b) Type B

Normalized channel size can be calculated from Equation III.29 :

$$\frac{R_i}{R_0} = \frac{[R_0 - Th(n)]}{R_0} \tag{III.29}$$

where R_i is the channel radius at certain cell density, R_0 is the initial channel radius.

$$\frac{k}{k_0} = \left(\frac{R_i}{R_0}\right)^2 \tag{III.30}$$

where k is the permeability at certain cell density and k_0 is the initial permeability.

Equations III.23 to III.30 show that normalized permeability (k/k_0) can be determined using cell density, fiber diameter, fiber fraction, thickness of a layer and contact area.

IV. MATERIALS AND METHODS

1 Cell Lines Used and Its Maintenance

1.1 γ-CHO

A recombinant Chinese Hamster Ovary cell line available at the Biotechnology Process Engineering Center of MIT was used for all the experiments on the anchorage-dependent cell cultivation systems. The cell line was provided by Dr. Walter Fiers of the University of Ghent. The cell line continuously expresses and secretes γ-interferon and is designated as γ-CHO cells. The cell line is anchorage-dependent and does not grow in suspension culture. (Perry and Wang, 1989)

The production of γ-interferon by γ-CHO cells was achieved by co-transformation of the cells with two plasmids, one coding for γ-interferon and the other coding for the enzyme dihydrofolate reductase (DHFR) (Scahill *et al*, 1983). DHFR catalyzes the reduction of dihydrofolate to tetrahydrofolate in the cell. Tetrahydrofolate is needed for single carbon transfer reactions for the productions of glycine, purines, and thymidylate. Methotrexate (or (+)-amethopterin), a 4-amino analog of folic acid, inhibits the activity of DHFR. By blocking these reactions, methotrexate inhibits the synthesis of protein and nucleotide precursors and leads to the death of the cells without DHFR gene (Schimke *et al.*, 1978). However, the cells with high copy numbers of DHFR gene (and correspondingly high copy numbers of the γ-interferon gene) will survive, proliferate and produce γ-interferon in the presence of methotrexate. Therefore, the presence of

methotrexate and the absence of nucleotides in the medium would provide the selection pressure for γ-interferon-producing cells.

To initiate a γ-CHO cell culture, a frozen vial of 1.5 ml of cell suspension was retrieved from a liquid nitrogen cell tank. Dimethyl sulfoxide (DMSO) was usually added in the medium for cryogenic storage because the presence of DMSO would prevent the formation of ice crystals during the freezing process. However, since DMSO is toxic to metabolizing cells, the cell suspension had to be thawed and diluted quickly to minimize the exposure of the warm cells to DMSO. After thawing, the cell suspension was introduced into a roller bottle (490 cm^2 surface area, Corning Glass Works, Corning, NY) containing 80 ml of culture medium. The medium is replaced the next day in order to remove the DMSO in the medium. The culture medium consisted of Dulbecco's Modification of Eagle's Medium (DMEM, Sigma Chemical Co., St. Louis, MO) supplemented with 5% dialyzed fetal bovine serum (FBS, Gibco), 4 mM of glutamine (Sigma Chemical), 2.5×10^{-7} M of methotrexate (Sigma Chemical), and antibiotics(10 units/ml penicillin (Sigma Chemical), and 10 μg/ml streptomycin (Sigma Chemical)). Dialyzed fetal bovine serum was used because of its deficiency in nucleotides which otherwise would be utilized by non-γ-interferon producing cells to grow regardless of the presence of methotrexate. The culture was maintained on a roller bottle of 3 rpm at 37°C. As the bottle rotated, cells attached on the inside surface of the polystyrene bottle and were alternately exposed to the liquid medium and the headspace gas. Cell culture in roller bottles would be gassed with CO_2 in the beginning to maintain a bicarbonate buffer system for an pH of approximately 7.2.

When the cell confluency is reached in the roller bottles, the cells are then split into

new bottles to continue growth. To detach the cells from the inside surface of a roller bottle, the medium was suctioned out, and the attached cells were rinsed with phosphate buffered saline (PBS) to remove the residual serum. A solution of 0.005% trypsin and 0.53 mM ethylenediamine tetraacetic acid (EDTA) in Hanks' balanced salt solution (Gibco) was then added, and the bottle was placed on the roller rack at 37°C for 5 minutes. After a vigorous striking by hand, cells were dislodged. Serum-containing medium was then added to the cell suspension to inactivate trypsin. The cell suspension was then divided and cultured in four new roller bottles. Inoculum of γ -CHO cells for experiments was also obtained in this manner.

In certain instances, γ-CHO cells were cultured in T-flasks (75 cm^2 surface area, Falcon). The procedure and culture conditions were very similar to those for cultivating in roller bottles, except that the cell culture in T-flasks was incubated motionlessly at 10% CO_2 atmosphere.

For cryogenic storage, cells were trypsinized, and resuspended in DMEM containing 5% dialyzed fetal bovine serum and 7.5% DMSO. Each ml of cell suspension was then pipetted into a 1.5-ml vial (Corning). The vials were then gradually frozen to -70°C and stored in a liquid nitrogen cell bank.

1.2 CRL-1606

The cell line used for suspension cell culture experiments was ATCC-CRL-1606 obtained from American Type Culture Collection (Rockville, MD). This is a mouse-

mouse hybridoma producing IgG monoclonal antibody against human fibronectin (Schoen *et al.*, 1982). The cells grow in suspension and do not aggregate or attach to the surface when cultivated in T-flasks or in spinner flasks (Aunins and Wang, 1989). The kinetics of growth and antibody production as a function of nutrient, serum , and waste product concentration at low cell concentrations has been established by Glacken *et al.* (1988).

To initiate a hybridoma culture, a vial of 1 ml aliquot of hybridoma was retrieved frozen from the liquid nitrogen cell tank. The culture was thawed rapidly and diluted 10-fold in culture medium. The composition of the culture medium is DMEM supplemented with 10% (v/v) fetal bovine serum (Sigma Chemical), 6 mM of glutamine,10 units/ml penicillin, and 10 μg/ml streptomycin. The culture was then centrifuged at 200 xg for 10 minutes to remove DMSO and resuspended in the culture medium at 2-3 $x10^5$ cells/ml. The hybridoma was cultivated at 37 °C in a 10% CO_2 atmosphere.

For extended storage, the cells were centrifuged and resuspended at $1x10^7$ cells/ml in DMEM supplemented with 10% (v/v) fetal bovine serum and 10% (v/v) DMSO. Each ml of the cell suspension was dispensed into a 1.5 ml vial and gradually frozen to -70°C and stored in liquid nitrogen cell tank.

In order to cultivate cells at low serum concentrations, the cells were adapted to a defined medium, Excell 300 (JRH Biosciences, CA), supplemented with 0.125% (v/v) of fetal bovine serum by serial dilution. The adaption procedure is as follows: Cells were cultured to a density of $3\text{-}5x10^5$/ml in Excell 300 with 5% fetal bovine serum. The cell solution was then diluted one to two-fold by adding Excell 300 without serum supplement. The procedure was repeated until the cells were growing in Excell containing 0.125% fetal bovine serum.

2. Materials

2.1. Glass Fibers

Glass fibers of 24 and 30 μm in diameters were provided by PPG, Pittsburgh, PA. The fibers from PPG were provided either as chopped fibers or in a mat form. The average length of chopped glass fibers was 0.6 cm. The fiber mat was manufactured in the following way. The glass fiber thread of specific diameter was first produced. Bundles of the glass fiber threads were then interwoven into a mat. The distances between the threads are in the order of microns and the distances between bundles range from 0.3 to 1 cm.

2.2. Antifoam

Medical emulsion C (Dow Corning Corporation, Midland, MICH) was used as an antifoaming reagent throughout the study in this thesis. The antifoam is a silicon defoamer containing 30% simethicon - a mixture of polymethylsiloxane and silicon dioxide. Other ingredients include methyl cellulose, sorbic acid, benzoic acid and water. A 5% (w/v) stock solution of medical emulsion C was prepared in phosphate buffered saline and was autoclaved before use.

2.3. Bioreactor

A four-liter air-lift fiber-bed bioreactor was constructed for the determination of both liquid flow rate and mass transfer coefficient and for the feasibility study of cell cultivation. Its dimensions are described in Table IV.1.

Table IV.1

Bioreactor Dimensions

Reactor	Dimension
Diameter of Reactor (Do)	13.0 cm
Diameter of Inner Draft Tube (Di)	variable
Height of the Reactor (H)	35.0 cm
Total Volume	4.0 liter
Working Volume	2.7 liter

To ensure the best reactor performance, it is necessary that the packing of the fiber bed be uniform to reduce channeling of the liquid flow. It is not easy to obtain loose fibers packed into beds without large void pockets or channels, especially along the walls of the inner and outer cylinder of the reactor (Osawa, 1992). These void pockets and channels would lead to nonhomogeneity of the flow in fibrous bed and also result in nonuniform cell growth within the fibrous bed. To overcome this problem, the glass fiber mat instead of loose fibers was used to build the fiber bed in the reactor. Fiber mat was first cut into doughnut-shaped discs to have exact cross-sectional area and diameters as the annular region of the bioreactor. The middle empty portion was for the inner draft tube. In order to prevent the channeling along the walls, precise diameter or a slightly greater outer diameter

and a slightly smaller inner diameter of the doughnut-shaped disc were preferred.

For the determination of both liquid flow rate and mass transfer coefficient, 26 layers of the PPG glass fiber mat (fiber diameter 24 μm) were stacked to build a 16 cm high fiber bed. The void fraction of the fiber bed was 91.5%. A large glass tube of 5.6 cm inner diameter was used for the draft tube. To allow studies on the effect of draft tube diameter, various inserts into the 5.6 cm diameter inner draft tube were made in order to vary the draft tube diameter.

In the cell cultivation experiments with γ-CHO and CRL-1606 cells, the draft tube used was 1.9 cm in diameter, yielding a Di/Do of 0.15. Eighteen layers of commercially available fiberglass mat (fiber diameter 24 μm) were stacked to obtain a 10 cm high fiber-bed with a void fraction of 91.5%. The surface-to-volume ratio in this fiber-bed was 150 cm^2/cm^3. In this reactor system, the total fiber-bed volume was 1.2 liters and the total working volume was 2.7 liters.

3. Experimental Methods

3.1 Treatment of the Glass Vessel Surfaces

Prior to cell cultivation, the inner surfaces of all the glass vessels used for cell culture, including petri dishes, spinner flasks, and the bioreactor were treated with Prosil-28 (PCR Inc., Gainesville, FL), an organosilane concentrate, to generate a water-repellent surface. This increased hydrophobicity of the glass would prevent cell attachment and growth to the various surfaces.

The procedure was as follows. The glass vessel was soaked in the 1% (v/v) prosil-28 in an aqueous solution for 30 seconds. The glass vessel was rinsed with water several times, dried, and then rinsed with deionized water. After sterilization, the vessel was ready to use.

3.2 Determination of Liquid Flow Rate

A pulse-tracer (acid or base) method was used to determine liquid flow rate. The liquid flow rate, Q_l, can be calculated by the cyclic period, t, from the on-line measurement using a pH meter and is expressed as :

$$Q_l = V_l / t \tag{IV.1}$$

where V_l is the volume of the liquid in the reactor.

3.3 Determination of Mass Transfer Coefficient

The sodium sulfite oxidation method was used for determining the volumetric mass transfer coefficient, k_la. As shown in the equation below, sodium sulfite is oxidized to sodium sulfate in the presence of cupric or cobalt ion.

$$Na_2SO_3 + \frac{1}{2}O_2 \xrightarrow[Cu^{+2}]{Co^{+2}} Na_2SO_4 \tag{IV.2}$$

Since the reaction is sufficiently fast, oxygen concentration in the bulk liquid can be considered to be zero. And with relatively large bubbles, the chemical reaction occurs to a negligible extent in the liquid film adhering to each bubble. Thus the bulk phase chemical reaction rate is therefor equal to the $k_la C^*$, and the k_la value can be obtained. From the bulk phase chemical oxidation, the oxygen transfer rate was measured by analyzing the exhaust gas with the mass spectrometer model MGA-1200 (Perkin-Elmer, Pomona, CA).

3.4 Determination of Pressure Drop

Pressure drop (ΔP) was determined based on the difference of liquid heights (Δh) as shown in Equation IV.3:

$$\Delta P = \Delta h \, (\rho_l - \rho_g) \, g \qquad \text{(IV.3)}$$

where Δh is the height difference of liquid inside and outside the manometer, ρ_l and ρ_g are the density of liquid and gas respectively, g is the gravity acceleration.

In the 4-liter reactor, Δh was measured by the glass tube manometer attached in the annular fiber bed as shown in Figure IV.1. In the 2.5x10 cm fiber bed column, Δh was obtained from the two open manometers fitted at both ends of the column as shown in Figure IV.2.

3.5 Determination of Hydrodynamic Permeability of Fiber Bed

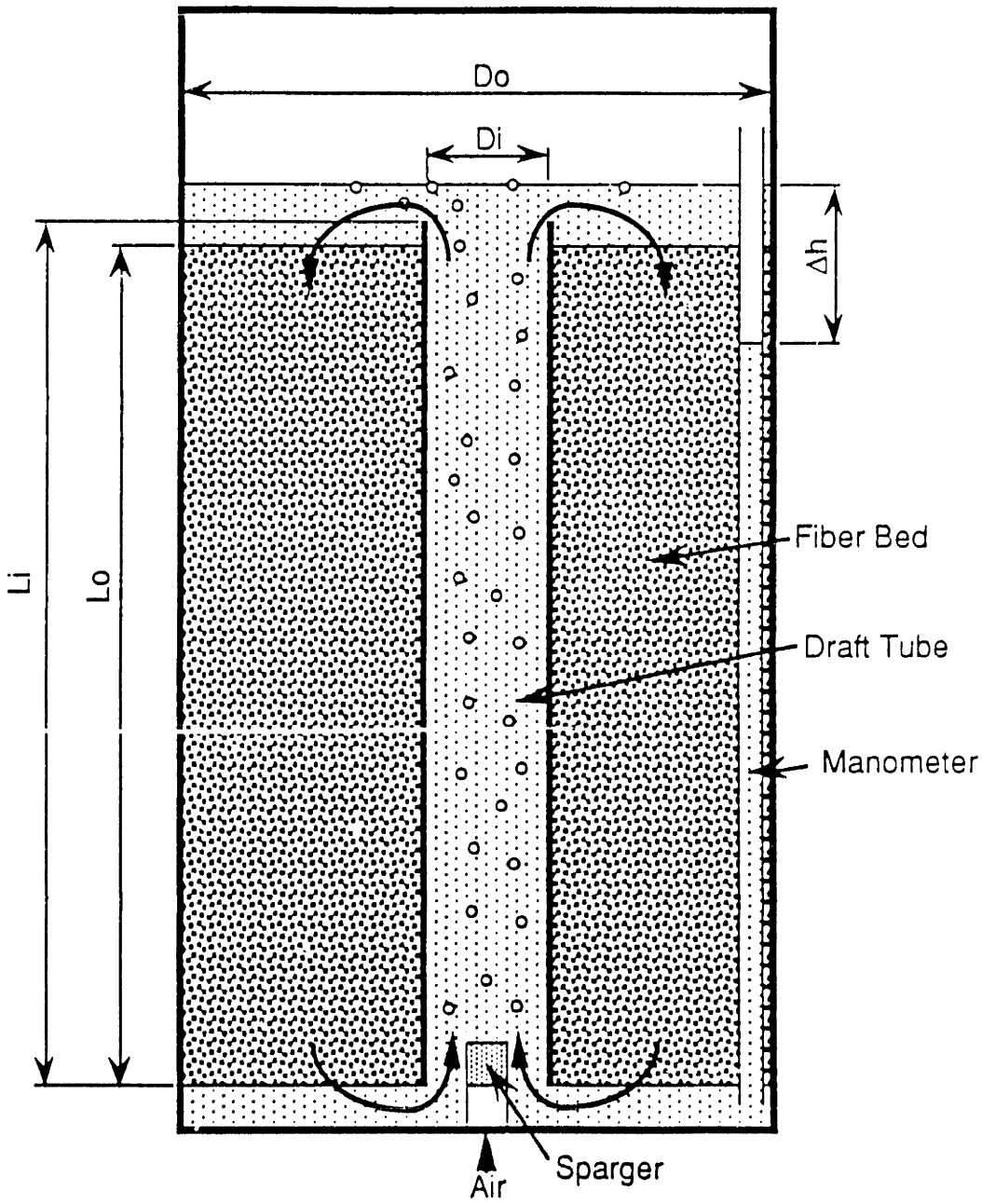

Figure IV.1 Configuration of the reactor. Air is introduced from the bottom of the draft tube and fiber is packed in the annulus. Glass tube manometer is attached for the measurement of pressure drop at the fiber bed.

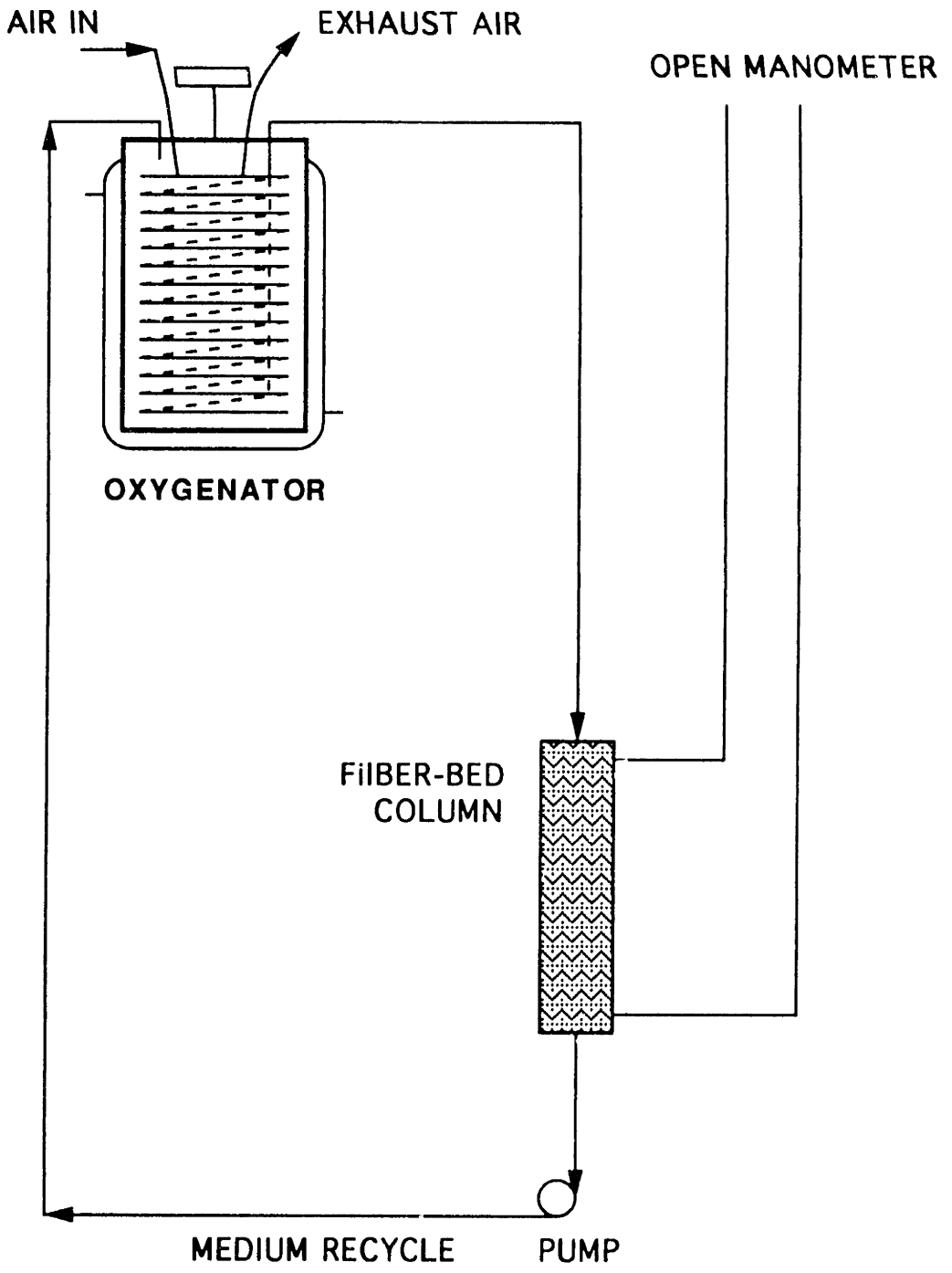

Figure IV.2 Experimental schematic for permeability and residence time distribution studies

Permeability was determined based on Darcy's law, where the hydrodynamic permeability is inversely proportional to the pressure drop across the fiber bed at a given flow rate, liquid viscosity and the cross-sectional area by the following equation:

$$k = \frac{\mu \frac{Q}{A}}{\left|\frac{\Delta P}{L}\right|} \qquad \text{(IV.4)}$$

where k is the permeability, Q is the liquid flow rate, μ is the fluid viscosity, A is the cross-sectional area of the column, ΔP is the pressure drop and L is the length of the fiber bed. Based on known viscosity, liquid flow rate, cross-sectional area, and measured pressure drop, the permeability of the fiber bed could be determined.

3.5.1 Comparison of Permeability between Different Fiber Packing

To compare the permeability of different fiber packing, a small fiber bed column with open manometer as shown in Figure IV.2 was used. The column was 10 cm long and 2.5 in diameter. Glass fibers were 24 μm in diameter and void fraction of the fiber bed was fixed to 91.5% by controlling the weight of the fiber packed. Three types of glass fibers packing were used and listed below:

a) chopped glass fibers packed to have the orientations of fibers perpendicular to the flow direction; b) chopped glass fibers randomly packed into a bed; and c) layers of matted fibers packed into a column.

3.6 Cell Growth on 24 μm and 30 μm Glass Fibers

Petri dishes with a diameter of 5 cm and height of 1.5 cm were used as the initial experiments on the effect of glass fiber diameters on cell growth. To thirty of the petri dishes, 0.25 gram of 30 μm glass fibers were added. To another thirty, 0.20 gram of 24 μm glass fibers were added. Therefore, the surface area in each bottle for cell attachment and growth was approximately 151 cm^2. The other 5 petri dishes containing no glass fibers served as the control.

Into each autoclaved petri dish, $5.3x10^5$ γ-CHO cells harvested from confluent roller bottle culture and 11 ml of the culture medium were added. The culture medium used was DMEM supplemented with 5% dialyzed fetal bovine serum, 4 mM of glutamine, $2.4x10^{-7}$ M methotrexate, and antibiotics (10 units/l of Penicillin and 10 mg/l of Streptomycin). The culture was shaken at about 5 rpm on a rotary shaker in an incubator at 37°C at 10% CO_2 atmosphere. The medium was replaced with fresh medium every three days. One or two of the bottles from each group were sacrificed to conduct nuclei counts.

A parallel experiment to investigate cell growth on 24 and 30 μm glass fibers was designed as follows. To a 250-ml glass vessel, either 1.5 grams of 30 μm glass fibers or 1.2 grams of 24 μm glass fibers, providing a surface area of about 910 cm^2, were added and autoclaved. $1.6x10^7$ cells and 125 ml of the culture medium (same as the petri dish experiment) were then added to each of the glass vessel containing the glass fibers. The experiment was carried out in duplicates. A sample of 3 ml medium was taken from each of the glass vessel every day to examine the glucose and lactate concentrations. At the end of

the cultivation experiment, free cells in the medium were counted following the usual cell count procedure and the cells attached on glass fibers in each glass vessel were enumerated by nuclei counts.

3.7 Effect of Antifoam on the Cell Growth and Productivity

3.7.1 For γ-CHO

The medium used for γ-CHO cell culture was DMEM/F12 Nutrient Mixture (1:1) supplemented with 1.2 % dialyzed fetal bovine serum, 4 mM L-glutamine, 2.4×10^{-7} M methotrexate, and antibiotics (10 units/l of Penicillin and 10 mg/l of Streptomycin). To a series of five 250 ml glass vessels (conducted in duplicate), 1.0 gram of 24 μm glass fibers and 50 ml of phosphate buffered saline were added. After sterilization, he phosphate buffered saline was discarded and 1×10^6 γ-CHO cells (harvested from confluent culture in T-flasks) were added to each vessel. Appropriate volumes of culture medium and 5% stock solution of medical emulsion C were added to yield an initial culture volume of 125 ml and antifoam concentrations of 0, 250, 500, 750, and 1000 ppm respectively. The cultures with various antifoam concentrations were then placed on a rotary shaker at 3 rpm and incubated at 37°C and 10% CO_2 atmosphere. Samples of 2 ml aliquots were taken from the vessels periodically to analyze glucose, lactate, and γ-interferon concentrations. Upon completion of the cultivation, nuclei counts were performed on the glass fibers in each of the vessels.

3.7.2 For Hybridoma ATCC-CRL-1606

The medium used for hybridoma cell culture was Excell 300 supplemented with 0.125% fetal bovine serum, 6 mM glutamine and antibiotics (10 units/l of Penicillin and 10 mg/l of Streptomycin). To a series of six 125 ml spinner flasks (conducted in duplicate), a cell suspension of $1x10^7$ hybridoma cells was added to each as inoculum. Appropriate volume of the 5% stock solution of medical emulsion C was added to give final concentrations of 0, 750, 1000, 1250, 1500 and 1750 ppm respectively. All the spinner flasks were then made up to 125 ml with the culture medium. Culture without antifoam was used as control. The spinner flasks were placed on magnetic stirrers set at about 75 rpm in an incubator at 37°C, 90% relative humidity and 10% carbon dioxide. Samples of 2 ml aliquots were withdrawn from the flasks daily for the analysis of cell number, glucose, lactate, and immunoglobulin G concentrations.

3.8 Operations and Technical Feasibility Studies

3.8.1 Cell Entrapment Kinetics

3.8.1.1 Single-Pass Process.

Five columns, each 3 cm in length and 0.55 cm in diameter, were packed with 24 μm glass fibers to yield a void fraction of 93%. DMEM/F12 Nutrient Mixture (1:1) was first placed into the packed bed, and a suspension of $2.4x10^6$ γ-CHO cells was then introduced into the column. Cells exiting the column were fractionally collected and counted with a hemocytometer using trypan blue as a dye in order to enumerate the outlet cell concentration versus time. After a single-pass of the cells through the column, glass

fibers in the columns were recovered, and the number of trapped cells in each of the five columns was quantified by citric acid/crystal violet nucleus counts.

3.8.1.2 Inoculation Studies

The study of the inoculation procedure was conducted in the 4-liter size reactor. Eighteen layers of the 24-μ glass fiber mat were packed to yield a void fraction of 91.5%. The medium filled in the reactor was Excell 300 supplemented with 0.25% fetal bovine serum and 100 ppm medical emulsion C. Inoculation was achieved by introducing a cell suspension of 4.9×10^9 CRL-1606 cells at the top of the reactor. This was followed by gas sparging at 0.5 VVM (gas volume per liquid volume per minute) for 5 minutes and 0.05 VVM for about one hour to distribute the cells within the entire fiber-bed. Free cell concentration in the solution was determined by hemocytometer cell counts every 5 to 10 minutes to record the free cell concentration as a function of time. At the end of the inoculation procedure, the reactor was dissembled and the cells entrapped in each layer of the fiber mat were enumerated through citric acid/crystal violet nucleus counts.

3.8.2 Model Systems

3.8.2.1 Anchorage-Dependent Cell Culture

Recombinant Chinese Hamster Ovary (γ-CHO) cells engineered to produce γ-interferon were used for all experiments. The medium used was Dulbecco's Modified Eagle's Medium/F12 Nutrient Mixture(1:1) supplemented with 1.2 % fetal bovine serum, 4

mM L-glutamine, 2.4×10^{-7} M methotrexate, and antibiotics (10 units/l of Penicillin and 10 mg/l of Streptomycin). Dow Corning medical emulsion C was added as an antifoam.

3.8.2.2 Suspension Cell Culture

Hybridoma ATCC-CRL-1606 was used for suspension cell culture. The medium used was a defined medium, Excell 300, supplemented with 0.125 to 0.3% fetal bovine serum, 6 mM glutamine and antibiotics (10 units/l of Penicillin and 10 mg/l of Streptomycin). Dow Corning medical emulsion C was added as an antifoam.

3.8.3 Operations

Figure IV.3 shows the experimental apparatus and the associated equipment for the cell cultivation process. Inoculation was achieved by introducing a cell suspension from the top of the reactor. This was followed by gas sparging at 0.5 VVM for 5 minutes to distribute the cells within the entire fiber-bed. The gas flow rate was controlled by a mass flow controller (Brooks 5850E, Emerson Electric Co., Hatfield, PA).

During the cultivation process, the pH was maintained within the range of 6.7 to 7.3 by adjusting the CO_2 content in the inlet gas flow. Since the reactor was operated in a perfusion mode, the feed was supplied continuously, and product and spent medium were continuously withdrawn.

During the cultivation, samples were drawn and analyzed off-line for glucose,

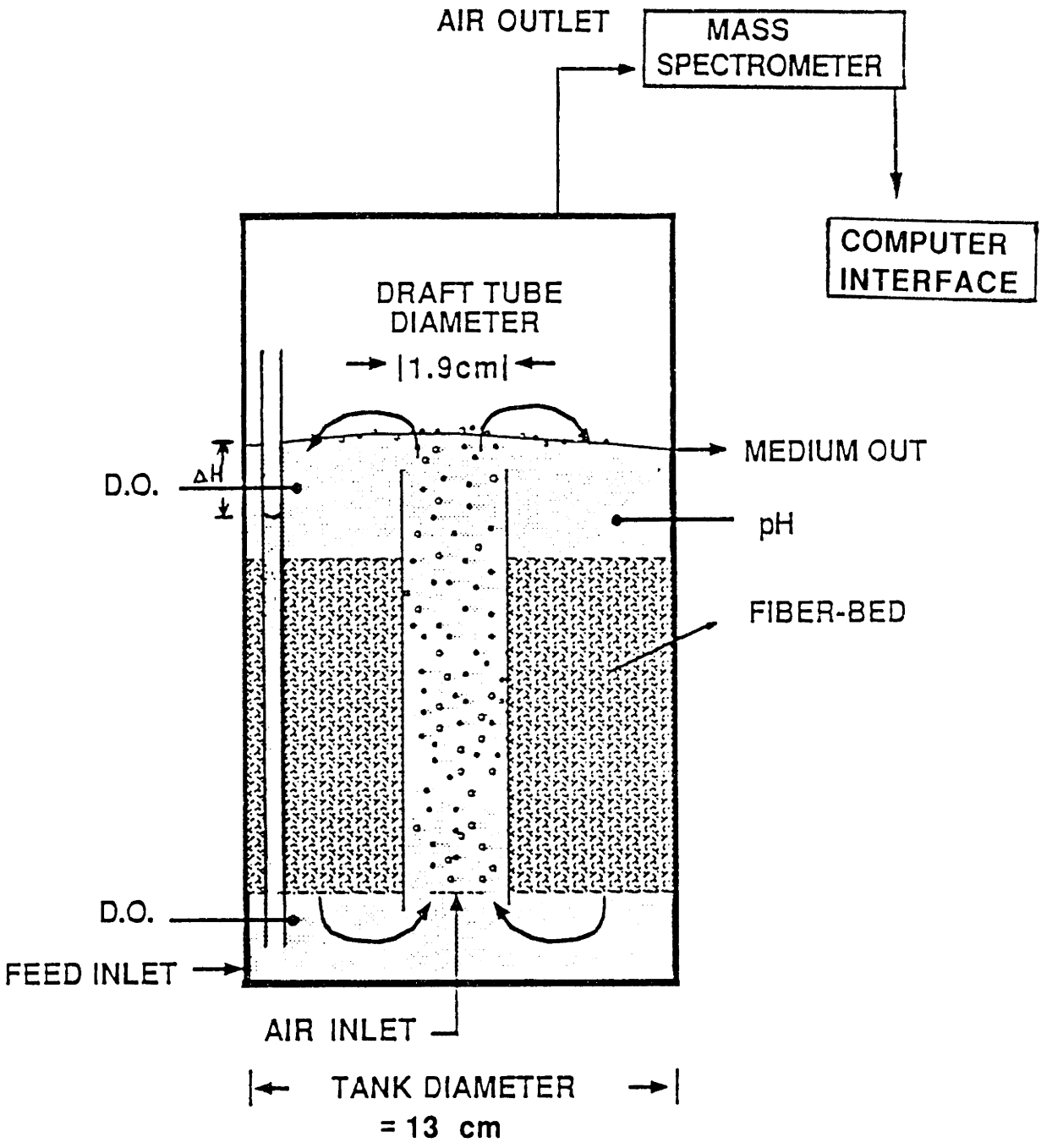

Figure IV.3 Schematic diagram and associated equipment of the airlift fiber-bed bioreactor

lactate and product (γ-interferon or IgG) concentrations. Trypan blue cell counts and citric acid/crystal violet nucleus counts by hemocytometer were used to determine the cell numbers in the inoculum and the fiber-bed respectively.

An *in situ* method for measuring the oxygen uptake rate (OUR) was employed during cell cultivation. Dissolved oxygen (D.O.) probes were mounted at the top and at the bottom of the annular fiber-bed. A material balance on the liquid side, using the top and bottom D.O. readings and liquid flow rate, provides an indication as to the oxygen consumption. The following equation was used to determine the OUR (mmole/l/hr) :

$$OUR = Q_l \frac{3600}{100} (DO_t - DO_b) \frac{C_A}{V_f} \qquad \text{(IV.5)}$$

where Q_l is the liquid flow rate, cm^3/s; C_A is the equilibrium dissolved oxygen concentration with air, 0.225 mmole/liter; DO_t and DO_b are percentage of dissolved oxygen by the top and bottom DO probe respectively; V_f is the volume of the fiber-bed, liter. The liquid flow rate, Q_l, was calculated using the following equation :

$$\begin{aligned} Q_l &= k \left|\frac{\Delta P}{L}\right| \frac{A}{\mu} \\ &= k \frac{\rho g \Delta H}{L} \frac{A}{\mu} \end{aligned} \qquad \text{(IV.6)}$$

As shown in Equation IV.6, Q_l is determined by hydrodynamic permeability of the fiber bed, (k), pressure drop ($\Delta P/L$), cross-sectional area A, and viscosity (μ) of the liquid. The pressure drop can be measured through the liquid height difference by an glass manometer as shown in Figure IV.3. However, the permeability, k, is a function of cell density in the fiber bed (will be presented in Section 4.4). Consequently, the Q_l changed as the cells

grew inside the fiber-bed. The cell density could be estimated based on lactate production rate; the relationship between cell density and permeability developed in Chapter 2 was then used to obtain the correct liquid flow rate during the cell cultivation. In this way, the oxygen uptake rate was obtained.

3.9 Effect of Cell Growth on Permeability and Residence Time Distribution

Cell line. Recombinant Chinese Hamster Ovary cells (γ-CHO) with encoded gene for γ-interferon and the murine hybridoma cell line, ATCC-CRL 1606, were used in the model systems for anchorage-dependent and anchorage-independent cell culture respectively.

Medium. For cultivating γ-CHO cells, the medium used was DMEM/F12 (1:1) supplemented with 5% dialyzed fetal bovine serum, 4 mM of glutamine and 0.125 μM of methotrexate. For hybridoma cells, the medium used was DMEM supplemented with 5% fetal bovine serum and 12 mM of glutamine.

The experimental set up for the cell culture is illustrated in Figure III.2. The fiber-bed column is 10 cm in length and 2.5 cm in diameter. Layers of glass fiber mats (8.5 grams) were packed into the column yielding a void fraction of 91%. The glass fiber mat consisted of randomly woven bundles of glass fiber of 24 μm in diameter. The two ends of the column were fitted with two long tubings acting as an open manometer to monitor pressure drop.

A 2-liter reactor (Applicon) equipped with a cage of medical grade silicone tubing (15 meters in length and 1 mm in diameter) was used as an external oxygenator. The gas introduced into the oxygenator was 5% carbon dioxide balanced with air. The oxygenated medium, maintained at 37°C, was recycled through the fiber-bed column at a rate of 1.6 ml/sec (equivalent to a linear velocity of 0.4 cm/sec) by a peristatic pump. The system was operated at a fed-batch mode by replacing the medium periodically. During cell cultivation, pressure drop was measured as cell growth progressed in order to determine the effect of cell growth on permeability.

Residence time distribution (RTD) for the fiber-bed column was determined before and after cell cultivation. The tracer used was 0.4 ml phenol red at 2 mg/ml and the flow rate used was 0.64 ml/sec. A pulse of phenol red was introduced into the column and the time variation of the absorbance was monitored at 430 nm using a flow cell and UV spectrophotometer. The absorbance at 820 nm was used as a negative control. An HP pamcode system was used for data acquisition. Two numerical values have been used to characterize a distribution (Levenspiel, 1972). The mean residence time is given by :

$$\text{Mean Residence Time } (\bar{t}) = \frac{\int_0^\infty t\, A_b\, dt}{\int_0^\infty A_b\, dt} \qquad \text{(IV.7)}$$

Since the distribution curve is only known at a number of discrete time values t_i, the mean residence time can be given by :

$$\text{Mean Residence Time } (\bar{t}) = \frac{\Sigma\, t_i\, A_{bi}\, \Delta t_i}{\Sigma\, A_{bi}\, \Delta t_i} \qquad \text{(IV.8)}$$

where A_{bi} is the absorbance at 430 nm at given time t_i and Δt_i is 0.5 second in our experiments.

The other important descriptive quantity is the spread of the distribution. This is commonly measured by the variance, δ^2, defined as :

$$\text{Variance } (\delta^2) = \frac{\int_0^\infty (t - \bar{t})^2\, A_b\, dt}{\int_0^\infty A_b\, dt} \qquad \text{(IV.9)}$$

Again, in discrete form :

$$\text{Variance } (\delta^2) = \frac{\Sigma (t_i - \bar{t})^2\, A_{bi}\, \Delta t_i}{\Sigma\, A_{bi}\, \Delta t_i} \qquad \text{(IV.10)}$$

The variance represents the square of the spread of the distribution and has a unit of $(\text{time})^2$.

Cell density was determined by nuclei counts after the fiber bed was dissembled. During cell cultivation, since there is no direct and nondestructive way to enumerate cells, the value of lactate production rate divided by the specific lactate production rate was used as an indication of cell density. During cell cultivation, off-line samples were analyzed for

lactate concentration.

4 Analytical Methods

4.1 Cell Enumeration

For freely suspended cells, the concentration was determined by a hemacytometer at 100X magnification with a phase contrast objective, and the viability was determined by trypan blue (2 g/l in phosphate buffered saline) exclusion (Freshney, 1983). For cells attached on glass fibers, cell number was determined either by citric acid/crystal violet nuclei counts (Freshney, 1983) or by DNA assay. For nuclei counts, samples were immersed in the solution containing 0.5 g/l crystal violet in 0.1 M citric acid. Nuclei released after the membrane lysis due to the acid treatment would be stained by crystal violet. The samples were allowed to stand in the solution for at least one day. They were vigorously shaken periodically to facilitate the release of the nuclei. The stained nuclei were then counted by a hemacytometer.

DNA assay was performed following the procedure of Giles and Myers (1965). The samples consisting of cell mass and glass fibers were first suspended in phosphate buffered saline (PBS) and then vigorously shaken to detach cells from glass fibers. After the glass fibers settled, the cell suspension was withdrawn and then serially diluted. To a 2.0 ml sample, 2.0 ml of glacial acetic acid containing 4% (w/v) diphenylamine and 0.2 ml of 0.16% (w/v) acetaldehyde solution were added. The solutions were mixed and incubated at room temperature overnight. Absorbance at 595 nm and 700 nm were measured and the difference correlated to calf thymus DNA standards (Sigma Chemical).

4.2 Glucose and Lactate

Glucose and Lactate were measured by assay kits provided by Sigma Chemical Co. The assays for glucose were employing enzymatic reactions by hexokinase and glucose-6-phosphate; whereas the assay for lactate was based on the reaction of lactate dehydrogenase.

4.3 γ-Interferon

A radioimmunoassay kit was obtained from Centocor (Malvern, PA), and included a solid-bound primary antibody, an ^{125}I-labelled secondary antibody, as well as standards and diluent. This solid phase radioimmunoassay was based on the "forward sandwich" principle. Polystyrene beads coated with one of the mouse monoclonal antibodies specific for γ-interferon were incubated with samples, properly diluted by PBS, or the appropriate standards and controls. During the incubation, the γ-interferon in the sample was bound to the solid phase. Unbound material in the sample was removed by the aspiration of PBS and washing off the beads. The other monoclonal antibody to γ-interferon, labeled with ^{125}I, was incubated with the beads, and, if γ-interferon was bound to the beads, the radiolabeled anti-γ-interferon then bound to the γ-interferon on the beads. Unbound labeled antibody was removed by aspiration and washing. The bound radioactivity was measured by counting the beads in a gamma-counter. The bound radioactivity was proportional to the concentration of the γ-interferon in the sample within the working range

of the assay. A standard curve was obtained by plotting the γ-interferon concentration of the standards versus bound radioactivity. The γ-interferon concentration of the samples and control, which were analyzed concurrently with the standards, was determined from the standard curve. In addition, no interference of the antifoam, medical emulsion C, to γ-interferon activity was observed.

4.4 Anti-Fibronectin Immunoglobulin G(IgG)

IgG concentrations were determined by the ORIGEN assay kit (IGEN, Rockville, MD). The assay was based on a homogeneous competitive format labeled mouse IgG and goat anti-mouse antibody immobilized on the solid phase. IgG in the sample competed with the labeled IgG for binding sites on the immobilized antibody. The label was a metal chelate, ruthenium tris(bipyridine), which luminesces when electrochemically excited. When it binds to the solid phase, its luminescence is modulated. Therefore, the luminescence signal would be directly proportional to the IgG in the sample (Lindell *et al.*, 1991). No interference of the antifoam, medical emulsion C, to IgG activity was observed.

V. RESULTS AND DISCUSSION

The objective of this thesis is to provide an alternative for animal cell culture through a novel bioreactor design. Within this overall objective a series of specific goals were developed and these include:

1) biological considerations on the use of small fibers as an alternative support for anchorage-dependent cells;

2) development of a hydrodynamic model for liquid circulation velocity, mass transfer coefficient, oxygen transfer and other pertinent properties for the bioreactor;

3) demonstration of the technical feasibility of cultivating anchorage-dependent and suspension cells in the bioreactor;

4) analysis on the scaleup potential of the bioreactor.

CHAPTER 1. BIOLOGICAL CONSIDERATIONS

1.1 Small Diameters Glass Fibers As an Alternative Support for Anchorage-Dependent Cells

Initial studies probed the feasibility of implementing small diameter glass fibers as an alternative support for the attachment and growth of anchorage-dependent cells. The beneficial features of using smaller fibers include firstly, high surface-to-volume ratio which consequently leads to high cell density as shown in the equations below:

$$S/V = 4\,(1-\varepsilon_2)/d_f \tag{1.1}$$

$$X_m = (S/V)\,X_A \tag{1.2}$$

where S/V is the surface-to-volume ratio of the fiber bed, ε_2 is the void fraction of bed, d_f is the fiber diameter, X_m is the achievable monolayer cell density in cells per unit volume, and X_A is the cell number per unit area at the confluent state. Since the growth of anchorage-dependent cells is surface-dependent, a higher surface-to-volume ratio allows for a higher cell density to be achieved. Since the surface-to-volume ratio of a fiber bed is inversely proportional to fiber diameter, this can be achieved by decreasing the fiber diameter. Secondly, at a constant surface-to-volume ratio, using smaller fiber diameters with higher void fractions results in higher hydrodynamic permeability which will be shown in Chapter 2. It will also be discussed that high hydrodynamic permeability is c[illegible]nt

mass transfer in the reactor.

Although Maroudas (1972) has set the threshold diameter for cell growth on beads to be 50 μm, anchorage-dependent cells could behave differently when grown on glass fiber of smaller diameter because the cells' cytoskeletal elements can align along the fiber axis (Dunn and Heath, 1976; Fisher and Tickle, 1981). Commercially available glass fibers of 24 and 30 μm in diameter were first examined for γ-CHO cell attachment and growth. These experiments were performed to assess the possibility of using glass fibers of small diameters as an alternative support for cell growth. As shown in Figure 1.1, the cell number increased from $3x10^3$ cells/cm^2 to about $1x10^5$ cells/cm^2 on both 24 and 30 μm glass fibers after 11 days of cultivation. The growth rate during the exponential phase was 0.0146 hr^{-1} (doubling time = 47.5 hours). This growth rate is comparable to that obtained in roller bottles where the typical doubling times ranged from 36 to 48 hours for γ-CHO cells. Cells growing on 24 and 30 μm glass fibers did not exhibit a significant difference in the growth rate. Figure 1.2 shows the microphotographs of a 12 days culture of γ-CHO cells on glass fiber. The cells in petri dishes without glass fibers did not multiply and disappeared after 5 days' cultivation time. This result is consistent with an earlier report by Perry and Wang (1989).

In the parallel experiment, glucose and lactate concentrations were monitored during the cultivation, and these are plotted on a cumulative basis in Figure 1.3. The trends of glucose and lactate metabolisms were very similar for cells growing on 24 and 30 μm glass fibers. The rates for glucose consumption and lactate production increased for the first 6 days before levelling off. During this time, the cell densities increased from $1.7x10^4$ cells/cm^2 to $6.8x10^4$ cells/cm^2 for the 30 μm fibers and to $6.6x10^4$ cells/cm^3 for the 24 μm

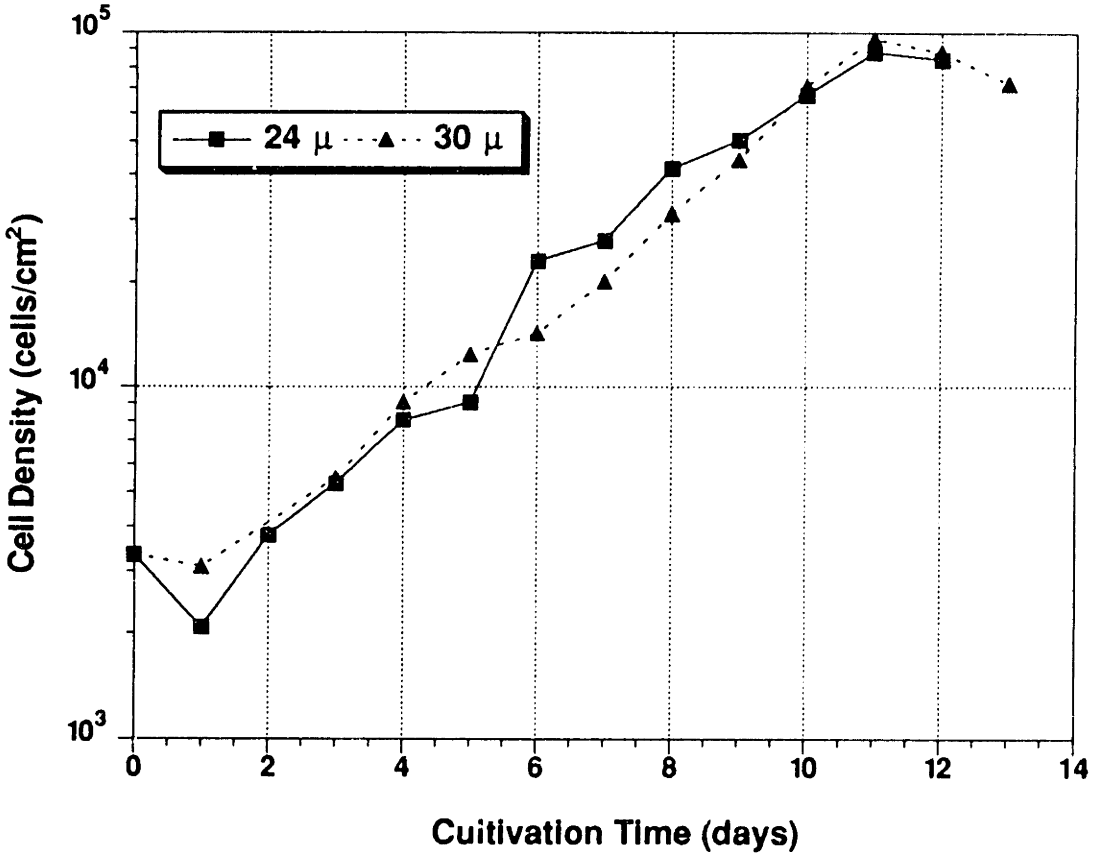

Figure 1.1 Cell growth on 24 μm and 30μm glass fibers

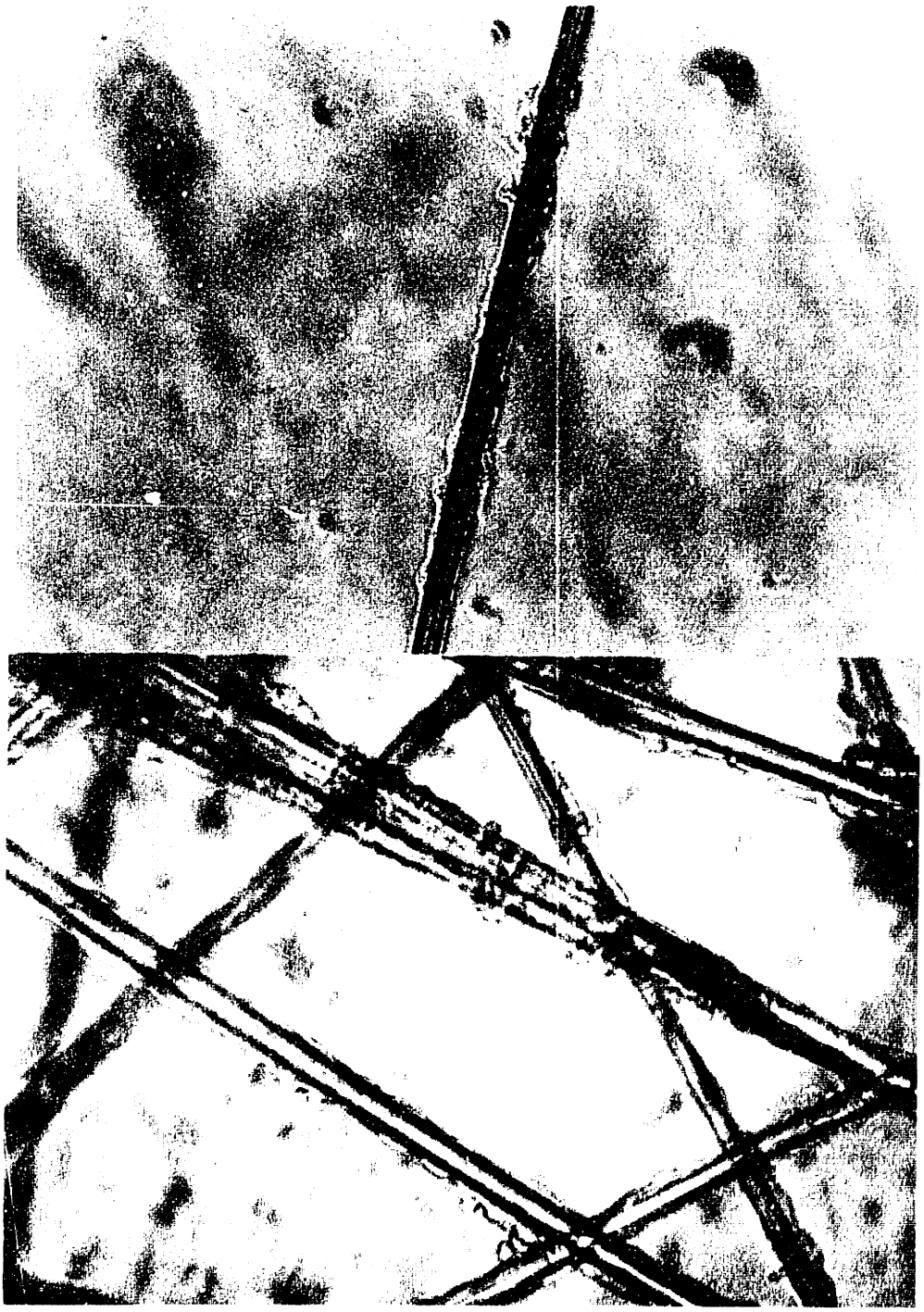

Figure 1.2 Photographs of γ CHO cells grown on 24 μm and 30 μm glass fibers. Top: 24 μm glass fibers, bottom: 30 μm glass fibers.

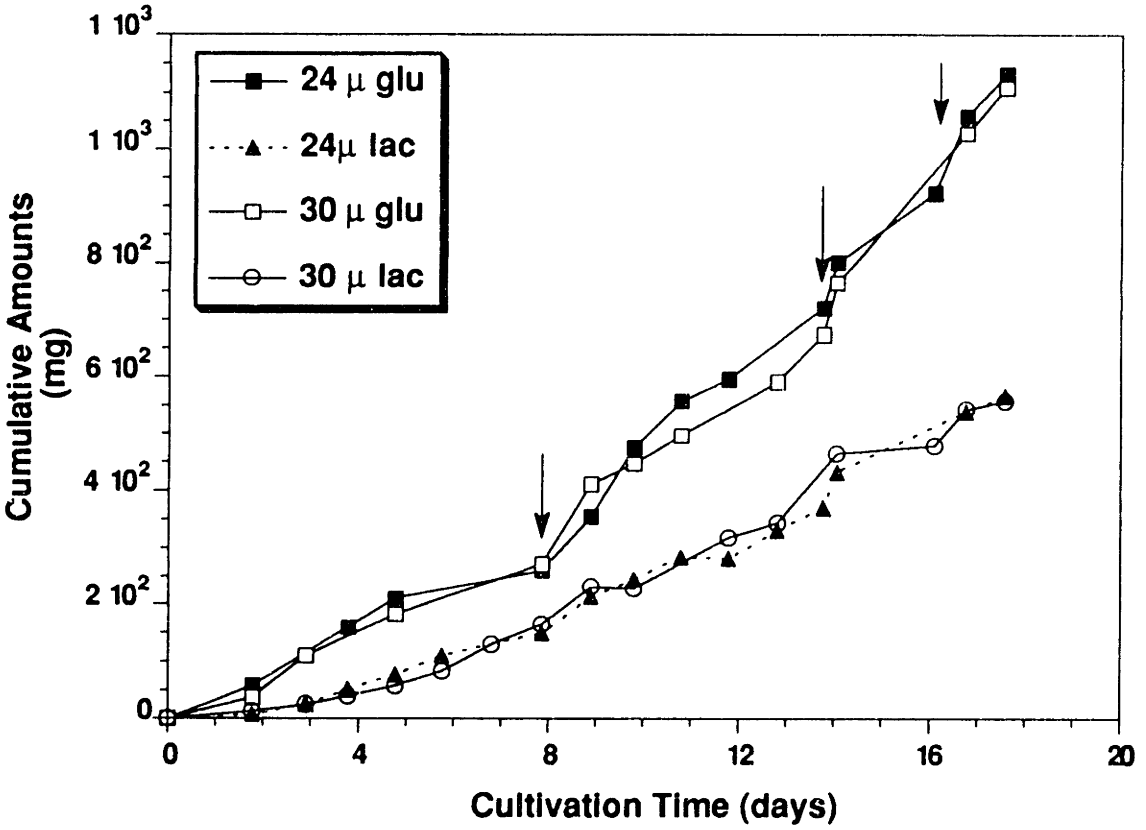

Figure 1.3 Cumulative glucose consumption and lactate production for CHO cells growing on 24 μm and 30 μm glass fibers (↓: medium change)

fibers. The free cell concentration in the medium was less than 0.5% of the total cells present in the glass vessel. We concluded that glass fibers of small diameters such as 24μm and 30 μm can be used as an alternative support for cell attachment and growth.

1.2 Study of Antifoam Effect

Due to the need for aeration, antifoam was added to suppress foaming during cell cultivation. Although there are reports regarding the use of antifoam in animal cell culture, the amounts of antifoams used are usually low due to the low gas flow rate required (Aunins *et al.*, 1986). Since high gas flow rates may be required for the operation of our bioreactor, it was necessary to find an effective, non-toxic antifoam. After a preliminary screening, medical emulsion C showed great promise in meeting the requirements. It was therefore chosen for detailed studies on the dependence of required concentration on gas flow rate and the effect of antifoam on cell growth and productivity.

1.2.1 Antifoam Requirement

The amounts of antifoam required for foam inhibition at various gas flow rates were investigated. Figure 1.4 shows two examples from these studies. The data were collected from cell cultivation experiments which will be presented in Chapter 3. The media used were DMEM/F12 supplemented with 1.25% dialyzed fetal bovine serum, 4 mM L-glutamine, 2.4×10^{-7} M methotrexate, and antibiotics (10 units/l of Penicillin and 10 mg/l of Streptomycin), and Excell 300 supplemented with 0.125% fetal bovine serum, 6 mM glutamine and antibiotics (10 units/l of Penicillin and 10 mg/l of Streptomycin). It was found that it is necessary to increase the antifoam concentration proportionally to the air

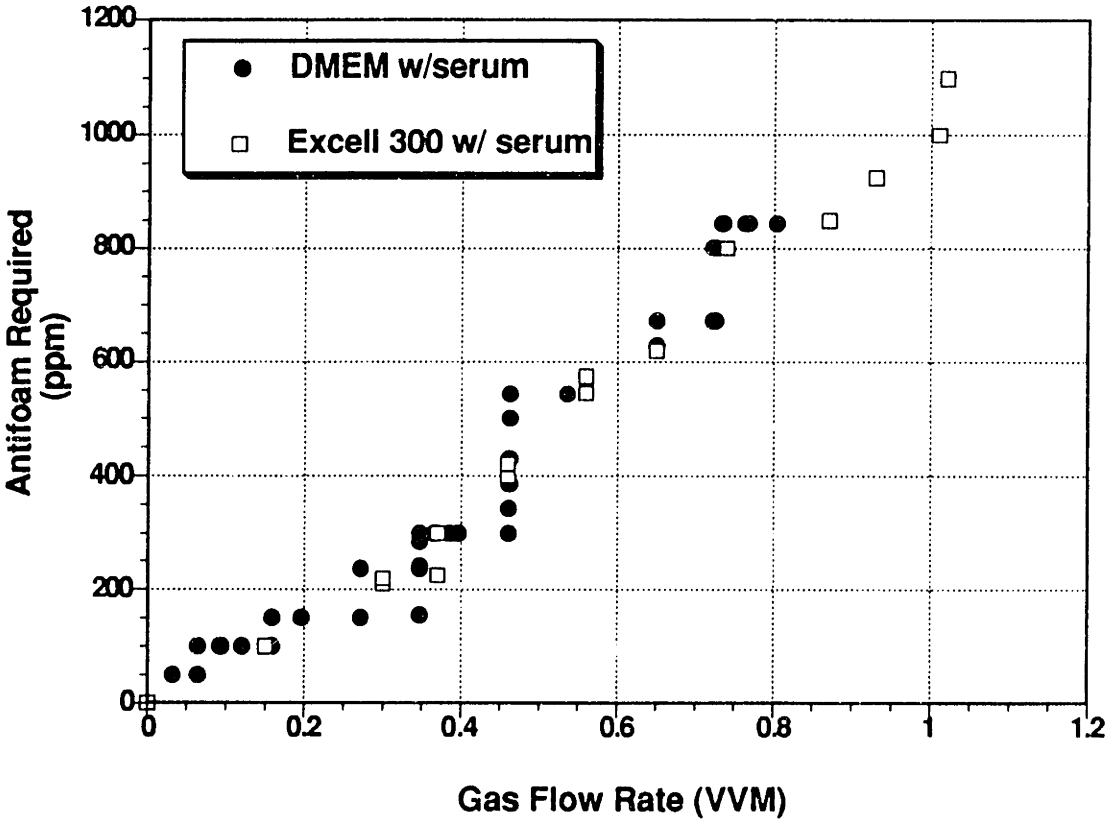

Figure 1.4 Antifoam requirement at various gas flow rates

flow rate. There is no significant difference in the antifoam requirement for the two types of media studied. Medical emulsion C at 1000 ppm was required for a gas flow rate of 1 VVM. This high level of antifoam present in the medium raised the concern of its toxicity effect on cell growth and product generation. The investigation on antifoam toxicity was therefore initiated and is described below.

1.2.2 Antifoam Toxicity

1.2.2.1 Anchorage-Dependent Cells

The effect of antifoam on the growth of γ-CHO cells is shown in Figures 1.5 to 1.7. The culture with various amounts of antifoam added showed similar metabolic pattern. The cumulative consumption of glucose and production of lactate are illustrated in Figures 1.5 and 1.6. Nearly identical production of γ-interferon were found for the various amounts of antifoam added. The total cell number in each glass vessel at the end of the experiment, obtained through nuclei counting, was 2.1×10^7, 2.2×10^7, 2.1×10^7, 2.0×10^7, and 2.1×10^7 for 0, 250, 500, 750 and 1000 ppm of antifoam added respectively. The deviations are within the experimental error. It is therefore concluded that the cell growth and γ-interferon production are not affected by medical emulsion C addition up to 1000 ppm.

1.2.2.2 Suspension Cells

The results on the growth of hybridoma cells ATCC-CRL-1606 in the presence of various concentrations of medical emulsion C are shown in Figure 1.8. The growth rate

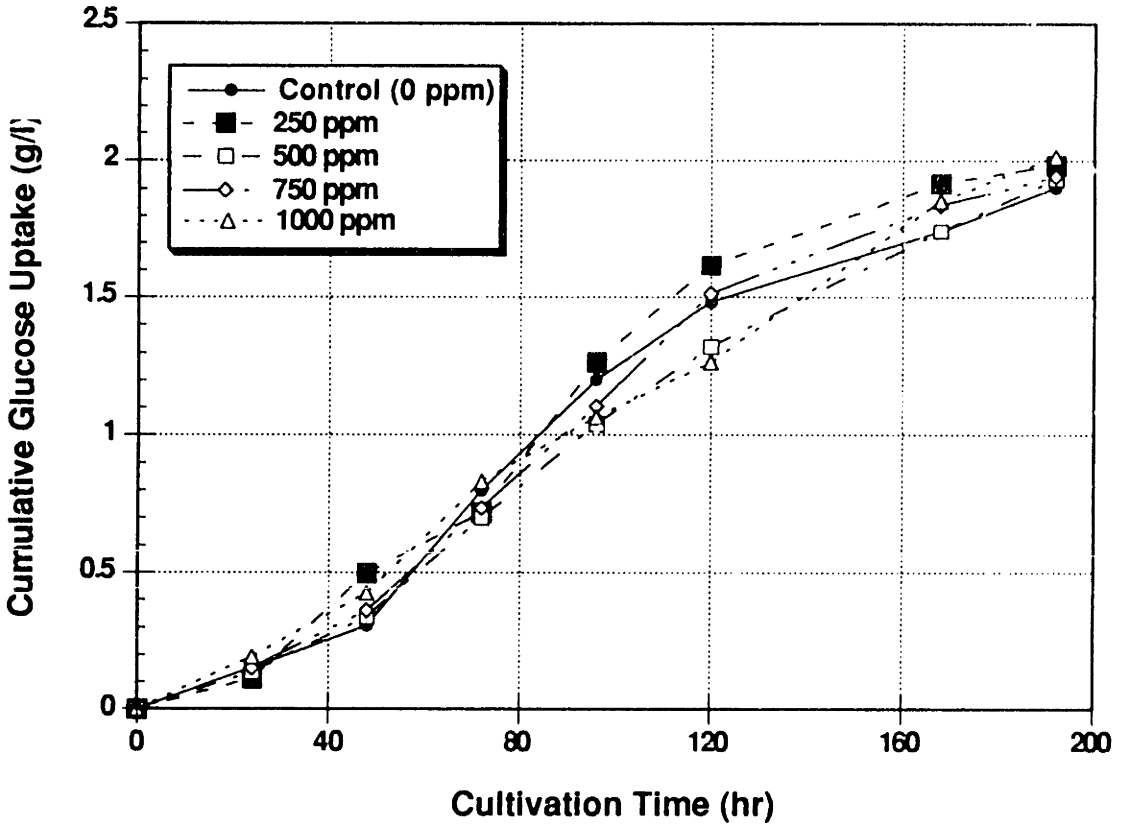

Figure 1.5 Antifoam effect on glucose uptake (CHO)

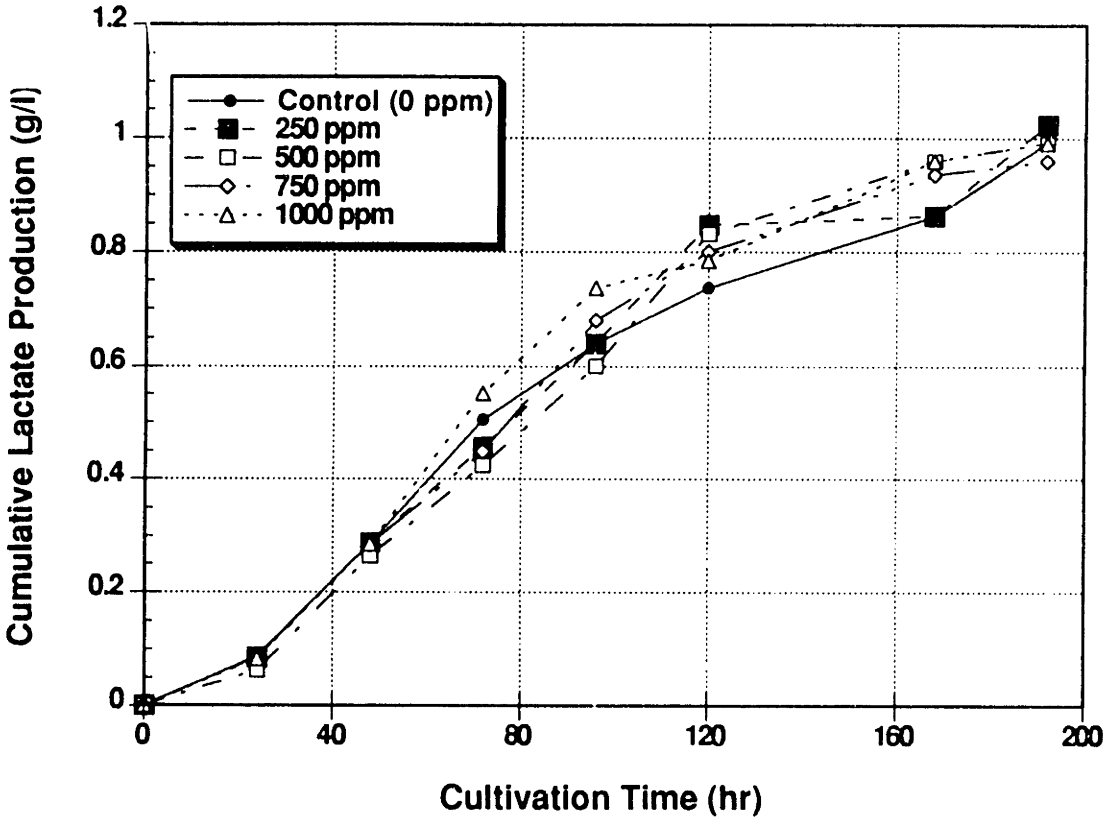

Figure 1.6 Antifoam effect on lactate production (CHO)

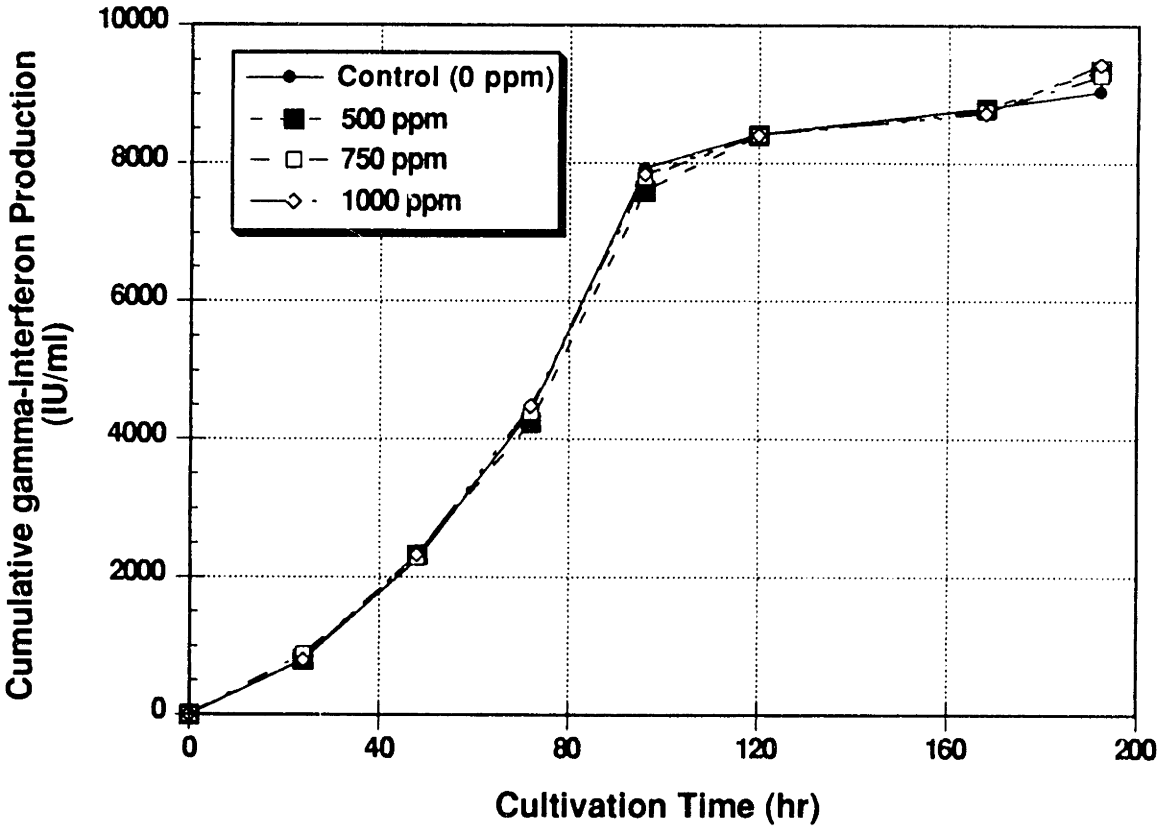

Figure 1.7 Antifoam effect on gamma-interferon production (CHO)

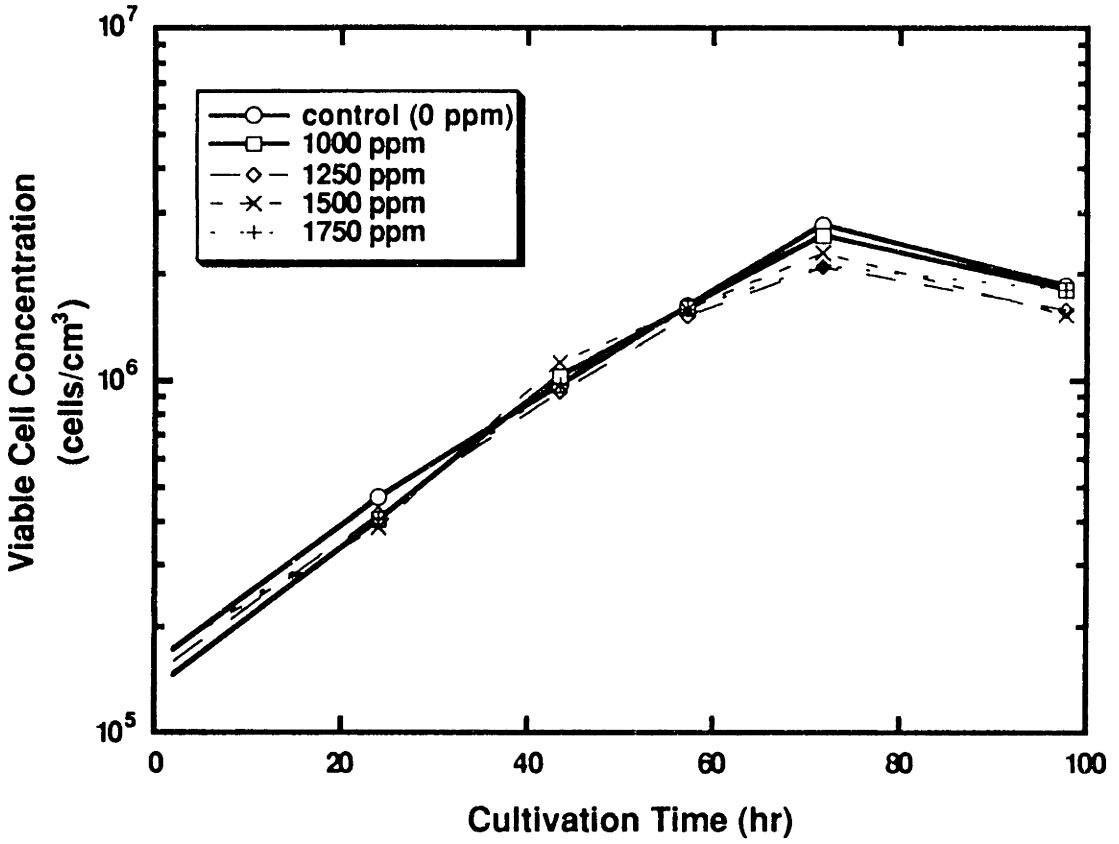

Figure 1.8 Effect of antifoam on cell growth (CRL-1606)

during the exponential phase was approximately 0.038 hr^{-1} (doubling time = 18 hours). Compared with the control, which contains no antifoam, there is no significant reduction in the cell growth with added antifoam up to 1750 ppm. The trends of glucose utilization and lactate production of the hybridoma cells in the presence of antifoam are essentially the same as those of the control as shown in Figures 1.9 and 1.10. The specific glucose uptake rate and lactate production rate in the exponential phase are 2.86×10^{-8} mg/cell/hr and 1.67×10^{-8} mg/cell/hr respectively. Figure 1.11 shows the cumulative production of anti-human fibronectin IgG at various antifoam concentrations. The production of IgG was not significantly affected as compared to the control. In conclusion, the specific IgG productivity in exponential phase is about 1.19×10^{-9} mg/cell/hr. The addition of medical emulsion C up to a concentration of 1750 ppm during the cultivation of hybridoma ATCC-CRL-1606 was not toxic to the cells and had no deleterious effect on the anti-human fibronectin IgG production.

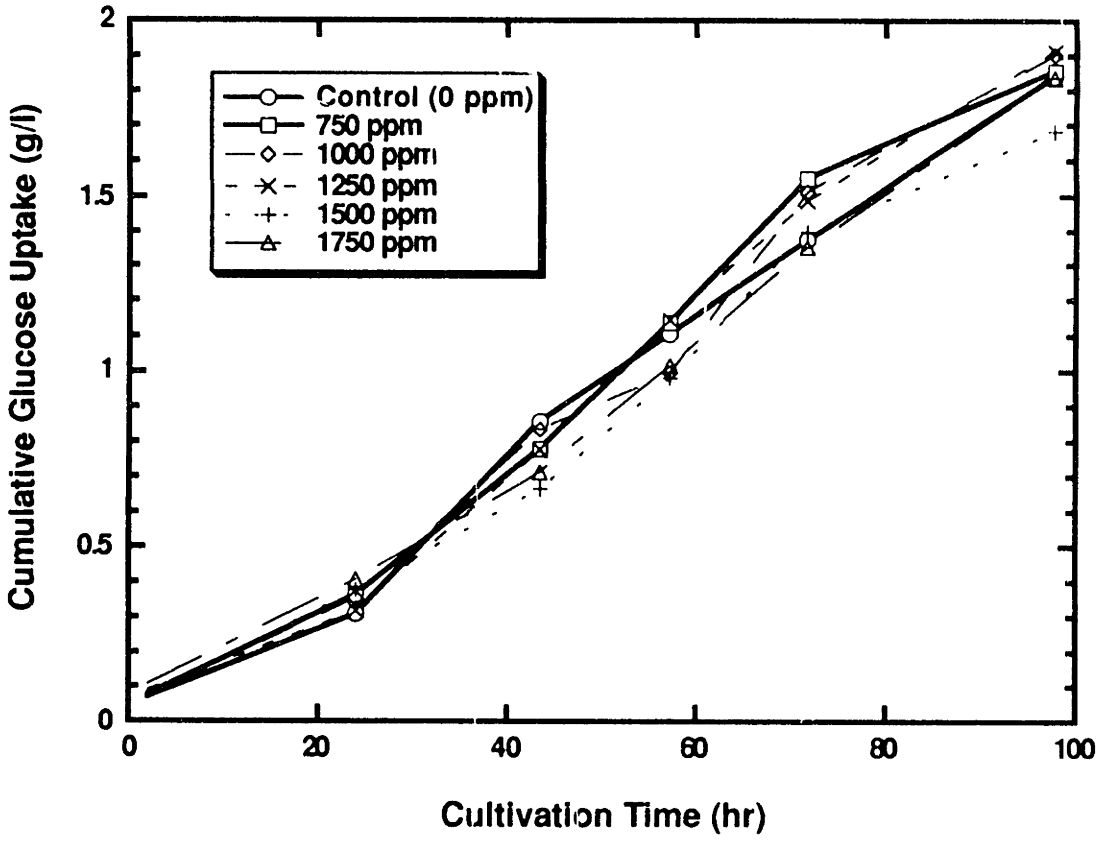

Figure 1.9 Effect of antifoam on glucose uptake (CRL-1606)

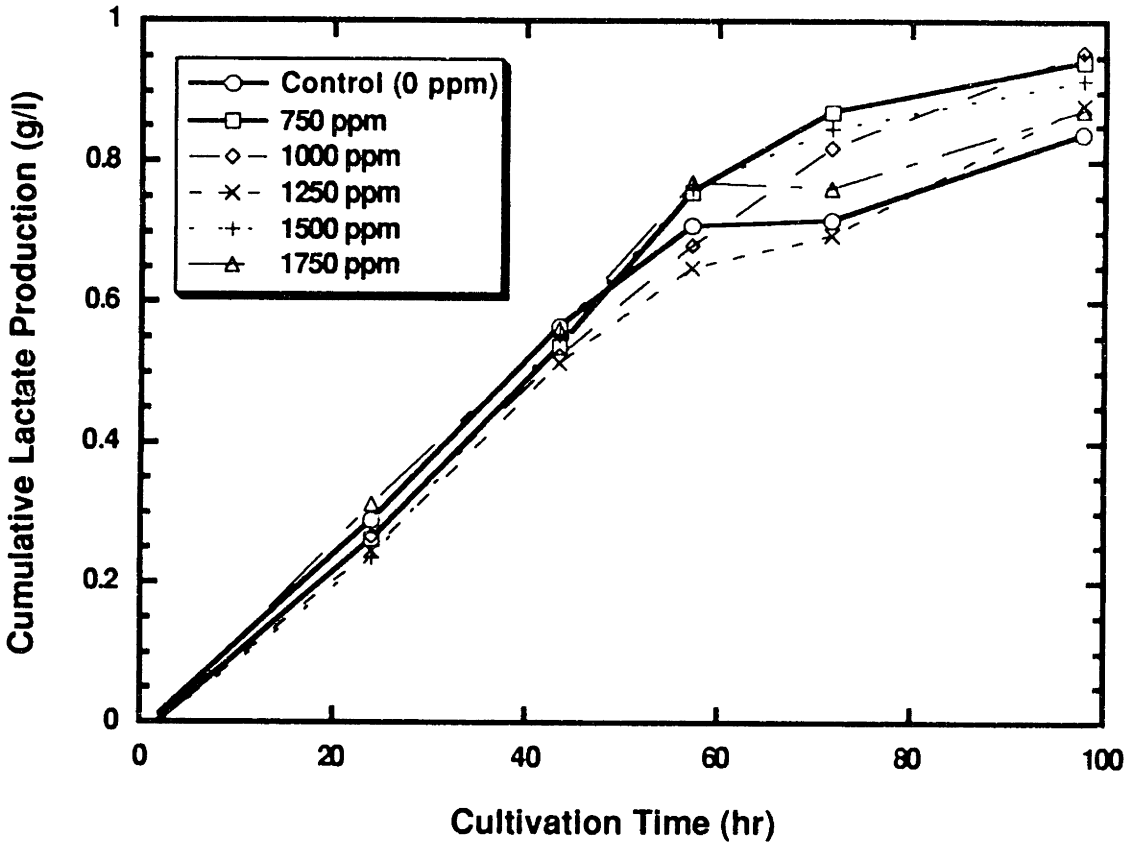

Figure 1.10 Effect of antifoam on lactate production (CRL-1606)

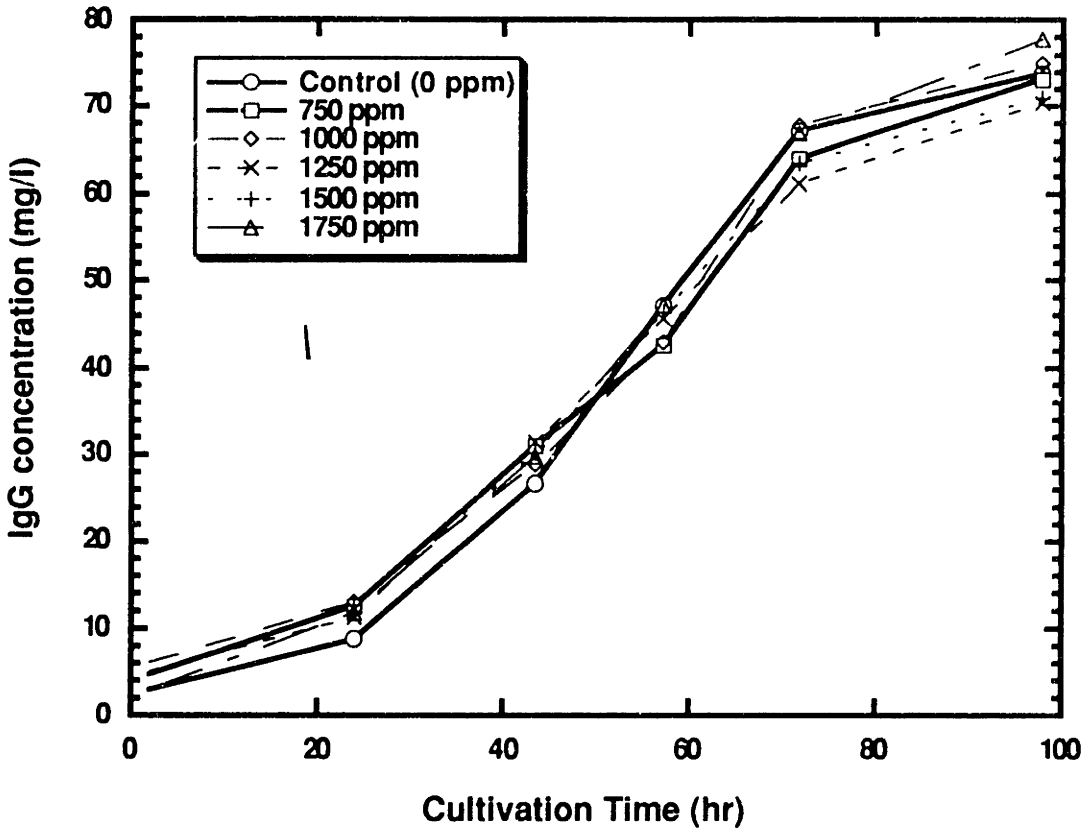

Figure 1.11 Effect of antifoam on IgG production (CRL-1606)

CHAPTER 2. A HYDRODYNAMIC MODEL

A model was proposed in Section III (Theoretical Analysis) to describe the hydrodynamics in the bioreactor. Liquid flow rate, mass transfer coefficient, oxygen transfer and the effect of permeability on oxygen transfer in the presence and absence of cells are considered in this chapter.

2.1 Liquid Flow Rate

Based on the momentum balance of driving force and the related resistance forces, such as the fiber bed hydrodynamic permeability as well as the bubble size, the liquid flow rate at various air flow rates and reactor geometry was obtained. The hydrodynamic permeability of the fiber bed, k, was calculated from pressure drop measurements and was found to be 2×10^{-5} cm^2. The calculated bubble size was about 0.08 cm in diameter. By using these two values, the liquid flow rate was predicted. Figure 2.1 shows the calculated and measured liquid flow rate at various ratios of draft tube diameter (Di) to reactor diameter (Do) and air flow rates. The theoretical calculations fit the experimental results quite well except at the lower Di/Do ratios. These differences are likely due to bubble coalescence and asymmetrical flow in the draft tube.

As shown in Figure 2.1, at a given air flow rate, the highest liquid flow rate was obtained at a Di/Do ratio ranging from 0.08 to 0.16. With the smaller Di/Do ratio, pressure drop in the draft tube reduces the liquid flow rate; and with the larger Di/Do ratio, reduction of gas hold up ultimately reflects the reduced liquid flow rate. Theoretically, the maximal liquid flow rate is shifted to the larger Di/Do ratio with increasing air flow rate. Compared

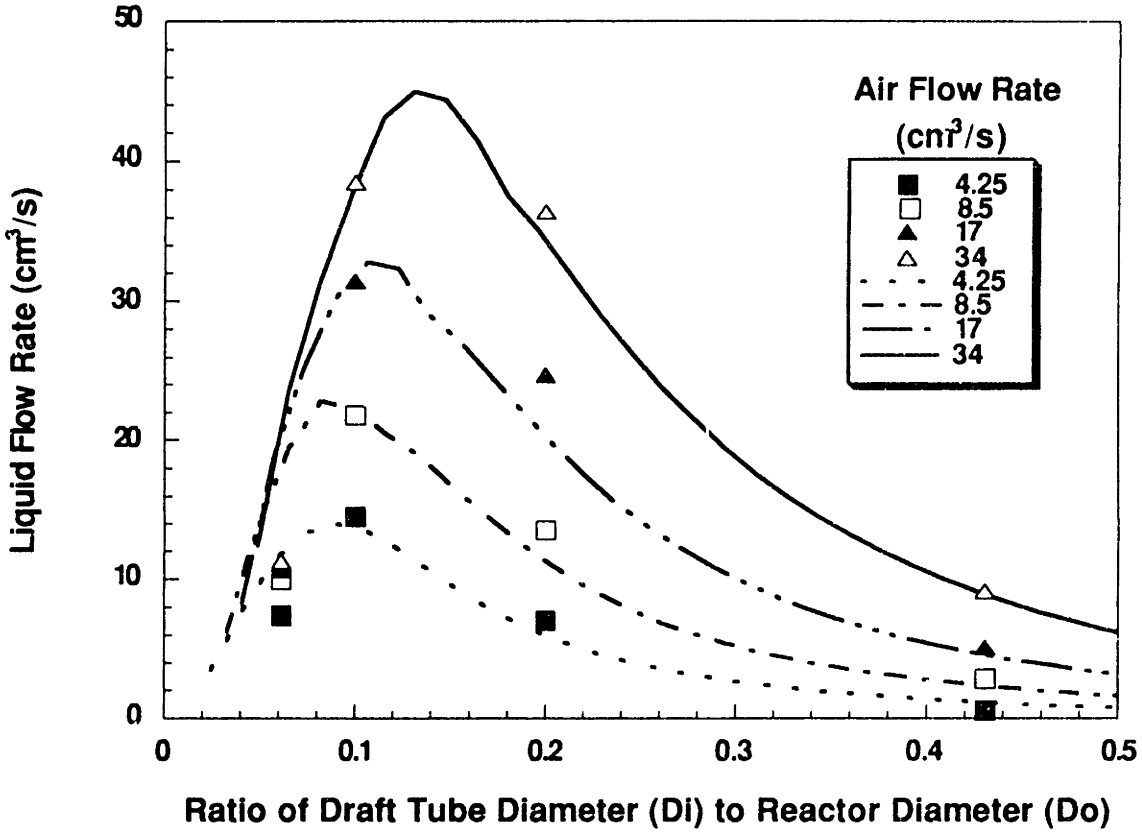

Figure 2.1 Liquid flow rate at various Di/Do ratios and air flow rates. Lines represent the calculated results and symbols represent the experimental results.

to the traditional airlift systems, which has no packing in the annular region, the liquid flow rate in our reactor is much lower due to the resistance from the packed glass fiber, and the optimal Di/Do ratio is much smaller than the optimal Di/Do ratio found in traditional airlift systems without packing (Wang *et al*, 1971; Jones, 1985).

2.2 Mass Transfer Coefficient

Figure 2.2 shows the calculated and measured volumetric mass transfer coefficient, k_la, at various Di/Do ratios and air flow rates. With the smaller Di/Do ratio, the measured values were greater than the calculated values. This is due to the effect of surface oxygenation, which was not included in the theoretical calculations. Unlike the liquid flow rate, the highest k_la was obtained with the largest draft tube diameter. The decrease in the liquid velocity in the case of the larger Di/Do ratio prolongs the residence time of the bubbles. Therefore, mass transfer from the bubbles to the liquid is enhanced.

2.3 Oxygen Transfer Rate

From the liquid flow rate and the mass transfer coefficient experiments, corroboration of the theoretical predictions with experimental results were confirmed: at least within the range of Di/Do ratios and air flow rates studied. Consequently, the oxygen transfer rate can be calculated by substituting the theoretical results from the liquid flow rates and the volumetric mass transfer coefficients into Equations III.15 to III.18.

Figure 2.3 shows the calculated reactor oxygen transfer rate versus Di/Do ratio at

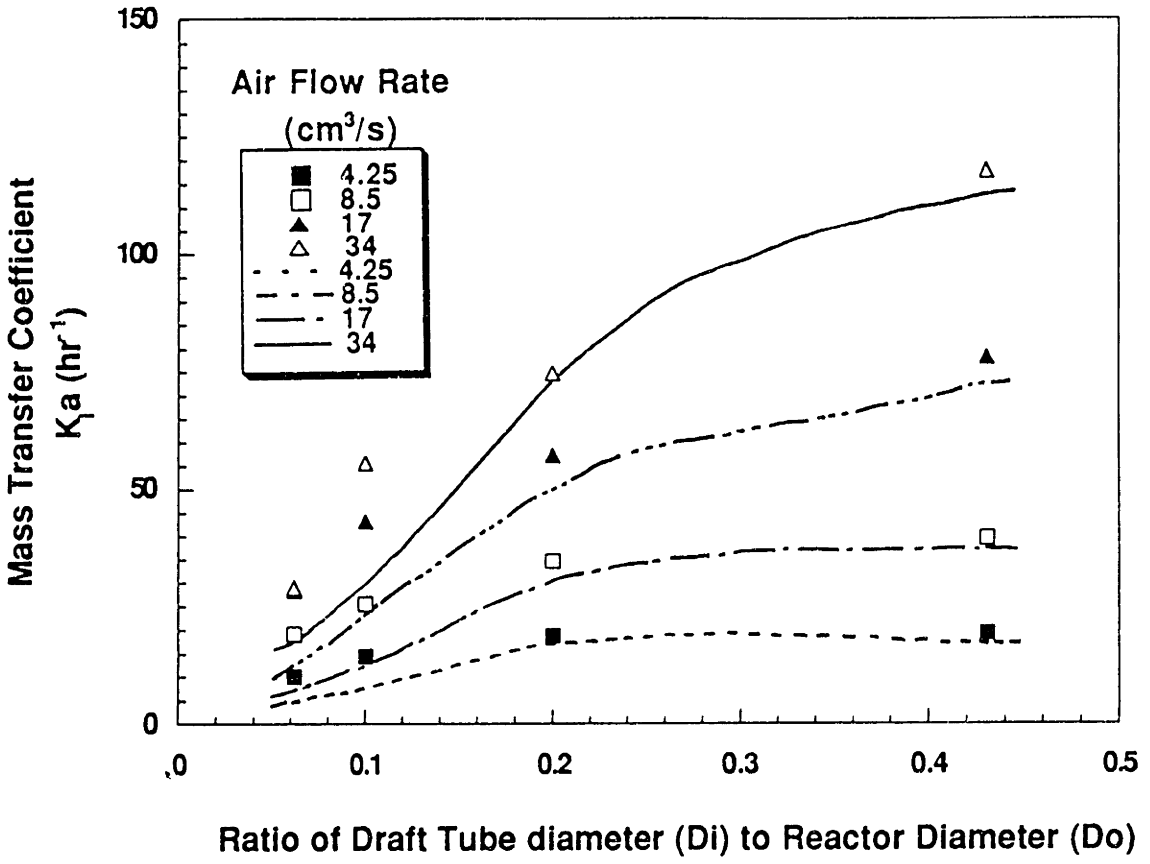

Figure 2.2 Volumetric mass transfer coefficient at various Di/Do ratios and air flow rates. Lines represent the calculated results and symbols represent the experimental results.

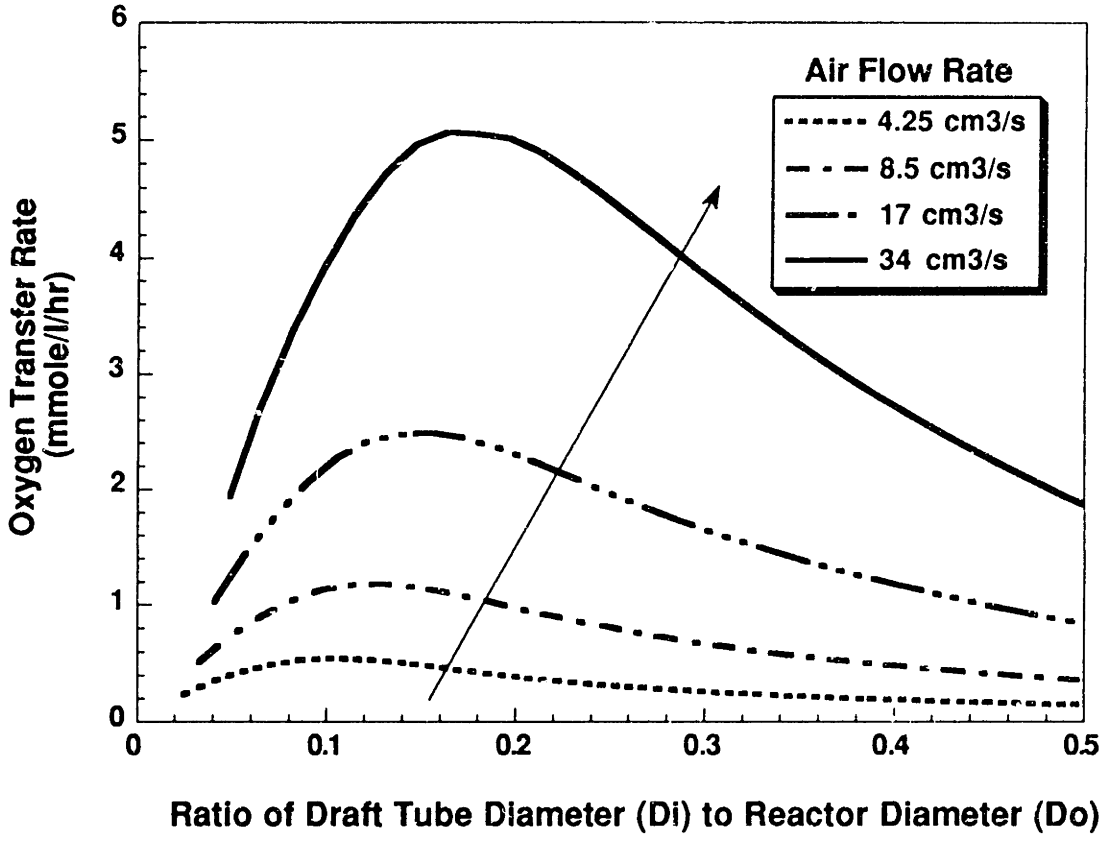

Figure 2.3 Effect of Di/Do on oxygen transfer rate at various air flow rates

various air flow rates. This figure graphically depicts that a distinctive maximum for the oxygen transfer rate was obtained for each air flow rate. This means that the highest oxygen transfer rate can be obtained at the optimal Di/Do ratio. Also seen in the figure is the shift of the optimal Di/Do to a higher value as the air flow rate is increased. The trend can clearly be seen by plotting the optimal Di/Do ratio versus air flow rate (Figure 2.4). The quantitative relationship between optimal Di/Do and air flow rate was found to be:

$$(Di/Do)_{opt} = 0.0797\ (Qg)^{0.219}. \qquad (2.1)$$

2.4 Effect of Permeability on Oxygen Transfer Rate

Figure 2.5 shows the effect of permeability of the fiber bed on the oxygen transfer rate at various Di/Do ratios and for a constant air flow rate of 51 cm^3/sec. The decrease in permeability led to a decrease in the oxygen transfer rate. This behavior is due to the coupling of permeability with hydrodynamic resistance. Decreasing permeability increases the hydrodynamic resistance of the fiber bed and thus decreases the liquid flow rate in the fiber-bed. Consequently, the oxygen transfer rate is also reduced. Figure 2.6 shows the relationship between the maximal oxygen transfer rate (max OTR) and the corresponding Di/Do ratio as a function of permeability. The optimal Di/Do ratio and maximal oxygen transfer rate increase as the permeability is increased, and the relationships are shown as:

$$\text{Max OTR} = 25.95 + 3.95 \log (k) \qquad (2.2)$$

$$\text{Opt Di/Do} = 0.734 + 0.113 \log (k) \qquad (2.3)$$

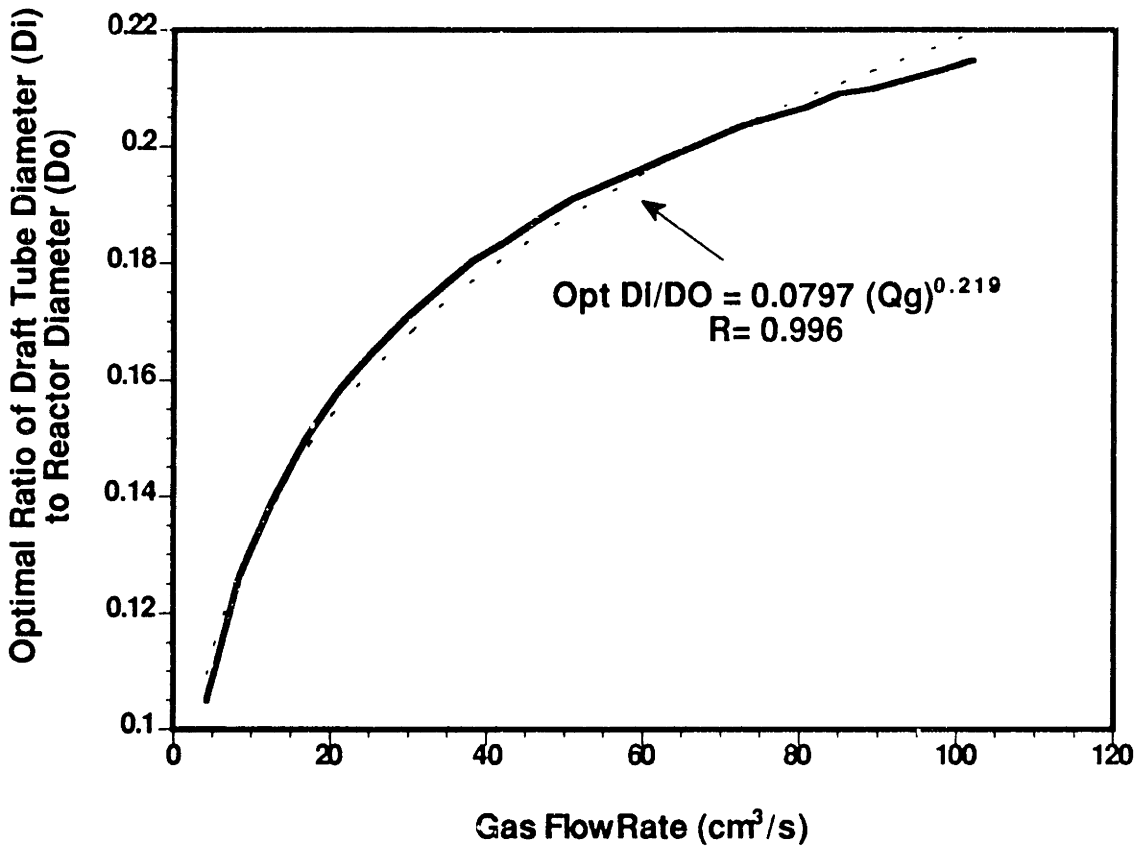

Figure 2.4 Optimal Di/Do at various air flow rates

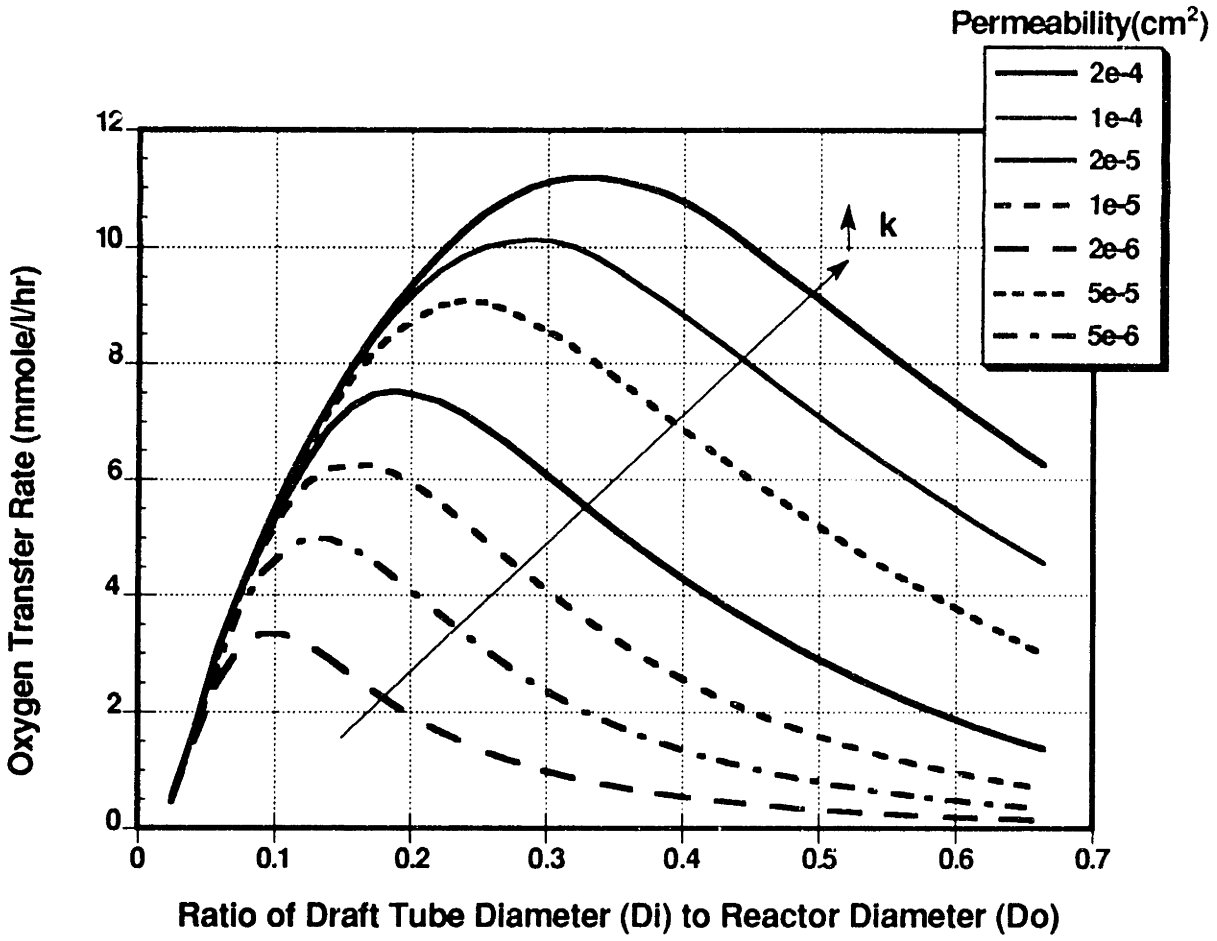

Figure 2.5 Effect of permeability on oxygen transfer rate

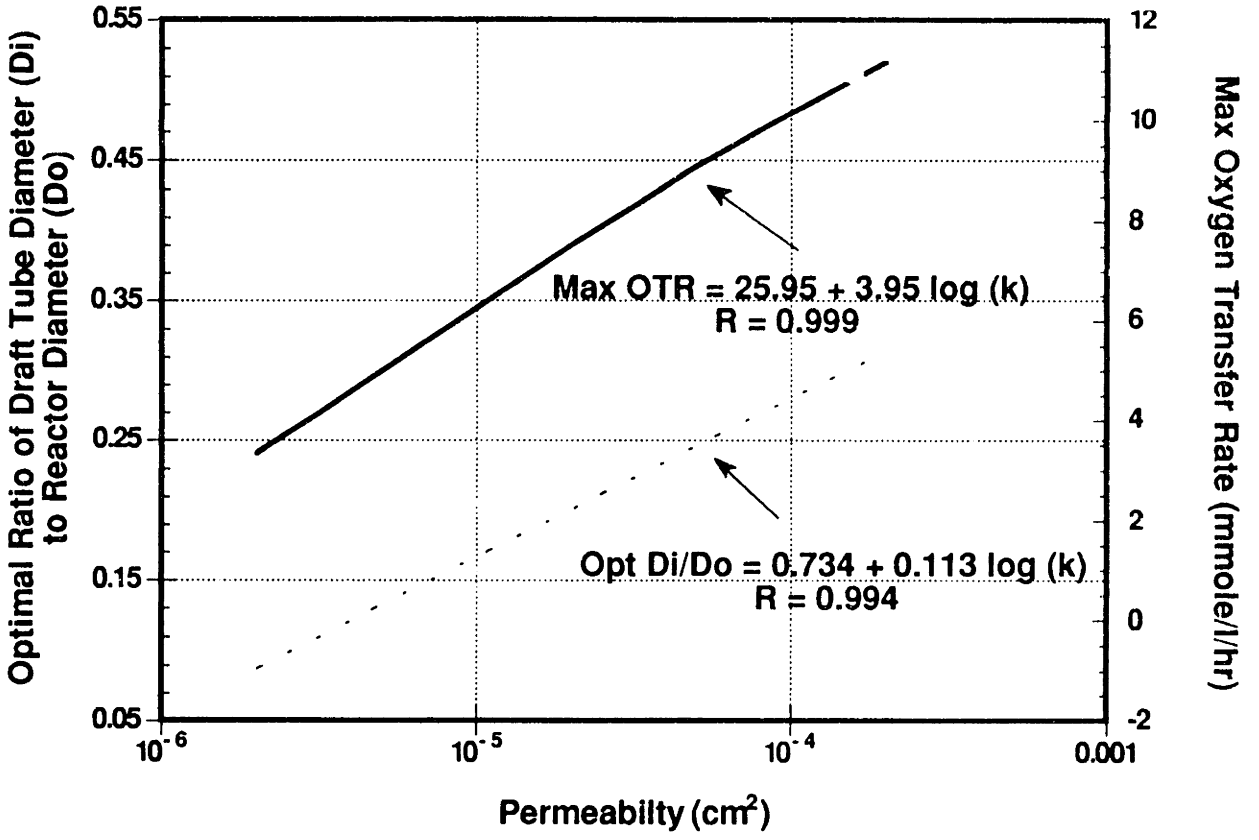

Figure 2.6 Effect of permeability on maximum oxygen transfer rate and optimal Di/Do ratio

Moreover, the hydrodynamic permeability determines the average shear stress in the fiber bed. The average shear stress (τ_{avg}) at the surface of the cells in the fiber-bed can be estimated by equating the viscous energy dissipation to the drag force on a fiber:

$$\tau_{avg} = \frac{F_D}{A_f} = -\frac{\Delta P}{Lo}\frac{1}{(S/V)} = \frac{\mu U_l \varepsilon_2}{k}\frac{d_f}{4(1-\varepsilon_2)} \qquad (2.4)$$

where F_D is the drag force; A_f, the surface area of fibers; ΔP, the pressure drop in the fiber-bed; Lo, the length of the bed; S/V, fiber surface-to-volume ratio of the reactor; μ, the liquid viscosity; U_l, the liquid velocity in the packed bed; ε_2, the void fraction of the packed bed; k, the permeability of the packed bed; and d_f, the diameter of fibers. As shown in Equation 2.4, the higher the permeability, the smaller the shear stress. Consequently, high permeability is desirable in order to reduce the shear stress experienced by the cells.

2.4.1 Permeability as a Function of Void Fraction, Fiber Diameter and Fiber Arrangement

In order to achieve high oxygen transfer and maintain low shear stress, an ideal fiber-bed in the annular region of the bioreactor should have a high permeability. The permeability is determined by void fraction, fiber diameter and fiber arrangement in the bed. In order to gain some useful information for the purpose of choosing the right fiber bed, the effect of void fraction and fiber diameter on permeability at various fiber arrangements were investigated.

Based on a model proposed by Spielman and Goren (1968), the dimensionless permeability (r^2/k) was used for this analysis. Figure 2.7 illustrates the relationship between dimensionless permeability and void fraction of the fiber bed for various arrangements. As seen in Figure 2.7, the dimensionless permeability is influenced by the fiber arrangement. The arrangement does not significantly affect the permeability at very high void fraction; whereas, at low void fraction, the permeability is heavily dependent on the fiber arrangement. For the highest permeability, the arrangement of all fibers parallel to the direction of flow is favored; for the lowest permeability, the arrangement of all fibers perpendicular to the direction of flow should be chosen. The random and alignment arrangements result in intermediate permeabilities.

Fiber diameter is also important in determining the permeability. For a constant void fraction, permeability is inversely proportional to the square of the fiber diameter. Figures 2.8 to 2.11 show the permeability at various fiber diameters, ranging from 12 to 200 μm, for each fiber arrangement. For each packing, the larger the fiber diameter, the greater the permeability. This is because at the same void fraction, specific surface area decreases as the fiber diameter increases. Consequently, larger fiber diameter results in a lower resistance which provides a higher permeability.

These results can be used for choosing the bed with a desired initial permeability. This is dependent on the fiber diameter, void fraction, and fiber arrangement. For example, both the 0.8 voidage, 200μm fiber and Case 3 packing and the 0.94 voidage, 100 μm fiber and Case 1 packing led to the same permeability of 10^{-4} cm^2. The high permeability can be achieved by choosing smaller fibers and higher void fraction (under the same surface to volume ratio), and the proper fiber arrangement. The fibers parallel to the flow would lead to high permeability and fibers normal to the flow lead to lower permeability.

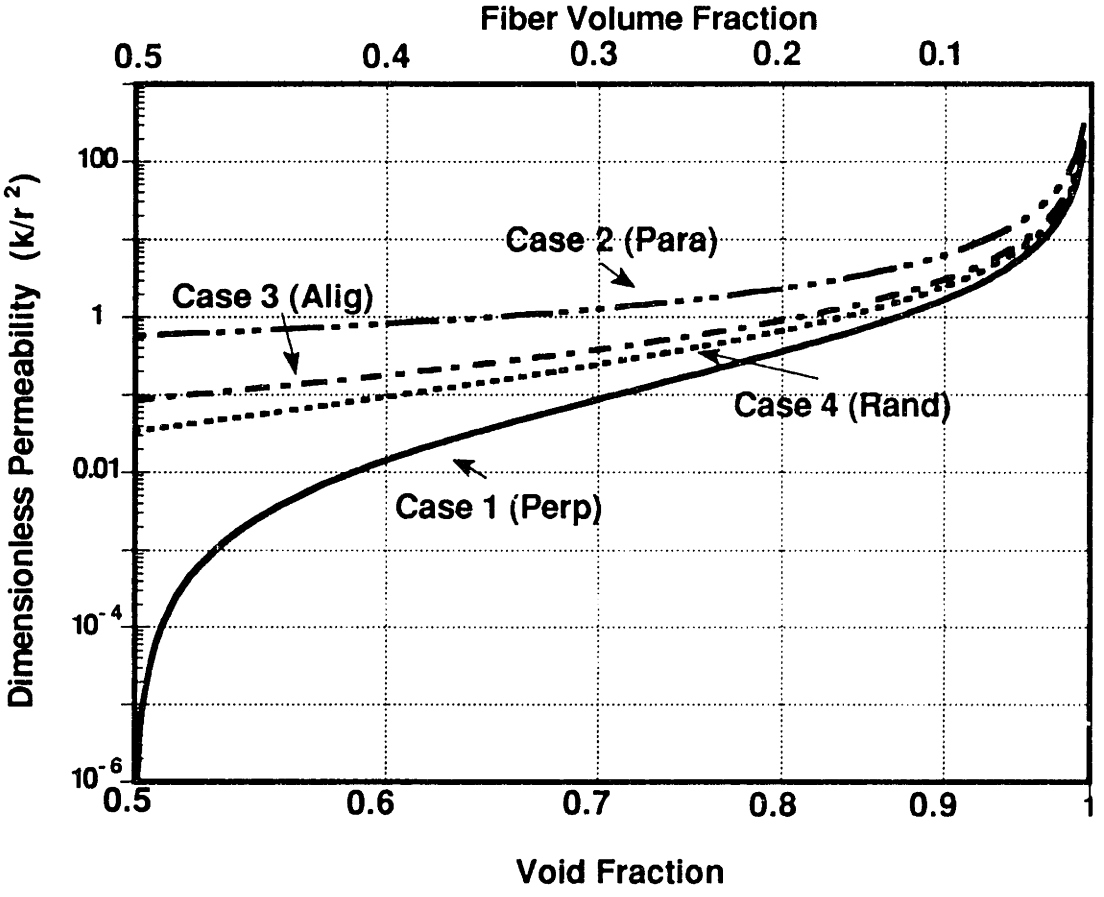

Figure 2.7 Dimensionless permeability versus void fraction for various fiber arrangements

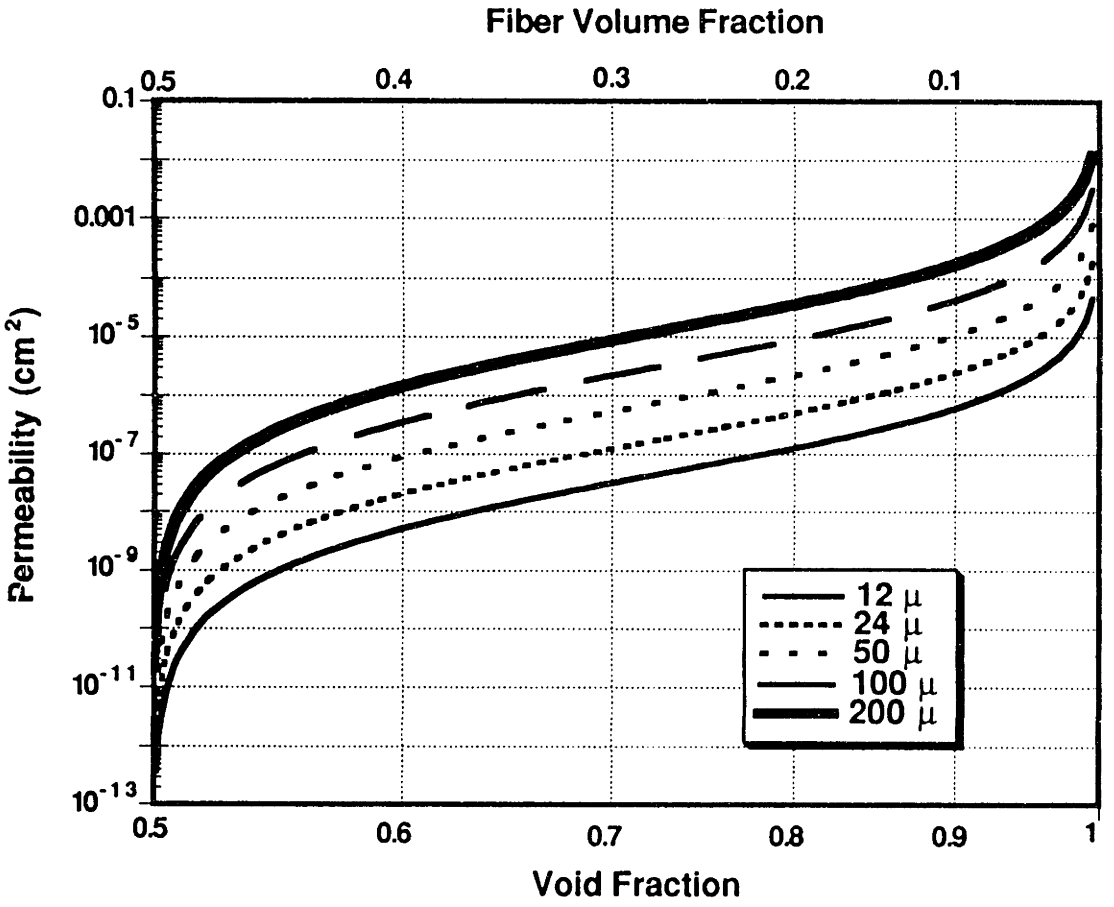

Figure 2.8 Effect of void fraction on permeability at various fiber diameters - Case 1 (perp)

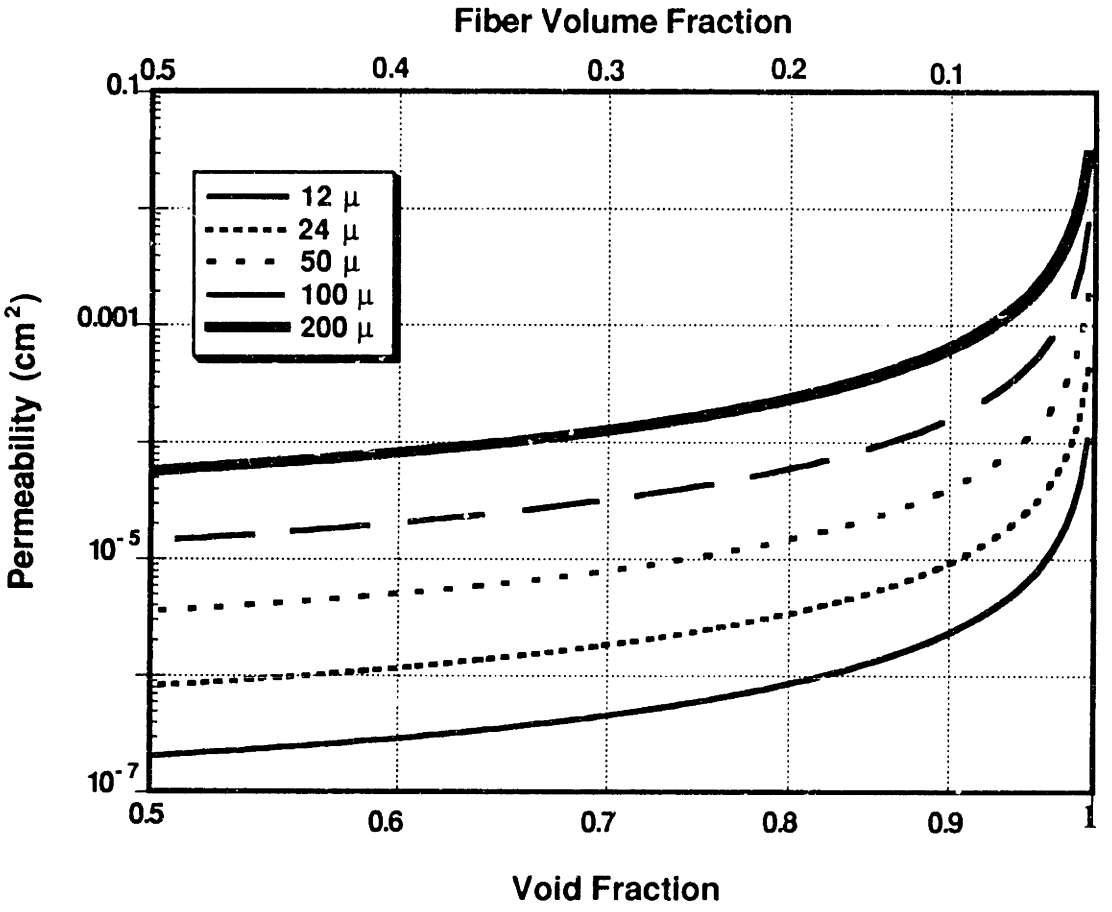

Figure 2.9 Effect of void fraction on permeability at various fiber diameters - Case 2 (para)

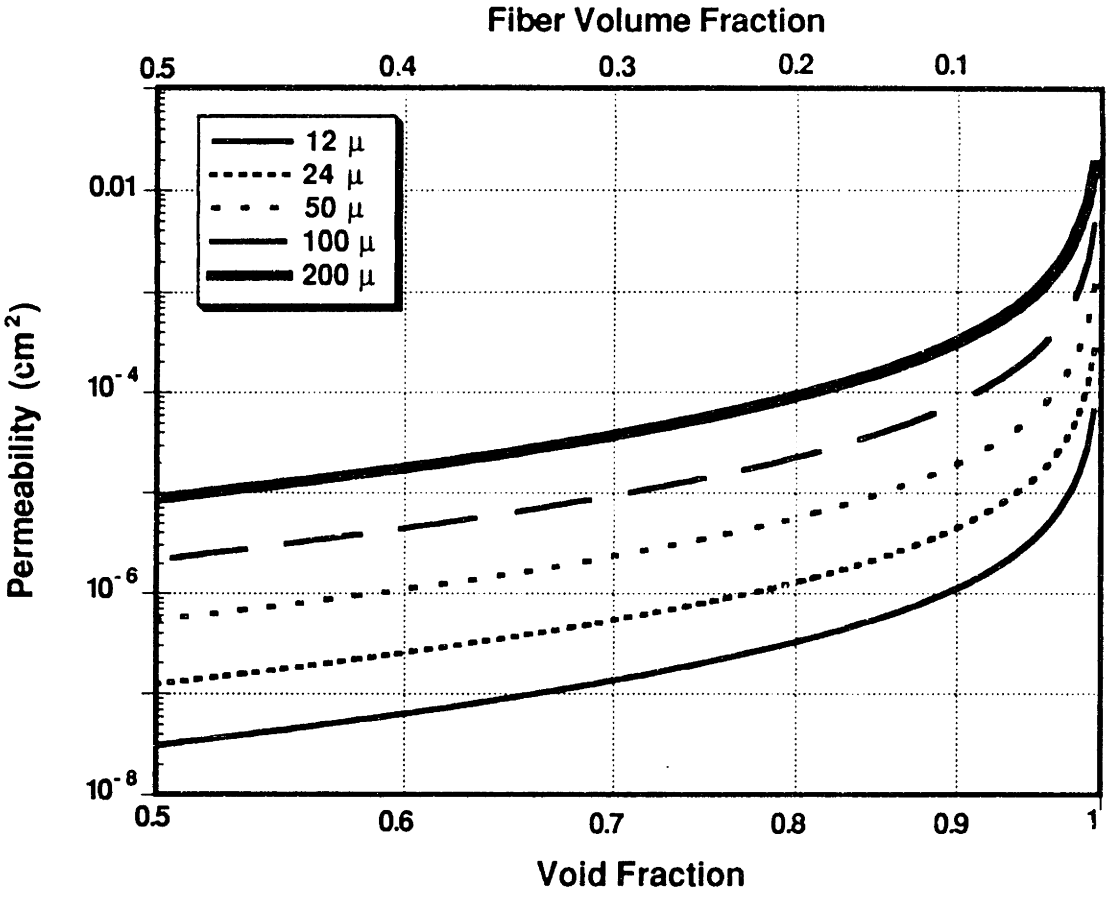

Figure 2.10 Effect of void fraction on permeability at various fiber diameters - Case 3 (alig)

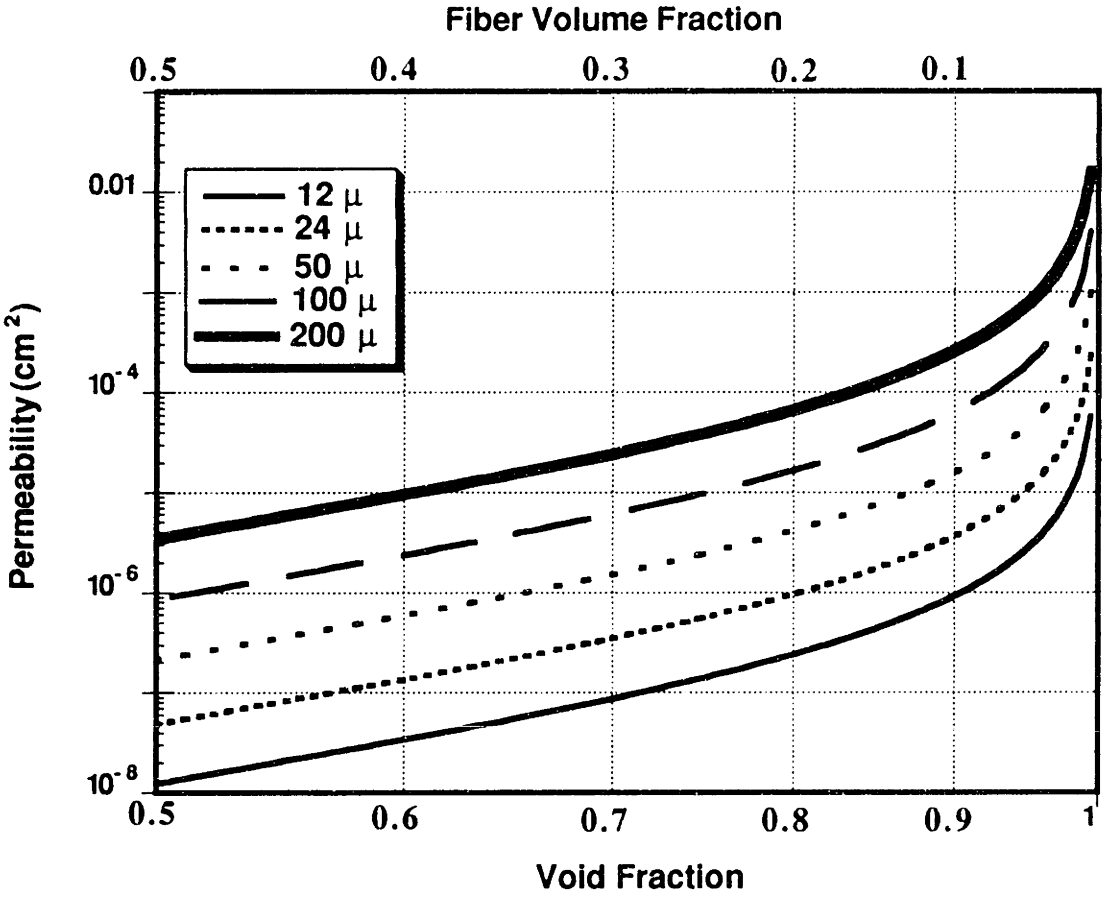

Figure 2.11 Effect of void fraction on permeability at various fiber diameters - Case 4 (rand)

The experimental data for both kinds of packing of chopped glass fibers compare very well with theoretical data, as shown in Table 2.1. However, the packing of layers of fiber mat resulted in permeability one order of magnitude higher than those of chopped fibers. This is probably due to the inhomogeneity of the fiber structure. Since fiber mat was used for all the other experiments, a permeability of 2×10^{-5} cm^2 was used for the fiber bed without cells throughout the study unless otherwise stated.

2.4.2 Effect of Cell Growth on Permeability

During cell cultivation, the accumulation of cell mass will change both the void fraction and the "apparent" fiber diameter. Consequently, the permeability of the fiber bed is expected to change during the cultivation process. A model to assess the effect of cell growth on permeability was developed by assuming that the square root of the hydrodynamic permeability is a characteristic channel radius. In other words, a decrease of the channel radius of a porous bed by a factor of x would lead to a decrease in the permeability by a factor of x^2. The change of the channel radius is due to multilayer cell growth and this was considered in order to establish the model.

At various times of cultivation, photomicrographs of cells showed that both γ-CHO and CRL-1606 cells anchored on the glass fibers and formed multilayers in the fiber bed. Some typical photomicrographs shown in Figure 2.12 illustrates the progression of cell growth on the fibers. Figure 2.12 (a) shows γ-CHO cells at a cell density of 1×10^7 cells/cm^3, yielding about 85% monolayer confluency. Figure 2.12 (b) shows γ-CHO cells

Table 2.1 Comparison between theoretical and experimental values

Type of Packing*	Theoretical k/r^2	Theorectical k(cm2)	Measured k(cm2)
Type a) Perpendicular, chopped fibers	2.05	2.95×10^{-6}	4×10^{-6}
Type b) Random, chopped fibers	2.99	4.30×10^{-6}	5×10^{-6}
Type c) Layers of mat			2×10^{-5}

*The fibers used were all 24 μ in diameter, and the void fractions were 91.5%.

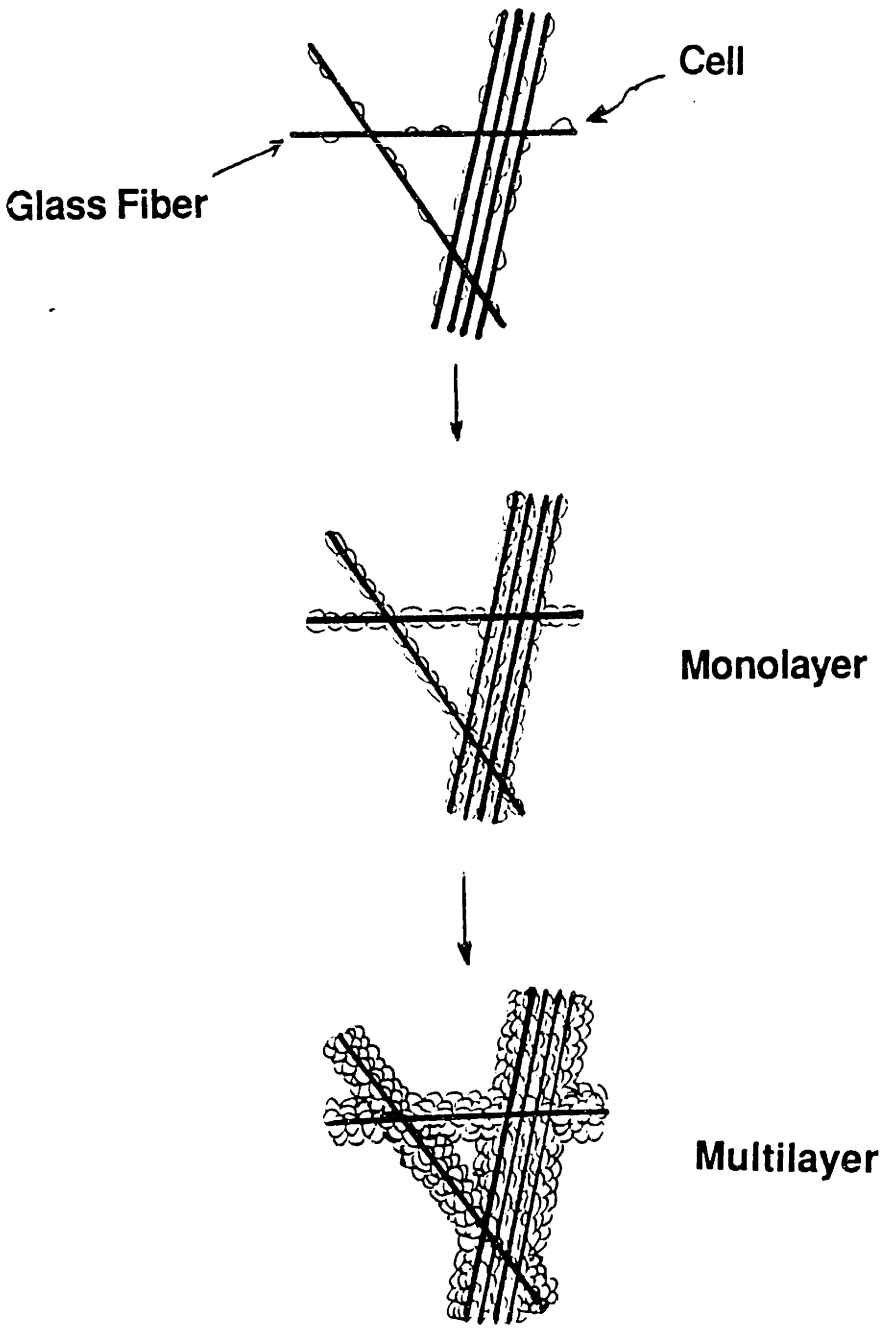

Figure 2.12 The progression of cell growth on the glass fibers

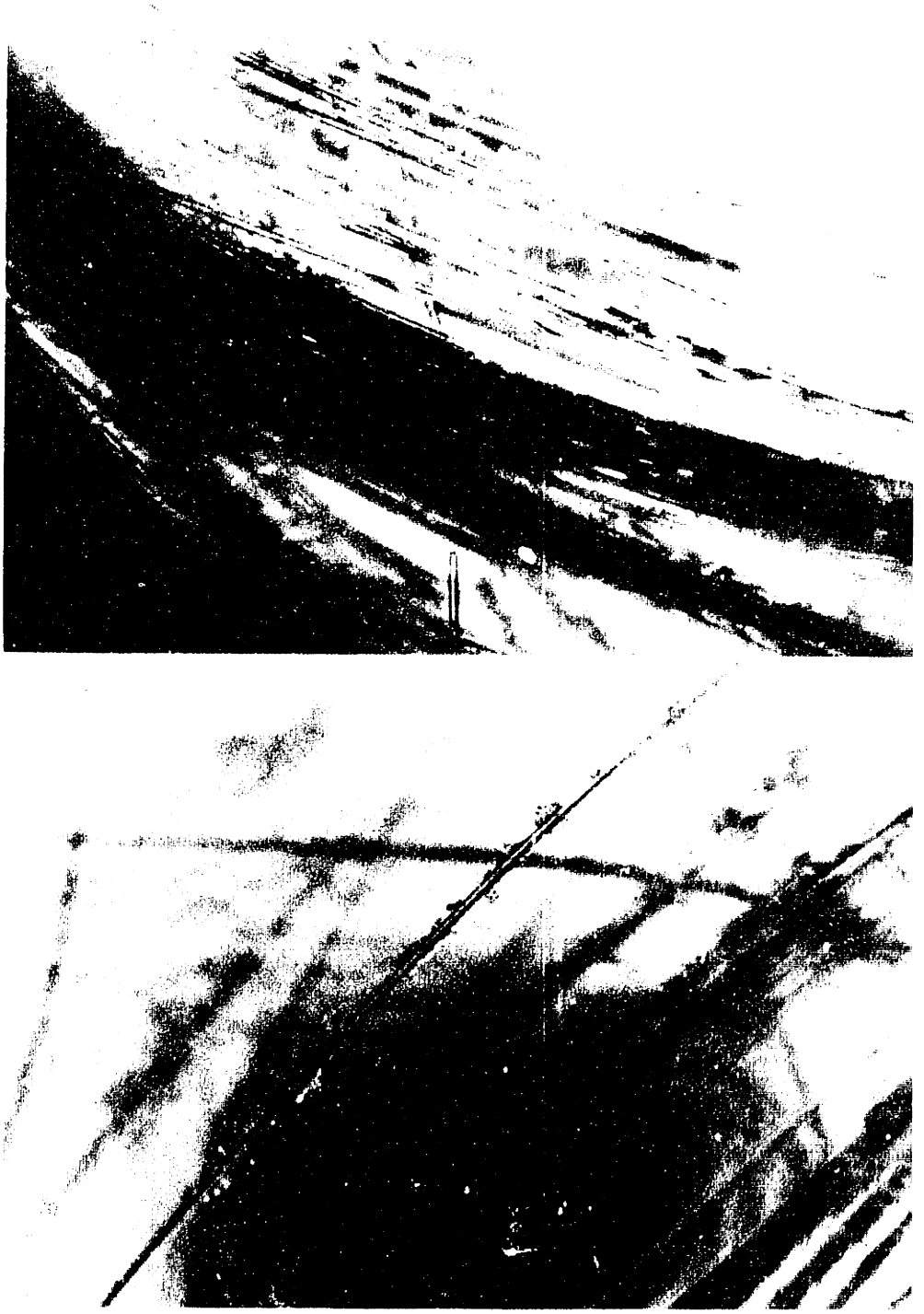

Figure 2.12 The progression of cell growth on the glass fibers (a) 1.2×10^7 cells/cm^3 of γ CHO

Figure 2.12 The progression of cell growth on the glass fibers
(b) 5.6×10^7 cells/cm^3 of γ-CHO

at a cell density of $5.6x10^7$ cells/cm^3, exhibiting the formation of multilayers of cells on the glass fibers. Figure 2.12 (c) shows CRL-1606 cells at a cell density of $6.7x10^7$ cells/cm^3, also exhibiting multilayer growth on the glass fibers.

These microphotographs illustrate the growth of the cells onto the fibers, effectively increasing the apparent fiber diameter and leading to a decrease in the channel size. From Equations III.23 to III.30 of the model, the number of layers, normalized radius and normalized permeability as a function of cell density may be calculated. These results are presented in Figures 2.13, 2.14 and 2.15. The thick solid lines in the figures represent the calculated results for γ–CHO cells and the dashed lines show the results for Type B close-packing of hybridoma cells and thin solid lines are for Type A close-packing of hybridoma cells. The cell density versus the number of layers is shown in Figure 2.13. Compared to hybridoma cells, γ–CHO cells build up more layers for the same cell density. This is because γ–CHO cells are larger and require a greater contact area.

For hybridoma cells, the cell arrangement in each plane is first considered. It is obvious that the arrangement in Figure III.1b is more closely packed than that in Figure III.1a. The former is the most desirable arrangement of the cell packing. However, the type of packing did not significantly affect the layer number. Although the Type B close-packing led to smaller layer number, the two lines are almost identical as seen in Figure 2.13. Based on the model, about 4 layers of cells would build up on the glass fibers for a cell density of $5.6x10^7$ γ-CHO cells/cm^3. This is consistent with what was observed from the microphotographs. For hybridoma cells at $2.4x10^8$ cells/cm^3, about 3.7 layers was calculated using the model, and this is again consistent with the experimentally observed value.

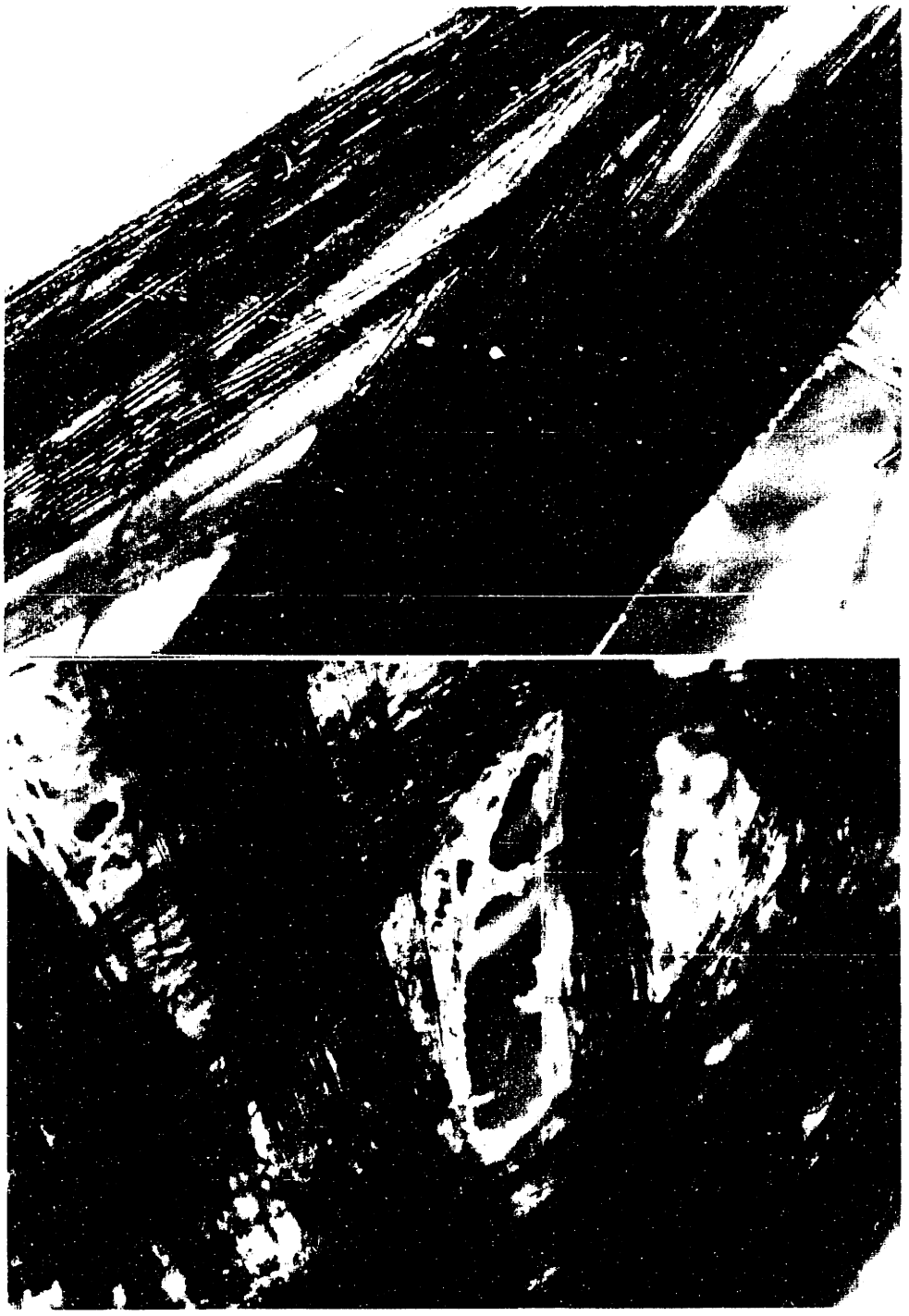

Figure 2.12 The progression of cell growth on the glass fibers (c) 6.1×10^7 cells/cm^3 of CRL-1606

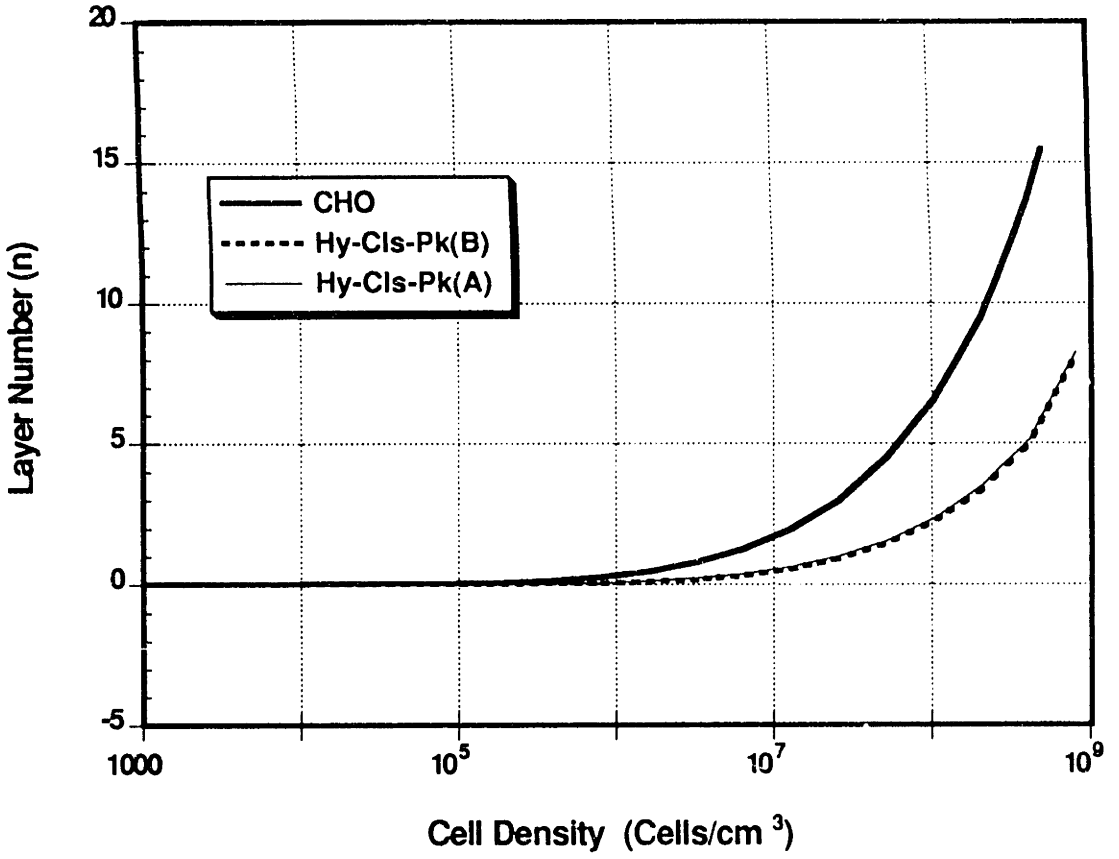

Figure 2.13 Layer number versus cell density

(Hy-Cls-Pk(B): Calculated data based on Type B close packing of hybridoma cells;
Hy-Cls-Pk(A): Calculated data based on Type A close packing of hybridoma cells)

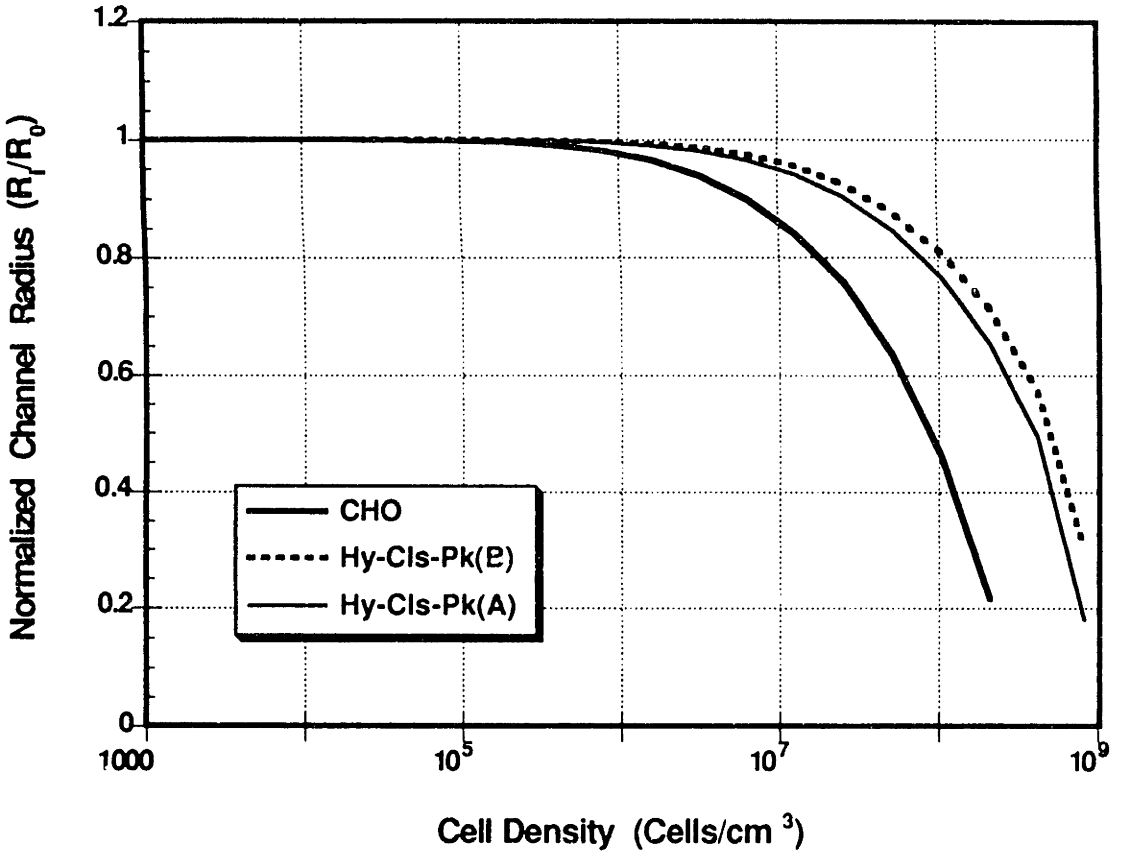

Figure 2.14 Effect of cell density on channel radius

(Hy-Cls-Pk(B): Calculated data based on Type B close packing of hybridoma cells;
Hy-Cls-Pk(A): Calculated data based on Type A close packing of hybridoma cells)

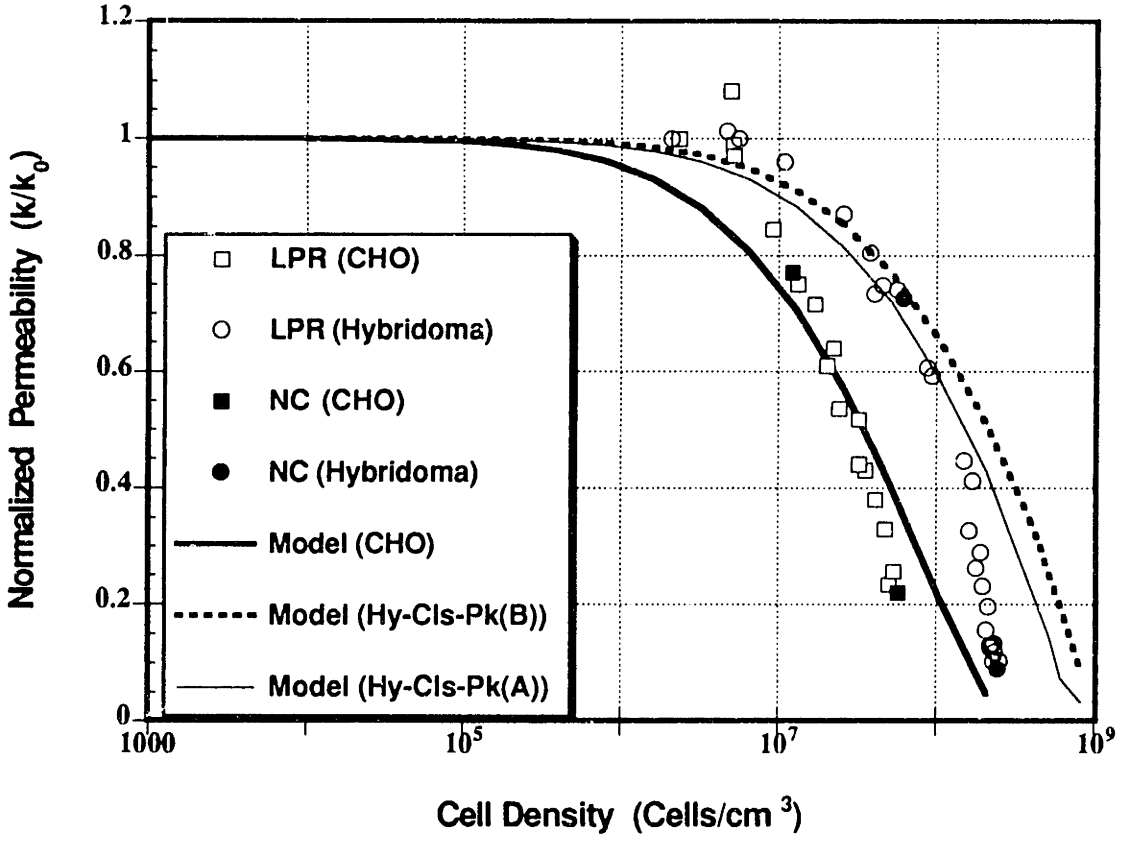

Figure 2.15 Effect of cell growth on permeability

(LPR: Experimental data obtained from lactate production rate;
NC: Experimental data obtained from nuclei counts;
Hy-Cls-Pk: Calculated data based on close packing of hybridoma cells)

Figure 2.14 illustrates the effect of cell density on the normalized channel radius. A cell density of about $2x10^8$ γ-CHO cells/cm^3 was required to reduce the channel radius 80 % of its original value, whereas nearly 10^9 cells/cm^3 of hybridoma cells were required to cause the same effect. The channel radius of Type B close-packing did not change as rapidly as Type A because of the smaller layer number for a given cell density.

Shown in Figure 2.15 is the effect of cell density on the permeability. The lines represent the theoretical values while the square and circle symbols represent the experimental data. The measured permeability of a fiber-bed without cells (k_0) was $2x10^{-5}$ cm^2. The solid symbols are the cell densities obtained from nuclei counts after each cell cultivation experiment and the open symbols are the calculated cell density derived from lactate production rate. It was found that during the initial cell growth, the permeability did not change significantly but does exhibit dramatic decreases at high cell density. The critical cell density before the permeability is affected appears to be $1x10^7$ cells/cm^3. The experimental data showed the same trends predicted from the theory. Some experimental data are also shown in Table 2.2. For γ–CHO cells, when the cell density reached $1.2x10^7$ cells/cm^3 and $5.6x10^7$ cells/cm^3, the permeability decreased to 77% and 21% of its initial value respectively. The corresponding channel radius decreased to 88% and 46% of the initial channel radius respectively. For CRL-1606, as the cell density increased to $6.1x10^7$ and $2.4x10^8$ cells/cm^3, the permeability decreased to 73% and 9% of the initial value, and the channel radii were reduced to 85% and 30% of the initial value correspondingly. As seen in Figure 2.15, the experimental data matched the model predictions quite well. The greater deviations were observed at the higher cell densities.

Table 2.2 Estimation of cells within reactor through permeability studies

Cell Line	Cell Number* (cells/cm^3)	Void	Calculated number of layers	Expt k/ko	Ri/Ro
γ-CHO	0	0.915	0	1	1
	1.2×10^7	0.89	1.9	0.77	0.88
	5.6×10^7	0.81	4.7	0.21	0.46
Hybridoma	0	0.915	0	1	1
	6.1×10^7	0.85	1.6(Type B); 1.7(Type A)	0.73	0.85
	2.4×10^8	0.69	3.7(Type B); 3.8(Type A)	0.09	0.30

* The cell number was obtained from nuclei counting.

Since the permeability is a function of cell density and permeability affects the maximal oxygen transfer rate, one can anticipate that the maximal oxygen transfer rate will vary as cell cultivation progresses. Increase in the cell density is expected to cause reductions in the maximal achievable oxygen transfer rate. A draft tube of 1.9 cm diameter and at a Di/Do of 0.15 was used for further cell cultivation experiments to demonstrate the feasibility of this bioreactor. Specifically, the experiments were performed to confirm the maximum oxygen transfer rate at the final stage of the cell cultivation. Although this draft tube diameter is sub-optimal during the initial phases of cell growth when the permeability is high, it provides higher oxygen transfer rate at the end of the cell cultivation when the permeability of fiber bed is low.

CHAPTER 3. OPERATIONS AND TECHNICAL FEASIBILITY

3.1 Entrapment Kinetics

Mechanistically, the fiber bed can immobilize cells through cell adhesion and at the same time can act as a depth filter to entrap the cells. Hence, our bioreactor can be used to immobilize both anchorage-dependent and suspension cells and therefore can be effectively operated in a perfusion mode for both types of cells.

Many studies have been conducted on entrapped suspension cells and their cultivation in packed beds (Ramirez and Mutharasan, 1989; Ramirez *et al.*, 1987; Marcipar, *et al.*, 1983). The void fractions and liquid flow rates employed were all much lower than those used in our fiber-bed reactor. Previously reported void fractions were typically 40 to 60 %, and the liquid velocity used were at least one order of magnitude lower than those achievable in our reactor system. In order to test our hypothesis on the entrapment of cells by the fiber-bed, the kinetics of cell entrapment by the fiber bed were studied.

Cell entrapment kinetics onto the fiber bed were examined by a single-pass experiment. As shown in Figure 3.1, only 33% of the input cells appeared at the outlet following a single-pass through the column. In the fiber-packed columns, the trapped cells were found to distribute in a descending manner; the retained cell concentrations in each fiber-packed column (from top to bottom) were 21%, 16%, 15%, 6%, and 10% of the inoculum. This indicates that the inoculation procedure needs more than one cycle in order to obtain a more complete entrapment of the cells in the fiber bed. Furthermore, if multiple passes are used during inoculation, the fraction of cell entrapped per pass can be expected to be lower. If we assume that the cell entrapment kinetics are concentration dependent, a

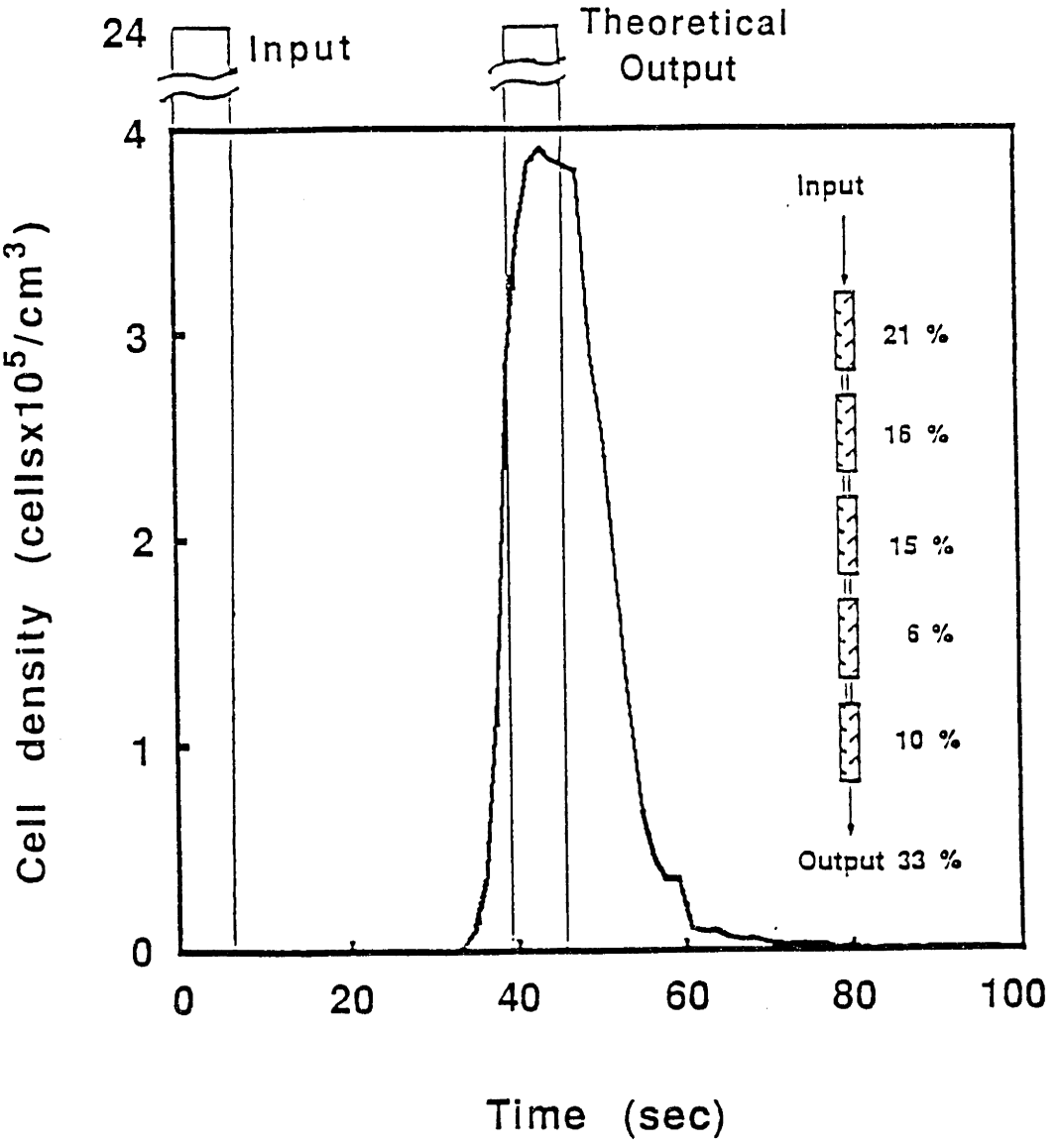

Figure 3.1 Single-pass entrapment of cells by the packed fiber bed

higher flow rate using multiple passes would allow a more even cell distribution within the different sections of the glass fiber packed bed. In addition, because the liquid flow in the reactor is driven by the gas flow, the cells are subject to bubble damage before their entrapment by the fiber bed. As a result, a shorter duration for inoculation is preferred to reduce the time period for the contact between gas bubbles and the cells. This analysis would therefore favor increased flow rate and using multipasses for inoculation.

An inoculation procedure which utilized a higher liquid flow rate and multiple cycles was therefore designed. Inoculation was achieved by introducing a cell suspension at the top of the reactor. This was followed by gas sparging at 0.5 VVM (corresponding to a liquid flow rate of 40 cm^3/sec) for 5 minutes and 0.05 VVM (corresponding to a liquid flow rate of 4 cm^3/sec) for the remainder of one hour in order to distribute the cells more uniformly within the entire fiber-bed. The cell concentration in the solution during this inoculation procedure was closely monitored. Figure 3.2 shows the cell concentration in the solution as a function of time. As shown in Figure 3.2, the cell concentration decreased from 1.5×10^6 cells/ml to about 4×10^3 cells/ml within 20 minutes, which corresponds to greater than 99 % of the inoculum entrapped in the fiber-bed.

An analysis of the data in Figure 3.2 allows one to assess the collection efficiency of the fiber bed for cell inoculation. If one assumes that when a cell once entrapped does not leave the fiber, a model to depict this phenomenon can be proposed. The average collection efficiency (E) per cycle at a given liquid flow rate can be estimated using the following equation:

$$C_n/C_0 = (1-E)^n \qquad (3.1)$$

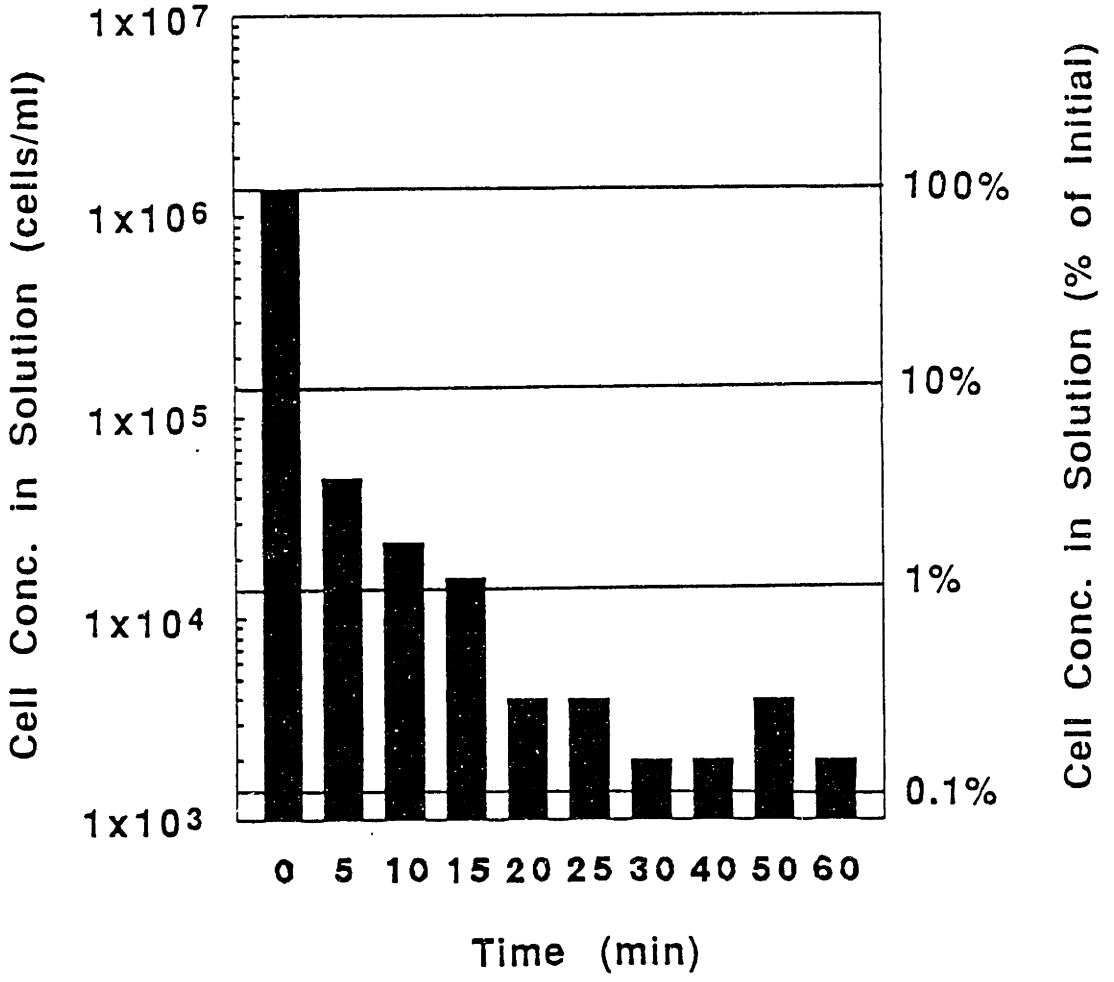

Figure 3.2 Kinetics of inoculum entrapment of suspension cells (CRL-1606)

where C_n is the free cell concentration in the solution after n cycles, C_0 is the initial free cell concentration in the solution, and n is the number of recirculation cycles. Under the experimental conditions, n is approximately equal to 11, and the calculated average collection efficiency is about 72% at each pass. This analysis and the model could prove useful for scale-up system during inoculation.

The cell distribution after the inoculation for CRL-1606 cells is shown in Figure 3.3. There is a slight descending distribution of the cells from the top to the bottom of the fiber bed. The difference between the top and the bottom is only about 30%.

Using this inoculation procedure, a continuous/perfusion cell cultivation was then initiated to cultivate anchorage-dependent and suspension cells. The methodology and control strategy employed were very similar for both types of cells and data obtained from the cell cultivation experiments are presented in the next section.

3.2 Cultivating Anchorage-Dependent Cells

For anchorage-dependent cells, γ-CHO cells were used in the experiments. The inoculum used was 3.6×10^8 cells per reactor, which is about 2.5 % of the calculated cell density at a monolayer confluency (1×10^5 cells/cm^2) in the fiber-bed. The packed bed operation was then commenced and the results of this study are presented below.

Figure 3.4 shows the gas flow rate and antifoam addition and requirement versus cultivation time. Gas flow rate was controlled in order to meet the oxygen demand of the

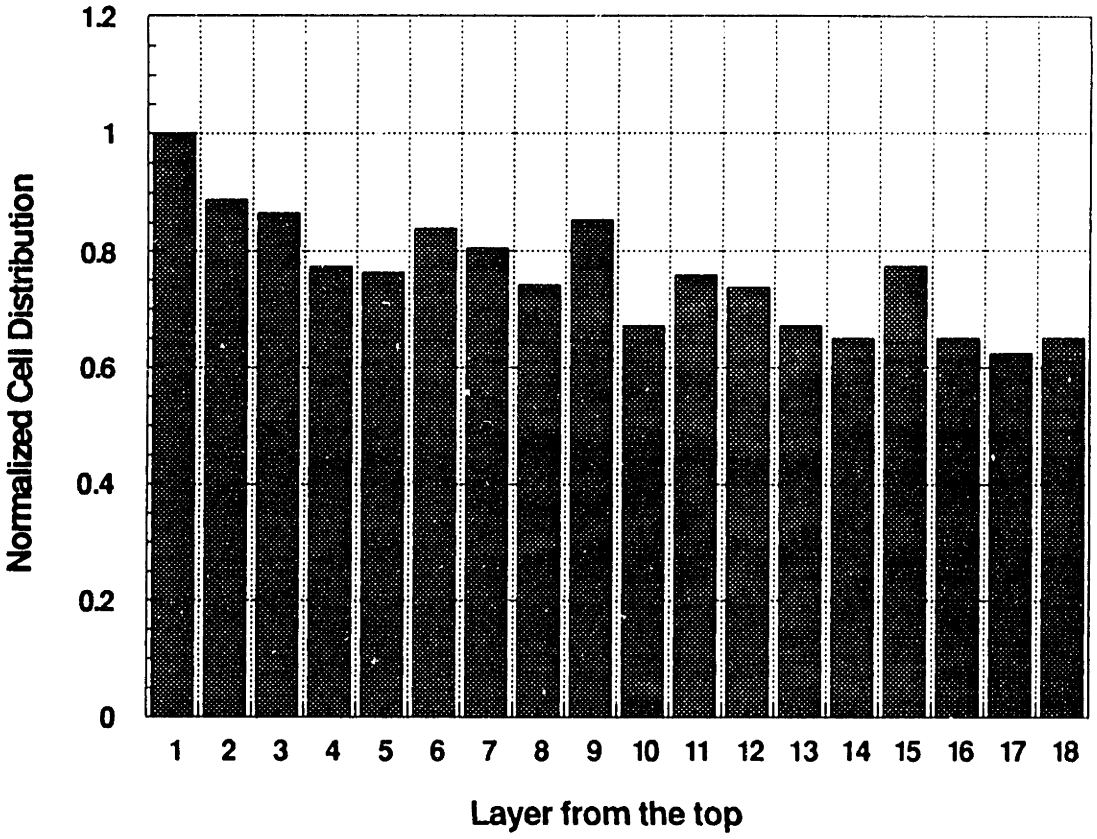

Figure 3.3 Initial cell distribution (CRL-1606)

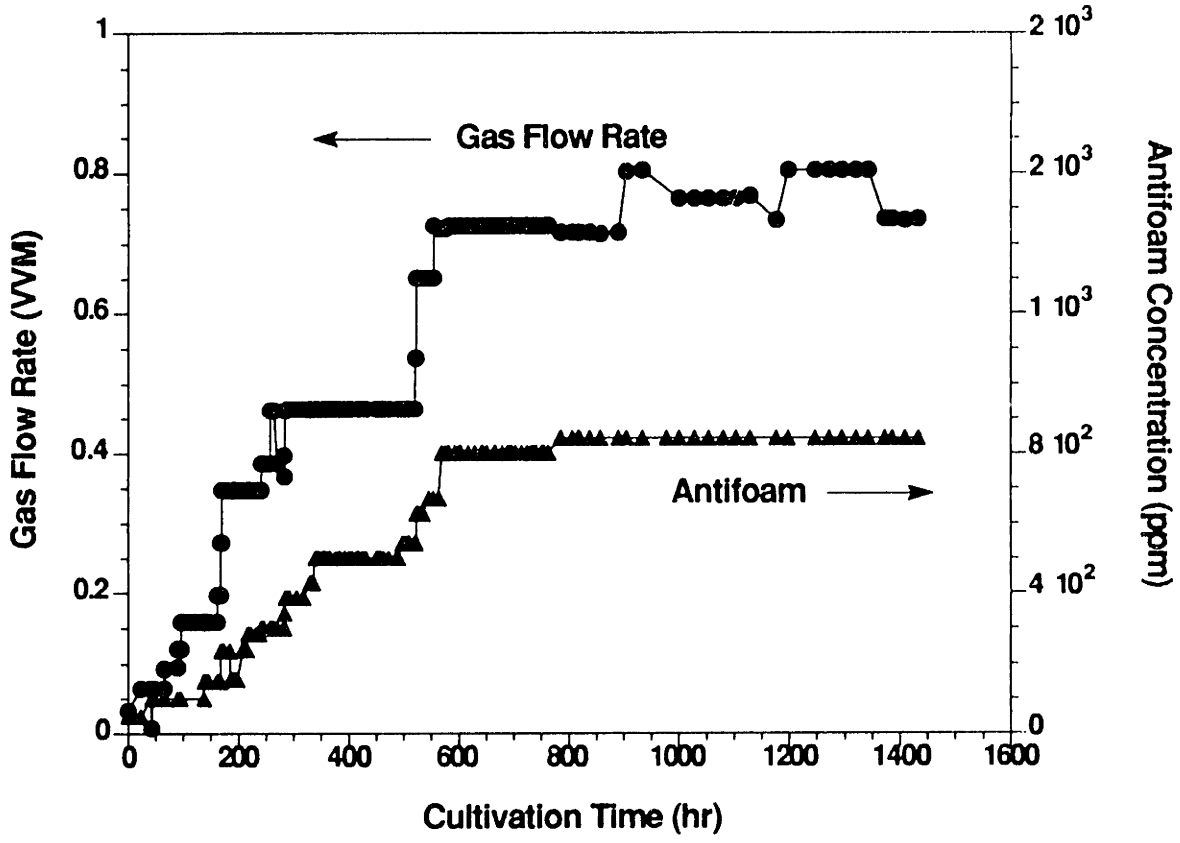

Figure 3.4 Gas flow rate and antifoam concentration during the cultivation process (CHO)

culture. The control strategy was to maintain the bottom dissolved oxygen concentration greater than 20% saturation by continuously increasing the gas flow rate. The gas flow rate required to meet the oxygen demand under this control strategy is shown in Figure 3.4. During the cultivation process, the gas flow rate was increased up to 0.80 VVM. This high gas flow rate, which is similar to that used in microbial fermentation, has seldom been reported in animal cell culture. This is because gas bubbles are detrimental to the cells unless the system is properly designed. In addition, the high cell density which requires this high gas flow rate is not usually encountered in most cell culture system.

The amount of antifoam added throughout the course of cell cultivation to suppress foaming is shown in Figure 3.4. The antifoam concentration was approximately 850 ppm at the very end of the cultivation process. This concentration is well within the safe range for γ-CHO cell cultivation found previously.

A perfusion rate of 200 ml/hr (equivalent to a dilution rate of 0.074 hr^{-1}) for the reactor operation was employed during the cell cultivation. Figure 3.5 shows the off-line analyses for the cumulative glucose consumption, lactate production, and γ-interferon production. The trends of glucose and lactate curves indicate a rapid cell growth during the initial phase although the rate decreases after about 400 hours. γ-Interferon was produced continuously throughout the reactor operation and the average calculated volumetric productivity (from Fig. 3.5) of γ-interferon was 2.1×10^6 IU/l/hr between 500 to 1500 hours from the start of the cultivation process. At the end of the cell cultivation, this bioreactor had produced a cumulative γ-interferon titer equivalent to 3×10^9 IU/liter. In addition, the estimated specific metabolic activities of γ-CHO cells during the final stages of bioreactor operation, which will be shown later, were quite comparable to those previous reported (Perry and Wang, 1989; Lutz, 1982).

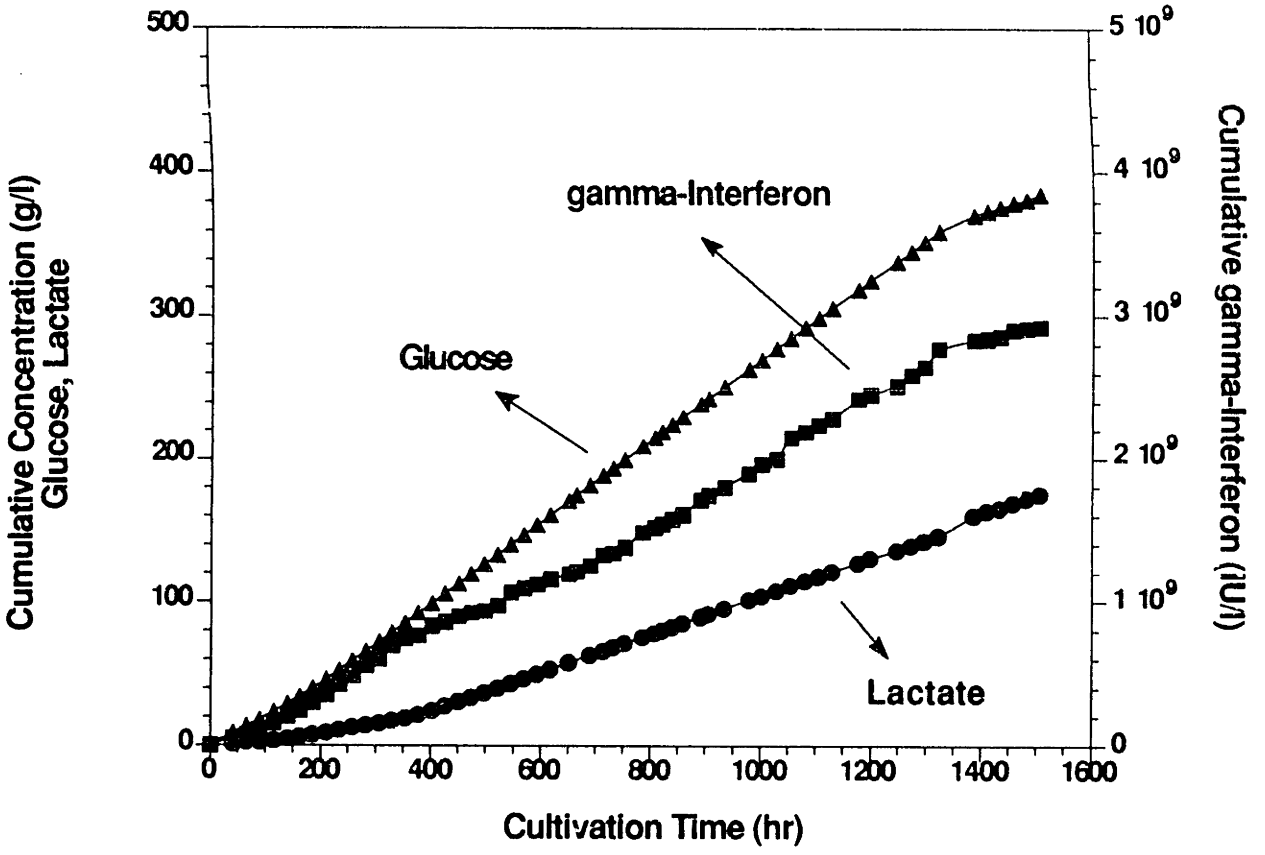

Figure 3.5 Cumulative glucose consumption, lactate production, and gamma-interferon production during the cultivation process (CHO)

The calculated liquid flow rate during the cultivation process is shown in Figure 3.6. The liquid flow rate was low initially due to the low gas flow; the step increases closely followed and resulted from the step increases of gas flow rate. The decrease in liquid flow rate following each step increase of the liquid flow rate was caused by the reduction in permeability due to cell mass accumulation. After about 800 hours the liquid flow rate reached a steady state of about 12 cm^3/ml.

At the highest gas flow rate, the liquid velocity was calculated to be 0.13 cm/s, corresponding to a Reynolds number in the packed bed of less than 1. This indicates that the flow in the annular fiber-bed section was in the laminar regime. At these conditions, very little detrimental hydrodynamic damage to the cells is expected. According to Equation 2.4, the calculated average shear stress at a liquid velocity of 0.13 cm/sec was found to be 0.3 $dyne/cm^2$. This shear stress is significantly lower than what is needed to cause shear damage to the cells (Sprague *et al*, 1987; Crouch *et al*, 1985; Stathopoulos and Hellums, 1985).

Figure 3.7 shows the volumetric oxygen uptake rate (OUR) by the cells during the cultivation process. The results in this figure are from the OUR calculated from the liquid side oxygen balance. As shown in Chapter 2, oxygen transfer rate is determined by liquid flow rate and mass transfer coefficient. The former is determined by gas flow rate and cell density, and the latter is determined by the gas flow rate. The initial pattern of oxygen uptake rate fluctuated due to the variations in the liquid flow rate. However, after 600 hours, even when liquid flow rate was decreased, the OUR continuously increased due to the increased mass transfer from the increase in the gas flow rate. In other words, the gas flow rate although increased at 600 hours did not lead to significant increase of liquid flow rate.

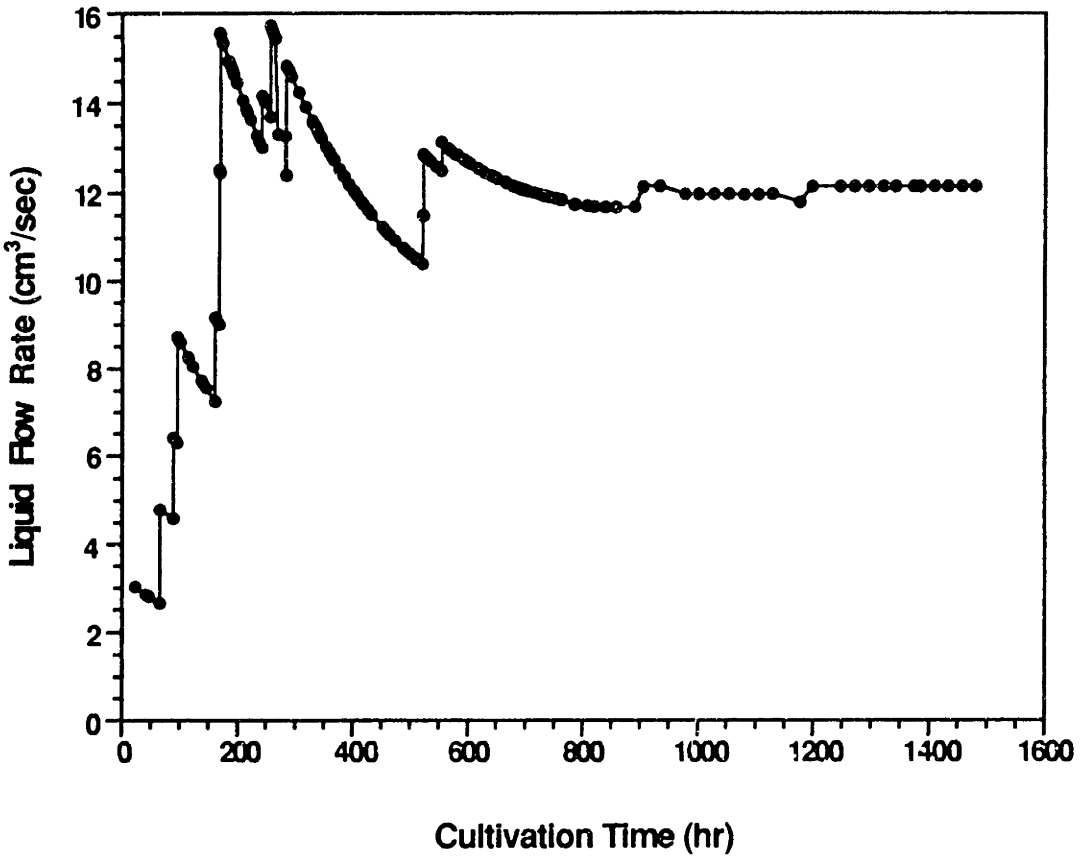

Figure 3.6 Liquid flow rate in the fiber bed during cultivation (CHO)

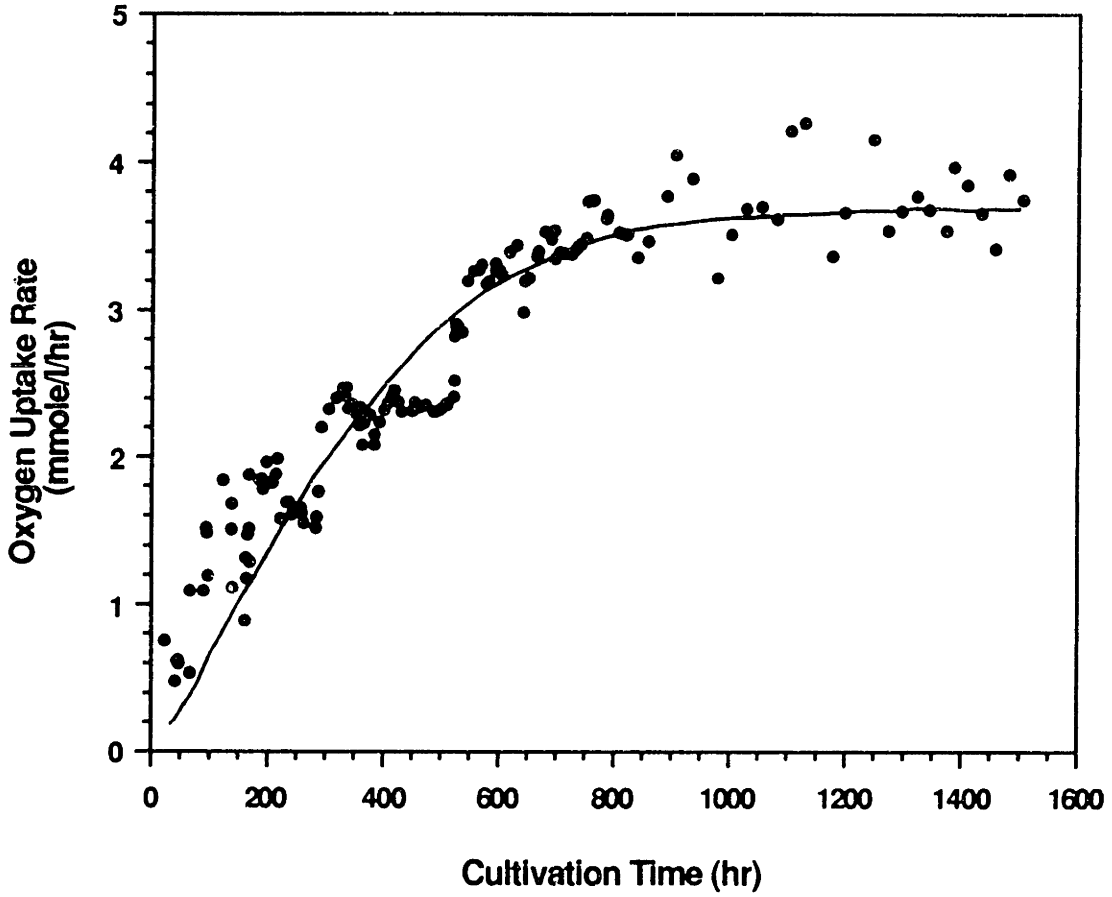

Figure 3.7 Oxygen uptake rate during cultivaiton process (CHO)

However, the increased gas flow rate does significantly increase the mass transfer coefficient. At about 800 hours into the cultivation, the OUR reached a steady state. The OUR at steady state was 4 mmole/l/hr. This high oxygen consumption rate is not often reported in the literature for mammalian cell cultivation due to the difficulty in measuring OUR in cell culture systems. One could also surmise that at this high OUR the cell density must be correspondingly high in the packed bed.

Based on the correlation between cell density and permeability which was presented in Chapter 2, the determination of permeability from *in situ* measurements of pressure drop allows us to calculate cell density during the cultivation process. Figure 3.8 shows the calculated normalized permeability and corresponding cell density in the fiber bed during the γ-CHO cultivation experiment. The permeability was normalized with respect to the permeability of the fiber bed before inoculation. As shown by the figure, the normalized permeability decreased as the cultivation progressed and reached a constant value of 0.19 at about 800 hours. This indicates that the cell density increased dramatically, leading to this reduction of permeability during the first 800 hours of the cultivation process. After that, the cell density reached a constant value and thus the permeability reached a constant value during the latter part of the cultivation process. The calculated cell densities during the cell cultivation are shown in the lower part of Figure 3.8. It was found that cell density increased from $3x10^6$ cells/cm^3 to $5.8x10^7$ cells/cm^3 during the first 800 hours and then remained constant during the final stage of the cultivation process. The calculated cell density at the final stage was $5.8x10^7$ cells/cm^3 which was quite close to $6.8x10^7$ cells/cm^3 obtained from nuclei counting performed upon the disassembled fiber bed at the end of cultivation process.

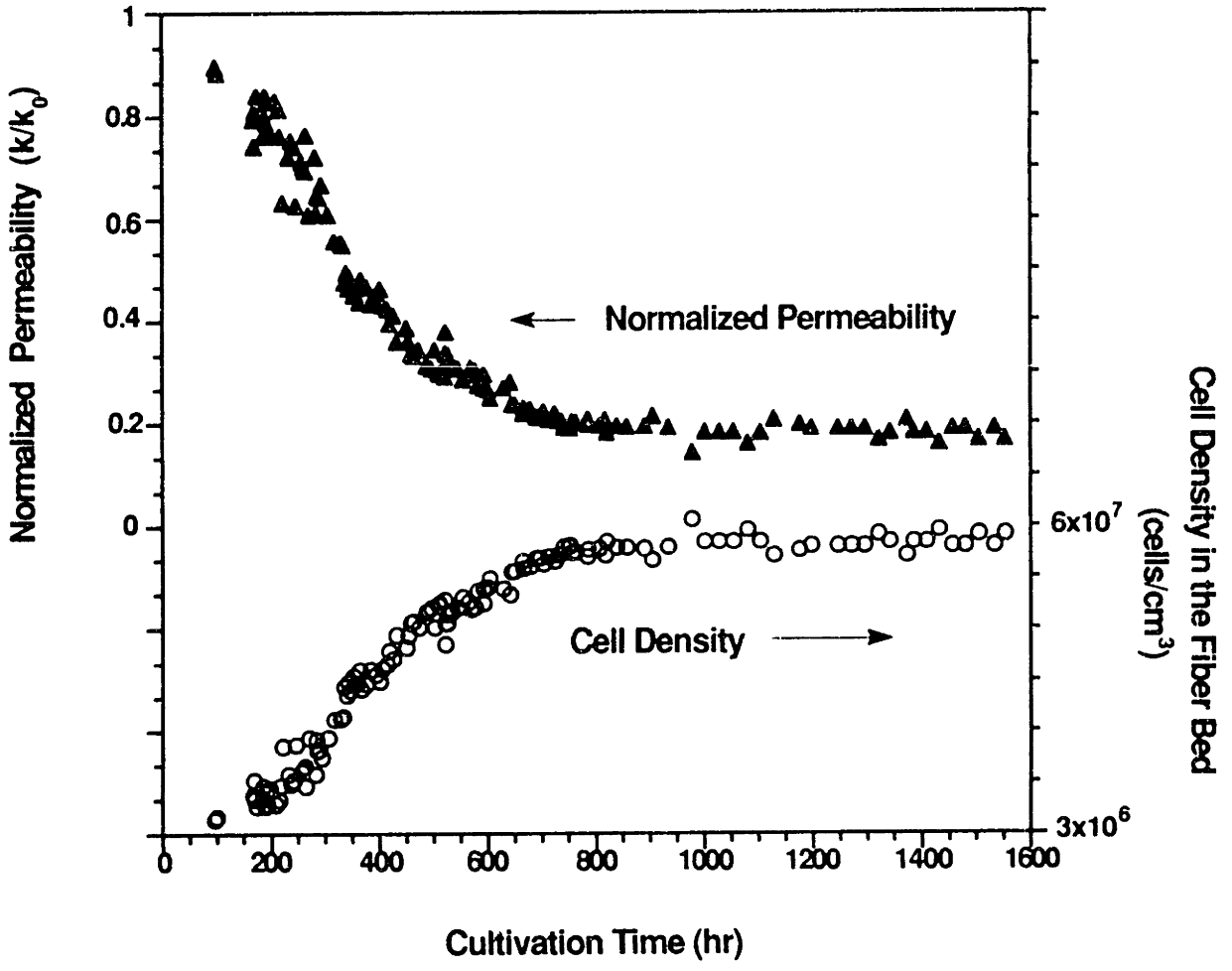

Figure 3.8 Normalized permeability and corresponding cell density in the fiber bed during cell cultivaiton (CHO)

The cell cultivation was successfully maintained for 66 days, and the termination of the process was not due to contamination or detrimental effects to the cells; rather, the cultivation was terminated after satisfactorily demonstrating the ability to maintain long-term operation. It is our belief that the operation could have continued indefinitely. Although OUR measurements did provide some instantaneous indication of cell growth, there is no direct and non-destructive way to enumerate cells in the fiber-bed during the cell cultivation. Therefore, nuclei counting was performed at the end of the cultivation process when the packed bed was dismantled. The cell distribution within the packed bed at the end of the experiment is shown in Figure 3.9. The cell distributions of two previous experiments terminated after 10 and 22 days are also included in the figure for comparison. All the cell concentrations were normalized by a factor of 5.57×10^9 which was the total number of cells for the top layer in the 66 day-run. As shown in this figure, the cell number increased dramatically between the tenth and the twenty-second day (the final total number of cells for the 22 day run was 5.7×10^{10}). This finding is consistent with what was observed in Figures 3.6, 3.7 and 3.8. In addition, the top layers had more cells than the bottom layers. This was probably due to the filtering effect of the inoculum which led to a descending distribution of cells in the fiber-bed. This conclusion is based on the results from the previous cell attachment kinetics experiment.

In addition, there were only 7×10^3 cells/cm^3 in the suspension, which represented less than 0.02% of the cells in the fiber-bed. This confirmed indirectly that the shear stress on the cells was quite small, and only a low fraction of the cells was detached from the fibers.

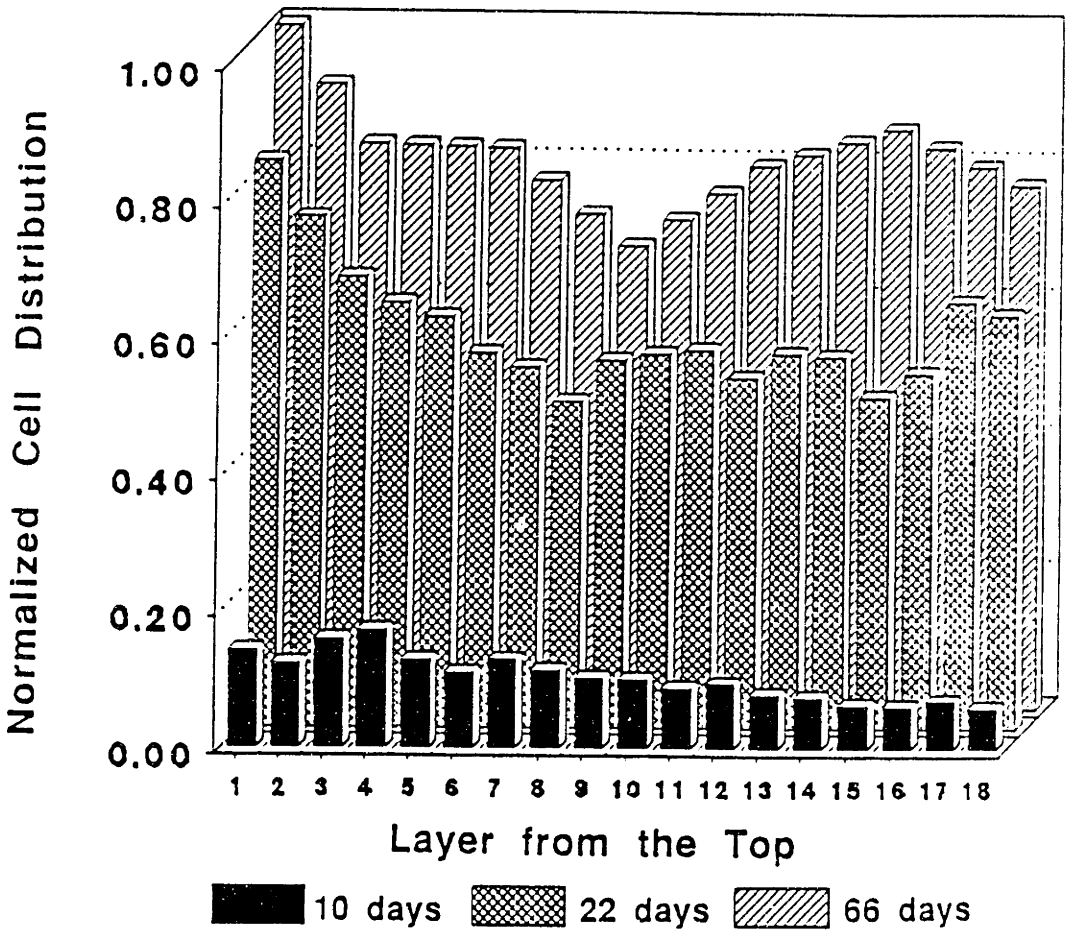

Figure 3.9 Cell distribution within the fiber bed at the end of cultivation process (CHO)

Although the cells in the fiber bed during the cell cultivation could not directly be enumerated, the culture kinetics could be obtained through the analysis of some independent measurements. These measurements include lactate production rate, oxygen uptake rate, and permeability during the course of cell cultivation.

Assuming the yield of cell from oxygen and the specific lactate production rate of γ-CHO cells are constant, the oxygen uptake rate and the lactate production rate divided by the specific rates can provide estimated cell number during cell cultivation. Figure 3.10 shows the results of cell density independently obtained from lactate production rate, OUR and permeability plotted against cultivation time during γ-CHO cultivation. The cell densities are normalized by the corresponding final cell densities obtained from each measurements. As seen in Figure 3.10, all three experimental results matched quite well, and showed rapid cell growth in the first 800 hours and reached a steady state. Based on the data in Figure 3.10, the growth rate at different times during the cultivation can be calculated. Initially, the growth rate was found to be 0.008 hr^{-1} which gradually decreased to almost zero at 800 hours. Since the dissolved oxygen was maintained greater than 20% air saturation, and the glucose concentrations in the spent medium throughout the time course and at the steady state were above 0.6 g/l as shown in Figure 3.11, it is unlikely that oxygen or glucose was limiting. In order to elucidate the cause for the decrease in growth rate at the steady state, the growth rate versus specific perfusion rate is examined. The specific perfusion rate is defined as perfusion rate divided by the corresponding cell number at a certain cultivation time. This parameter is an indication of the amount of medium (volume) supplied to each cell per unit time. A high specific perfusion rate means that fresh medium is supplied to the cells faster. As shown in Figure 3.12, growth rate was

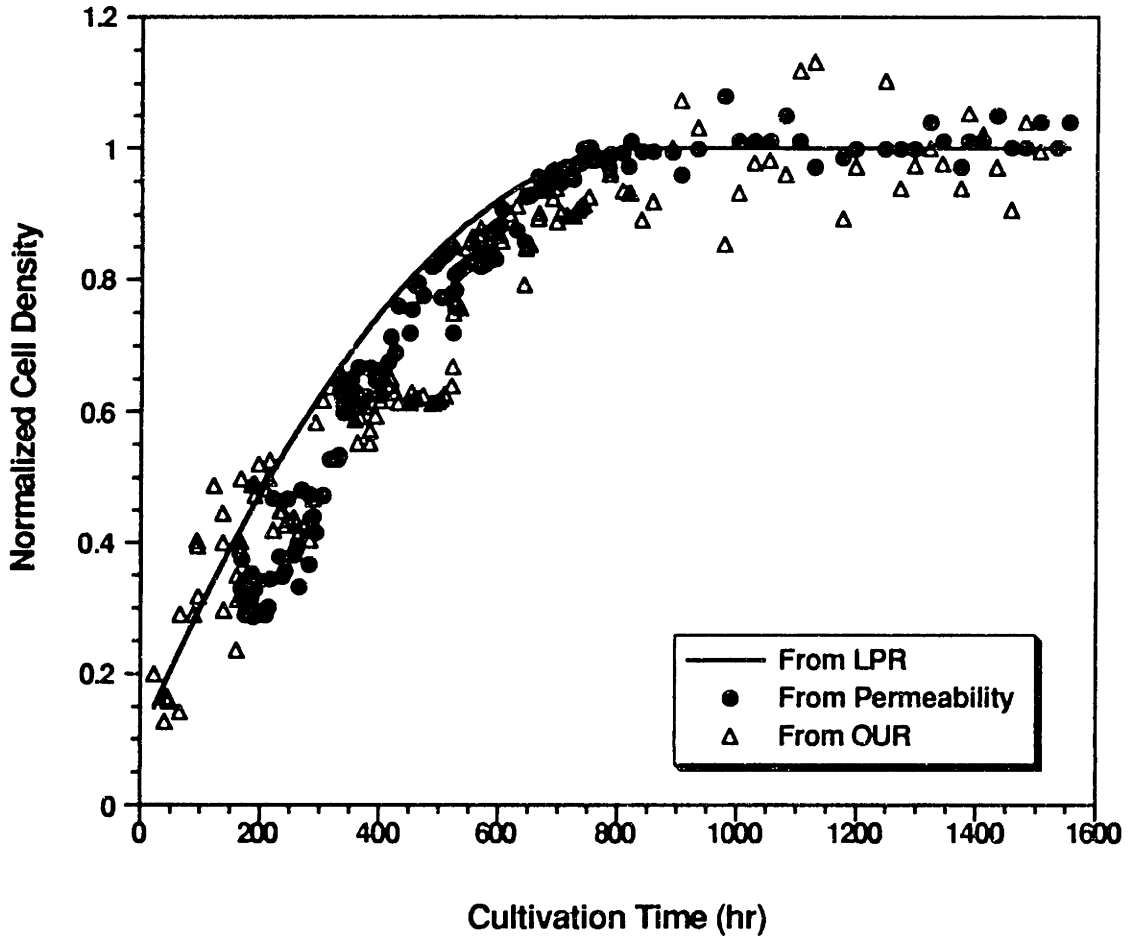

Figure 3.10 Normalized cell density versus cultivation time (CHO)

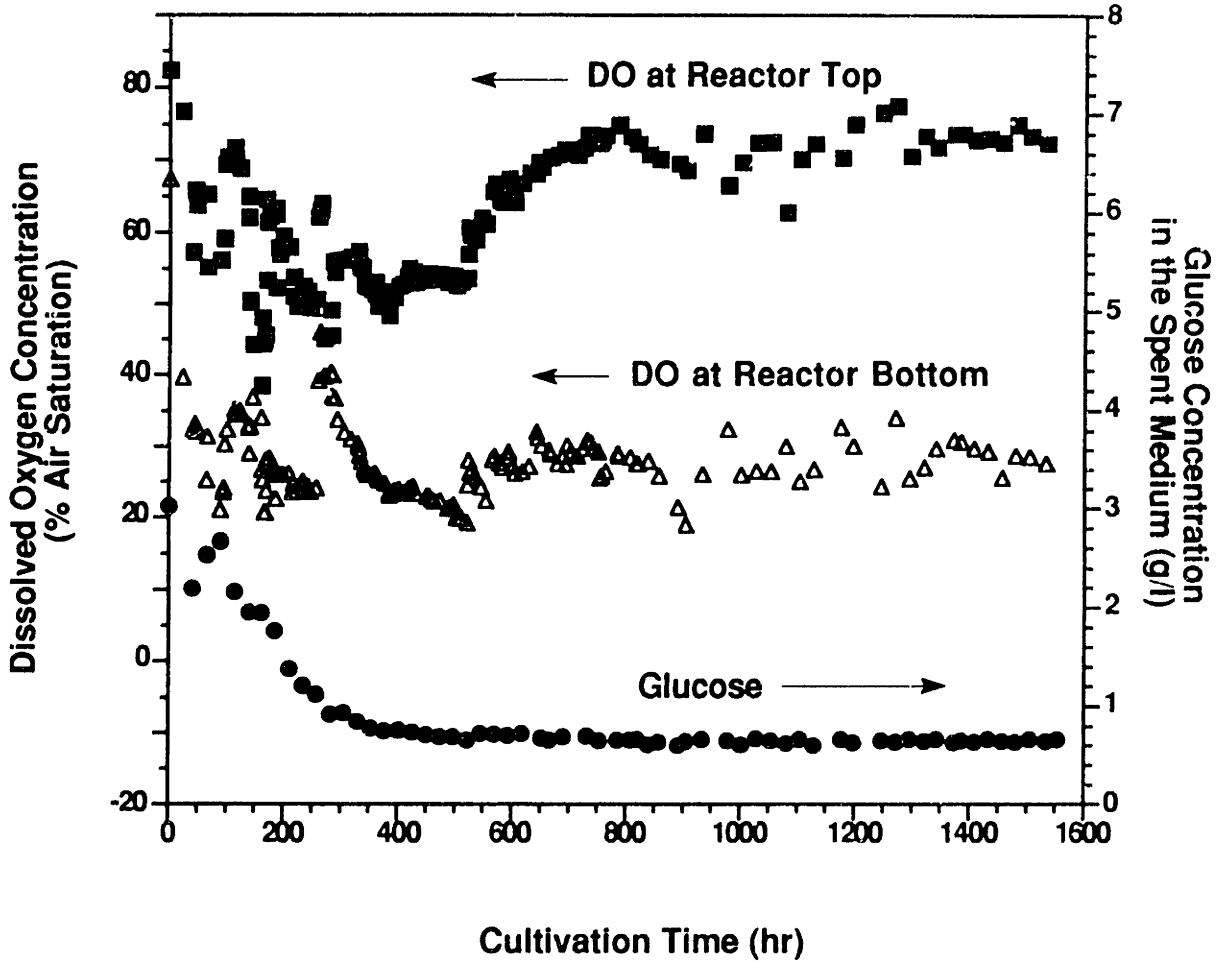

Figure 3.11 Dissolved oxygen concentration at the top and bottom of the reactor and glucose concentration in the spent medium during the cell cultivaiton (CHO).

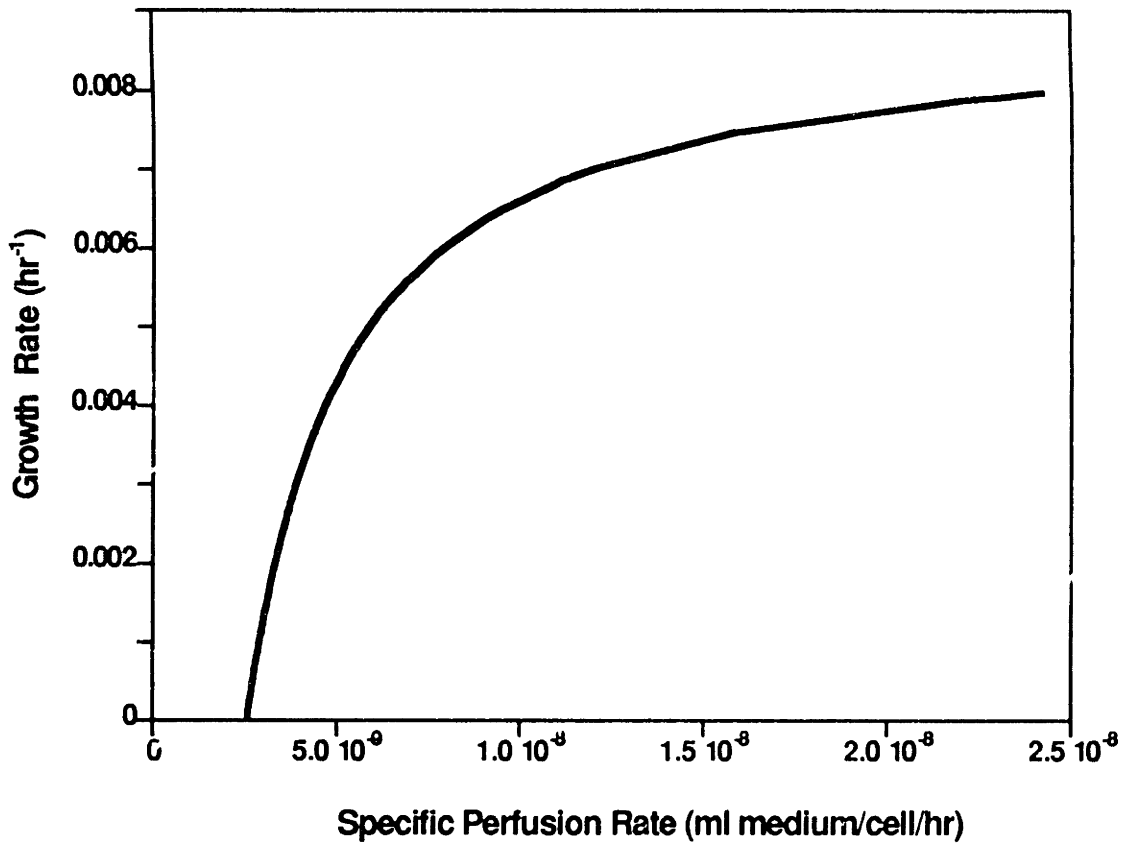

Figure 3.12 Effect of specific perfusion rate on gorwth rate (CHO)

affected by the specific perfusion rate. At high specific perfusion rate where cell density was low, the growth rate was maximum, and at low specific perfusion rate where cell density was high, the growth rate was greatly reduced. This clearly indicates that the culture at steady state was either substrate-limited or waste product inhibited. The maximum cell growth rate achieved at high specific perfusion rate (0.008 hr^{-1}) was comparable to those in the usual roller bottle experiments. However, at a perfusion rate of 200 ml/hr, a total cell number of $4x10^{10}$ (correspondingly to a specific perfusion rate of $1.0x10^{-9}$ ml/cell/hr) led to 50% reduction of the maximum growth rate. Higher perfusion rates should lead to higher achievable cell densities.

A summary of the data from the 66 day experimental study is shown in Table 3.1. As stated previously, the experiment lasted 66 days and was terminated due to our assurance of its ability to operate over prolonged period. The total number of cells which was inoculated was $3.6x10^{8}$ cells per reactor. Based on the cell enumeration performed after dismantling the packed bed, there was a total of $8.2x10^{10}$ cells per reactor. From these cell enumerations, it is possible to calculate the cell concentration at inoculation and at the end of a 66 day run. The calculated values showed an inoculum concentration of $3.0x10^{5}$ cells/cm^3 in the packed bed and $6.8x10^{7}$ cells/cm^3 at the end of the experiment. The latter value is quite impressive since this high cell density was reached with convective nutrient transport. In particular, the reactor was able to meet the oxygen demands of the cells without deleterious effects. From the initial and final cell concentrations, a calculated multiplication ratio of 230 was achieved. During steady state, γ-interferon was produced at a rate of $2.1x10^{6}$ IU/l/hr, and correspondingly the concentration of γ-interferon in the medium was $2.7x10^{4}$ IU/ml.

Also shown in Table 3.1 are the various specific rates which were calculated from

Table 3.1 Summary of cell cultivation results (γ-CHO)

	Inoculum	Final
Cultivation Time		66 days
Total Cell Number (cells/reactor)	3.6×10^8	8.2×10^{10}
Cell Concentration in Fiber-Bed (cells/cm^3)	3.0×10^5	6.8×10^7
Multiplication Ratio		230
Perfusion Rate (hr^{-1})		0.074
Oxygen Uptake Rate (mmole/l/hr)		4
γ-Interferon Production (IU/l/hr)		2.1×10^6
Steady State γ-Interferon Concentration (IU/ml)		2.7×10^4
Specific OUR (mmole/cell/hr)		5.9×10^{-11}
Specific Glucose Consumption Rate (mg/cell/hr)		8.8×10^{-9}
Specific Lactate Production Rate (mg/cell/hr)		5.6×10^{-9}
Specific γ-Interferon Production Rate (IU/cell/hr)		7.0×10^{-5}

the total cell concentration at the end of the experiments. The specific oxygen uptake, glucose consumption and lactic acid production rates are quite comparable to those previously reported (Perry and Wang, 1989; Lutz, 1983). In addition, the specific γ-interferon productivity also compares well with those reported in the literature (Perry and Wang, 1989; Lutz, 1983). All these results again confirm that the environment of the cells in the glass-fiber reactor is quite adequate to sustain cell growth and product synthesis at a high cell density.

3.3 Cultivating Suspension Cells

The medium used was Excell 300 supplemented with 0.25 to 0.5 % fetal bovine serum. 2.24×10^9 ATCC-CRL 1606 cells were inoculated into the bioreactor to yield a cell concentration of 1.87×10^6 cells/cm^3.

The gas flow rate was controlled to maintain the bottom D.O. at a value greater than 10% of saturation. As shown in Figure 3.13, gas flow rate was increased up to 1 VVM, and 1000 ppm of antifoam was added to suppress foaming at the end of the cell cultivation process. In the beginning (0 to 300 hours), the inlet gas was composed of air and 10% carbon dioxide. As the cultivation proceeded, oxygen content in the inlet gas was raised due to the high oxygen demand of the culture, with the inlet gaseous oxygen composition ranging from 0.13 to 0.46 atm between 300 to 500 hours as shown in Figure 3.14.

Shown in Figure 3.15. the dilution rates employed ranged from 0.08 to 0.13 hr^{-1} (equivalent to perfusion rates of 216 to 350 ml/hr) during the cultivation process. The off-line analyses for the cumulative glucose consumption and lactate production are shown in

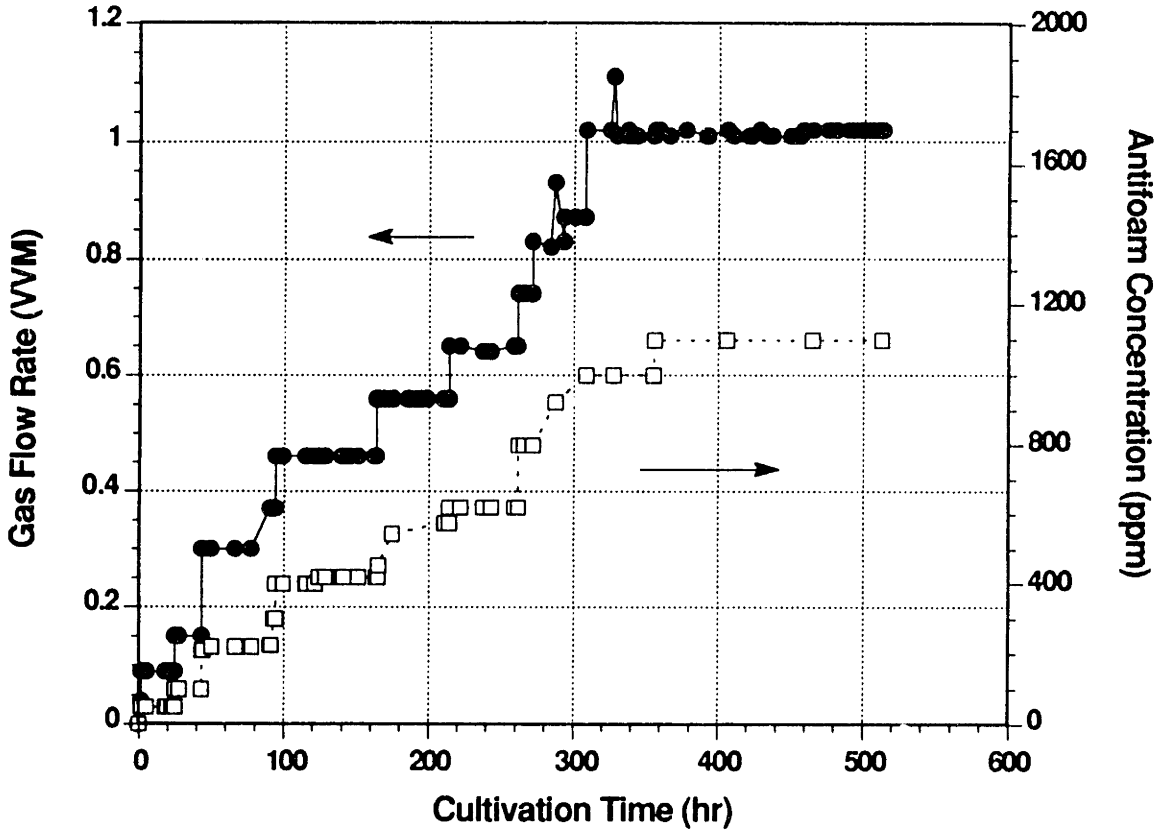

Figure 3.13 Gas flow rate and antifoam concentration during the cultivation process (CRL-1606)

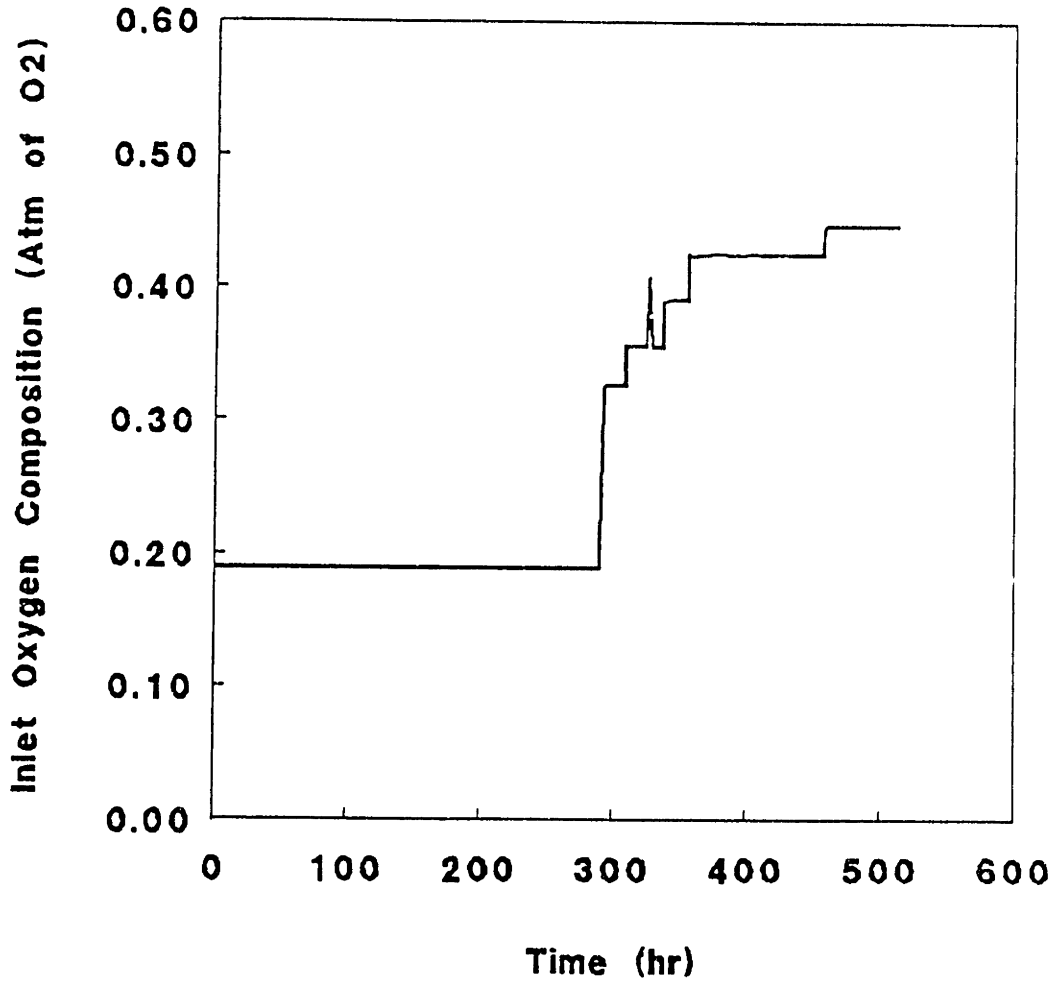

Figure 3.14 Inlet gaseous oxygen composition during cultivation (CRL-1606)

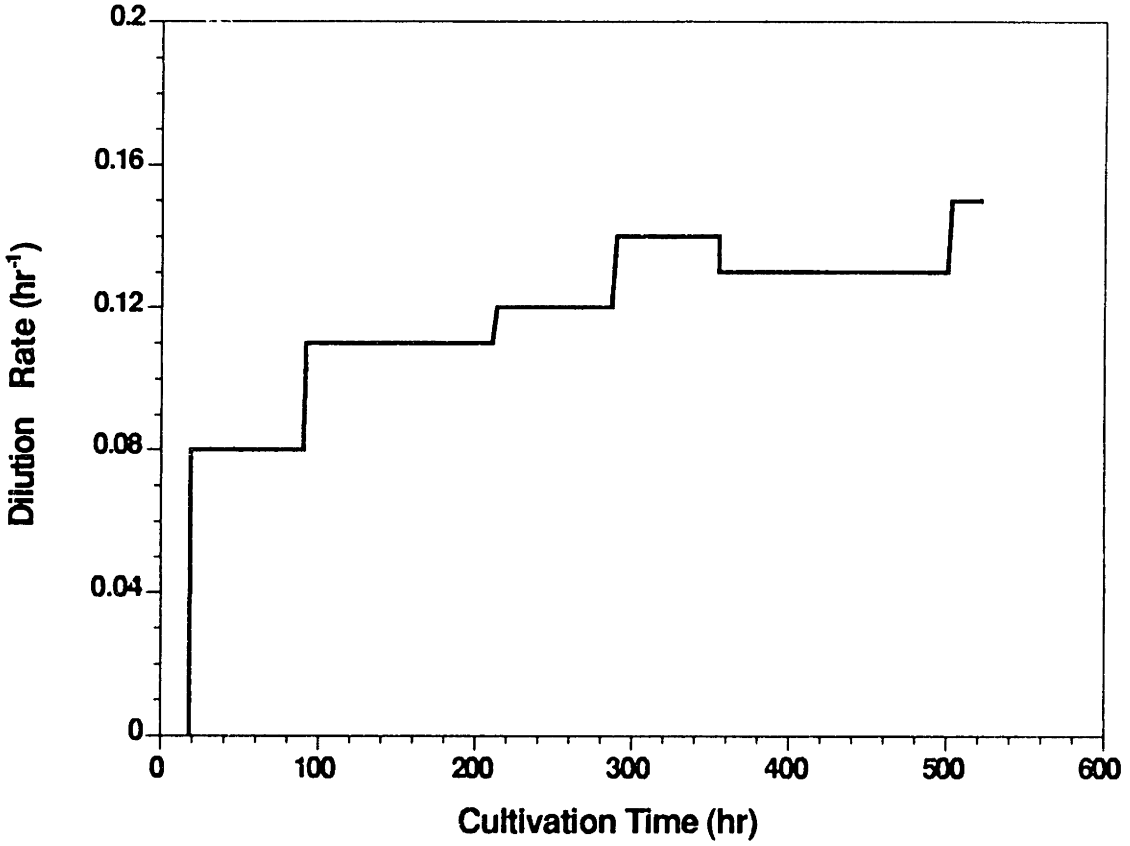

Figure 3.15 Dilution rate during cell cultivation (CRL-1606)

Figure 3.16. The trends of glucose consumption and lactate production rates are very similar, and both of them indicate rapid cell growth at the beginning and the attainment of a steady state toward the end of the process. After 22 days of cultivation, about 240 g/l of glucose was consumed and about 160 g/l of lactate was produced.

Liquid flow rate during the suspension cell cultivation was obtained through similar calculations as in the γ–CHO cell cultivation and is shown in Figure 3.17. The step increases in the liquid flow rate was due to the increasing of gas flow rate. The decrease after each step increase was due to the reduction in permeability resulting from cell accumulation. The highest liquid flow rate of 23 cm^3/sec occurred at 100 hours into the operation of the bioreactor; after that, liquid flow rate gradually decreased to about 13 cm^3/sec and steady state was reached. Again, the fiber bed was operated in the laminar flow regime and, even at the highest liquid flow rate, the shear stress was less than 1 dyn/cm^2 which is below the critical shear stress leading to cell damage.

Similar to that observed in the previous section on γ–CHO cultivation, the volumetric oxygen uptake rate (OUR) is determined by both liquid flow rate and mass transfer coefficient. As shown in Figure 3.18, even when the liquid flow rate decreased, the OUR increased due to the increase in gas flow rate. The significant increase of OUR at 300 hours was due to the increase of oxygen content in the inlet gas line. After that time, the OUR was maintained at about 13 mmole/l/hr. This high oxygen demand indicates that a very high cell density must have been achieved. In addition, the OUR obtained in our experiments is approaching that obtained for procaryotic fermentations (O'Connor, *et al.*, 1992).

Figure 3.19 shows the IgG concentration and cumulative IgG production during the

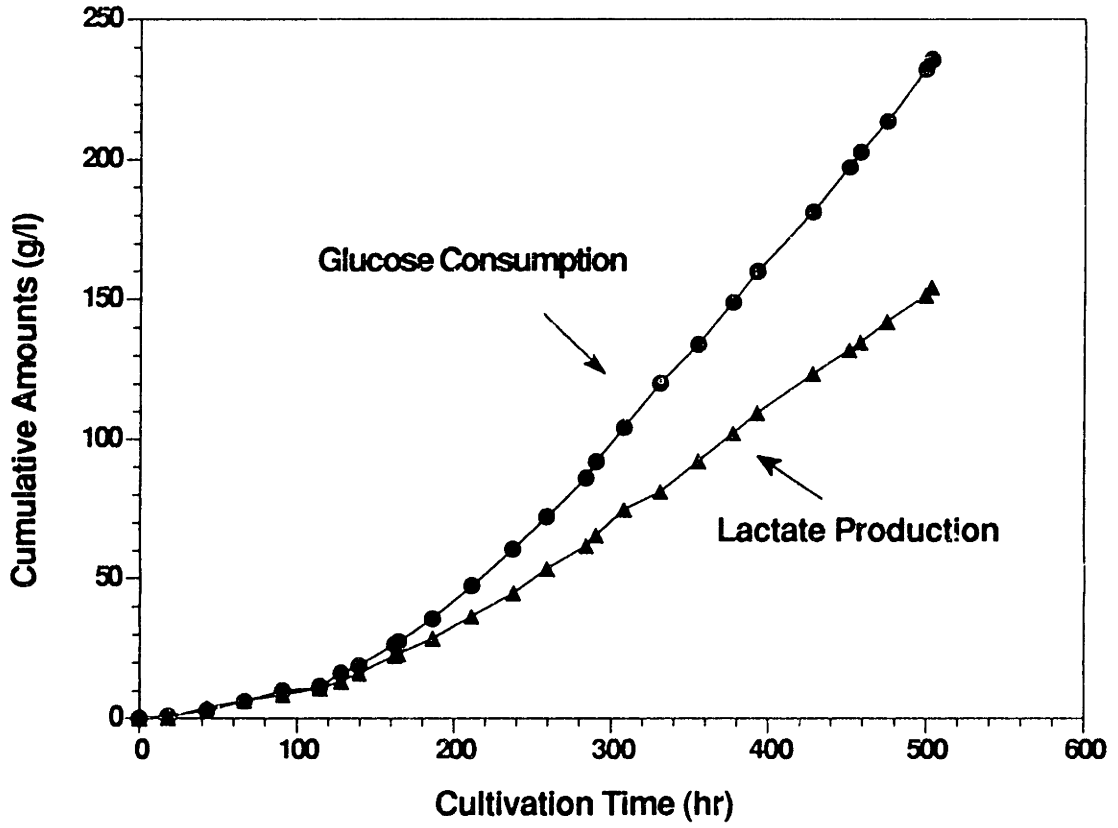

Figure 3.16 Cumulative glucose consumption and lactate production during the cultivation process (CRL-1606)

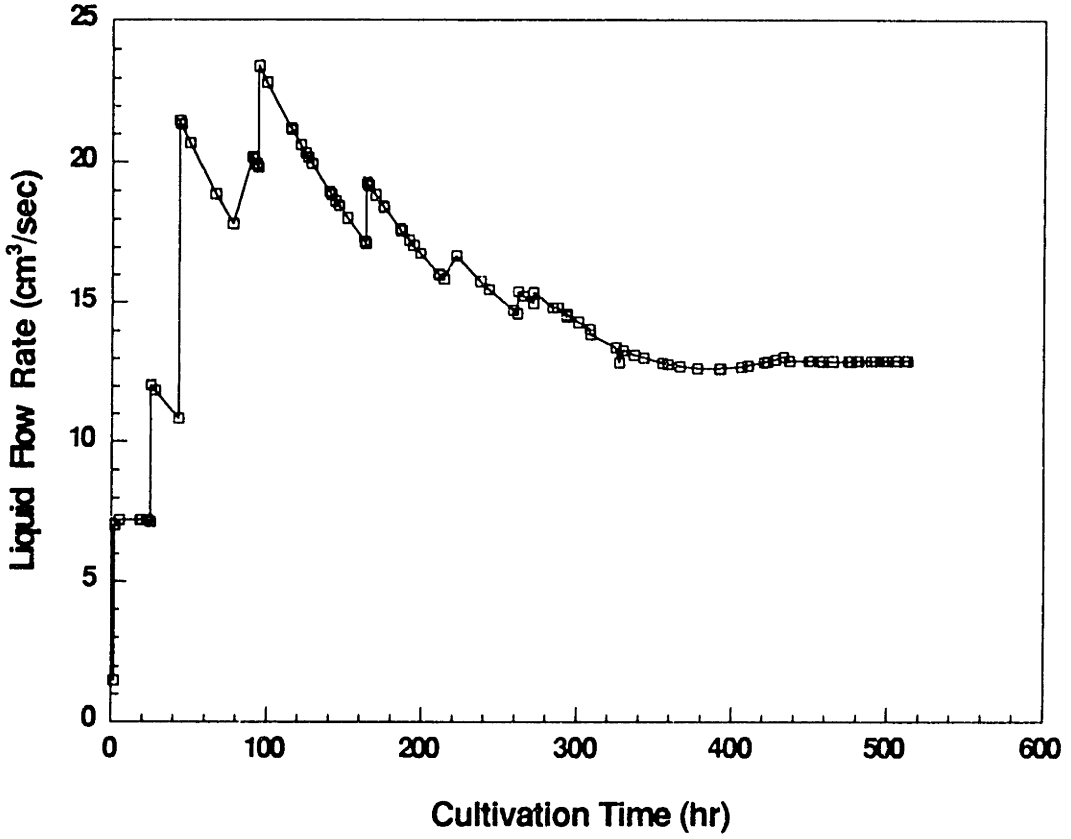

Figure 3.17 Liquid flow rate during the cultivation process (CRL-1606)

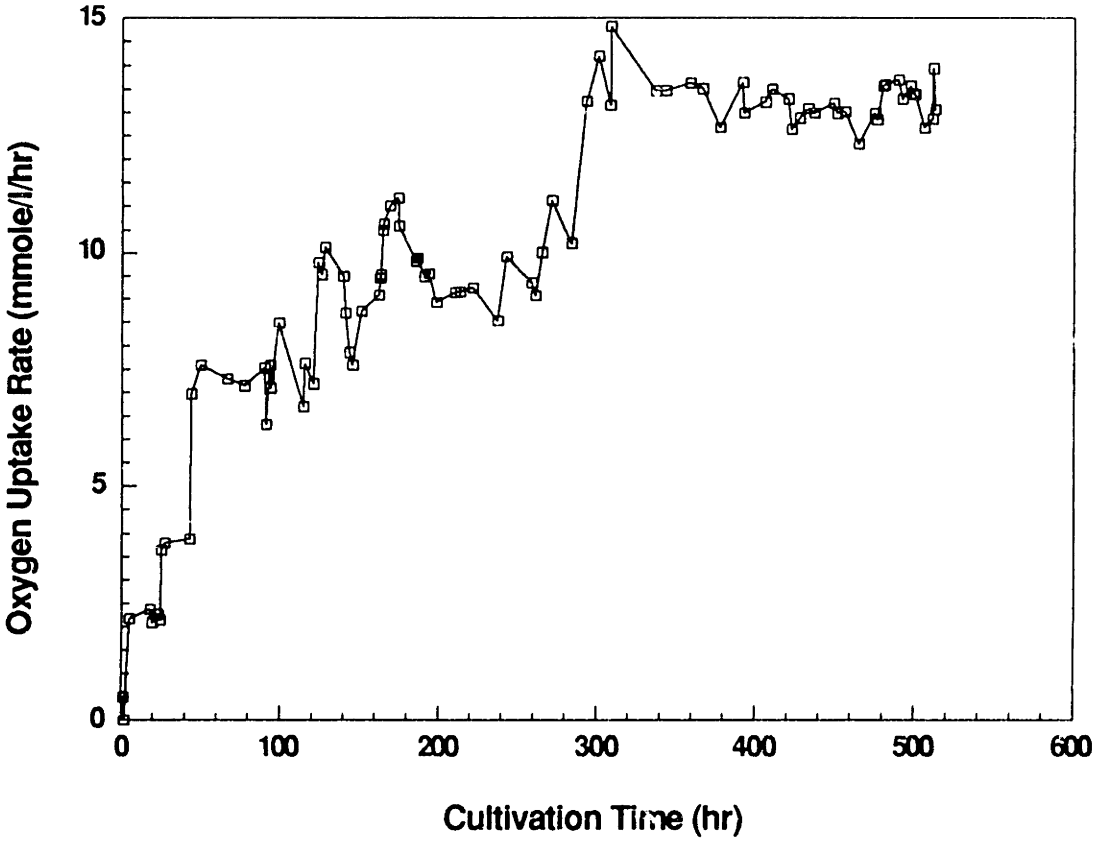

Figure 3.18 Oxygen uptake rate during cultivation process (CRL-1606)

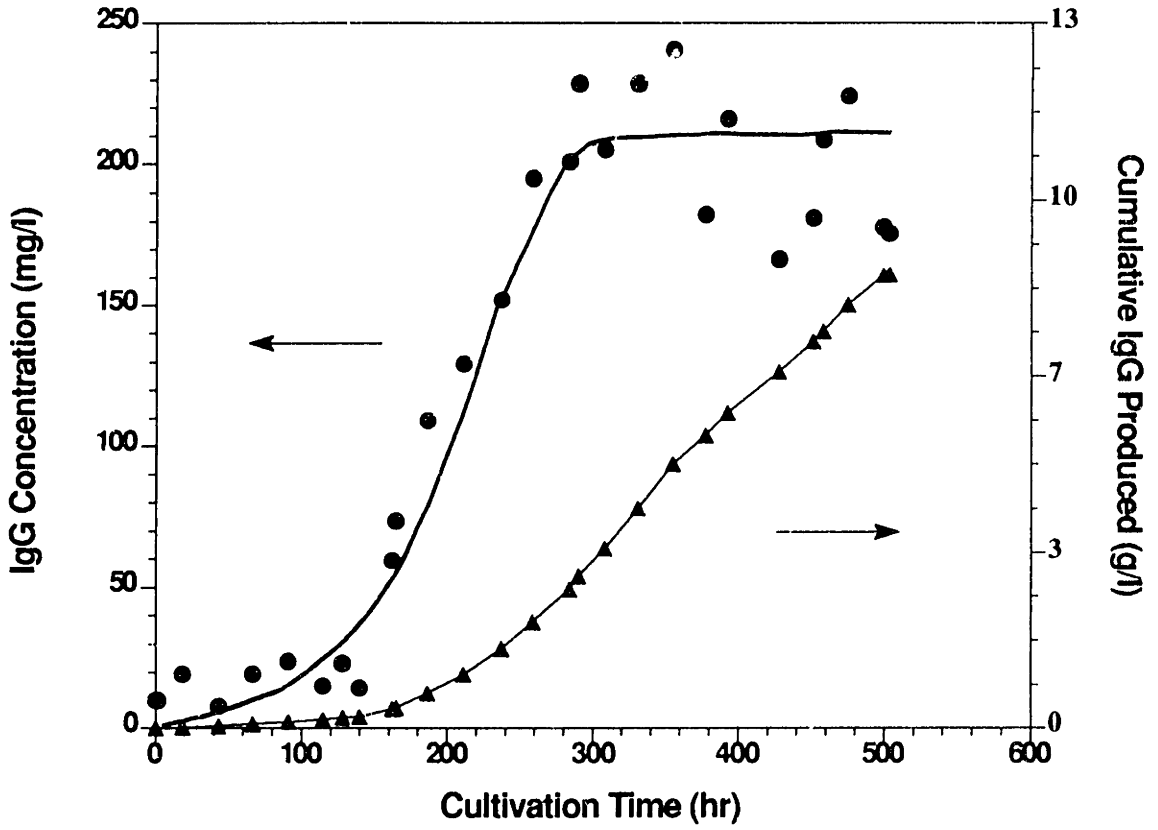

Figure 3.19 IgG Concentration and cumulative IgG production during the cultivation process (CRL-1606)

cultivation. IgG was produced continuously throughout the course of cell cultivation. At steady state, the IgG concentration was 225 mg/l, and the volumetric productivity was 28 mg/l/hr. It was noted that the high concentration of IgG at steady state was maintained even at as a high perfusion rate as 0.13 hr^{-1}, and nearly 9 g/l of IgG was produced during the 22 days in culture.

The cell cultivation was continued for 22 days, and the accumulation of cells in the fiber-bed could easily be seen by the naked eye (shown in Figure 3.20). Figure 3.21 shows the fiber mat before and after cell cultivation. The photograph on the top is the glass fiber mat before inoculation while on the bottom is the same fiber mat accumulated with cells.

Cell density and its axial distribution in the fiber bed was determined by cell counting after the experiment was terminated and these are shown in Figure 3.22. The cell density ranged from $4.5x10^8$ cells/cm^3 at the top to $1.4x10^8$ cells/cm^3 at the bottom, yielding a total cell number in the reactor of $2.0x10^{11}$ cells. These are among the highest cell concentrations reported to date. Cells were also distributed in a descending manner along the axial direction from top to bottom. However, the gradient in the case for CRL-1606 is steeper than the γ-CHO case. Possible reasons for the observations include (1) cell migration during cultivation, (2) uneven inoculum distribution, and (3) substrate limitation.

In view of the cell distribution shown in Figure 3.22, a detailed analysis of these data is presented in order to explain the experimental observations. As previously presented, the internal liquid recirculation rates ranged from 13 to 23 cm^3/sec. This corresponds to an internal liquid flow rate ranging from 46.8 to 82.8 liters per hour. On the other hand the perfusion rates during operation were significantly lower, ranging from

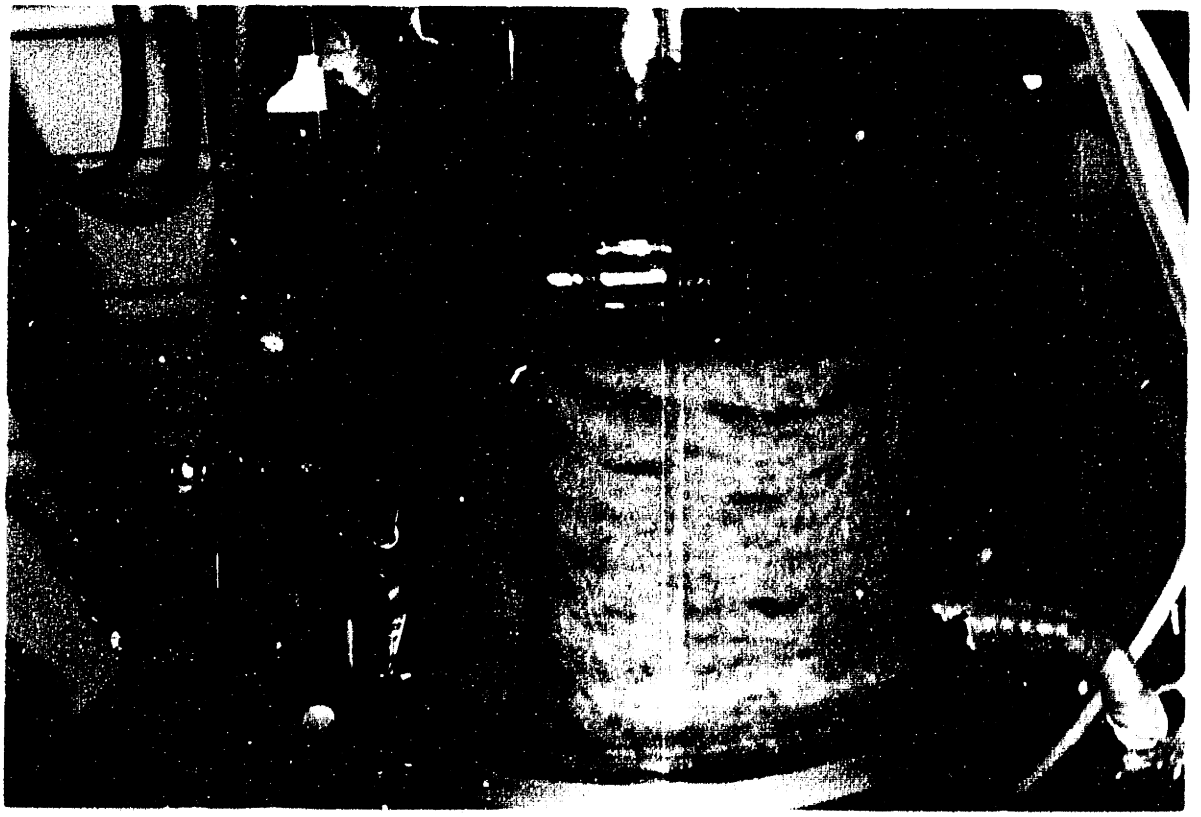

Figure 3.20 Photograph of fiber bed at the end of cultivation (CRL-1606)

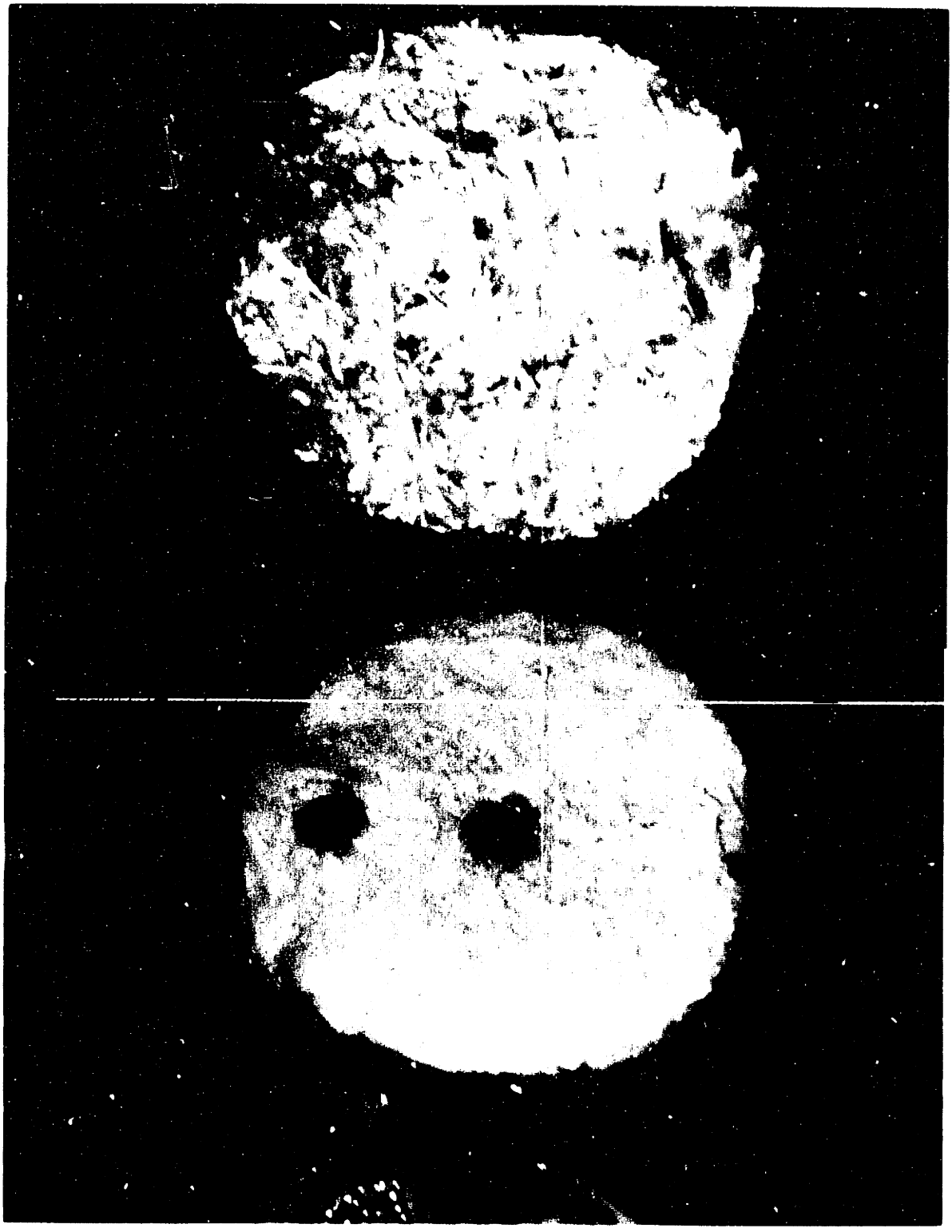

Figure 3.21 Photographs of glass fibers before and after CRL-1606 cultivation.
Top: Fibers before cell cultivation; bottom: fibers after cell cultivation.

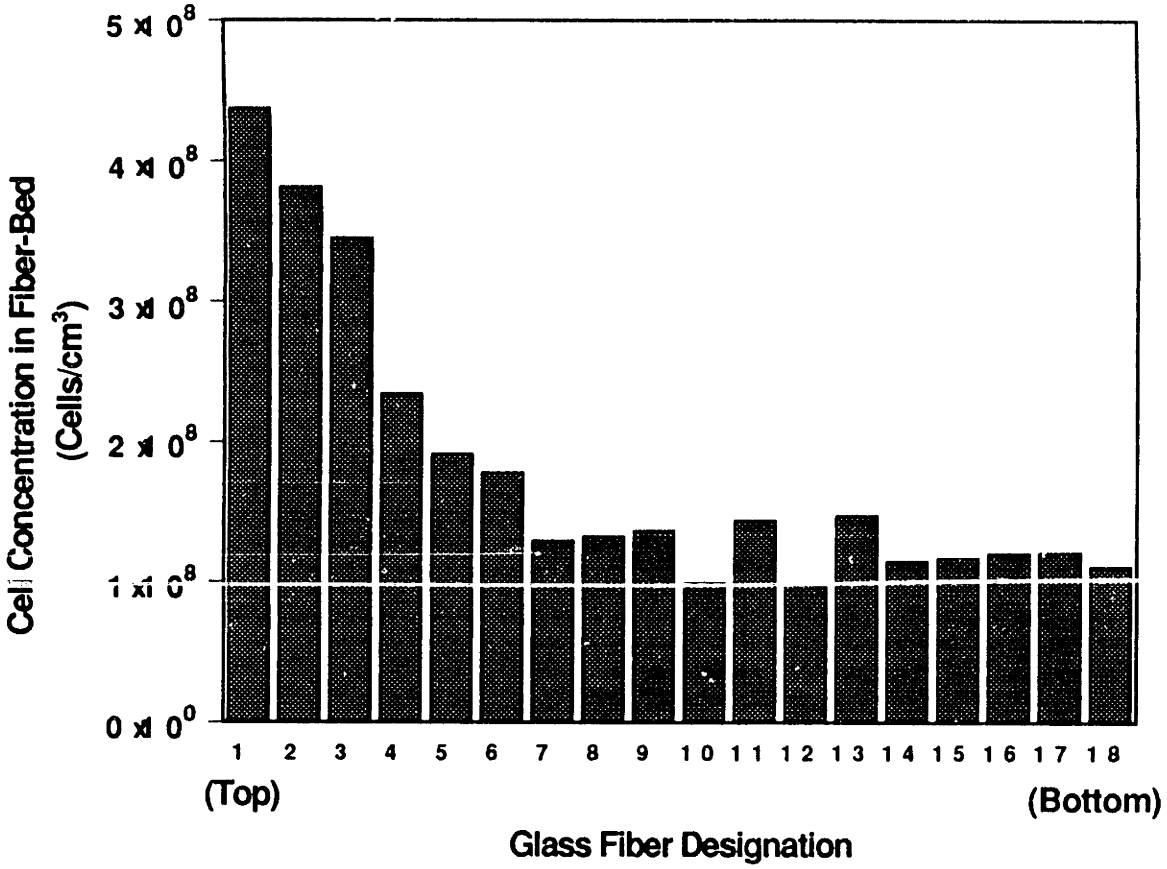

Figure 3.22 Cell distribution at termination of cultivation (CRL-1606)

0.216 to 0.350 liters per hour. At these high internal recirculation rates, there is a corresponding high probability that the entrapped cells can be dislodged from the fiber bed. However, the dislodged cells from the top layer can be subsequently entrapped due to the medium flow from recirculation into the fibers on a lower layer in the bioreactor. It is therefore hypothesized that this phenomenon of cell dislodgement and re-entrapment occurred throughout the course of the cell cultivation process.

This hypothesis can be reinforced by several other observations. First of all, it was shown in Figure 3.3 that the method of inoculation yielded a descending cell concentration from top of the bioreactor to the bottom of the bioreactor. This descending cell concentration at the end of the cultivation was similarly observed in Figure 3.22. The second observation which also enforces this hypothesis is based on the free cell concentration and cell viability as shown in Figure 3.23. As seen from this figure, the free cell concentration throughout the cultivation process was quite low (~ 10^4 cells/cm^3). These low free cell concentrations again substantiate the hypothesis that cell dislodging is accompanied by a rapid entrapment within the fiber bed bioreactor. Therefore, the cells exiting the bottom of the fiber bed are "re-inoculated" onto the top layers of the bioreactor. This re-inoculation cell distribution would probably behave quantitatively to the initial inoculation pattern; leading to a higher cell concentration at the top and descending towards the bottom portion of the reactor. Additional data from the radial cell distributions will be presented later in this thesis to further substantiate the hypothesis.

In order to investigate the culture kinetics, a methodology similar to that employed for γ-CHO culture was used to analyze the CRL-1606 cultivation results. Assuming that the yields of cells from oxygen and glucose are constants, the cell densities can be obtained based on oxygen uptake and glucose consumption. Permeability calculated from the

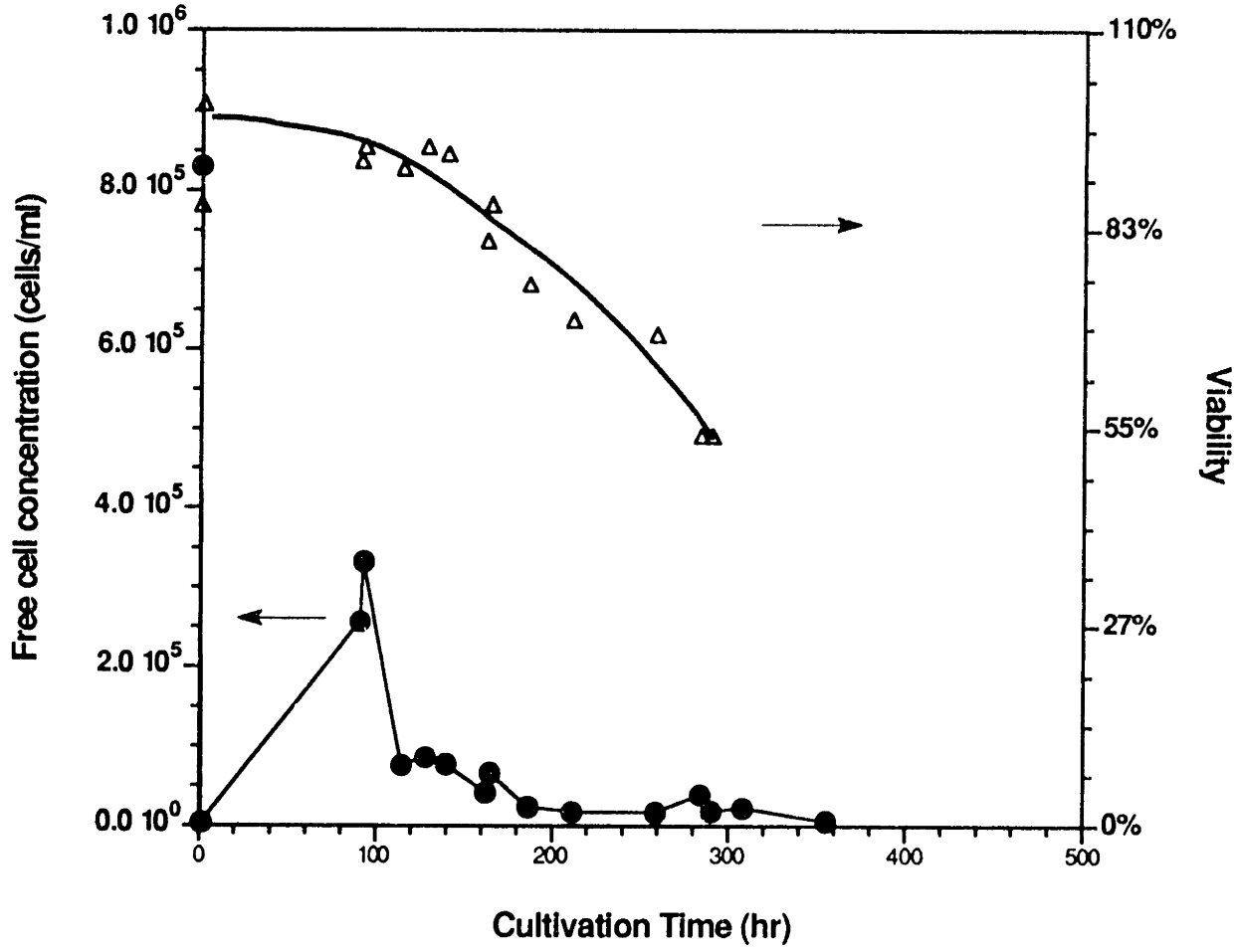

Figure 3.23 Free cell concentration and corresponding viability during cultivaiton (CRL-1606)

pressure drop measurement can also predict the cell density inside the fiber bed. Figure 3.24 shows the normalized cell density obtained based on glucose consumption, oxygen uptake and permeability during the cultivation. As seen in Figure 3.24, the cell density increased rapidly in the first 300 hours and reached a constant value at the final stages. The relationship between growth rate and specific perfusion rate was again examined and plotted in Figure 3.25. It is obvious that the growth rate of the culture was a function of specific perfusion rate and the culture is either substrate-limited or waste product inhibited. At high specific perfusion rate, where the perfusion rate was high and/or cell density was low, the growth rate was high at 0.023 hr^{-1}; at low specific rate, where the perfusion rate was low and cell density was high, the growth rate was greatly reduced due to the unavailability of certain critical nutrient(s) or the accumulation of certain waste product(s). Since the glucose and glutamine concentrations in the spent medium were still above 1.4 g/l and 0.7 mM at the final stage respectively, and the oxygen was maintained at 10% air saturation, it was unlikely that glucose, glutamine or oxygen was limiting. In addition, at steady state, the lactate concentration in the spent medium was about 0.8 g/l which is much lower than the inhibition constant in Monod's growth model for CRL-1606 (Glacken *et al.*, 1988), therefore the culture was not lactate-inhibited. Although the ammonia concentration was not measured, the usual specific ammonia production rate ranges from $0.15\text{-}0.7 \times 10^{-10}$ mmole/cell/hr under various dissolved oxygen concentrations (Zupke, 1992), consequently, the predicted ammonia concentration under the perfusion rate operating at final stage would be much lower than the inhibition constant of ammonia in Monod's growth model for CRl-1606. As a result, the critical factor which caused the reduction of growth rate was probably not ammonia either. It is more likely that certain amino acid or growth factor is limiting. Although the limiting factor was not identified, Figure 3.25 provides useful information for process control. For example, to support 1×10^{11} cells at a growth rate of 0.02 hr^{-1}, a perfusion rate of 600 ml/hr would be required.

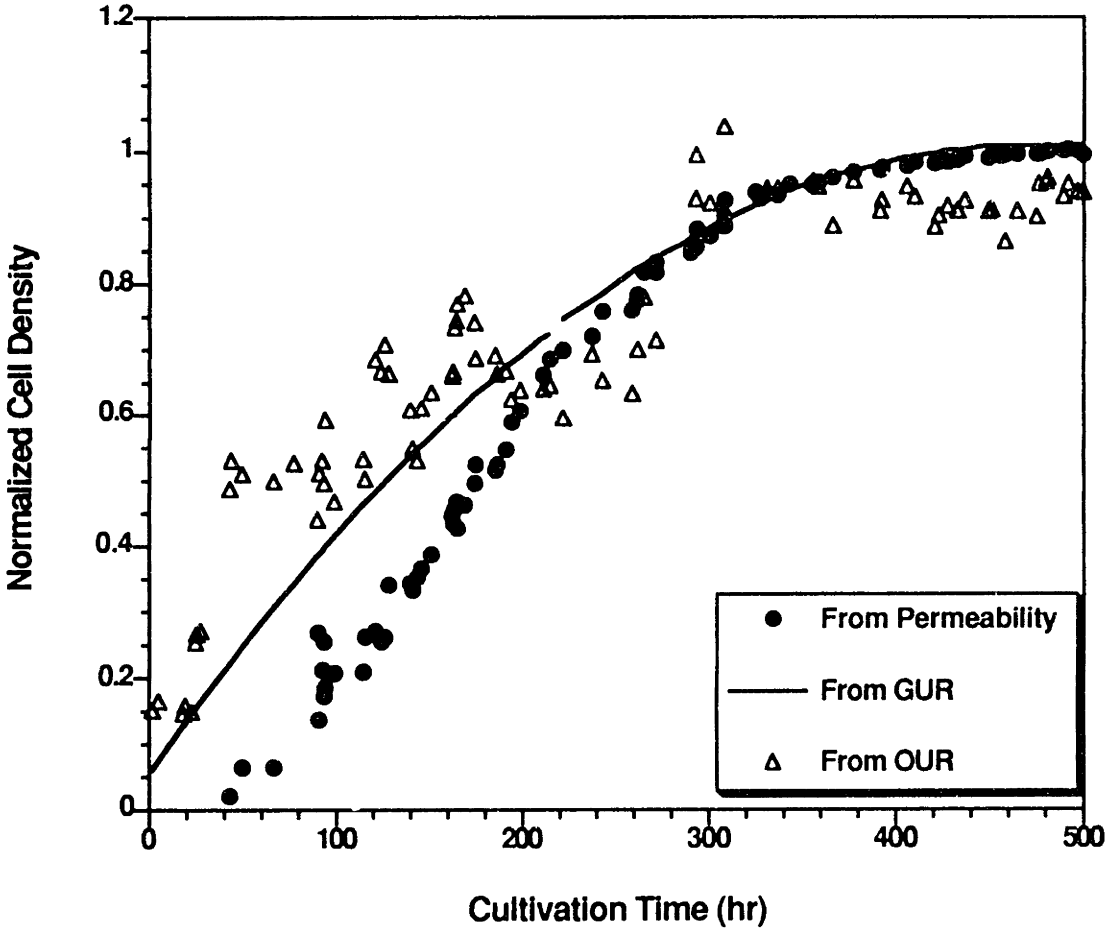

Figure 3.24 Normalized cell density versus cultivation tIme (CRL-1606)

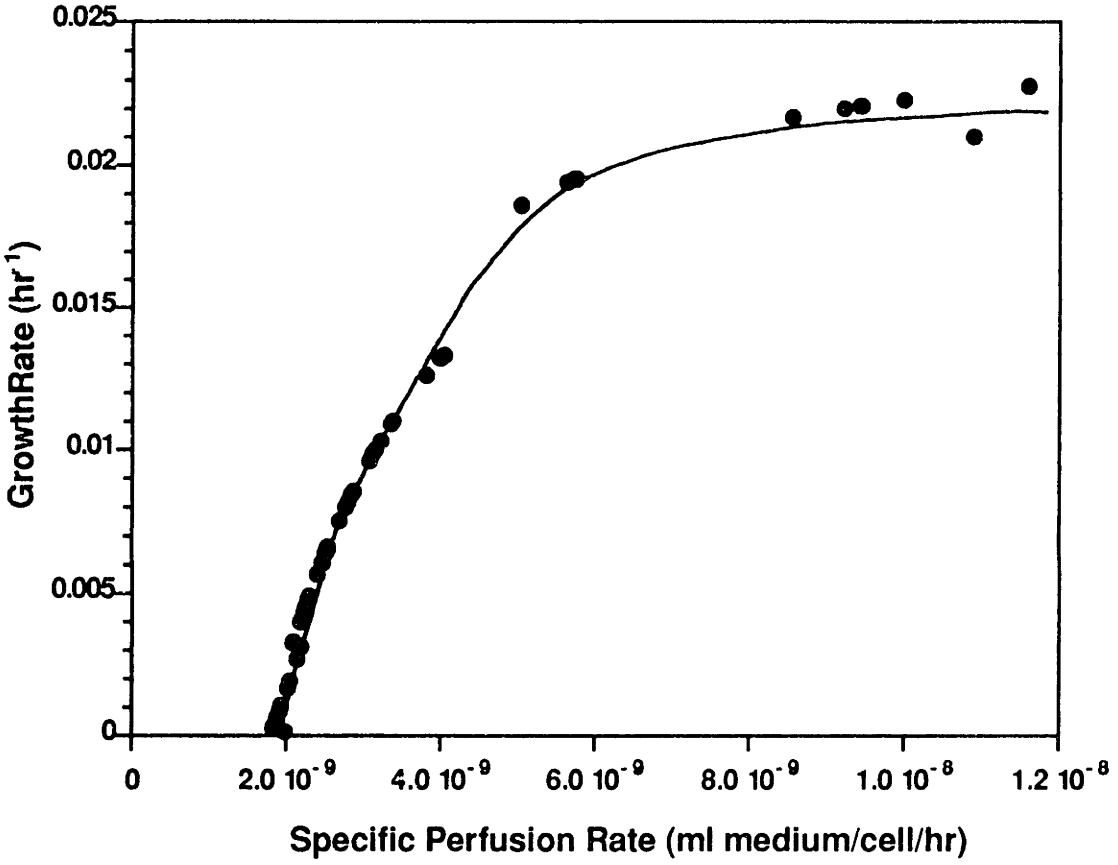

Figure 3.25 Effect of specific perfusion rate on growth rate (CRL-1606)

Based on this analysis, it was concluded that the culture was limited by the specific perfusion rate. The gradient of cell distribution may be partly due to the gradient of the limiting nutrient along the length of the reactor.

The cultivation results of hybridoma CRL-1606 cells in the bioreactor are summarized in Table 3.2. The reactor was operated for 22 days. During this period of time, total cell number increased from 2.3×10^9 cells to 2.0×10^{11} cells in the reactor, corresponding to cell densities of 1.9×10^6 cells/cm^3 and 1.7×10^8 cells/cm^3 respectively. The perfusion rate used ranged from 0.08 to 0.13 hr^{-1}. At steady state, an oxygen uptake rate of 13 mmole/l/hr was achieved. IgG was produced at a rate of 28 mg/l/hr, corresponding to an IgG concentration of 220 mg/l. The different specific rates were calculated from the total cell concentration at the end of the process. At the final stages of bioreactor operation, specific rates for oxygen uptake, glucose consumption, lactate production and IgG production were 1.0×10^{-11} mmole/cell/hr, 1.2×10^{-8} mg/cell/hr, 7.2×10^{-9} mg/cell/hr, 5.8×10^{-10} mg/cell/hr, respectively. Probably due to a different medium composition, the specific IgG production rate was about 50% of that reported by Glacken (Glacken, 1987). However, the volumetric productivity was greatly increased due to the very high cell density.

3.4 Effects of Channeling

When high cell densities are achieved in this bioreactor, one of the potential problem is channeling, or the existence of stagnant regions in the fibrous bed. The inhomogeneity of the fluid flow may cause some inhomogeneous cell growth in the bed

Table 3.2 Summary of cell cultivation results (CRL-1606)

	Inoculum	Final
Cultivation Time		22 days
Total Cell Number (cells/reactor)	2.3×10^9	2.0×10^{11}
Cell Concentration in Fiber-Bed (cells/cm^3)	1.9×10^6	1.7×10^8
Multiplication Ratio		87
Perfusion Rate (hr^{-1})		0.08-0.13
Oxygen Uptake Rate (mmole/l/hr)		13
Ig G Production (mg/l/hr)		28
Steady State IgG Concentration (mg/l)		220
Specific OUR (mmole/cell/hr)		1.0×10^{-10}
Specific Glucose Consumption Rate (mg/cell/hr)		1.2×10^{-8}
Specific Lactate Production Rate (mg/cell/hr)		7.2×10^{-9}
Specific IgG Production Rate (mg/cell/hr)		5.8×10^{-10}

and this may affect the bioreactor performance. In order to assess the potential channeling in the fiber bed, especially at high cell densities, various studies such as the axial and radial cell distributions in the fiber bed, channel radius change and residence time distribution (RTD) of the fiber bed were performed as discussed below.

3.4.1 Cell Distribution

Cell distribution at the end of the cell cultivation experiments was examined axially and radially in order to assess possible unevenness in cell distributions. As mentioned previously, the cells within the packed bed at the end of the γ-CHO cultivations and CRL-1606 cells showed descending distributions along the axial direction from top to bottom of the reactor as shown in Figure 3.9 and Figure 3.22. This behavior has been hypothesized to be due to the filtering effect within the fiber bed.

In order to gain a better insight into the quantitative distributions of cells on the fibers, several types of experiments were performed. The first set of experiments was performed to analyze the sectioned distributions of γ-CHO cells within a given axial position in the bioreactor at the end of the cultivation press. These experiments were macroscopic in nature where the fibers were sectionized and their cell distributions were then quantified. The results from the γ-CHO cells are shown in Figure 3.26.

The fiber mats from the top, middle and bottom of the reactor were cut into three equal sizes after the 66 days cultivation. Each section was then quantified with respect to the total cells within each section. These results are shown in Figure 3.26. It can be seen

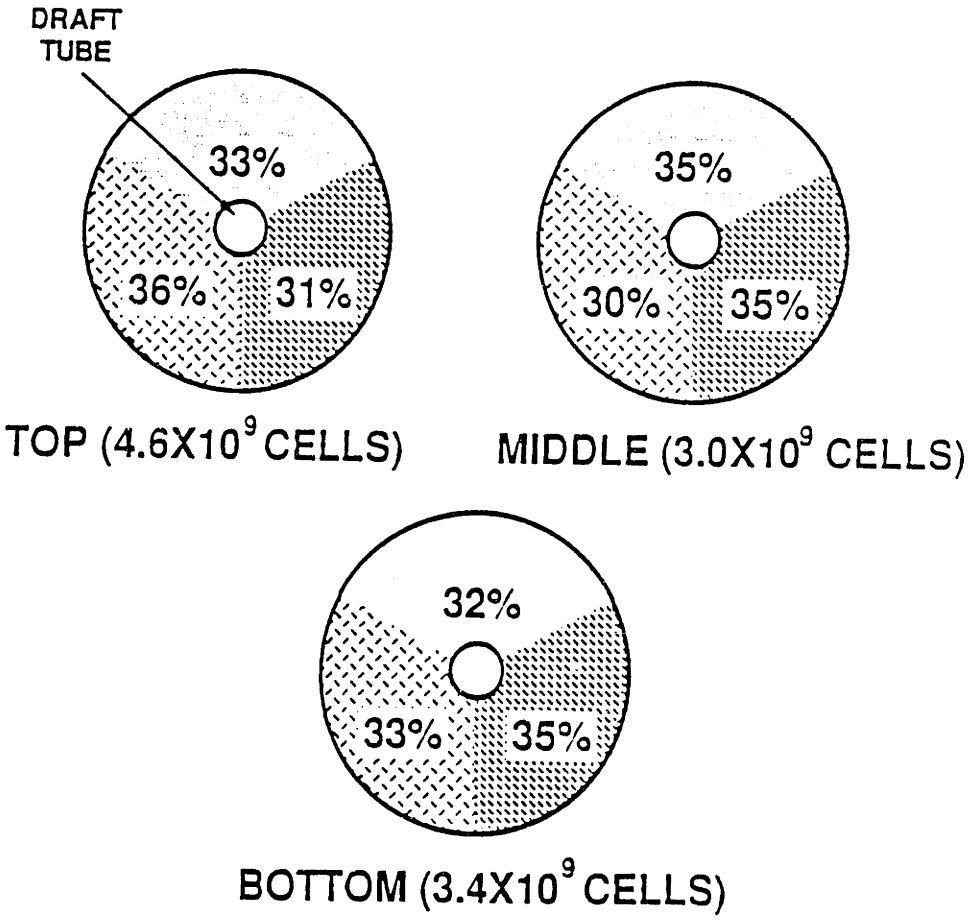

Figure 3.26 Cell distribution within fiber bed (CHO)

from this figure that the total number of cells in each of the three equal sections do not vary significantly even though the total number of cells from the top layer ($4.6x10^9$ cells) was different from the middle and lower layers ($3.0x10^9$ and $3.4x10^9$ cells, respectively). From these results, although macroscopically, we conclude that within the fiber bed the cell distribution is reasonably uniform at a given axial position in the reactor.

To provide an additional indicator on the cell distribution, a second set of experiments was performed using the CRL-1606 suspension cells. In this case, the radial cell distribution was the focus of our study. The experiments were performed using various fiber mats after the 22-day cultivation. More specifically, fiber mats from the middle of the reactor (8th layer) and bottom of the reactor (16th layer) were examined after 22 days of cultivation. The results are shown in Figure 3.27.

In these experiments, the fiber mats were sectioned radially and the cell concentration enumerated quantitatively. The center of the reactor represented the origin for the radial distribution studies. Approximately 1 cm away from the origin, the inner draft tube resided where no fibers are present. Successive radial sections from the draft tube to the outer radius of the fibers were analyzed through the DNA assay for quantifying the cell concentration distributions.

The results shown in Figure 3.27 yielded two useful and confirmatory sets of results. First of all, the radial distributions of the cells are not significantly different along the radial directions. For example, in the middle of the bioreactor, the highest cell concentration was about $1.6x10^8$ cells per cm^3 and the lowest was $1.3x10^8$ cells per cm^3. At the bottom of the reactor, the highest and lowest cell concentrations were $1.4x10^8$ and $1.1x10^8$ cells/cm^3. It is therefore an conclusion that the distribution of the cells within each

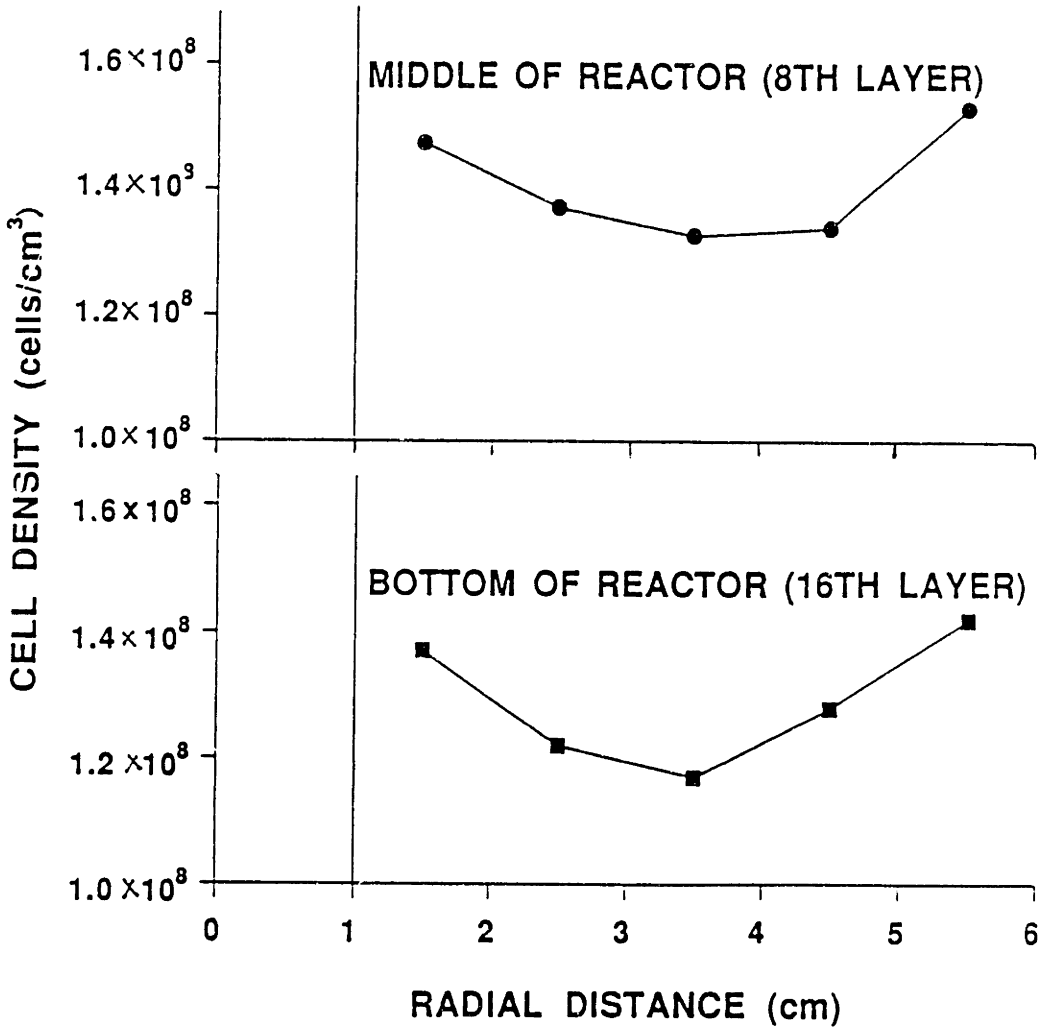

Figure 3.27 Radial cell distribution at the end of cultivation (CRL-1606)

fiber mat layer is reasonably uniform.

The more interesting observation was the shape of the cell distribution curves for both the middle and bottom layers. Both layers exhibited a "parabolic" profile reminiscent of the velocity profile for laminar fluid flow: highest at the center and lowest at the walls. Since the flow within the entire fiber space is within the laminar flow regime. This could further corroborate the previously hypothesized dependence of cell dislodgement and re-entrapment on fluid velocity. Specifically, due to the higher velocity at the center of the annulus, the dislodgement of cells is correspondingly the greatest. Therefore these results further reinforce the earlier hypothesis of the cell distribution data where the axial cell concentration results were presented.

The uniform cell distributions in both radial and axial directions of the fiber bed suggest that on a macroscale, no serious problem due to channeling was expected for cell cultivation in this type of packed-bed bioreactor system within the cell density ranges we investigated. However, it was noted that in the part where the glass fibers cross each other and at the intersections, cells tend to accumulate and form more layers. Visual evidence showed that there was some bridging of cells when the fibers were very close to each other (shown in Figure 3.28). At a cell density of 2×10^8 cells/cm^3 of CRL-1606 culture, some clumps bigger than 300 μm were observed. This led to the blockage of some small channels. Based on the analysis of diffusional penetration depth shown in Appendix, the cells in the middle of the big clumps could encounter nutrient deprivation. This is probably the primary reason for the 25% of non-viable cells observed at the end of the CRL-1606 cell cultivation.

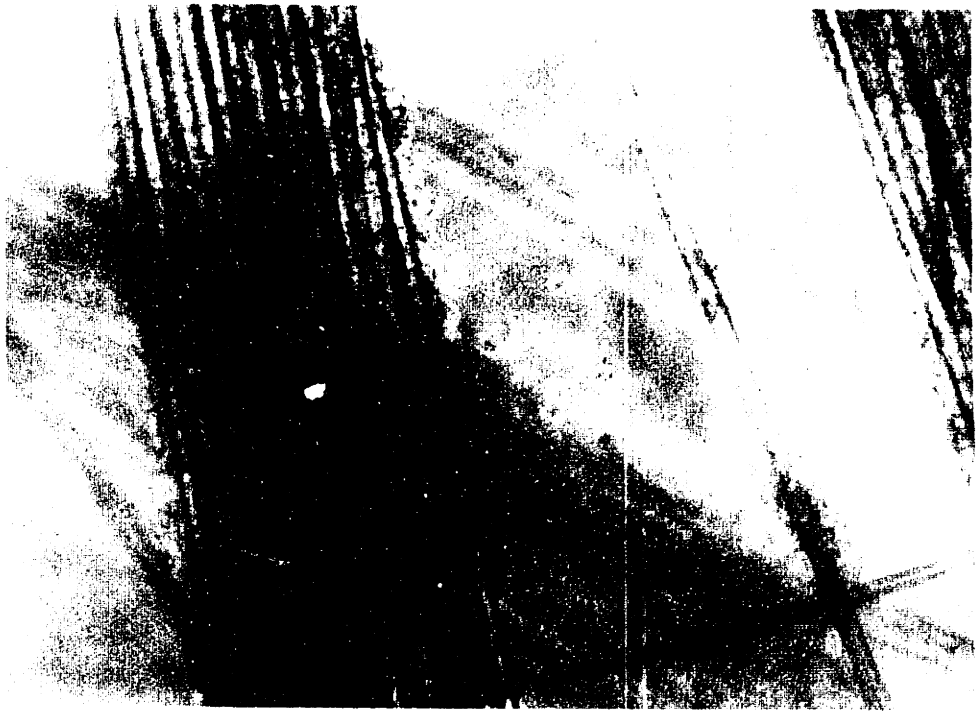

Figure 3.28 Photograph of blockage of small channels

fiber mat layer is reasonably uniform.

The more interesting observation was the shape of the cell distribution curves for both the middle and bottom layers. Both layers exhibited a "parabolic" profile reminiscent of the velocity profile for laminar fluid flow: highest at the center and lowest at the walls. Since the flow within the entire fiber space is within the laminar flow regime. This could further corroborate the previously hypothesized dependence of cell dislodgement and re-entrapment on fluid velocity. Specifically, due to the higher velocity at the center of the annulus, the dislodgement of cells is correspondingly the greatest. Therefore these results further reinforce the earlier hypothesis of the cell distribution data where the axial cell concentration results were presented.

The uniform cell distributions in both radial and axial directions of the fiber bed suggest that on a macroscale, no serious problem due to channeling was expected for cell cultivation in this type of packed-bed bioreactor system within the cell density ranges we investigated. However, it was noted that in the part where the glass fibers cross each other and at the intersections, cells tend to accumulate and form more layers. Visual evidence showed that there was some bridging of cells when the fibers were very close to each other (shown in Figure 3.28). At a cell density of $2x10^8$ cells/cm^3 of CRL-1606 culture, some clumps bigger than 300 μm were observed. This led to the blockage of some small channels. Based on the analysis of diffusional penetration depth shown in Appendix, the cells in the middle of the big clumps could encounter nutrient deprivation. This is probably the primary reason for the 25% of non-viable cells observed at the end of the CRL-1606 cell cultivation.

packed bed.

3.4.3 Residence Time Distribution (RTD)

The RTD for the fiber bed operating with γ–CHO and hybridoma cells at various cell densities are shown in Figures 3.29 and 3.30 respectively. These RTD profiles were obtained at a constant flow rate of 0.134 cm/s. The RTD for the column without cells showed slight tailing of the tracer. Similar to the principle of size exclusion chromatography, this tailing resulted from the tracer having to travel through the more tortuous pathways (i.e. through small channels). More importantly, Figures 3.29 and 3.30 indicated that cell growth in the fiber bed affected the mean residence time of the RTD curves. Table 3.3 lists some results which were calculated from the RTD experiments. At a constant flow rate, mean residence time (MRT) can be calculated from the void volume of the column and the liquid flow rate as shown in Equation 3.2.

$$(MRT)_{calculated} = \text{void volume / liquid flow rate} \qquad (3.2)$$

The mean residence times tabulated in Table 3.3 were obtained through actual measurements, as well as the calculated mean residence time based on void volume and liquid flow rate in the fiber-bed column (Equation 3.2).

Comparing the column without cells and the column with 1.2×10^7 γ-CHO cells/cm^3, the measured mean residence time was nearly identical to the calculated mean residence time. For the columns with higher cell densities (5.6×10^7 γ-CHO cells/cm^3,

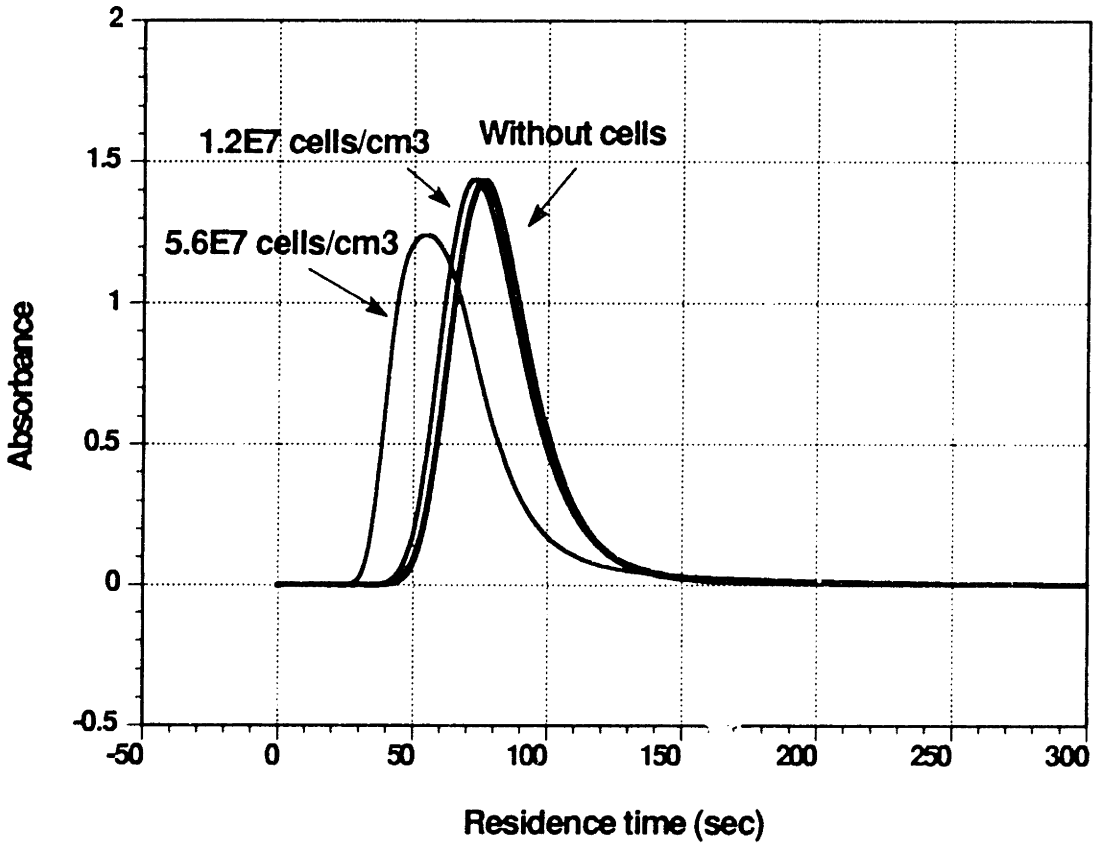

Figure 3.29 Residence time distribution in the fiber bed for CHO cells at different cell concentrations

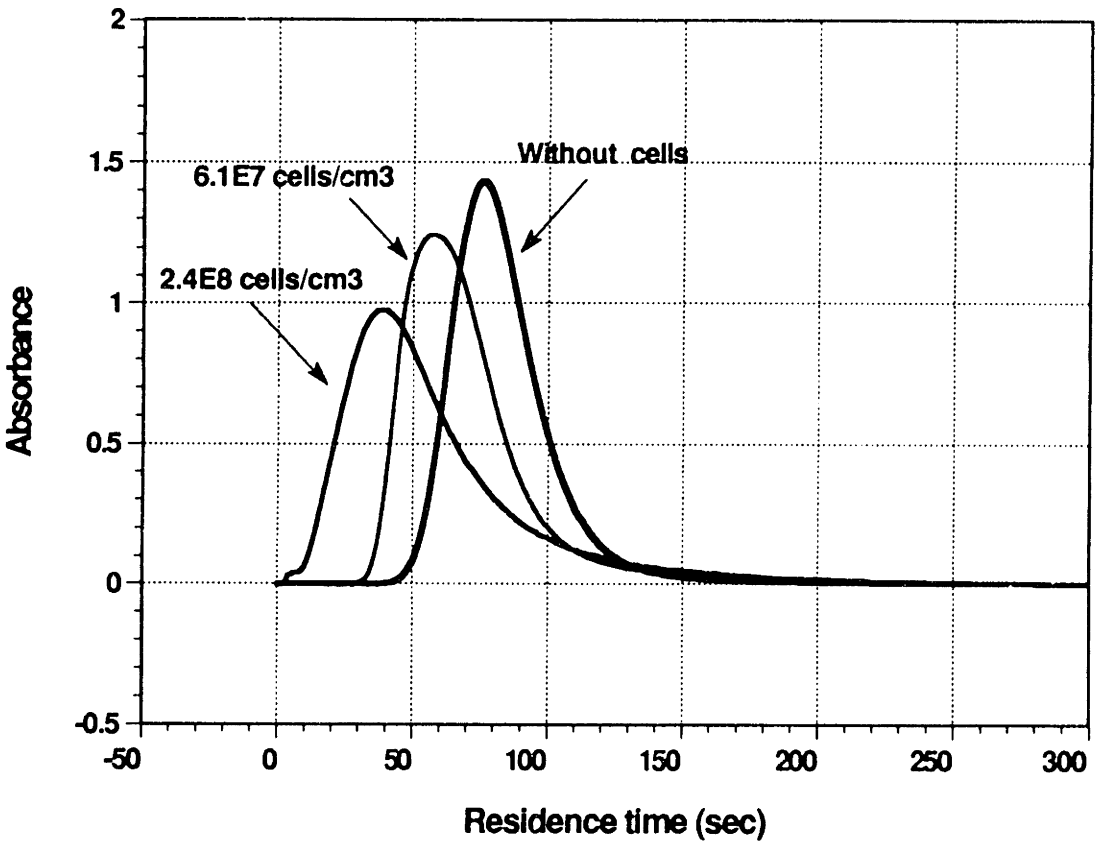

Figure 3.30 Residence time distribution for hybridoma ATCC-CRL-1606 at different cell concentrations

Table 3.3 Data on residence time distribution studies

Cell Line	Cell Number* (cells/cm^3)	Void Fraction	Measured				Calculated			
			MRT ** (sec)	Variance	$D/U_l L$	*Dax* *** (cm^2)	MRT (sec)	Apparent Void Fraction	Pe'****	*Dax* (cm^2)
CHO	0	0.915	68.7±0.4	247±52	0.001	0.0013	68.3	0.92	33	0.00046
	1.2×10^7	0.89	67.4±0.2	396±44	0.025	0.0034	66.3	0.90	83	0.0013
	5.6×10^7	0.81	54.9±0.3	904±85	0.013	0.018	60.5	0.74	160	0.0061
Hybridoma	0	0.915	68.7±0.4	247±52	0.001	0.0013	68.3	0.92	33	0.00046
	6.1×10^7	0.86	58.2±0.3	989±79	0.016	0.021	63.8	0.78	78	0.0017
	2.4×10^8	0.69	46.6±0.3	1806±157	0.053	0.071	51.7	0.63	137	0.0183

* The cell number was obtained from nuclei counting.

** MRT = Mean residence time

*** *Dax* = Axial dispersion coefficient

**** $Pe' = U_l r / D_f$

$6.1x10^7$ hybridoma cells/cm^3, or $2.4x10^8$ hybridoma cells/cm^3), the peaks from the tracer appeared earlier than expected. This early appearance of the tracer suggested some channeling of fluid and possibly the presence of stagnant regions in the reactor at high cell densities. The magnitude of this non-ideal fluid behavior can be estimated by calculating the experimental void volume of the fiber bed. The experimental void volume can be obtained by multiplying measured MRT with liquid flow rate operated and shown in Table 3.3. For the column without cells and the column with $1.2x10^7$ γ-CHO cells/cm^3, the experimental void fraction is quite close to value based on the actual void fraction of the fiber bed. However, for the columns with higher cell densities ($5.6x10^7$ γ-CHO cells/cm^3, $6.1x10^7$ hybridoma cells/cm^3, or $2.4x10^8$ hybridoma cells/cm^3), there were deviations between the experimental void fraction and the actual void fraction based on cell size and occupancy. For example, at a cell density of $2.4x10^8$ cells/cm^3, the void fraction of the fiber-bed was calculated to be 0.69 based on cell size and cell occupancy but the experimental void fraction calculated from measured MRT was only 0.63. Assuming that the latter number is accurate, these results suggest that about 6% of the fiber bed volume suffered from liquid channeling. This comparison suggests that a small portion of the bed encountered channeling, probably resulting from the blockage of small channels by the cells as shown in Figure 3.28. The channels in the fiber bed can roughly be categorized into two groups; one large group has sizes on the order of millimeters and the other group having smaller sizes on the order of microns. Based on visual observation, at high cell densities, the small channels were all blocked and the big channels were reduced in size due to the multilayer growth. This blockage of the small channels resulted in the formation of more uniform large channels. The shift in the mean of the channel size distribution can be illustrated in Figure 3.31. Additional information can be derived from further analysis of the tracer behavior in the presence and absence of cell growth. More specifically, the increased spreading of the tracer can be used as a measure of fluid dispersion.

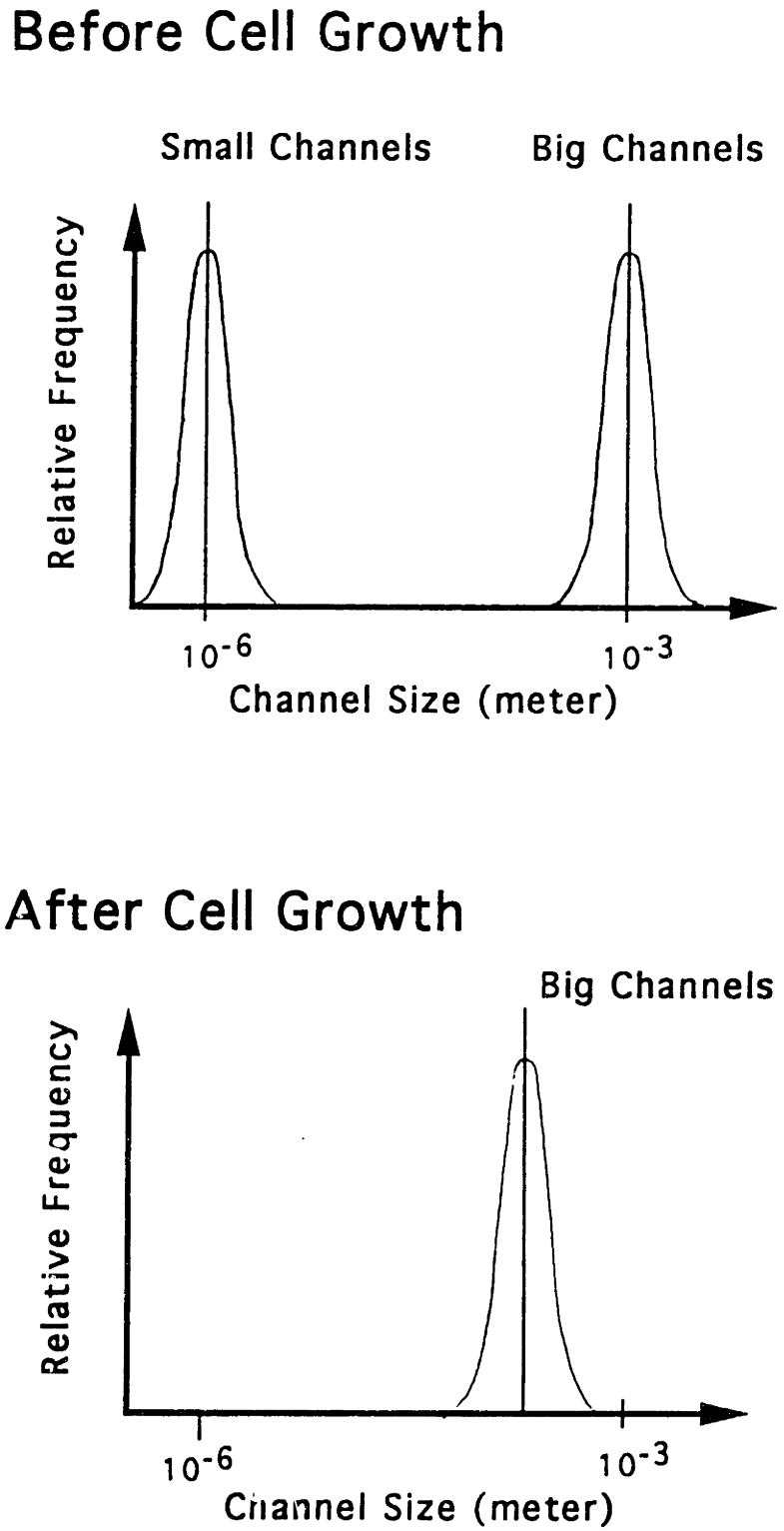

Figure 3.31 Shift in channel radius due to cell growth

The variance of the distribution is an important parameter to characterize peak spreading. It can be calculated by numerical integration of the concentration with respect to time as described in the Materials and Methods section. The variance can be related to axial dispersion coefficient based on an axial dispersion model as given below:

$$\text{Variance}/(\text{MRT})^2 = 2(D_{ax}/U_lL) \tag{3.3}$$

where D_{ax} is axial dispersion coefficient, U_l is the liquid velocity and L is the bed length. Axial dispersion is due to the axial fluid velocity gradient and the axial dispersion coefficient is used to characterize the degree of backmixing during flow. The dimensionless group (D/U_lL) is called the reactor dispersion number and its quantitative value measures the extent of axial dispersion. When (D/U_lL) approaches zero, there is negligible dispersion, hence plug flow. However, as (D/U_lL) increases, there is increasing dispersion and backmixing can be anticipated (Levenspiel, 1972).

The variance from the RTD profiles (Figure 3.29 and Figure 3.30) increased from 250 to 2000 as the cell density increased from 0 to 2.4×10^8 cells/cm^3. The corresponding calculated (D/U_lL) varied from 0.001 to 0.053 and the axial dispersion coefficients varied from 0.0013 to 0.071 as listed in Table 3.3. The values of (D/U_lL) at various cell densities were all relatively small; however, they increased as the cell density increased. It suggests that the increase of the cell density in the fiber bed led to a greater extent of axial dispersion in the fiber bed. The cause of this increase in axial dispersion can be explained by using the model developed by Koch and Brady (Koch and Brady, 1986).

Koch and Brady (1986) developed a theory for determining the dispersion in fibrous beds. Based on their model, the axial dispersion coefficients can be calculated and the equation used for the fibers normal to the flow is :

$$D_{ax}=D_f\left\{\frac{\pi}{8}\frac{r}{k^{1/2}\phi}|Pe'| + 5.835\frac{\phi\, r^2}{k}|Pe'|\ln|Pe'|\right\} \qquad (3.4)$$

where D_{ax} is the axial effective diffusivity, D_f is the diffusivity in the fluid, k is the permeability of fiber bed, ϕ is the volume fraction of fibers in the fiber bed, r is the fiber radius, Pe' is the Peclet number based on fiber radius ($U_l r/D_f$), and U_l is average velocity. The tracer used in the RTD experiments was phenol red (phenolsulfonphthalein). Its diffusivity was estimated by Wilke and Chang correlation (1955), and was found to be about 4.9×10^{-6} cm^2. The permeability (determined experimentally) and the "apparent" fiber radius (calculated based on the model of multilayer cell growth) were used for calculating the axial dispersion coefficient. Table 3.3 lists the calculated Pe' and axial dispersion coefficients.

The calculated Peclet number based on fiber radius (Pe') ranged from 33 to 160. More importantly, the axial dispersion coefficients increased from 0.00046 to 0.018 cm^2 as the cell density increased from 0 to 2.4×10^8 cells/cm^3. These values showed the same trend as the values obtained from experimental RTD profiles. Osawa (1992) reported that axial dispersion increases directly with the fiber diameter and inversely with void fraction. Consistent with Osawa's findings, our results suggest that the greater dispersion at the high cell densities was due to the larger "apparent" fiber diameter and the lower void fraction resulting from multilayer cell growth.

From the RTD studies, it can be concluded that as cell density increased, there was a small number of stagnant regions and the increase in peak variance was primarily due to the increase in axial dispersion which resulted from the reduction in void fraction and increase in "apparent" fiber diameter.

Based on these theoretical and experimental analyses, it seems that, on a macroscale, no serious problem due to channeling will result during cell cultivation in this type of packed-bed bioreactor system. This is further substantiated by the previous observations that within the cell density ranges investigated uniform cell distributions in both the radial and axial directions of the fiber bed were observed. In addition, the channels were still quite open for fluid flow even at very high cell densities. However, on a microscale, due to the inhomogeneous structure of the fiber mat, it was observed that the accumulation of cells resulted in the blockage of small channels. RTD studies also showed that there was a small amount of stagnant regions and that the reduction in void fraction and increase in fiber diameter caused the increase in axial dispersion at high cell density.

CHAPTER 4. SCALEUP POTENTIAL

In order to assess the scaleup potential of the modified air-lift fiber-bed bioreactor, the equations presented in the hydrodynamic model in Theoretical Analysis have been used to calculate the achievable oxygen transfer rate for various reactor volumes. Since the reactor configuration proposed in this thesis is a simple concentric loop reactor, the geometric scaling parameters which were considered for the various reactor volumes were the ratio of draft tube diameter (Di) to reactor diameter (Do) and the aspect ratio (ratio of reactor height to reactor diameter). Reactor height, draft tube height, and fiber bed height were assumed to be constant in the simulations. By performing parametric analyses using Equations III.1 to III.18, trends in the reactor characteristics and performances were obtained and the scaleup potential was evaluated.

Before calculating the scaleup potential, the permissive air flow rate must be defined. Air flow rate is limited by the foam formation due to serum proteins and other surface active agents in the medium. Despite the availability of some mechanical foam breaking methods (Goldberg and Rubin, 1967), an antifoam is usually used to curb the excess foaming in the reactor. As shown previously in Figure 1.1, it was necessary to increase the antifoam concentration due to the increase in the air flow rate. In this case, to maintain the antifoam concentration below 1000 ppm, which has proven to be non-toxic for γ-CHO and CRL-1606 cells, air flow rate of 1 VVM (gas flow rate per reactor volume) was chosen. In the following calculations, an air flow rate (60 Q_g/V_l) of 1 VVM was used.

The scaleup calculation was first performed for the reactor without cells and thus a constant permeability was employed. The scaleup potential for the reactor at various cell

densities will then be presented.

4.1 Reactors without Cells

In order to assess the scaleability of the bioreactor in terms of its ability to transfer oxygen, the highest oxygen transfer rates for various aspect ratios (ratio of reactor height to reactor diameter) ranging from 0.1 to 100 and various reactor volumes ranging from 1 to 10,000 liters were first determined. At the given gas flow rate (1 VVM), the highest oxygen transfer rate as a function of the aspect ratio at different reactor volumes was obtained from the variation of achievable oxygen transfer rate at each Di/Do ratio ranging from 0.1 to 0.5. These maximal oxygen transfer rates at various aspect ratios and reactor volumes are shown in Figure 4.1.

As seen from this figure, the maximal achievable oxygen transfer rate increases as the reactor volume increases. This is primarily due to the higher liquid flow rate and higher mass transfer coefficient obtained at the higher gas flow rate (Qg). Although the VVM is the same, the actual gas flow rate (Qg) and superficial gas velocity are higher for the large reactor volumes. The correlation between the maximal oxygen transfer rate and the reactor volume was found to be:

$$\text{Max OTR} = 8.67 + 1.33 \log (V) \qquad (4.1)$$

Also seen in Figure 4.1 , the maximal oxygen transfer rate is affected by both aspect ratio and reactor volume. A clear optimal aspect ratio exists at each reactor volume. The optimal aspect ratio decreases as the reactor volume increases. The correlation between the aspect

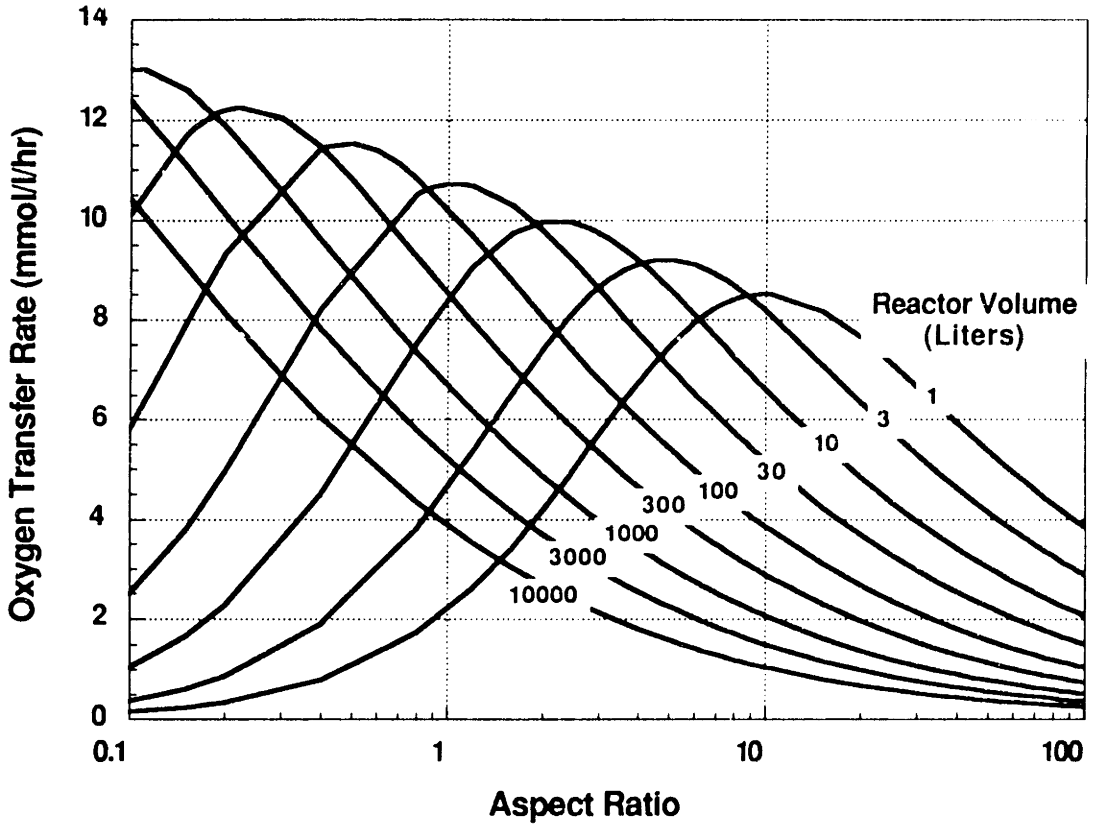

Figure 4.1 Oxygen transfer rate at various aspect ratios and reactor volumes

(Aspect ratio: Ratio of reactor height to reactor diameter)

ratio and the reactor volume was found to be:

$$\text{Opt AR} = 9.7\ V^{-0.65} \tag{4.2}$$

With an aspect ratio less than optimum, reduction of gas hold up causes a decrease in oxygen transfer rate; with a value greater than optimum, an increase in bed height reduces oxygen transfer.

Although a low aspect ratio results in small pressure drop, from a practical point of view, an aspect ratio less than 1 will cause the following problems: (a) unsymmetrical flow in the draft tube leading to the reduction of gas hold up, and (b) packed density heterogeneity causing channeling and reduced nutrient supply. Hence, a reactor should be designed with an aspect ratio of at least greater than 1 despite its deviation from the optimum. As seen from Figure 4.1, for reactors larger than 100 liters and aspect ratios greater than one, increasing the aspect ratio results in decreasing oxygen transfer rate. Consequently, maximal oxygen transfer rate occurs at an aspect ratio equal to one. Therefore, an aspect ratio of one was chosen for reactors larger than 100 liters in the scaleup calculations. As for reactors less than 100 liters, the optimal aspect ratio occurs at the maximal oxygen transfer rate as seen from Figure 4.1.

The effect of the deviations of aspect ratio on the maximal oxygen transfer rate and corresponding Di/Do ratio is shown in Figures 4.2a and 4.2b. The solid lines indicate the condition without aspect ratio restriction and the dashed lines illustrate the one for which the aspect ratio has to be equal to or greater than one. Due to the restriction of aspect ratio (*i.e.*, aspect ratio ≥ 1), the oxygen transfer rates in the reactors larger than 100 liters are away from its maximum. As shown in Figure 4.2a, the larger the reactor, the more

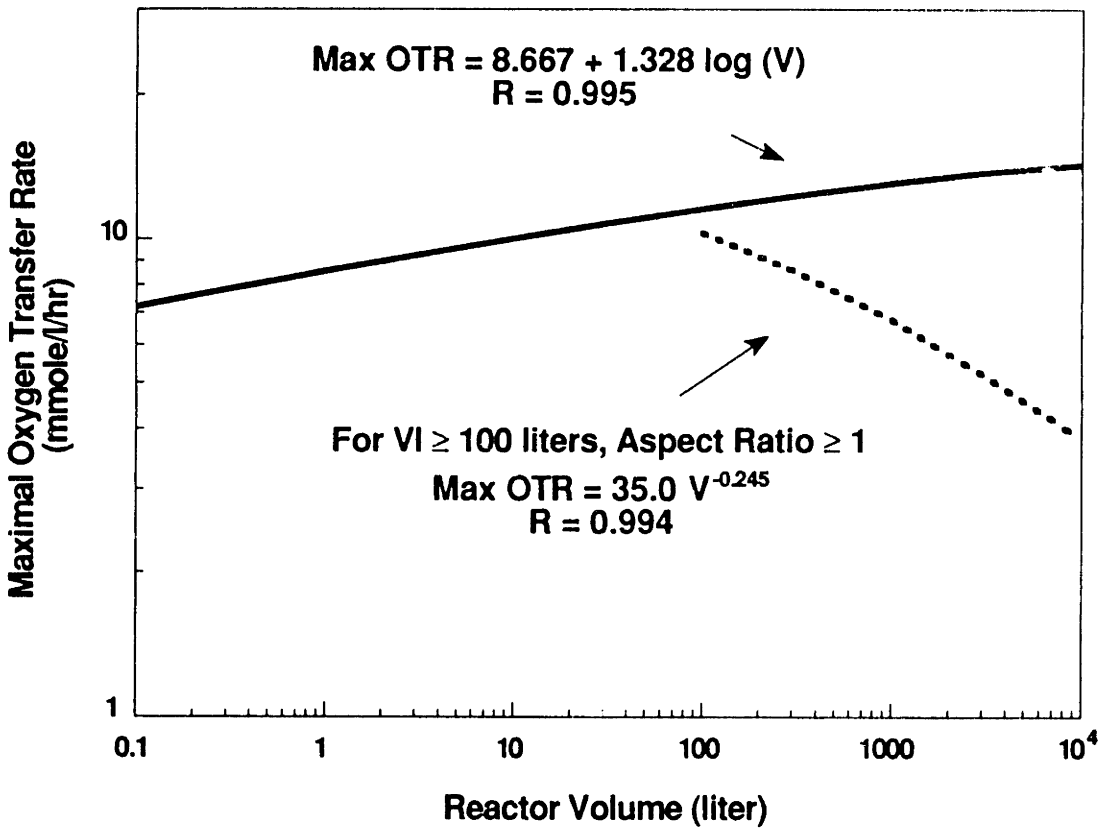

Figure 4.2a Maximum oxygen transfer rate versus reactor volume

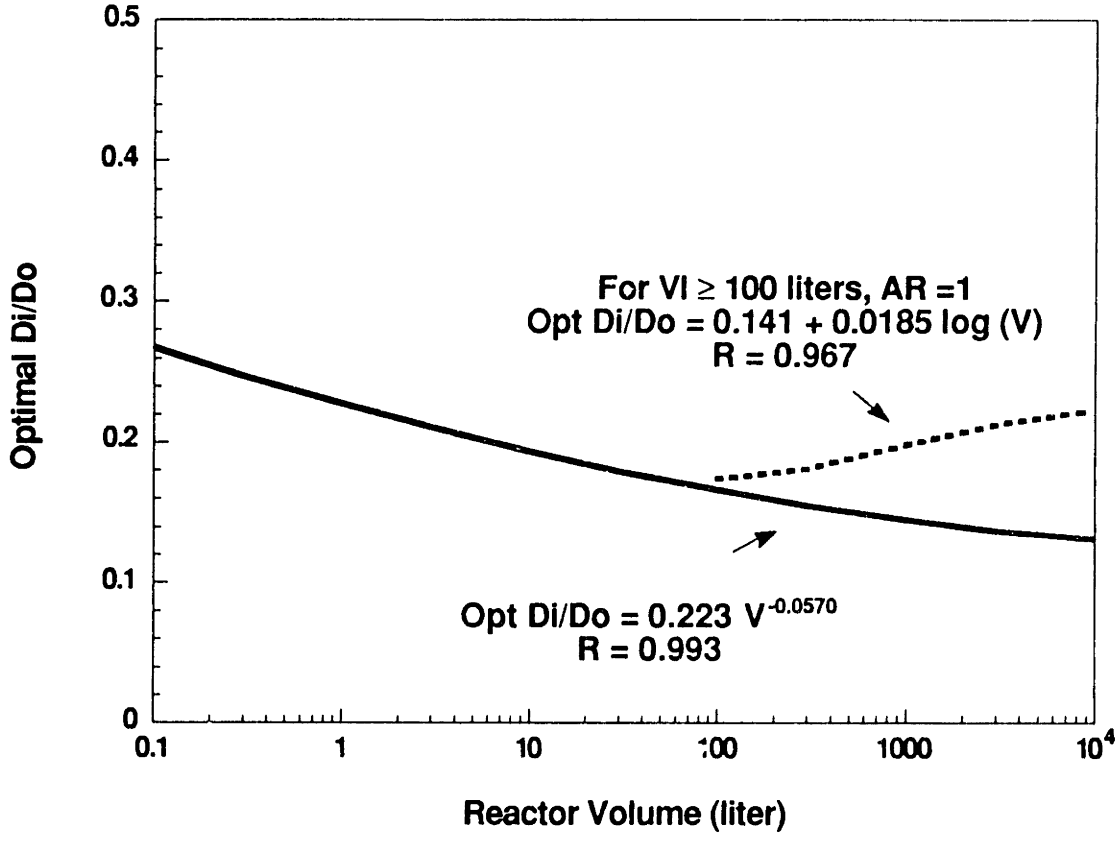

Figure 4.2b Optimal Di/Do ratio versus reactor volume

(Di/Do: ratio of draft tube diameter to reactor diameter;
AR: Ratio of reactor height to reactor diameter)

significant the deviation. As a result, with the restriction of aspect ratio, the maximal oxygen transfer rate increased with the reactor volume and decreased as the reactor became larger than 100 liters. Under the aspect ratio restriction, the correlation between the maximal oxygen transfer rate and the reactor volume for reactors larger than 100 liters was found to be:

$$\text{Max OTR} = 35.0\ V^{-0.24} \tag{4.3}$$

The maximal oxygen transfer rate decreases exponentially as the reactor volume increases. However, even at a very big scale, such as 10,000 liters of volume, the main point to note is that oxygen transfer rates higher than 4 mmole/l/hr are still achievable.

Compared to the corresponding Di/Do ratios for the maximal achievable oxygen transfer rate without aspect ratio restriction, the corresponding Di/Do ratios resulting from the restriction in aspect ratio were higher as shown in Figure 4.2b. For both cases (with and without aspect ratio restriction), the optimal Di/Do ratios range from 0.13 to 0.27 at various reactor volumes. Compared to those of the traditional airlift fermentors, these optimal Di/Do ratios are relatively low (Hach, 1973; Weiland, 1984; Koide *et al.*, 1984; Jones, 1985; Blenke, 1985). This is good in the sense that the *in situ* oxygenator takes only a small portion of the reactor and the reactor can be more efficiently used for growing cells in its annular region.

4.2 Reactors with Cells

It is known that cell growth affects permeability (shown in Chapter 2) and

consequently affects oxygen transfer in the reactor. The optimal geometry for oxygen transfer rate in the reactors of 2.5, 250, and 1000 liters was therefore analyzed for various cell densities. The scaleup method was similar to that for the reactor analysis without cells. In these cases for the reactors with cells, different void fractions and permeabilities at various cell densities were taken into consideration. The void fractions and permeabilities of the fiber bed for various cell densities used in the scaleup calculations are listed in Table 4.1. The void fractions used ranged from 0.90 to 0.81 and the permeabilities used ranged from $1.8x10^{-5}$ to $1.1x10^{-5}$ cm^2. These values were obtained from the multilayer cell growth model for hybridoma cells. In this case, we only consider aspect ratios greater than one due to the geometric limitations discussed previously.

Figures 4.3, 4.4 and 4.5 show the effects of aspect ratio on the achievable oxygen transfer rate at cell densities of $1x10^7$, $5x10^7$ and $1x10^8$ cells/cm^3 respectively. For all three cell densities, the effect of aspect ratio on oxygen transfer at three reactor volumes shows the same trend. For the 2.5-liter reactor, the optimal aspect ratio at which maximal oxygen transfer occurs was about 1.4 for all three cell densities. For the 250- and the 1000-liter reactors, since oxygen transfer rate is inversely proportional to the aspect ratio in the range between 1 and 10, aspect ratio of one has to be chosen as previously discussed. Therefore, the optimal geometry and the achievable oxygen transfer rate for 2.5, 250, and 1000-liter reactor at various cell densities are listed in Table 4.2. Based on the optimal aspect ratio, the 2.5-liter reactor has a height of 18.4 cm and a diameter of 13.2 cm. The optimal reactor height and reactor diameter are 68.3 cm for the 250-liter and 108.4 cm for the 1000-liter reactor. As shown in Table 4.2, at a given reactor volume, the optimal Di/Do ratios gradually decreased as the cell density increased. This is due to the permeability decrease as shown previously in Figure 2.5. Again, the optimal Di/Do ratios are all very low (around 0.2) compared to the traditional airlift fermentors. The calculated draft tube

Table 4.1 Parameters used in the scaleup calculation for reactors at various cell densities

Cell density (cells/cm^3)	Void fraction	Permeabilty (k) (cm^2)
$1x10^7$	0.90	$1.8x10^{-5}$
$5x10^7$	0.86	$1.5x10^{-5}$
$1x10^8$	0.81	$1.1x10^{-5}$

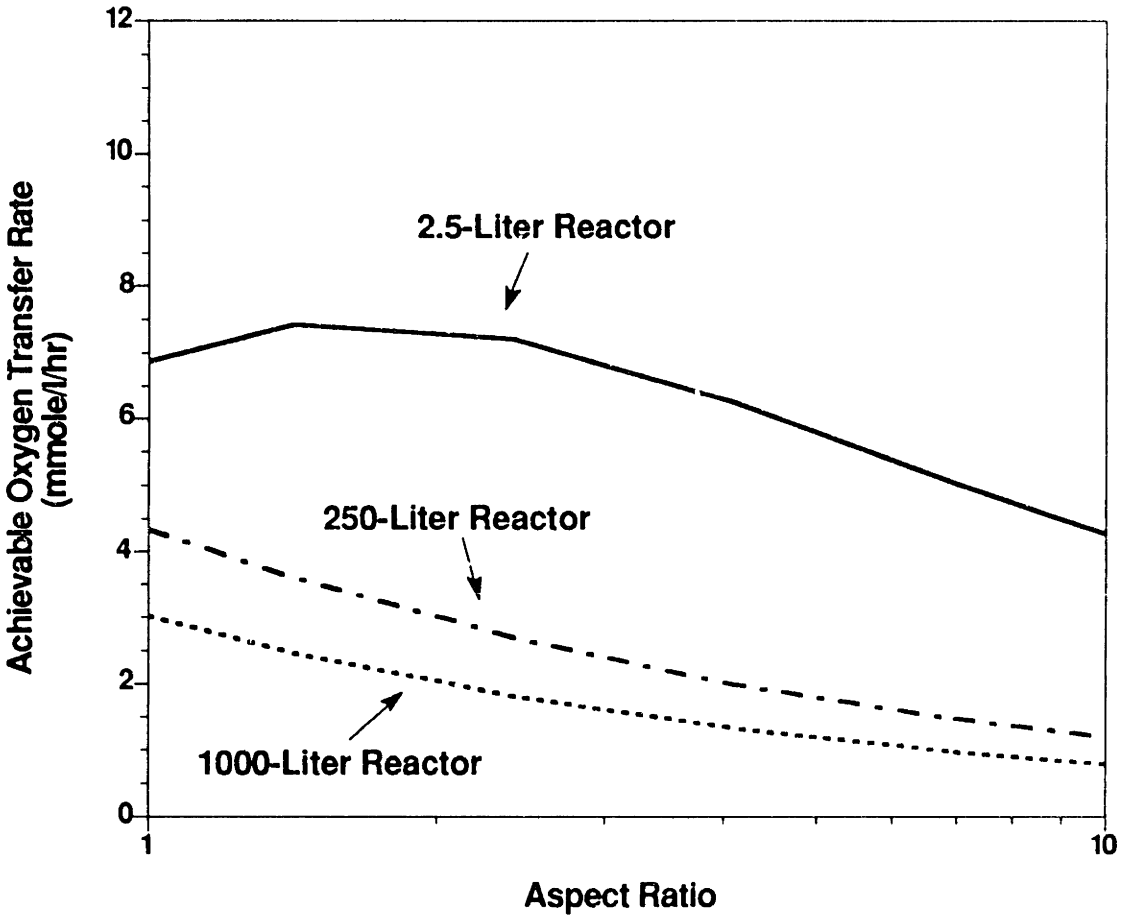

Figure 4.3 Effect of aspect ratio on oxygen transfer at $1x10^7$ cells/cm^3

(Aspect ratio: Ratio of reactor height to reactor diameter)

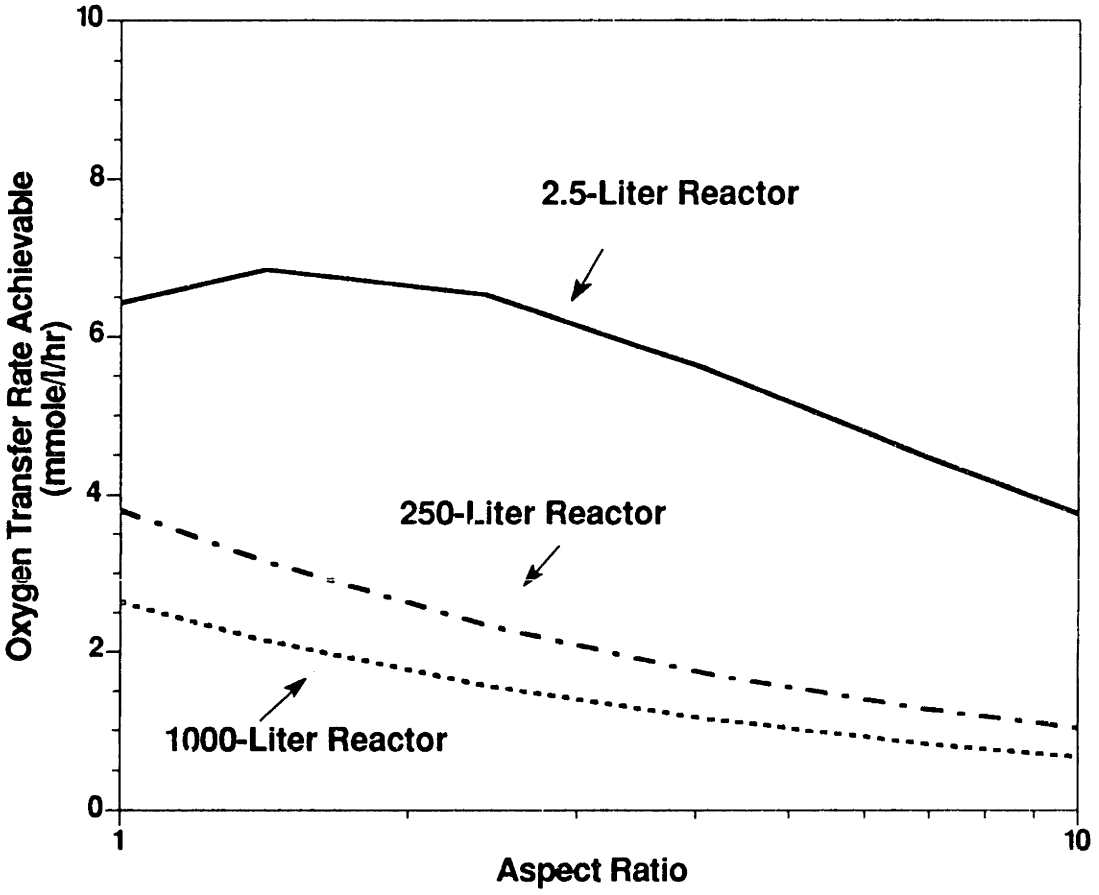

Figure 4.4 Effect of aspect ratio on oxygen transfer at $5x10^7$ cells/cm^3

(Aspect ratio: Ratio of reactor height to reactor diameter)

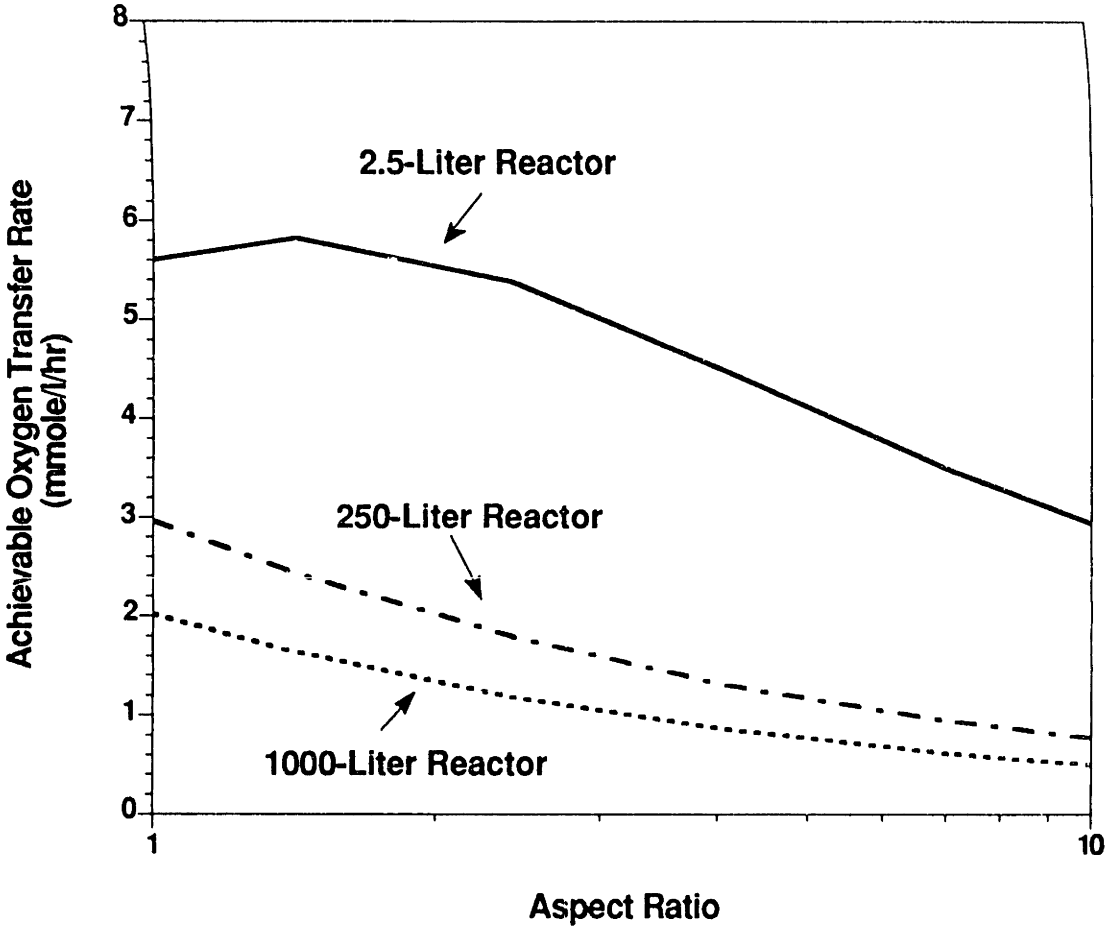

Figure 4.5 Effect of aspect ratio on oxygen transfer at $1x10^8$ cells/cm^3

(Aspect ratio: Ratio of reactor height to reactor diameter)

Table 4.2 Optimal geometry and the maximal achievable oxygen transfer rate for 2.5-, 250-, and 1000-liter reactor at various cell densities.

Cell density ($cells/cm^3$)	2.5-liter reactor		250-liter reactor		1000-liter reactor	
	Opt geometry	Max OTR achievable (mmole/l/hr)	Opt geometry	Max OTR achievable (mmole/l/hr)	Opt geometry	Max OTR achievable (mmole/l/hr)
$1x10^7$	AR= 1.4 Di/Do=0.234 H=Lo=Li=18.4 cm Do=13.2 cm Di=3.1 cm	7.41	AR=1 Di/Do=0.192 H=Lo=Li=Do =68.3 cm Di=13.1 cm	4.3	AR=1 Di/Do=0.196 H=Lo=Li=Do =108.4 cm Di=21.2 cm	3.0
$5x10^7$	AR=1.4 Di/Do=0.22 H=Lo=Li=18.4 cm Do=13.2 cm Di=2.9 cm	6.84	AR=1 Di/Do=0.184 H=Lo=Li=Do =68.3 cm Di=12.6 cm	3.8	AR=1 Di/Do=0.190 H=Lo=Li=Do =108.4 cm Di=20.6 cm	2.7
$1x10^8$	AR=1.4 Di/Do=0.196 H=Lo=Li=18.4 cm Do=13.2 cm Di=2.6 cm	5.82	AR=1 Di/Do=0.170 H=Lo=Li=Do =68.3 cm Di=11.6 cm	2.9	AR=1 Di/Do=0.177 H=Lo=Li=Do =108.4 cm Di=19.2 cm	2.0

AR = Aspect ratio = Ratio of reactor height to reactor diameter
Di = Diameter of inner draft tube
Do = Diameter of reactor
H = Height of reactor
Lo = Height of fiber bed
Li = Height of inner draft tube

diameters ranged from 3.1 to 2.6 cm, 13.1 to 11.6 cm, and 21.2 to 19.2 cm for 2.5-, 250-, and 1000-liter reactors respectively.

Also seen from Figures 4.3 to 4.5, the achievable oxygen uptake rates shift downwards gradually due to the decrease of permeability of the fiber bed. The maximal achievable oxygen transfer rate for various sizes of the reactor and various cell densities are listed in table 4.2. The maximal achievable oxygen transfer rate decreased as the cell density increased because of consequent decrease in the permeability. For cell densities ranging from $1x10^7$ cells/cm^3 to $1x10^8$ cells/cm3, the maximal achievable oxygen transfer rates ranged from 7.41 to 5.82 mmole/l/hr for the 2.5-liter reactor; from 4.3 to 2.9 mmole/l/hr for the 250-liter reactor; and from 3.0 to 2.0 mmole/l/hr for the 1000-liter reactor. Since the typical specific oxygen uptake rates range from $1x10^{-11}$ mmole/cell/hr to $2x10^{-10}$ mmole/cell/hr (Glacken *et al.*, 1983), the oxygen requirement for cell densities of $1x10^7$, $5x10^7$, and $1x10^8$ cells/cm3 are 0.1 to 2 mmole/l/hr, 0.5 to 10 mmole/l/hr, and 1 to 20 mmole/l/hr respectively. Therefore, we conclude that the maximal oxygen transfer rate by air sparging can certainly meet the requirements of the cell lines with low specific oxygen uptake rates at high cell densities. However, cell lines with high specific oxygen uptake rates may be starved of oxygen under these conditions. One possibility to increase the oxygen transfer rate is to increase the oxygen composition in the sparged gas. This has been successfully demonstrated in the cell cultivation experiment for CRL-1606 cells. Due to the concern of oxygen toxicity, there is a limit to the maximum oxygen content in the inlet gas line. Therefore, for the cell lines with high specific oxygen uptake rate, it is difficult to maintain cell densities higher than $5x10^7$ cells/cm^3 for the 250- and the 1000-liter reactors.

In conclusion, for large scale reactors such as 250-liter and 1000-liter in size, having

an aspect ratio of 1, the oxygen supplied would be able to meet the oxygen demand of high cell densities. For some cases, increasing the oxygen content in the inlet gas line may be necessary. The reactor is therefore scaleable.

VI. SUMMARY AND CONCLUSIONS

The objective of the thesis is to provide an alternative for animal cell culture using a novel bioreactor designed to overcome some of the problems in animal cell cultivation. The conclusions from this thesis are summarized below:

Bioreactor Design

Based on cell anchorage onto glass fibers and sparging of air through an inner draft tube, the design of a novel bioreactor was developed. The bioreactor consists of an inner draft tube and an annular packed glass fiber bed. Cells are immobilized in the annular glass fiber bed and medium fills both the draft tube and the annular region. Air is introduced from the base of the draft tube and oxygenates the medium in the draft tube; and bubbles disengage at the upper fluid surface. The hydrostatic pressure difference between the aerated fluid in the draft tube and the bubble-free fluid in the annular fiber-bed results in the global circulation of the medium in the bioreactor.

This bioreactor design provides the following unique characteristics: (1) the reactor can provide a very high surface-to-volume ratio in the annular section by choosing glass fibers of small diameter; (2) *in situ* oxygenation with no external loop can be achieved; (3) the cells are not exposed to gas-liquid interfaces since no gas bubble is entrained by the oxygenated medium in the annular region; (4) nutrients are convectively supplied to the immobilized cells when the fluid is flowing through such a system; (5) very little hydrodynamic cell damage can result since low turbulence and low shear stress occur due

to the low liquid velocity in the annular fiber-bed; (6) no mechanical agitation or external pump is required. Consequently, the avoidance of moving parts prevents cell damage by local high-shear regions and also decreases the risk of contamination; (7) the reactor can be operated in a batch or continuous/perfusion mode; and (8) the reactor is quite scaleable.

Biological Considerations

Experiments of growing recombinant, γ-interferon producing Chinese Hamster Ovary cells (γ-CHO) on glass fibers of 24 and 30 μm diameters were performed in order to confirm the feasibility of this fiber-bed bioreactor. It has been shown that glass fibers of diameter as small as 24 μm are able to support cell attachment and growth. Using the 24 μm glass fibers increased the surface-to-volume ratio of the reactor and also increased the hydrodynamic permeability of the fiber bed.

Within the concentration range used, Medical Emulsion C, which was found to be effective in suppress foaming in the experiments and was also shown to be non-toxic to the growth and productivity of γ-CHO and CRL-1606 cells.

Hydrodynamic Model

In order to determine the optimal reactor configuration in terms of ratio of inner draft tube diameter (Di) to reactor diameter (Do), a hydrodynamic model was developed to describe the bioreactor. Using the model, liquid flow rates and volumetric mass transfer

coefficients were predicted and were shown to be in agreement with experimental results. Oxygen transfer rate in this reactor, calculated based on liquid flow rate and mass transfer coefficient, could be improved by optimizing the Di/Do ratio. Since permeability of the fiber bed significantly affects oxygen transfer and optimal Di/Do ratio in the reactor, the desired permeability can be obtained by selecting the appropriate void fraction, fiber diameter and fiber arrangement in the fiber bed. A high permeability is desirable for high oxygen transfer and lower shear stress. The high permeability can be achieved by choosing smaller fibers and higher void fraction (maintaining the same surface to volume ratio), and the proper fiber arrangement. Permeability was also affected by the accumulation of cells in the fiber bed. A model of multilayer cell growth in the fiber bed was developed to describe the effect of cell growth on permeability. It was found that during the initial stages of cultivation, permeability does not change significantly. The permeability decreased dramatically after the cell density reaches $1x10^7$ cells/cm^3 due to the significant reduction in void fraction of the fiber bed and the increase of apparent fiber diameter resulting from cell accumulation.

Feasibility Study

In order to examine the operational and the technical feasibility of the bioreactor, cell cultivation experiments were conducted in a 4-liter prototype reactor. After demonstrating the ability for effective cell entrapment by the fiber bed, continuous/perfusion cultivations for recombinant Chinese Hamster Ovary cells, γ-CHO, (an anchorage-dependent cell line) and hybridoma ATCC-CRL-1606 (a suspension cell line) were performed. The controlling strategy was to maintain the dissolved oxygen concentration at the bottom of the reactor greater than 10% saturation by increasing gas

flow rate. Since both cultures were specific-perfusion-rate limited, the cultivation processes were maintained at steady state during the latter times of the cultivation. High cell densities ($6.8x10^7$ cells/cm^3 for γ-CHO and $1.8x10^8$ cells/cm^3 for CRL-1606) were maintained due to the convective nutrient transport. In particular, oxygen was efficiently supplied without detrimental effects, and the actual oxygen transfer rates were as high as 4 mmol/l/hr and 13 mmole/l/hr for γ-CHO and CRL-1606 cells respectively. The production of desired product was sustained 66 days for γ-CHO and 22 days for CRL-1606 cells. During the steady states, high productivities ($2.1x10^6$ IU γ-interferon/l/hr of γ-CHO and 28 mg IgG /l/hr of CRL-1606) corresponding to high product concentrations ($2.7x10^4$ IU/ml for γ-interferon and 220 mg/l for IgG) were achieved. Being able to maintain the necessary conditions stably for high cell density and continuous product synthesis for a long period of time, the designed bioreactor provides an excellent alternative for cultivating both anchorage-dependent and suspension cells.

In order to elucidate potential channeling in the fiber bed at high cell densities, the cell distribution in the fiber bed at the end of the cell cultivation, the change in channel radius due to cell growth, and residence time distribution (RTD) of the fiber bed before and after cell cultivation were investigated. Macroscopically, no serious problem due to channeling was concluded within the fiber bed. This was concluded since the cell distribution in the fiber bed at the end of cultivation experiments was quite uniform in both axial and radial directions. In addition, the channels were seen through microphotographs to be quite open for fluid flow even at high cell densities. However, visual observations showed an extensive cell mass buildup which could block small channels and also form big clumps around the intersections of the fibers. Due to diffusional resistances, this might lead to the starvation of cells in the middle of clumps. RTD studies also showed that there

were small amount of stagnant regions and that the axial dispersion at high cell density primarily resulted from the reduction in void fraction and increase in fiber diameter.

Scaleup Potential

Theoretical scaleup calculations of the air-lift fiber-bed bioreactor have been performed for volumes ranging from 1 to 10,000 liters where oxygen transfer rate of 10 to 4 mmole/l/hr, respectively, can be maintained. Since cell growth in the fiber bed affects the permeability and achievable oxygen transfer, the scaleability of reactors of 2.5 liters, 250 liter and 1000 liters at various cell densities was also considered. The permeabilities at various cell densities were assessed by the model of multilayer cell growth. The reactor is quite amenable to scaleup because high oxygen transfer rates (higher than 2 mmole/l/hr) was achievable even at high cell density such as $1x10^8$ cells/cm^3 for the large reactor volume (1000 liters). Increasing oxygen content in the inlet gas could also lead to higher oxygen transfer rate.

VII. RECOMMENDATIONS FOR FUTURE RESEARCH

1. Uniformity in Axial Cell Distribution for Suspension Cells.

The distribution of CRL-1606 cells in the fiber bed decreased along the axial direction (from top to the bottom) as presented in Figure 3.22. A uniform cell distribution is desired for the efficient utilization of the entire reactor. One possible cause for this descending distribution is cell dislodgement and re-entrapment in the fiber bed as discussed in Section 3.3. The mechanisms for particle collection by fibrous materials include direct interception, diffusion deposition, gravitational deposition, electrostatic deposition, inertial deposition and deposition influenced by molecular forces (Pich, 1966; Spielman and Goren, 1968). However, it is unclear how these mechanisms relate to the fiber bed structure (such as void fraction, fiber diameter, and fiber arrangements) and parameters such as liquid circulation velocity and cell density. A systematic and detailed study is therefore recommended to define the factors which determine the collection efficiency and to test the model of cell dislodgement and re-entrapment.

If the hypothesis of dislodgement and re-entrapment is correct, a more uniform cell distribution may be obtained by inoculating the fiber bed with reversed density distribution; *i.e.*, higher cell density at the bottom and lower at the top. During the cultivation process, cells are dislodged from the bottom and are re-inoculated back to the top of the fiber bed. The rate of dislodgement and the rate of re-entrapment could be manipulated if the mechanisms of cell dislodgement and entrapment were known. This would enable one to achieve a more uniform cell density in the fiber bed at the end of cultivation process.

2. Devising Control Strategies Based on On-Line Measurements:

Cell concentration determines the reactor performance in terms of productivity because it affects the permeability of the fiber bed and thus the achievable oxygen transfer rate. The cell density also determines nutrient demand, especially that for oxygen. In addition, cell concentration also determines volumetric productivity and product titer. Therefore, during the cultivation process, the determination of cell concentration is one of the most important parameter for the quantitative definition of the reactor's performance. Although it has been difficult to directly and non-destructively enumerate cells in the fiber bed during cell cultivation, glucose consumption, oxygen consumption, lactate production and permeability have been shown to be adequate to estimate the cell concentration. On-line measurements of these parameters can therefore allow us to estimate cell concentration, understand culture kinetics, and, consequently, directly monitor and control the cultivation process.

The methods for on-line measuring these parameters are available. For example, concentrations of glucose and lactate can be determined on-line by employing biosensors or HPLC (Scheirer and Merten, 1991). The on-line oxygen uptake rate can be obtained either by the liquid side or the gas side oxygen balance. The liquid side oxygen balance method requires the measurements of liquid flow rate in the fiber bed and dissolved oxygen concentrations at the top and the bottom of the fiber bed. The liquid flow rate can be determined *in situ* using a tracer. Possible tracers include cold water, salt solutions, dyes, sugars, or radioactive isotopes (Swaine and Daugulis, 1988). The dissolved oxygen (DO) concentrations can be directly measured by DO probes. The gas side oxygen balance can be assessed by analyzing gas compositions in the inlet and outlet gas lines using a mass

spectrometer. In addition, the hydrodynamic permeability of the fiber bed can also be measured on-line by *in situ* measurements of pressure drop and liquid flow rate during cell cultivation based on Darcy's law.

The culture kinetics may be regulated via the deliberate manipulation of the specific perfusion rate since the culture in the cell cultivation experiments presented in Chapter 3 were specific-perfusion-rate limited. A strategy for medium perfusion can be devised based on the cell concentration estimated from on-line measurements. For example, the process goal may be to keep a short initial cell growth phase and a steady state of high cell density to obtain sustained high productivity. Rapid achievement of the desired cell density will be obtained if the specific perfusion rate during the initial stage is such that nutrients are adequately supplied and the growth rate of cells is at its maximum. Once the desired steady-state cell density is achieved, the specific perfusion rate can be adjusted to reduce the growth rate and maintain the cell density at steady state. The volumetric productivity at the steady state is then dependent on the cell density achieved and the specific productivity per cell.

3. Medium Formulation for High Cell Density

Nutrient depletion can limit productivity by reducing both the maximum achievable cell concentration and the specific productivity (Glacken, 1991). Continuous perfusion systems, which continuously supply fresh medium to and withdraw spent medium from the bioreactor, are ideal for providing nutrients. The nutrients, especially the limiting one, can be supplied as required by increasing the perfusion rate. This, however, will lower the concentration of desired products and increase the wash-out of the non-limiting medium

components. The low product concentrations decrease separation efficiencies and consequently increase separation costs. The excess wash-out of the non-limiting nutrients results in higher cost of the raw materials which are not efficiently utilized. Consequently, the production costs will be high for this type of operation. Cell cultivations in the fiber-bed bioreactor were limited by specific-perfusion-rate and not by oxygen transport. The media used for the cultivation experiments are limiting in certain nutrients. An increase in perfusion rate is required to support cell growth at high cell density. Low perfusion rate at high cell densities with high product concentrations can be achieved with better medium formulation. In addition, better medium formulation would also save on non-limiting nutrients and, therefore, be more economical.

The first challenging step in re-formulating the culture medium is to identify the limiting nutrients and their concentrations required for the culture. A thorough review on serum free media was performed by Kitano (1991) to better understand the relationship between medium composition and the proliferation of cells and the synthesis of desired products. The necessity of including carbon and energy source, amino acids, vitamins, inorganic salts, growth factors, hormones and miscellaneous supplements in the culture medium has been recognized during the development of serum free medium. Quite a few models, unstructured (Miller *et al.*, 1988; Bree *et al.*, 1988) or structured (Batt *et al.*, 1989), have been developed to investigate cell metabolism and product synthesis. Shu and Shuler (1991) developed a mathematical model to describe growth response to a variety of amino acid supplements for *E. coli* culture. A similar stoichiometric approach may be employed to predict growth rates of animal cell culture as a function of nutrient concentrations. Once the specific consumption rate of the particular limiting nutrient component is experimentally determined, the required concentration at certain cell density can be calculated. The appropriate adjustment of the nutrient concentration in the medium would support cell

proliferation at high cell density without increases in perfusion rate.

4. Cell Distribution on a Fiber Mat

In the permeability model presented in Chapter 2, photomicrographs of cell culture were presented to show the multilayer cell growth and cell distribution on a fiber mat. More quantitative assessment is required to obtain a better understanding of cell layer formation and their distribution.

A method for morphological characterization has been reported using an electron digitizer (Metz *et al.*, 1981). The method is slow, labor-intensive, and not very accurate. An alternative based on image analysis was recently developed (Reichl *et al.*, 1992; Packer and Thomas, 1990). In this new method, a television camera is mounted on a microscope and the video signal of the field of view is sent to a computer for image processing and analysis. The image is captured in digital form, and then analyzed to obtain required measurements. Image analysis has been successfully used to measure morphological characteristics of filamentous microorganisms such as the frequency distribution of pellet size, mean pellet size, content of pellets, and pellet shape. The system allows for a fast and reproducible analysis and can be fully automated to perform on-line analysis. Similar analysis can be used to quantify cell distribution on a fiber mat. The quantitative data obtained can be related to the model of cell layers and permeability. Furthermore, these data of cell distribution may provide information required to estimate the effect of nutrient penetration on the cell layers.

5. Local Liquid Velocity within Fiber Bed

As previously mentioned, the liquid flow rate in the fiber bed can be measured *in situ* by the tracer method. Based on Darcy's law, the permeability of the fiber bed can be determined on-line by *in situ* measurements of liquid flow rate and pressure drop. Hence, based on the model of multilayer cell growth, the cell concentration in the fiber bed can be assessed on-line by the measurement of bed permeability during the cell cultivation process.

The detectors for liquid flow rate measurement can be placed at various positions in the fiber bed. By aligning the detectors in the same horizontal and vertical planes in the fiber bed, radial and axial velocity profiles can be possibly obtained. These radial and axial velocity profiles would be useful to elucidate the potential channeling problem in the fiber bed.

6. Determination of the Optimum Fiber Diameterand the Effect of Curvature on Cell Metabolism

For the same void fraction of a fiber bed, decreasing the fiber diameter increases surface-to volume ratio, and provides higher permeability. In this thesis, glass fibers of 24 μm diameter have been shown to be a good support for cell growth and product synthesis. In a separate experiment, it was shown that cells could attach on glass fibers of 15 μm diameter. However, further studies on growth and product kinetics were not performed. When anchorage-dependent cells attach onto a support, they are likely to conform to the shape of the support. It is possible that this adaptation may result in a change in their

metabolism rates. Singhvi *et al.* (1991) are currently studying the effects of roughness on adhesion strength and cell function. Therefore, it is suggested that more systematic research be conducted in order to determine the optimum fiber diameter required for cell attachment and growth, and the effect of curvature on cell metabolism.

7. Fiber Bed with Alternative Fiber Arrangement.

In this thesis, a fiber mat in which fibers were oriented normal to the flow was employed for cell cultivation experiments, The permeability of the fiber bed is high due to the inhomogeneity of the fiber bed structure. However, this inhomogeneity led to microscale channeling at high cell densities. A theoretical analysis shows that the fibers arranged parallel to the flow would be more desirable to generate high permeability. A technique which will allow equal interspacing of the fibers to avoid channeling while maintaining mechanical strength would be desirable. Specifically, a fiber bed with fibers parallel to the flow should result in improved reactor performance with respect to achievable cell density and oxygen transfer.

8. Mechanisms for Protein Product Instability during Sparging

Air was sparged into the bioreactor during cell cultivation in order to meet the high oxygen demand of the cells. It has been reported that the interfacial surfaces resulting from sparging can lead to protein denaturation (Donaldson *et al.*, 1980). Additionally, the protein product may also be oxidized by the oxygen. The elucidation of mechanisms and kinetics of inactivation of protein products will allow for the prevention or the reversal of the

unfavorable effect, and will add information to process optimization, especially the selection of perfusion rate and gas flow rate.

NOMENCLATURE

A	cross-sectional area of a porous bed (cm^2)
A_b	Absorbance at 430 nm
A_c	contact area for a cell on the fiber (cm^2)
A_d/A_r	the cross-sectional area ratio of the downcomer to the riser of a concentric airlift reactor
A_f	surface area of fibers (cm^2)
a	gas-liquid interfacial area per unit liquid volume (cm^2/cm^3)
C	distribution parameter for non-uniform radial flow
C_A	the equilibrium dissolved oxygen concentration with air, 0.225 mmole/liter
C_l	dissolved oxygen concentration (mmol/liter)
C*	liquid phase oxygen concentration which is in equilibrium with the bulk gas phase (mmol/liter)
d	bubble diameter (cm)
D_{ax}	Axial effective diffusivity (cm^2/s)
D_f	diffusivity in the fluid (cm^2/s)
d_f	the diameter of fiber (cm)
Di	the diameter of the inner column of the reactor (cm)
Do	the diameter of the reactor (cm)
DO_t, DO_b	percent saturation of the air at the top and bottom of the reactor respectively (%)
E	Average efficiency of a fiber bed for entrapping cells
F_D	drag force (dyne)
Fr	Froude number,
f_{TP}	two phase friction factor
g	gravity acceleration (cm/s^2)
H	proportionality constant of the solubility of oxygen (atm mol H_2O/mol O_2)
k	hydrodynamic permeability (cm^2)
K_c	contraction coefficient
k_l	mass transfer coefficient (cm/h)
K_n	modified Bessel function of 2nd kind, order n
k_0	the initial permeability of a fiber bed (cm^2)
L	height (cm)
Lo	the length of the packed bed (cm)
M_{H2O}	molecular weight of water (g/mol)
N(n)	cell number on the nth layer
N_f	the number of fibers
OTR	oxygen transfer rate (mmol/liter/h)
OUR	oxygen uptake rate per unit volume(mmol/liter/h)
Pe'	Peclet number based on fiber radius,
pO_2	partial pressure of oxygen (atm)
Q_g	gas flow rate (cm^3/s)
Q_l	liquid flow rate (cm^3/s)
R	gas constant (liter atm/mmol/K)
r	radius of glass fiber (cm)
Re	Reynolds number
R_i	the channel radius at certain cell density (cm)

R_0	the initial channel radius (cm)
Sc	Schmidt number
Sh	Sherwood number
S/V	surface-to-volume ratio (cm^2/cm^3)
T	temperature (K)
t	cyclic period of pH change (s)
Th	the thickness of one layer of cell (cm)
Th(n)	the total thickness of n layers of cells (cm)
U	velocity (cm/s)
$U_{b,\infty}$	terminal rise velocity of a bubble (cm/s)
U_l	the liquid velocity (cm/s)
U_s	superficial velocity (cm/s)
V	the reactor volume (cm^3)
V_f	volume of the fiber bed region (cm^3)
V_l	liquid volume in the reactor (cm^3)
We	Weber number
X	cell density ($cells/cm^3$)
X_A	cell number per unit area in the confluent state ($cells/cm^2$)
X_c	cell density ($cells/cm^3$)
X_m	monolayer cell density ($cells/cm^3$)
Y_{O2}	specific oxygen consumption rate of a cell (mmol/cell/h)
Δh	manometer reading (cm)
ΔP	pressure drop of the fiber bed (dyn/cm^2)
$\left(\frac{\Delta P}{\Delta L}\right)$	pressure drop per unit length (g/cm^3)
δ	average pore diameter of the porous sparger (cm)
δ_{O2}	oxygen diffusivity (cm^2/h)
ε_g	gas hold up
ε_2	the void fraction of the packed bed
Φ_l	parameter which is a function of a dimensionless variable, χ, defined by Lockhart-Martinelli (1949)
ϕ , ϕ_f	volume fraction of glass fiber in the fiber bed
μ	liquid viscosity (poise)
ρ	density (g/cm^3)
χ	two phase flow modules defined in Equation III.6
Ψ	parameter defined in Equation III.18
τ	shear stress ($dyne/cm^2$)

subscripts

g	gas (air)
l	liquid
TP	gas-liquid two phase
i	draft tube
o	fiber bed (reactor)
in	inlet
out	outlet
t	top
b	bottom

REFERENCES

Abaev, G.N., E.K.Popov, P.G.Schtern, S.V.Turuntaev, A.K.Kristinin, N P.Rogozina, I.S.Luk'janenko, N.S.Gurfein, V.F.Luchagin, V.M.Kostelkin and V.N.Koleskin. 1981. In: V.V. Struminsky (editor), *Aerodinamika v Teknologicheskikh Processakh*, pp.79-91, Moscow: Nauka.

Aerov, M.E., O. M. Todes and D.A. Narinsky. 1979. Apparatuses with Stationary Packed Beds, pp. 176, Liningrad: Khimiji.

Addison, W.E. 1961. The Close Packing of Spheres. In: *Structural Principles in Inorganic Compounds*. p.44. New York: John Wiley and Sons, Inc.

Applegate, M.A. 1991. Development and Characterization of Macroporous Ceramic Matrix Bioreactors for Mammalian Cell Culture. *Ph.D. Thesis*, M.I.T. Cambridge, MA.

Arthur, J.R., J.W. Linnet, E.J. Raynor and E.P.S. Sington. 1950. The Flow of an Air Stream Through a Layer of Granules. *Trans. Faraday Soc.* **46**: 270-281.

Atkinson, B. and F. Mavituna. 1983. *Biochemical Engineering and Biotechnology Handbook*, pp.773,784. London: Macmillan.

Aunins, J.G., and D.I.C. Wang. 1989. Induced Flocculation of Animal Cells in Suspension Culture. *Biotechnol. Bioeng.* **34**:1127-1132.

Aunins, J.G., M.S. Croughan, D.I.C. Wang and J.M. Goldstein. 1986. Engineering Developments in Homogeneous Culture of Animal Cells: Oxygenation of Reactors and Scaleup. *Biotechnol. Bioeng.* **17**: 699-723.

Avgerinos, G.E., D. Drapeeau, J.S. Socolow, J. Mao, K. Hsiao and R.J. Broeze. 1990. Spin Filter Perfusion System for High Density Cell Culture: Production of Recombinant Urinary Type Plasminogen Activator in CHO Cells, *Bio/Technology*, **8**: 54-58.

Backer, M.P., L.S. Metzger, P.L. Slaber, K.L. Nevitt, and G.B. Boder. 1988. Large-Scale Production of Monoclonal Antibodies in Suspension Culture. *Biotechnol. Bioeng.* **32**: 993-1000.

Batt, B.C., R.H. Davis, D.S. Kompala. 1990. Inclined Sedimentation for Selective Retention of Viable Hybridomas in a Continuous Suspension Bioreactor. *Biotechnol. Prog.* **6**: 458-464.

Batt, B.C. and D.S. Kompala. 1989. A Structured Kinetic Modeling Framework for the Dynamic of Hybridoma Growth and Monoclonal Antibody Production in Continuous Suspension Cultures. *Biotechnol. Bioeng.* **34**: 515-531.

Bayer, E. 1960. In: R.W.P. Scott (editor), *Gas Chromatography*, p.236. London: Butterworths, .

Bejan, A. 1984. Principles of Convection Through Porous Media. In: *Convection Heat Transfer*, pp.343-350. New York: John Wiley & Sons,

Belfort, G. 1989. Membranes and Bioreactors: A Technical Challenge in Biotechnology. *Biotechnol. Bioeng.* **33**: 1047-1066.

Bello, R.A. 1981. A Characterization Study of Airlift Contactors for Applications to Fermentation. *Ph.D. Thesis*, University of Waterloo, Ontario.

Bello, R.A., C.W. Robinson, and M. Moo-Young. 1984. Liquid Circulation and Mixing Characteristics of Airlift Contactors. *Canad. J. Chem. Eng.* **62**: 573-577.

Bello, R.A., C.W. Robinson, and M. Moo-Young. 1985 a. Prediction of the Volumetric Mass Transfer Coefficient in Pneumatic Contactors. *Chemical Engineering Science*, **40**(1): 53-58.

Bello, R.A., C.W. Robinson, and M. Moo-Young. 1985 b. Gas Holdup and Overall Volumetric Oxygen Transfer Coefficient in Airlift Contactors. *Biotechnology and Bioengineering*, **27**: 369-381.

Berg, G.J., and B.G.D. Bodeker. 1988. Employing Ceramic Matrix for the Immobilization of Mammalian Cells in Culture, In: R.E. Spier and J.B. Griffiths (editors), *Animal Cell Biotechnology*, **3**: 321-335. London: Academic Press.

Birch, J.R., P.W. Thompson, R. Boraston. 1985. Production of Monoclonal Antibodies in Large-Scale Cell Culture System. *J. Tissue Culture Methods*, **8**: 147-154.

Blenke, H. 1979. Loop Reactors. In: T. K. Ghose, A. Fiechter, and N. Blakebrough (editors), *Advances in Biochemical Engineering*, **13:** 121-214. Berlin: Springer-Verlag.

Blenke, H. 1985. Chapter 21: Biochemical Loop Reactors. In: H.J. Rehm and G. Reed (editors), *Biotechnology*, **2:** 465-517, W.G: Weinheim.

Bliem, R., Konopitzky, K, and Katinger, H. 1991. Industrial Animal Cell Reactor Systems: Aspects of Selection and Evaluation. In: A. Fiechter (editor), *Advances in Biochemical Engineering*, vol.44, pp.1-27. Springer-Verlag Berlin Heidelberg.

Bree, M.A., P. Dhurjati, R.F. Geoghegan Jr. and B. Robnett. 1988. Kinetic Modelling of Hybridoma Cell Growth and Immunoglobulin Production in a Large-Scale Suspension Culture. *Biotechnol. Bioeng.* **32**: 1067-1072.

Brennan, A.J., J. Shevitz, and J.D. Macmillan. 1987. A Perfusion System for Antibody Production by Shear-Sensitive Hybridoma Cells in a Stirred Reactor. *Biotechnol. Techniques*, **1**: 169-174.

Brosemer, R.W. and W.J. Rutter. 1961. The Effect of Oxygen Tension on the Growth and Metabolism of a Mammalian Cell. *Exp. Cell Res.* **25**: 101-113.

Brown, P.C., M.A.C. Costello, R.Oakley, and J.L. Lewis. 1985. Applications of the Mass Culturing Technique (MCT) in the Large Scale Growth of Mammalian Cells. In: J. Feder and W. Tolbert (editors), *Large Scale Mammalian Cell Culture*, pp.59-78. Orlando: Academic Press.

Burbidge, C. 1979. The Mass Culture of Human Diploid Fibroblasts in Packed Beds of Glass Beads. *Dev. Biol. Stand.* **46**: 169-172.

Chakravarty, M., H.D. Singh, J.N. Baruah and M.S. Iyengar. 1974. Liquid Velocity in a Gas-Lift Column. *Indian Chemical Engineers,* **16**(3):17.

Chang, H. N. and M. Moo-Young. 1988. Estimation of Oxygen Penetration Depth in Immobilized Cells. *Appl. Microbiol. Biotech.* **29**:107.

Chen, Y.Y. 1990. Personal Communication. Institute of Physics, Academia Sinica, Taipei, Taiwan, R.O.C.

Cherry, R.S. and E.T. Papoutsakis. 1986. Hydrodynamic Effects on Cells in Agitated Tissue Culture Reactors. *Bioprocess Eng.* **1**: 29-41.

Cherry, R.S. and E.T. Papoutsakis. 1990. Understanding and Controlling Fluid-Mechanical Injury of Animal Cells in Bioreactors. In: R.E. Spier and J.B. Griffiths (editors), *Animal Cell Biotechnology*, **4**: 71-121. London: Academic Press.

Chisti, M. Y. and M. Moo-Young. 1987. Airlift Reactors: Characteristics, Applications and Design Considerations. *Chem. Eng. Comm.* **60**: 195-242.

Chisti, M. Y. and M. Moo-Young. 1988. Prediction of Liquid Circulation Velocity in Airlift Reactors with Biological Media. *J.Chem.Tech. Biotechnol.* **42**: 211-219.

Collins, R. E. 1961. In: *Flow of Fluids through Porous Materials*, pp.10-21. Oklahoma: PennWell Publishing Co

Comer, M.J., M.J. Kearns, J. Wahl, M. Munster, T. Lorenz, B. Szperalski, S. Koch, U. Behrendt, H. Brunner. 1990. Industrial Production of Monoclonal Antibodies and Therapeutic Proteins by Dialysis Fermentation. *Cytotechnol.* **3**: 295-299.

Crouch, C.F., H.W. Fowler and R.E. Spier. 1985. The Adhesion of Animal Cells to Surfaces: The Measurement of Critical Surface Shear Stress Permitting Attachment or Causing Detachment. *J. Chem. Tech. Biotechnol.* **35**(B): 273-281.

Croughan, M.S. 1988. Hydrodynamic Effects on Animal Cells in Microcarrier Bioreactors. *Ph.D. Thesis*, M.I.T. Cambridge, MA.

Croughan, M.S., J.F. Hamel and D.I.C. Wang. 1987. Hydrodynamic Effects on Animal Cells Grown in Microcarrier Cultures. *Biotechnol. Bioeng.* **29**: 131-141.

Croughan, M., E. Sayre, and D.I.C. Wang. 1989. Viscous Reduction of Turbulent Damage in Animal Cell Culture. *Biotechnology and Bioengineering,* **33**: 862-872.

Croughan, M.S., and D.I.C. Wang. 1989. Growth and Death in Overagitated Microcarrier Cell Culture. *Biotechnology and Bioengineering*, **33**: 731-744.

Croughan, M.S., and D.I.C. Wang. 1991. Hydrodynamic Effects on Animal Cells in Microcarrier Bioreactors. In: C.S. Ho and D.I.C. Wang (editors), *Animal Cell Bioreactors*, pp.213-249. Boston: Butterworth-Heinemann.

Cumming, D.A. 1991. Glycosylation of Recombinant Protein Therapeutics: Control and Functional Implications. *Glycobiol.* **1**: 115-130.

Danes, B.S., M.M. Broadfoot and J. Paul. 1963. A Comparative Study of Respiratory Metabolism in Cultured Mammalian Cell Strains. *Exp. Cell Res.* **30**: 369-378.

Darcy, H. 1856. In: *Les fontainer publiques de la ville de Dijon*, Paris: Dalmont.

Deckwer, W.D. 1980. Access of Hydrodynamic Parameters Required in the Design and Scale-Up of Bubble Column Reactors. In: S.H. Fogler (editor), *Chemical Reactors*, p.213. ACS Monograph.

De Nevers, N. 1968. Bubble Driven Fluid Circulations. *AIChE J.* **14**: 222-226.

Dewey, C.F., Bussolari, S.R., Gimbrone, M.A., and Davies, P.F. 1981. The Dynamic Response of Vascular Endothelial Cells to Fluid Shear Stress. *J. Biomech. Eng.* **103**: 177-185.

Dodge, T. C. and W.S. Hu. 1986. Growth of Hybridoma Cells under Different Agitation Conditions, *Biotechnol. Lett.* **8**: 683-686.

Donaldson, T.L., E.F. Boonstra, and J.M. Hammond. 1980. Kinetics of Protein Denaturation at Gas-Liquid Interfaces. *J. Colloid and Interface Science,* **74**(2): 441-450.

Drummond, J.E. and M. I. Tahir. 1984. Laminar Viscous Flow Through Regular Arrays of Parallel Solid Cylinders. *Int. J. Multiphases Flow,* **10**: 515-540.

Duff, R.G. 1985. Microencapsulation Technology: A Novel Method for Monoclonal Antibody Production. *Trends Biotechnol.* **3**: 167-170.

Dunn, G.A. and Heath, J.P. 1976. A New Hypothesis of Contact Guidance in Tissue Cells. *Exp. Cell Res.* **101**: 1-14

Dussap, G. and Gros, J.B. 1982. Energy Consumption and Interfacial Mass Transfer Area in an Air-Lift Fermentor. *Chem. Eng. J.* **25**: 151-162.

Duval, D., C. Demangel, K. Munier-Jolain, S. Miossec, and I. Geahel. 1991. Factors Controlling Cell Proliferation and Antibody Production in Mouse Hybridoma Cells: I. Influence of the Amino Acid Supply. *Biotechnology and Bioengineering,* **38**: 561-570.

Edwards , M.F. and J.F. Richardson. 1968. Gas Dispersion in Packed Beds. *Chem. Eng. Sci.* **23**: 109-123.

Emery, A.N., M. Lavery, B. Williams, and A. Handa. 1987. Large-Scale Hybridoma Culture. In: C. Webb and F. Mavituna (editors), *Plant and Animal Cells: Process Possibilities*, pp.137-146. Chichester: Ellis Horwood.

Esclade, L.R.J., S. Carrel, P. Peringer. 1991. Influence of the Screen Material on the Fouling of Spin Filters. *Biotechnol. Bioeng.* **38**: 159-168.

Fields, P.R., F.R.G. Mitchell, and N.K.H. Slater. 1984. Studies of Mixing in a Concentric Tube Air-Lift Reactor Containing Xantham Gum by Means of an Improved Flow Follower. *Chem. Eng. Commun.* **25**: 93-104.

Fisher,P.E. and C. Tickle. 1981. Differences in Alignment of Normal and Transformed Cells on Glass Fibres. *Exp. Cell Res.* **131**: 407-410

Fleischaker, R.J. and A.J. Sinskey. 1981. Oxygen Demand and Supply in Cell Culture. *Europ. J. Appl. Microbiol. and Biotechnol.* **12**: 193-197.

Freedman, D. 1969. The Shaker in Bioengineering. *Process Biochem.* **4**(3): 35-40.

Freedman, W. and J.F. Davidson. 1969. Hold-Up and Liquid Circulation in Bubble Columns. *Trans. Instn Chem. Engrs*, **47**: T251-T262.

Freshney, R.I. 1983. *Culture of Animal Cells. A Manual of Basic Technique.* New York: Alan R. Liss, Inc.

Gammon, M.C., M.H. Banas, L.E.Boccumini, N.H. Sigal, and H.J. Zweerink. 1990. Heterohybridomas that Secrete High Levels of Pseudomonas-Specific Therapeutic Human Monoclonal Antibodies: their Generation and Large Scale Growth in an Automated Hollow Fibre Cell Culture System. *Cytotechnology*, **3**: 51-60.

Gbewonyo, K. 1982. Enhancing Gas-Liquid Mass Transfer Rates in Mycelial Fermentations through Confinement of Cell Growth. *Ph.D. Thesis*. M.I.T. Cambridge, MA.

Giles, K.W. and A. Myers. 1965. An Improved Diphenylamine Method for the Estimation of Deoxyribonucleic Acid. *Nature*, **206**: 93.

Glacken, M.W. 1987. Development of Mathematical Descriptions of Mammalian Cell Culture Kinetics for the Optimization of Fed-Batch Bioreactors. *Ph.D. Thesis*, MIT, Cambridge, MA.

Glacken, M.W. 1991. Bioreactor Control and Optimization. In: C.S. Ho and D.I.C. Wang (editors), *Animal Cell Bioreactors*, p.373-404, Boston: Butterworth-Heinemann.

Glacken, M.W., E. Adema, and A.J. Sinskey. 1988. Mathematical Descriptions of Hybridoma Culture Kinetics: Initial Metabolic Rates. *Biotechnol. Bioeng.* **32**: 491-506.

Glacken, M.W., R.J. Fleischaker, and A.J. Sinskey. 1983. Mammalian Cell Culture: Engineering Principles and Scale-Up. *Trends in Biotechnology*, **1**(4): 102-108.

Green, M., G. Henle, and F. Deinhardt. 1958. Respiration and Glycolysis of Human Cells Grown in Tissue Culture. *Virol.* **5**: 206-219.

Greenkorn, R.A. 1983. In: *Flow Phenomena in Porous Media*, pp.1-9. NY: Marcel Dekker.

Griffiths, J.B. 1988. Overview of Cell Culture Systems and Their Scale-Up. In: R.E. Spier and J.B. Griffiths (editors), *Animal Cell Biotechnology*, **4**: 149-166. London: Academic Press.

Griffiths, J.B. 1990. Advances in animal cell immobilization technology. In: R.E. Spier and J.B. Griffiths (editors), *Animal Cell Biotechnology*, **3**: 179-221. London: Academic Press.

Griffiths, B. and D. Looby. 1991. Fixed immobilized beds for the cultivation of animal cells. In: C.S. Ho and D.I.C.Wang (editors), *Animal Cell Bioreactors*, pp.165-190. Boston: Butterworth-Heineman.

Goldberg, M. and E. Rubin. 1967. *I&EC Process Design and Development*, **6**:195.

Gunn, D.J. 1969. Theory of Axial and Radial Dispersion in Packed Beds.*Trans. Instn. Chem. Engrs*, **47**: T351-T359.

Hach, R. T. 1973. Experimental and Theoretical Studies of Oxygen Transfer in the Airlift Fermentor, *Ph.D. Thesis*, MIT, Cambridge, Mass.

Handa, A., A.N. Emery, and R.E. Spier. 1987 a. On the Evaluation of Gas-Liquid Interfacial Effects on Hybridoma Viability in Bubble Column Bioreactors. *Develop. biol. Standard.* **66**: 241-253.

Handa, A., A.N. Emery, and R.E. Spier. 1987 b. Detrimental Effects of Sparger Aeration on Suspended Mammalian Cell Cultures and Their Prevention. In: O. M. Neijssel, R. R. van der Meer and K. Ch. A. M. Luyben (editors), *Proc. 4th European Congress on Biotechnology* **3**: 601-604, Amsterdam (Netherlands): Elsevier Science Publishers B.V.

Handa-Corrigan, A. 1990. Oxygenating Animal Cell Cultures: the Remaining Problems. In: R.E. Spier and J.B. Griffiths (editors), *Animal cell biotechnology*, **4:** 122-132. London: Academic Press.

Handa-Corrigan, A., Emery, A.N., and Spier, R.E. 1989. Effect of Gas-Liquid Interfaces on the Growth of Suspended Mammalian Cells: Mechanisms of Cell Damage by Bubbles. *Enzyme Microb. Technol.* **11**: 230-235.

Happel, J. 1959. Viscous Flow Relative to Arrays of Cylinders. *AIChE J.* **5**: 174-177.

Hasimoto, H. 1959. On the Periodic Fundamental Solutions of the Stokes Equations and their Application to Viscous Flow Past a Cubic Array of Spheres. *J. Fluid Mech.* **5**: 317-328.

Hayman, E.G., N.G. Ray, and P.W. Runstadler Jr. 1987. Production of Biomolecules by Cells Cultured in Tri-Dimensional Collagen Microspheres. In: G.W. Moody and P.B. Baker (editors), *Bioreactors and Biotransformations*, pp.132-140. London and New York: Elsevier.

Hayter, P.M., E.M.A. Curling, A.J. Baines, N. Jenkins, I. Salmon, P.G. Strange, J.M. Tong, and A.T. Bull. 1992. Glucose-Limited Chemostat Culture of Chinese Hamster Ovary Cells Producing Recombinant Human Interferon-γ. *Biotechnol. Bioeng.* **39**: 327-335.

Heifetz, A.H., J.A. Braatz, R.A. Wolfe, R.M. Barry, D.A. Miller, and B.A. Solomon. 1989. Monoclonal Antibody Production in Hollow Fiber Bioreactors Using Serum-Free

Medium. *BioTechniques*, **7**: 192-199.

Himmelfarb, P., P. S. Thayer, H.E. Martin. 1969. Spin Filter Culture: The Propagation of Mammalian Cells in Suspension. *Science*, **164**: 555-557.

Hirtenstein, M.and J. Clark. 1980. In: R. Richards and K.Rajan (editors), *Tissue Culture in Medical Research*, Oxford: Pergamon.

Hsu, Y. C. and M. P. Dudukovic. 1980. Gas Holdup and Liquid Recirculation in Gas-Lift Reactors. *Chem. Engng, Sci.* **35**: 135-141.

Hu, W.-S. and Peshwa, M.V. 1991. Animal cell bioreactors-recent advances and challenges to scale-up. *The Canadian J. of Chem. Eng.* **69**: 409-420.

Huyten, F. H., W. Beersum and G. W. A. Rijnders. 1960. 3rd Symposium on Gas Chromatography,1960, Edinburgh, Preprints of papers, pp174-186, London: Butterworths.

Hupe, K.-P., U. Busch, and K. Winde. 1969. Investigation of Separation Columns for Production Scale Gas Chromatography. *J. Chromatogr. Sci.* **7**: 1-6.

Iijima, S., T. Mano, M. Taniguchi, and T. Kabayashi. 1988. Immobilization of Hybridoma Cells with Alginate and Urethane Polymer and Improved Monoclonal Antibody Production. *Appl. Microbiol. Biotechnol.* **28**: 572-576.

Jackson, G.W. and D.F. James. 1982. The Hydrodynamic Resistance of Hyaluronic Acid and Its Contribution to Tissue Permeability, *Biorheology*, **19:** 317-330.

Jackson, G.W. and D.F.James. 1986. The Permeability of Fibrous Porous Media. *The Canadian Journal of Chemical Engineering*. **64**: 364-374.

Jager, V., W. Eichner, and J. Lehmann. 1989. Production of Human PDGF-A in a Stirred Tank Perfusion Reactor and in a Hollow Fibre Reactor System. In: R.E. Spier, J.B. Griffiths, J. Stephenne, and P.J. Crooy (editors), *Advances in Animal Cell Biology and Technology for Bioprocesses*, pp. 323-326. London: Butterworths.

Jensen, M.D. 1981. Production of Anchorage Dependent Cells: Problems and Their Possible Solutions. *Biotechnol. Bioeng.* **23**: 2703-2716.

Jones, A. G., Liquid Circulation in a Draft-Tube Bubble Column. 1985. *Chem Engng. Sci.* **40**: 449-462.

Joshi, J.B., V.V. Ranade, S. Gharat and S.S. Lele. 1990. Sparged Loop Reactors. *Can. J. Chem. Eng.* **68**:705-741.

Kaminsky, M., J. Klawiter, and J. S. Kowalczyk. 1982. Characteristics of the Slurry Method of Packing Chromatographic Columns. *J.Chromatogr.* **243**: 225-244.

Katinger, H.W.D.,W. Scheirer and E. Kromer. 1979. Bubble Column Reactor for Mass Propagation of Animal Cells in Suspension Culture. *Ger. Chem. Eng.* **2**: 31-38.

Kilburn, D.G. and F.C. Webb. 1968. The Cultivation of Animal Cells at Controlled

Dissolved Oxygen Partial Pressure. *Biotechnology and Bioengineering,* **10**: 265-271.

King, G.A., A.J. Kaugulis, P. Faulkner and M.F.A. Goosen. 1987. Alginate-polylysine Microcapsules of Controlled Membrane Molecular Weight Cutoff for Mammalian Cell Culture Engineering, *Biotechnol. Prog.* **3**: 231-240.

Kitano, K. 1991. Serum-Free Media. In: C.S. Ho and D.I.C. Wang (editors), *Animal Cell Bioreactors,* p.73-106, Butterworth-Heinemann.

Klawiter, J., M. Kaminsky, and J. S. Kowalczyk. 1982. Investigation of the Relationship Between Packing Methods and Efficiency of Preparative Columns. *J.Chromatogr.* **243**: 207-225.

Knazek, R.A., P.M. Guillino, P.O. Kohler, and R.L. Dedrick. 1972. Cell Culture on Artificial Capillaries: An Approach to Tissue Growth in vitro. *Science* .**178**: 65-67.

Koch, D.L. and J.F. Brady. 1986. The Effective Diffusivity of Fibrous Media. *AIChE Journal,* **32**(4): 575-591.

Koide, K., S. Iwamoto, Y. Takasaka, S. Matsuura, E. Takahashi and M. Kimura. 1984. Liquid Circulation, Gas Holdup and Pressure Drop in Bubble Column with Draft Tube. *J. Chem Eng, Jpn.* **17**(6): 611-618.

Koide, K., M. Kimura, H. Nitta and H. Kawabata. 1988. Liquid Circulation in Bubble Column with Draft Tube. *J. Chem Eng, Jpn.* **21**(4): 393-399.

Ku, K., M.J. Kuo, J.Delente, B.S. Wildi, and J. Feder. 1981. Development of a Hollow-Fiber System for Large-Scale Culture of Mammalian Cells, *Biotechnol. Bioeng.* **23**: 79-95.

Kubota, H., Y. Hosono, and K. Fujie. 1978. Characteristic Evaluations of ICI Air-Lift Type Deep Shaft Aerator. *J. Chem. Eng. Jpn.* **11**(4): 319-325.

Kunas, K.T. and E.T. Papoutsakis. 1989. Increasing Serum Concentrations Decrease Cell Death and Allow Growth of Hybridoma Cells at Higher Agitation Rates. *Biotechnol. Lett.* **11**: 525-530.

Kunas, K.T., E.T. Papoutsakis. 1990. Damage Mechanisms of Suspended Animal Cells in Agitated Bioreactors with and without Bubble Entrainment. *Biotechnol. Bioeng.* **36**: 476-483.

Kuwabara, S. 1959. The Forces Experienced by Randomly Distributed Parallel Circular Cylinders or Spheres in a Viscous Flow at Small Reynolds Number. *J. Phys. Soc. of Japan* **14**: 527-532.

Lamont, A.G.W. 1958. Air Agitation and Pachuca Tanks. *Can. J. Chem. Engng.* **8**:153-160.

Langmuir, I. 1942. Report of Smokes and Filters, Part IV of a report for the Office of Scientific Research and Development. OSRD No.865. Ser. No. 353. In:W.H. Rodebush, *et al.* (editors), *Filtration of Aerosols and the Development of Filter Materials.*

La Van, M. D. and T. Vermeulen. 1984. Channeling and Bed-Diameter Effects in Fixed Bed Adsorber Performance. *AIChE Symposium Series*, No. 233, Vol. 80, p.34-43.

Lavery, M. and A.W. Neinow. 1987. Oxygen Transfer in Animal Cell Culture Medium. *Biotechnology and Bioengineering*, **30**: 368-373.

Lazar, A., L. Silberstein, A. Mizrahi, and S. Reuveny. 1988. An Immobilized Hybridoma Culture Perfusion System for Production of Monoclonal Antibodies, *Cytotechnol.* **1**: 333-338.

Lehnert, J. 1972. "Berechnung von Mischvorgangen in schlanken Schlaufenreaktoren." Verfahrenstechnik **6**(2): 58-64.

Levenspiel, O. 1972. Chapter 9 Nonideal Flow. In: *Chemical Reaction Engineering*, 2nd edition, P.253-268, New York: John Wiley & Sons, Inc.

Lim, F. 1982. Encapsulation of biological material, U.S. Patent, no. 4, 352, 883, granted Oct.5, 1982, assigned to Damon Biotech. Needham Heights, MA.

Lim, F. 1988. Microencapsulation of Living Mammalian Cells. In: A. Mizrahi (editor), *Advances in Biotechnological Processes*, **7**: 185-197. New York: Alan R. Liss, Inc.

Lipmaa, E.T., and P.O. Luiga. 1966. in *Gazovaja Khromatographija*, Dzerzhinsk, pp.330-335.

Lindell, P.I., L. Hall, T.G. Wu, C.L. Cooney. 1991. Comparison of an Electrochemiluminescent Homogeneous Immunoassay and an ELISA for Monitoring Productivity in Mammalian Cell Bioreactors. *Biotechnol. Techniques*, **5**: 187-192.

Lockhart, R.W. and R.C. Martinelli. 1949. Proposed Correlation of Data for Isothermal Two-Phase, Two-Component Flow in Pipes. *Chem. Engr. Progr.* **45**: 39-48.

Looby, D., and J.B. Griffiths. 1988. Fixed Bed Porous Glass Sphere (Poro Sphere) Bioreactors for Animal Cells. *Cytotechnology*, **1**: 339-346.

Luan, Y.T., R. Mutharasan, and W.E. Magee. 1987. Strategies to Extend Longevity of Hybridomas in Culture and Promote Yield of Monoclonal Antibodies. *Biotechnol. Lett.* **9**: 691-696.

Lutz, A. A. 1982. An Analysis of Human Immune Interferon Production by Recombinant Chinese Hamster Ovary Cells. *Master Thesis*. M.I.T. Cambridge, MA.

Lydersen, B.K. 1987. Perfusion Cell Culture System Based on Ceramic Matrices. In: B.K. Lydersen *(editor), Large-Scale Cell Culture Technology*, pp.113-144. New York: Hanser Publications.

Lydersen, B.K., G.G. Pugh, M.S. Paris, B.P. Sharma, and L.A. Noll. 1985 a. Ceramic Matrix for Large Scale Animal Cell Culture. *BioTechnology*, **3**: 63-67.

Lydersen, B.K., J. Putnam, E. Bognar, M, Patterson, G.G. Pugh, and L.A. Noll. 1985 b. The Use of a Ceramic Matrix in a Large Scale Cell Culture System. In: J. Feder and W.

Tolbert, (editors), *Large-Scale Mammalian Cell Culture*, pp.39-58. Orlando: Academic Press.

Maiorella, B., G. Dorin, A. Carion, and D. Harano. 1991. Crossflow Microfiltration of Animal Cells. *Biotechnol. Bioeng.* **37**:121-126.

Marcipar, A., P. Henno, E. Lentwojt, A. Roseto and G.Broun. 1983. Ceramic Supported Hybridomas for Continuous Production of Monoclonal Antibodies. *Annals of N.Y. Academy of Science,* **413**: 416-420.

Margaritis, A. and Sheppard, J.D. 1981. Mixing Time and Oxygen Transfer Characteristics of a Double Draft Tube Airlift Fermentor. *Biotechnol. Bioeng.* **23**: 2117-2135.

Maroudas, N.G. 1972. Anchorage Dependence: Correlation between Amount of Growth and Diameter of Bead, for Single Cells Grown on Individual Glass Beads. *Exp. Cell Res.* **81**: 104-110.

Merchuk, J.C. 1986. Gas Hold-Up and Liquid Velocity in a Two-Dimensional Air Lift Reactor. *Chem. Eng. Sci.* **41**(1): 11-16.

Merchuk, J.C. and Stein,Y. 1981. Local Hold-Up and Liquid Velocity in Airlift Reactors. *AIChE J.* **27**(3): 377-388.

Metz, B., E.W. deBruijn, and J.C. van Suijdam. 1981. Method for Quantitative Representation of the Morphology of Molds. *Biotechnol. Bioeng.* **23**: 149-162.

Miller, W.M., H.W. Blanch, and C.R. Wilke. 1988. A Kinetic Analysis of Hybridoma Growth and Metabolism in Batch and Continuous Suspension Culture: Effect of Nutrient Concentration, Dilution Rate, and pH. *Biotechnol. Bioeng.* **32**: 947-965.

Miltenburger, H.G., and P.David. 1980. Mass Production of Insect Cells in Suspension. *Dev. Biol. Std.* **46**: 183-186.

Miyahara, T., M. Hamaguchi, Y. Sukeda, and T. Takahashi. 1986. Size of Bubbles and Liquid Circulation in a Bubble Column with a Draught Tube and Sieve Plate. *Can. J. Chem. Engng.* **64**: 718-725.

Mizrahi, A., G.V. Volsoeller, Y. Yagi, and G.E. Moore. 1972. The Effect of Dissolved Oxygen Partial Pressure on Growth, Metabolism and Immunoglobulin Production in a Permanent Human Lymphocyte Cell Line Culture. *P.S.E.B.M.* **139**: 118-122.

Mohandas, N. 1976. Red Cells Adhering to a Glass Surface: Deformation in a Well-Defined Fluid Shear Field. *Nouvelle Revue Francaise d'Hematologie.* **16**(3): 357-362.

Montagnon, B., J.C. Vincent-Falquet, and B. Fanget. 1984. Thousand Litre Scale Microcarrier Culture of Vero Cells for Killed Polio Virus Vaccine. *Dev. Biol. Stand.* **55**: 37-42.

Morales, M., C.W. Spinn and I.M.Smith. 1951. *Ind. Eng.Chem.* **43**: 225-232.

Murdin, A.D., J.S. Thorpe, and R.E. Spier. 1987 a. Immobilization of Hybridoma in

Packed Bed Reactors. In: R.E. Spier and J.B. Griffiths (editors), *Modern Approaches to Animal Cell Technology*, pp.420-436. Guildford: Butterworth.

Murdin, A.D., R. Wilson, N.F. Kirkby, and R.E. Spier. 1987 b. Examination of a Simple Model for the Diffusion of Oxygen into Dense Masses of Animal Cells. In: R.E. Spier and J.B. Griffiths (editors), *Modern Approaches to Animal Cell Technology*, pp.353-363. Guildford: Butterworth.

Murhammer, D.W. and C.F. Goochee. 1988. Scaleup of Insect Cell Cultures:Protective Effects of Pluronic F-68. *Bio/Technology* **6**: 1411-1418.

Murhammer, D.W. and C.F. Goochee. 1990. Sparged Animal Cell Bioreactors: Mechanism of Cell Damage and Pluronic F-68 Protection. *Biotechnol. Prog.* **6**: 391-397.

Nelson, K. L. 1988 a. Industrial-Scale Mammalian Cell Culture, Part 1: Bioreactor Design Considerations. *Biopharm. Manufacturing*, February, p.42-46.

Nelson, K.L. 1988 b. Industrial-Scale Mammalian Cell Culture, Part II: Design and Scaleup. *BioPharm. Manufacturing*, March, pp.34-50.

Nilsson, K. 1987. Methods for Immobilizing Animal Cells. *Trends in Biotechnology*. **5**: 73-78.

Nilsson, K., J. Almgren, C. Nilsson, A.-C. Peterson. 1991. The Use of Macroporous Gelatin Microcarriers, Cultisphere-G in Fluidised Bed Bioreactors and for the Culture of Hybridoma Cells. In: R.E. Spier, J.B. Griffiths, and B. Meignier (editors), *Production of Biologicals from Animal Cells in Culture*, pp.434-438. London: Butterworths.

Nilsson, K., F. Buzsaky, and K. Mosbach. 1986. Growth of Anchorage-Dependent Cells on Macroporous Microcarriers. *Bio/Technology*, **4**: 989-990.

Nilsson, K., W. Scheirer, O.W. Merten, L. Ostberg, E. Liehl, H.W.D. Katinger, and K. Mosbach. 1983. Entrapment of Animal Cells for Production of Monoclonal Antibodies and Other Biomolecules. *Nature*, **302**: 629-630.

Nottendamper, R., A. Steiff, and P.-M. Weinspach. 1983. Experimental Investigation of Hydrodynamics of Bubble Columns. *Ger. Chem. Eng.* **6**: 147-155.

O'Connor, G.M., F. Sanchez-Riera, and C.L. Cooney. 1992. Design and Evaluation of Control Strategies for High Cell Density Fermentations. *Biotechnol. Bioeng.* **39**: 293-304.

Onken, U., and P. Weiland. 1980. Hydrodynamics and Mass Transfer in an Airlift Loop Fermentor. *Eur. J. Appl. Microbiol. Biotechnol.* **10**: 31-40.

Onken, U., and P. Weiland. 1983. Airlift Fermentors: Construction, Behavior, and Uses. In: A. Mizrahi and L. Van Wezel (editors), *Advances in Biotechnological Processes*, **1**: 67-95. New York: Alan R. Liss, Inc.

Orazem, M. E. and L.E. Erikson. 1979. Oxygen Transfer Rates and Efficiencies in One- and Two-Stage Airlift Towers. *Biotechnol. Bioeng.* **21**: 69-88.

Orton , D., and Wang, D.I.C. 1990. Effects of Gas Interfaces on Animal Cells in Bubble Aerated Bioreactors. Paper Presented at the 1990 Annual AIChE Meeting, November 11-16, 1990, Chicago, IL.

Osawa, A.E. 1992. The Use of Fibrous Beds for the Chromatographic Separation of Proteins. *Ph.D. Thesis*, M.I.T. Cambridge, MA.

Packer, H.L. and C.R. Thomas. 1990. Morphological Measurements on Filamentous Microorganisms by Fully Automated Image Analysis, *Biotechnology and Bioengineering*, **35**: 870-881.

Papoutsakis, E.T. 1991. Fluid-Mechanical Damage of Animal Cells in Bioreactors. *Trends in Biotechnology*, **9**: 427-437

Perkins, T.K. and C.C. Johnston. 1963. *Soc. Petrol Eng. J.* **3**: 70

Perry, S. D. and Wang, D.I.C. 1989. Fiber Bed Reactor Design for Animal Cell Culture. *Biotechnol. Bioeng.* **34**: 1-9.

Petersen, J. F., McIntire, L. V., and Papoutsakis, E. T. 1988. Shear Sensitivity of Cultured Hybridoma Cells (CRL-8018) Depends on Mode of Growth, Culture Age and Metabolite Concentration. *Journal of Biotechnology*, **7**: 229-246.

Pich, J. 1966. Chapter IX. Theory of Aerosol Filtration by Fibrous and Membrane Filters. In: C.N. Davies (editor), *Aerosol Science*, p.223-286. London and New York: Academic Press.

Pollard, R. and Khosrovi, B. 1978. Reactor Design for Fermentation of Fragile Tissue Cells. *Process Biochemistry*, May, p.31-37.

Pullen, K.F., Johnson, M.D., Philips A.W., Ball, G.D., and Finter, N.B. 1985. Very Large Scale Suspension Cultures of Mammalian Cells. *Dev. Biol. Stand.* **60**: 175-177.

Quraishi, A.Q., R.A. Mashelkar, and J.J. Ulbrecht. 1977. Influence of Drag Reducing Additives on Mixing and Dispersing in Agitated Vessels. *AIChE J.* **23**: 487-492.

Radlett, P.J., R.C. Telling, J.P. Whiteside, and M.A. Maskell. 1972. The Supply of Oxygen to Submerged Cultures of BHK 21 Cells. *Biotechnol. Bioeng.* **14**: 437-445.

Ramirez, O.T., R. Mutharasan. 1989. Physical Immobilization Characteristics of a Hybridoma in a Glass Bead Packed-Bed Reactor. *Biotechnol. Bioeng.* **33**: 1072-1076.

Ramirez, O.T., R. Mutharasan and W.E. Magee. 1987. A Novel Immobilized Hybridoma Reactor for the Production of Monoclonal Antibodies. *Biotechnology Techniques*, **1**(4): 245-250.

Ranz, W.E., Marshall, W.-R. 1952. Evaporation from Drops. *Chem. Eng. Prog.* **48**: 141.

Ray, N.G., A.S. Tung, P.W. Runsdtadler, and J.N. Vournakis. 1991. Enhanced Productivity of Hybridoma and Recombinant CHO Cultures by Environmental Manipulation in Fluidised Bed Reactors. In: R.E. Spier, J.B. Griffiths and B. Meignier

(editors), *Production of Biologicals from Animal Cells in Culture*, pp.502-511. London: Butterworths.

Reichl, U., R. King, and E.D. Gilles. 1992. Characterization of Pellet Morphology During Submerged Growth of *Streptomyces tendae* by Image Analysis. *Biotechnology and Bioengineering*, **39**: 164-170.

Reiter, M., G. Bluml, T. Gaida, N. Zach, F. Unterluggauer, O. Doblhoff-Dier, M. Noe, R. Plail, S. Huss and H. Katinger. 1991. Modular Integrated Fluidized Bed Bioreactor Technology, *Bio/Technology*, **9**: 1100-1102.

Reiter, M., O. Hohenwater, T.Gaida, N. Zach, C. Schmatz, G. Bluml, F. Weigan, K. Nilsson and H. Katinger. 1990. The Use of Macroporous Gelatin Carriers for the Cultivation of Mammalian Cells in Fluidized Bed Reactors, *Cytotechnol.* **3**: 271-277.

Reiter, T., Penman, S., and Capco, D.G. 1985. Shape-Dependent Regulation of Cytoskeletal Protein Synthesis in Anchorage-Dependent and Anchorage-Independent Cells. *J. Cell Sci.* **76**: 17-33.

Rietema, K. 1982. Science and Technology of Dispersed Two-Phase Systems-I and II. *Chemical Engineering Science*, **37**(8): 1125-1150.

Rietema, K. and S.P.P. Ottengraf. 1970. Laminar Liquid Circulation and Bubble Street Formation in a Gas-Liquid System. *Trans. Instn Chem. Engrs.* **48**: T54-T62.

Rousseau, I. and J.D. Bu'lock. 1980. Mixing Characteristics of a Simple Airlift. *Biotechnol. Lett.* **2**: 475-480.

Runstadler, P.W. and S.R. Cernek. 1988. Large-Scale Fluidized Bed, Immobilized Cultivation of Animal Cells at High Densities. In: R.E. Spier and J.B. Griffiths (editors), *Animal Cell Biotechnology*, **3**: 305-320. London: Academic Press.

Sangani, A.S. and A. Acrivos. 1982. Slow Flow Past Periodic Arrays of Cylinders with Application to Heat Transfer. *Int. J. Multiphases Flow*, **8**: 193-206.

Scahill, S.J., R. Devos, J. Van der Heyden, W. Fiers. 1983. Expression and Characterization of the Product of a Human Interferon cDNA Gene in Chinese Hamster Ovary Cells. *Proc. Natl Acad. Sci. USA.* **80**: 4654-4658.

Scheirer, W. 1988. High-density Growth of Animal Cells within Cell Retention Fermenters Equipped with Membranes, In: R.E. Spier and J.B. Griffiths (editors), *Animal Cell Biotechnology*, **3**: 263-281. London: Academic Press.

Scheirer, W. and O.-W. Merten. 1991. Instrumentation of Animal Cell Culture Reactors. In: C.S. Ho and D.I.C. Wang (editors), *Animal Cell Bioreactors*, p.405-443, Boston: Butterworth-Heinemann.

Schimke, R.T., R.T. Kaufman, F.W. Alt, R.F. Kellems. 1978. Gene Amplification and Drug Resistance in Cultured Murine Cells. *Science*, **202**: 1051-1055.

Schoen, R.C., K.L. Bentley, R.J. Klebe. 1982. Monoclonal Antibody Against Human

Fibronectin Which Inhibits Cell Attachment. *Hybridoma*, **1**: 99-108.

Scholz, M. and W.-S. Hu. 1990. A Two-Compartment Cell Entrapment Bioreactor with Three Different Holding TImes for Cells, High and Low Molecular Weight Compounds, *Cytotechnol.* **4**: 127-137.

Schugerl, K., J. Luckn and U. Oels. 1977. Bubble Column Bioreactors. In: T.K. Ghose, A. Fiechter, and N. Blakebrough (editors), *Advances in Biochemical Engineering*, 7:1-84. Berlin: Springer-Verlag.

Schwartz, C.E. and J.M.Smith. 1953. Flow Distribution in Packed Beds. *Ind. Engng Chem.* **45**: 1209-1218.

Shah, Y.T., B.G. Kelkar, S.P. Godbole and W.-D. Deckwer. 1982. Design Parameters Estimations for Bubble Column Reactors. *AIChE J.* **28**(3): 353-379.

Shiloach, J., J.B. Kaufman, and R.M. Kelly. 1986. Hollow Fiber Microfiltration Methods for Recovery of Rat Basophilic Leukemia Cells (RBL-2H3) from Tissue Culture Media. *Biotechnol. Prog.* **2**: 230-233.

Shimazaki, K., N. Nishimura, H. Shibai. 1986. New Separation System for Mammalian Cells with Large-Scale Centrifugation. *Ann. NY Acad. Sci.* **469**: 63-72.

Shirai, Y., K. Hasimoto, H. Yamaji and M. Tokashi. 1987. Continuous Production of Monoclonal Antibody with Immobilized Hybridoma Cells in an Expanded Bed Fermentor. *Appl. Microbiol. Biotechnol.* **26**:495-499.

Shu, J. and M.L. Shuler. 1991. Prediction of Effects of Amino Acid Supplementation on Growth of *E. coli* B/r. *Biotechnology and Bioengineering*, **37**: 708-715.

Siegel, M.H., M. Hallaile and J.C. Merchuk. 1988. Air-Lift Reactors: Design, Operation, and Application. In: A. Mizrahi (editor), *Advances in Biotechnological Process*, **7**: 79-124. NY: Alan R. Liss, Inc.

Siegel. M.H., J.C. Merchuk and K. Shugerl. 1986. Paper Presented ar the *International Conference on Bioreactor Fluid Dynamics*, Cambridge (England), 15-17 April, 1986.

Singhvi, R., G.N. Stephanopoulos, and D.I.C. Wang. 1991. Effect of Substratum Morphology on Animal Cell Adhesion and Behavior. Paper Presented at AIChE Annual Meeting, Los Angeles, CA, Nov. 1991. Paper no. 254d.

Sinskey, A.J., R.J. Fleischaker, M.A. Tyo, D.J. Giard, and D.I.C. Wang. 1981. Production of Cell-Derived Products: Virus and Interferon. *Annals New York Academy of Sciences*, 47-59.

Sparrow, E.M. and A.L. Loeffler Jr. 1959. Longitudinal Laminar Flow Between Cylinders Arranged in Regular Array. *AIChE J.* **5**: 325-330.

Spielman, L. and S.L. Goren. 1968. Model for Predicting Pressure Drop and Filtration Efficiency in Porous Media. *Envir. Sci. Tech.* **2**: 279-287.

Spier, R.E. 1985. Monolayer Growth Systems: Heterogeneous Unit Processes. In: *Animal Cell Biotechnology*, **1**: 243-263. London: Academic Press Inc. Ltd.

Spier, R.E. 1991. Large-Scale Mammalian Cell Culture. Methods, Applications and Products. *Current Opinion in Biotechnology*, **2**: 375-379.

Spier, R.E., and J.B. Clarke. 1980. Variation in the Susceptibility of BHK Populations and Cloned Cell Lines to Three Strains of FMD Virus. *Arch. Virol.* **63**: 1-9.

Spier, R.E. and B. Griffiths. 1982. An Examination of the Data and Concepts Germane to the Oxygenation of Cultured Animal Cells. *Develop. biol. Standard.* **55**: 81-92.

Spier, R.E., and K. McCullough. 1990. *The Large-Scale Production of Monoclonal Antibodies in vitro*, Cambridge: Cambridge University Press.

Spier, R. E. and J.P. Whiteside. 1976. The Production of Foot and Mouth Disease Virus from BHK21C13 Cells Grown on the Surface of Glass Spheres. *Biotechnol. Bioeng.* **18**: 649-657.

Spier, R.E. and J.P. Whiteside. 1990. The Oxygenation of Animal Cell Cultures by Bubbles. In: R.E. Spier and J.B. Griffiths (editors), *Animal cell biotechnology*, **4**: 133-148. London: Academic Press.

Sprague, E.A., B.L. Steinbach, R.M. Nerem, and C.J. Schwartz. 1987. Influence of a Laminar Steady-State Fluid-Imposed Wall Shear Stress on the Binding, Internalization, and Degradation of Low-Density Lipoproteins by Cultured Arterial Endothelium. *Circulation*, **76**: 648-656.

Stanek, V. and J. Szekely. 1972. The Effect of Non-uniform Porosity in Causing Flow Maldistributions in Isothermal Packed Beds. *CanJ. Chem.Eng.* **50:** 9-14.

Stathopoulos, N.A. and J.D. Hellums. 1985. Shear Stress Effects on Human Embryonic Kidney Cells *in vitro*. *Biotech. Bioeng.* **27**: 1021-1026.

Stephanopoulos, G.N., R. Singhvi and S. Park. 1989. Porous Ceramic Microcarriers for Animal Cell Culture. Paper Presented at ACS Pacifichem Meeting, Honolulu, Haiwaii, Dec. 1989.

Struminsky, V.V. and M.A. Pavilikhina. 1981. Experimental Investigations of the Velocity Distribution at the Catalyst Packed Bed Outlet. *Aerodynamics in Processes*, pp.63-74. Nauda, Moscow.

Swaine, D.E. and A.J. Daugulis. 1988. Review of Liquid Mixing in Packed Bed Biological Reactors. *Biotechnology Process*, **4**(3): 134-148.

Taguchi, H. and A. E. Humphrey. 1966. Dynamic Measurement of Volumetric Oxygen Transfer Coefficient in Fermentation Systems. *J. Ferment. Tech.* (Jap.) **44**: 881-889.

Takazawa, Y., M. Tokashiki, K. Hamoto, H. Murakami. 1988. High Cell Density Perfusion Culture of Hybridoma Cells Recycling High Molecular Weight Components. *Cytotechnol.* **1**: 171-178.

Taylor, W.G., R.F. Camalier, and K.K. Stanford. 1978. Density-Dependent Effects of Oxygen on the Growth of Mammalian Fibroblasts in Culture. *J. Cell Physiol.* **95**: 33-40.

Telling, R.C. and R. Elsworth. 1965. Submerged Culture of Hamster Kidney Cells in a Stainless Steel Vessel. *Biotechnol. Bioeng.* **7**: 417-434.

Tharakan, J.P. and P.C. Chau. 1986 a. A Radial Flow Hollow Fiber Bioreactor for the Large-Scale Culture of Mammalian Cells.*Biotechnol. Bioeng.* **28**: 329-342.

Tharakan, J.P. and P.C. Chau. 1986 b. Operation and Pressure Distribution of Immobilized Cell Hollow Fiber Bioreactors. *Biotechnol. Bioeng.* **28**: 1064-1071.

Tharakan, J. P., S. L. Gallagher and P. C. Chau. 1988. Hollow-Fiber Bioreactors for Mammalian Cell Culture. In: A. Mizrahi (editor), *Advances in Biotechnological Processes*, **7**: 153-184. New York: Alan R. Liss, Inc.

Tolbert, W.R., C. Lewis Jr., P.J. White, J. Feder. 1985. Perfusion Culture Systems for Production of Mammalian Cell Biomolecules. In: J. Feder and W. Tolbert (editors), *Large Scale Mammalian Cell Culture*, London: Academic Press.

Tokashiki, M. 1991. High Density Cell Culture. In: C.S. Ho and D.I.C.Wang (editors), *Animal Cell Bioreactors*, pp.327-356. Boston: Butterworth-Heinemann.

Tokashiki, M.,and T. Arai. 1989. High Density Culture of Mouse-Human Hybridoma Cells Using a Perfusion Culture Apparatus with Multi-Settling Zones to Separate Cells from the Culture Medium. *Cytotechnology*, **2**: 5-8.

Tokashiki, M., T. Arai, K. Hamamoto, K. Ishimaru. 1990. High Density Culture of Hybridoma Cells Using a Perfusion Culture Vessel with an External Centrifuge. *Cytotechnology*, **3**: 239-244.

Tramper, J., D. Joustra, and J.M. Vlak. 1987. Bioreactor Design for Growth of Shear-Sensitive Insect Cells. In: C. Webb and F. Mavituna (editors), *Plant and Animal Cells: Process Possibilities*, Chichesster (England): Ellis Horwood Ltd.

Tramper, J., J.B. Williams and D. Joustra. 1986. Shear Sensitivity of Insect Cells in Suspension. *Enzyme Microb. Technol.* **8**: 33-36.

Turner, J. C. R. 1966. On Bubble Flow in Liquids and Fluidised Beds. *Chem. Eng. Sci.* **21**: 971-974.

Tyo, M.A., B.J.Bulbulian, B. Zaspeo, and T.J. Murphy. 1988. Large-scale Mammalian Cell Culture Utilizing ACUSYST Technology, In: R.E. Spier and J.B. Griffiths (editors), *Animal Cell Biotechnology*, **3**: 357-371. London: Academic Press.

van Wezel, A.L. 1967. Growth of Cell-Strains and Primary Cells on Microcarriers in Homogeneous Culture. *Nature* (London), **216**: 64-65.

van Wezel, A.L. 1982. Cultivation of Anchorage-dependent Cells and Their Applications. *J. Chem. Technol. Biotechnol.* **32**: 318-323.

van Wezel, A.L. and C.A.M. van der Velden-de Groot. 1978. Large Scale Cultivation of Animal Cells in Microcarrier Culture. *Process Biochemistry*, **13**(3): 6-8.

Varani, J., M. Dame and T. F. Beals. 1983. Growth of Three Established Cell Lines on Glass Microcarriers. *Biotechnol. Bioeng.* **25**: 1359-1372.

Verlaan, P., J. Tramper, K. Van't Riet and K.Ch.A.M. Luyben. 1986 a. Paper Presented at the *International Conference on Bioreactor Fluid Dynamics*, Cambridge (England), 15-17 April, 1986, Paper 07.

Verlaan, P., J. Tramper and K. Van't Riet. 1986 b. A Hydrodynamic Model for an Airlift - Loop Bioreactor with External Loop. *The Chemical Engineering Journal*, **33**: B43-B53.

Volkov, S.A., K.F. Khalilov, V.I. Reznikov, V.Yu. Zel'venskii and K.I. Sakodynsdii. 1986 a. Longitudinal Spreading in Gas and Liquid Chromatography and Its Connection with Packed Bed Structure and the Velocity of the Mobile Phase. *Journal of Chromatography*, **364**: 39-51.

Volkov, S.A., V.I. Reznikov, V.Yu. Zel'vensdy, K.I. Sakodynsdy and F. Ya. Frolov. 1979. On the Inhomogeneity of the Gas Flow Velocity Field in Chromatographic Columns. *Teor. Osnovy Khim. Teknol.* **13**: 455-458.

Volkov, S.A., V.I. Reznikov, K.F. Khalilov, V.Yu. Zel'vensdy and K.I. Sakodynsdy. 1986 b. Nonuniformity of Packed Beds and Its Influence on Longitudinal Dispersion. *Chemical Engineering Science*. **41**(2): 389-397.

Volkov, S.A., V.Yu. Zel'vensdy, and K.I. Sakodynsdii. 1972. *Neftekhimiya*, **12**: 912-919.

Vournakis J.N., and P.W. Runstadler, Jr. 1991. Optimization of the Microenvironment for Mammalian Cell Culture in Flexible Collagen Microspheres in a Fluidized-Bed Bioreactor. In: C.S. Ho and D.I.C.Wang (editors), *Animal Cell Bioreactors*, pp.305-326. Boston: Butterworth-Heinemann.

Wang, D.I.C., R.T. Hatch and C. Cuevas. 1971. Engineering Aspects of Single-Cell Protein Production from Hydrocarbon Substrate: The Airlift Fermentor. In: *Proceedings of the 8th World Petroleum Congress*, p.149-156. Moscow,

Weiland, P. 1984. Influence of Draft Tube Diameter on Operation Behaviour of Airlift Loop Reactors.*Ger.Chem.Eng.* **7**: 374-385.

Weiland P. and U. Onken. 1981. Differences in the Behaviour of Bubble Columns and Airlift Loop Reactors. *Ger. Chem. Eng.* **4**: 174-181.

Whiteside, J.P., S. Farmer and R.E. Spier. 1985. The Use of Caged Aeration for the Growth of Animal Cells on Microcarriers. *Develop. biol. Standard*, **60**: 283-290.

Whiteside, J.P. and R.E. Spier. 1981. The Scale-Up from 0.1 to 100 Liters of a Unit Process System Based on 3 mm Diameter Glass Spheres for the Production of Four Strains of FMDV from BHK Monolayer Cells. *Biotechnol. Bioeng.* **23**: 551-565.

Wilke, C.R. and P. Chang. 1955. Correlation of Diffusion Coefficients in Dilute Solutions. *Am. Inst. Chem. Eng. J.* **1**: 264-270.

Wohler, W., H.W. Rudiger and E. Passage. 1972. Large-Scale Culturing of Normal Diploid Cells on Glass Beads Using a Novel Type Culture Vessel. *Exp. cell Res.* **74**: 571-573.

Wohlpart, D., J. Gainer and D. Kirwaan. 1991. Oxygen Uptake by Entrapped Hybridoma Cells. *Biotechnol. Bioeng.* **37**: 1050-1053.

Wudtke, M. 1988. Studies on the Damage of Animal Cells by Mechanical Means. *Ph.D. Thesis*, University of Hannover, Braunschweig, West Germany.

Yoshida, H., M. Kamihira, S. Iijima, and T. Kobayashi. 1989. Continuous Production of Anti-Erythropoitin Antibody by Immobilized Hybridoma Cells. *J. Chemical Engineering Jpn.* **22**(3): 282-286.

Yu, C.P. and T.T. Soong. 1975. A Random Cell Model for Pressure Drop Prediction in Fibrous Filters. *J of Applied Mech. Trans ASME,* **22**: 301-304.

Zuber, N. and Findlay, J.A. 1965. Average Volumetric Concentration in Two-Phase Flow Systems. *Transactions of the ASME (C), J. Heat transfer*, November, p.453-468.

Zupke, C. 1992. Personal Communications. M.I.T. Cambridge, MA

Appendix: Penetration Depth

Chang and Moo-Young (1988) used a simple model to calculate the oxygen penetration depth in immobilized cells by assuming zero order kinetics in the presence of several external oxygen transport resistances in various systems, such as fluidized bed reactor, hollow fiber reactor and microencapsulation device. It was indicated that the typical penetration depths of oxygen are in the range of 500 to 1000 μm for immobilized or encapsulated animal and plant cells. Murdin *et al.* (1987 b) have also calculated the diffusion of oxygen into immobilized cell masses and compared the values with experimental measurements of the metabolism of hybridoma cells in a slab of agarose.

The penetration depth is determined by specific oxygen uptake rate of the cells and the oxygen concentration in the solution. A simplified treatment of the problem of oxygen transfer into dense cell mass can be made based on the following assumptions:

(1) specific oxygen uptake rate is independent of oxygen concentration. This zero order kinetics is considered because Km values of oxygen are usually very small, less than 10% of the ambient oxygen concentration in the liquid saturated with air. The possible effect of this assumption is to make the model poorly fitting into reality at low oxygen concentration.

(2) The system is at steady-state condition.

(3) The effective diffusivity of oxygen through the dense cell mass is constant, and the value is about half of the free-diffusion value.

(4) One-dimensional flow through cell mass.

(5) No effectively viable cells exist beyond the region where oxygen concentration is lower than a certain critical value.

Therefore, (A.1)

$$Ds \frac{\partial^2 Cs}{\partial x^2} = Rs$$

where Ds is the effective diffusivity of oxygen in dense cell masses (cm^2/s), Cs is the nutrient concentration (mmolar), x is the distance (cm), and Rs is the volumetric oxygen consumption rate (mmole/l/s), which is equal to the product of specific oxygen uptake rate (r') and cell density (Xc).

Boundary conditions:

$x = 0$, $Cs = Cs^b$ (oxygen concentration in the bulk solution)

$x = x_p$, $Cs = Cs^{cr}$ (critical oxygen concentration)

$$\frac{\partial Cs}{\partial x} = 0$$

where penetration depth of viable cells, x_p, is unknown. It can be solved through Equation A.1 combined with the three boundary conditions above to give:

$$x_p = \sqrt{2 \frac{Ds}{Rs} (Cs^b - Cs^{cr})} \quad (A.2)$$

Therefore, the penetration depth depends on the oxygen concentration outside the cell mass and the volumetric oxygen uptake rate of the cells. The specific oxygen uptake rate used was 5.9×10^{-11} and 1.0×10^{-10} mmole/cell/hr for γ-CHO and hybridoma CRL-1606 respectively, which were obtained from our cultivation experiments. Assume that Cs^{cr} is 10% air saturation, Figure A.1 shows the penetration depth versus dissolved oxygen concentration in the bulk solution for γ-CHO and hybridoma CRL-1606. Based on the

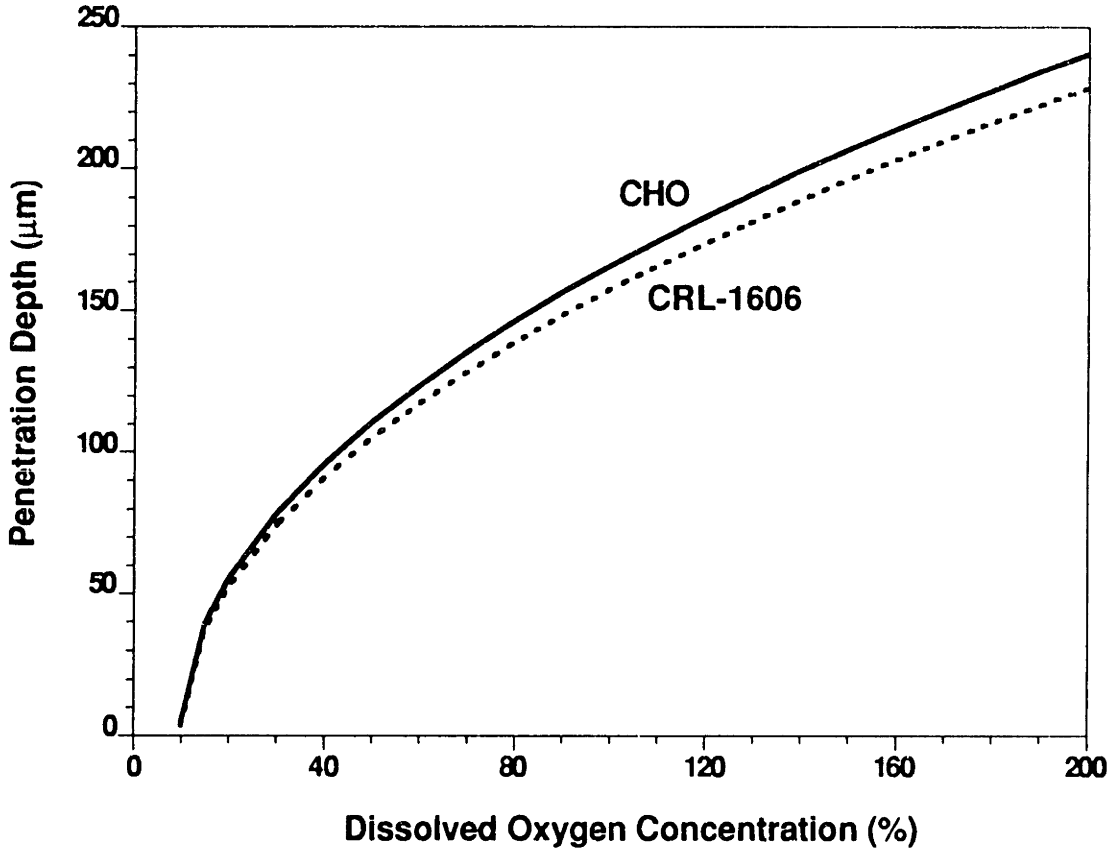

Figure A.1 Effect of dissolved oxygen concentration on penetration depth

multilayer growth model, the total number of layers as a function of dissolved oxygen concentration can be calculated and is shown in Figure A.2.

The graphs are useful in providing information for oxygen diffusion. For example, for a hybridoma CRL-1606 cell culture in a fiber bed, if the fiber is equally spaced, a cell density of $2x10^8$ cells/cm^3 would result in 4 layers of cells anchored on the fibers. The thickness of these 4 layers of cells is smaller than the penetration depth as long as the dissolved oxygen concentration is higher than 15%.

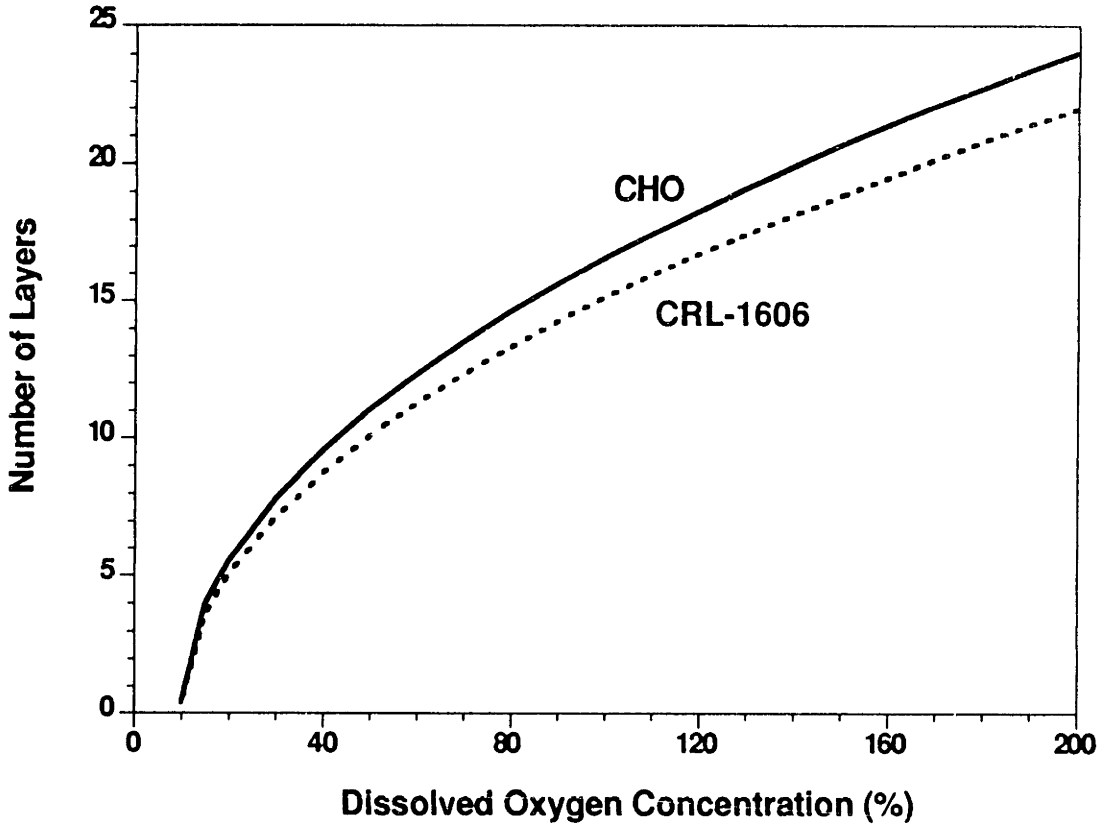

Figure A.2 Effect of dissolved oxygen concentration on the number of layers penetrated